A Decision Support System for Indirect Potable Reuse Based on Integrated Modeling

Adnan Ghaffar Lodhi

Dissertation submitted to the faculty of the Virginia Polytechnic Institute and State University in partial fulfillment of the requirements for the degree of

Doctor of Philosophy

In

Civil Engineering

Adil N. Godrej Committee Chair

John C. Little

Zhiwu Wang

Dipankar Sen

April 24, 2019

Manassas, VA

Keywords: Decision Support System; Integrated Modeling; Indirect Potable Reuse; National Water Model; Water and Wastewater Treatment; Weather Forecasting

Copyright © Adnan G. Lodhi

A Decision Support System for Indirect Potable Reuse Based on Integrated Modeling

Adnan G. Lodhi

Abstract

Optimal operation of water reclamation facilities (WRFs) is critical for an indirect potable reuse (IPR) system, especially when the reclaimed water constitutes a major portion of the reservoir's safe yield. It requires timely and informed decision-making in response to the fluctuating operational conditions, e.g., weather patterns, plant performance, water demand, etc. Advanced integrated modeling techniques can be used to develop reliable operational strategies to mitigate future risks associated with water quality without needing high levels of financial investment.

The Upper Occoquan Service Authority (UOSA) WRF, located in northern Virginia, discharges nitrified reclaimed water directly into a tributary of the Occoquan Reservoir, one of the major water supply sources for Fairfax County. Among the many operational challenges at UOSA, one is to regulate the nitrate concentration in its reclaimed water based on the denitrifying capacity of the reservoir. This study presents an integrated model that is used to predict future reservoir conditions based on the weather and streamflow forecasts obtained from the Climate Forecast System and the National Water Model. The application captures the dynamic transformations of the pollutant loadings in the streams, withdrawals by the water treatment plant, WRF effluent flows, and plant operations to manage the WRF performance. It provides plant operators with useful feedback for correctly targeting the effluent nitrates using an intelligent process simulator called IViewOps.

The platform is powered by URUNME, a new software that fully automates the operation of the reservoir and process models integrating forecasting products, and data sources. URUNME was developed in C#.NET to provide out-of-the-box functionality for model coupling, data storage, analysis, visualization, scenario management, and decision support systems. The software automatically runs the entire integrated model and outputs data on user-friendly dashboards, displaying historical and forecasting trends, on a periodic basis. This decision support system can provide stakeholders with a holistic view for the design, planning, risk assessments, and potential improvements in various components of the water supply chain, not just for the Occoquan but for any reservoir augmentation type IPR system.

A Decision Support System for Indirect Potable Reuse Based on Integrated Modeling

Adnan G. Lodhi

General Audience Abstract

In an indirect potable reuse (IPR) system, reclaimed water from an advanced wastewater treatment facility is blended with a natural water source, such as a reservoir, to augment drinking water supply. Reliable operation of such a system is critical, especially when the reclaimed water constitutes a major portion of the withdrawals from the reservoir for treatment and distribution. One example of such an IPR system is the Upper Occoquan Service Authority (UOSA) water reclamation facility (WRF) which discharges its reclaimed water into the Occoquan Reservoir, a key water resource for Fairfax County.

Integrated environmental modeling (IEM) provides a comprehensive approach towards the design and operation of water resource systems in which water supply, drainage, and sanitation are simulated as a single entity rather than independent units. In IEM, different standalone models, each representing a single subsystem, are linked together to analyze the complex interactions between various components of the system. This approach can be used for developing operational support tools for an IPR system to ensure timely and informed decision-making in response to the fluctuating conditions, e.g., weather patterns, plant performance, water demand, etc.

The overarching goal of this research was to integrate different models and the data sources and develop a decision support system (DSS) to manage the UOSA-WRF performance. This resulting integrated model is used to predict future reservoir conditions based on the weather and streamflow forecasts obtained from the National Weather Service. The application runs various future scenarios to capture the possible variations of the pollutant loadings in the streams, withdrawals by the water treatment plant, WRF effluent flows, and plant operations and provide feedback to plant operators. The entire integrated model is operated periodically to output data on user-friendly dashboards, displaying historical and forecasting trends. The DSS provides stakeholders with a holistic view for the design, planning, risk assessments, and potential improvements in various components of the water supply chain, not just for the Occoquan but for any reservoir augmentation type IPR system.

Dedication

To

Huma

Acknowledgments

I would like to thank my advisor Dr. Adil Godrej for giving me the opportunity to conduct this interesting research and for all his help and support. I would also like to extend my deepest appreciation to Dr. Dipankar Sen for playing an instrumental part during my entire Ph.D. research career. He has taught me a great deal and I cannot thank him enough for the time and guidance he has bestowed on me during the last few years.

I am extremely grateful to Dr. John C. Little and Dr. Zhiwu Wang for being part of my research and serving on my committee. I can never forget the late Dr. Thomas Grizzard for believing in me and appreciating my work. I miss you, Tom!

Many thanks to all the field, laboratory, and administrative staff at the OWML for treating me like family. Especially Barb Angelotti for sharing all those laughs. I am also extremely grateful for all the input I received from Bob Angelotti and Matt Brooks from the Upper Occoquan Service Authority.

I want to remember my parents for all their love and support, especially my mother without whom I could have never reached far in life. I would also like to thank Brig. Sardar Javed Ashraf, my adopted father and mentor, for always being there for me and providing ceaseless encouragement for all my academic endeavors.

And last but not least, I would like to extend my deepest gratitude to my wife, Huma, who has always been there for me through thick and thin. I could have never finished my Ph.D. without her relentless emotional support, love, and devotion towards my work. Finally, many thanks to my daughters, Mayher and Danya, for always bringing a smile on my face. You two are amazing and Baba loves you so much.

Table of Contents

Chapter 1 Research Objectives 1
1.1 Introduction 1
1.2 Study Motivation 1
1.2.1 A Generic Integrated Environmental Modeling Software 1
1.2.2 Nitrate Regulation in Occoquan Reservoir 2
1.2.3 Advanced Physicochemical Modeling 4
1.3 Study Objectives 5
1.3.1 URUNME 'You Run Models Easily' 5
1.3.2 Occoquan Decision Support System 5
1.3.3 IViewOps4 Physicochemical Model 5
1.4 Document Organization 5
1.5 References 6
Chapter 2 Background Information 9
2.1 Occoquan Watershed 9
2.2 Upper Occoquan Service Authority 10
2.3 Occoquan Watershed Monitoring 11
2.4 Occoquan Reservoir Model 11
2.5 IViewOps 13
2.6 Climate Forecast System 14
2.7 National Water Model 15
2.8 References 15
Chapter 3 URUNME: A Generic Software for Integrated Environmental Modeling 18
3.1 Abstract 18
3.2 Introduction 18
3.2.1 Built-In Integrated Models 19
3.2.2 Coupled Integrated Models 19
3.2.3 Need for a Generic IEM Software 20
3.3 Software Architecture 23
3.3.1 User Interface 24
3.3.2 Process and Functions 25
3.3.3 Open Modeling Interface 27
3.3.4 Parameters and Variables 28

3.3.5 Embedded Database 30
3.3.6 Unit Converter 31
3.4 Features and Capabilities 31
3.4.1 Diagram / Process Panel 32
3.4.2 Symbols 32
3.4.3 Functions 32
3.4.4 Run Engine 38
3.4.5 Panels 38
3.4.6 Commands 39
3.5 Case Studies 40
3.5.1 Data Analysis 40
3.5.2 Web Data Download 43
3.5.3 Auto Calibration 45
3.5.4 Loose Model Coupling 46
3.5.5 OpenMI based Coupling 48
3.5.6 Scenario Management 50
3.5.7 Decision Support Systems 50
3.6 Summary 52
3.7 Acknowledgments 53
3.8 References 54
Chapter 4 A decision support system for indirect potable reuse based on integrated modeling and futurecasting 69
4.1 Abstract 69
4.2 Introduction 69
4.2.1 Study Area 71
4.3 Methods 73
4.3.1 IViewOps (Intelligent View of Operations) Model 76
4.3.2 Climate Forecast System – Weather Model 76
4.3.3 National Water Model 77
4.3.4 Occoquan Reservoir Model 77
4.3.5 Hypolimnetic Oxygenation System Model 79
4.3.6 Decision Support System 81
4.4 Results and Discussion 87
4.4.1 Calibration of the Coupled Model 87
4.4.2 Bias Correction for CFS 89

4.4.3 Futurecasting 90
4.4.4 Process Optimization 95
4.5 Conclusion 95
4.5.1 Future Applications of URUNME based DSS 96
4.6 Acknowledgment 97
4.7 References 98
Chapter 5 Expansion of the Activated Sludge Model (ASM2d) for simulating advanced processes in water reuse systems 125
5.1 Abstract 125
5.2 Introduction 125
5.1.1 Upper Occoquan Service Authority 127
5.1.2 IViewOps3 127
5.3 Methods 129
5.3.1 pH (Acid/Base Systems) 129
5.3.2 Precipitation 131
5.3.3 Oxidation 132
5.3.4 Adsorption 137
5.3.5 Effect of temperature 140
5.3.6 Effect of ionic strength 140
5.3.7 Open source model library 141
5.4 Results and Discussion 142
5.4.1 Influent 143
5.4.2 Headworks 143
5.4.3 Secondary Treatment 144
5.4.4 Digestion and Solids Handling 145
5.4.5 Chemical Phosphorus (P) Removal 146
5.4.6 Activated Carbon Contactors 147
5.4.7 Disinfection and Final Effluent 148
5.5 Recommendations 149
5.6 Conclusion 149
5.7 Acknowledgment 150
5.8 References 150
Chapter 6 Summary and Conclusions 196
6.1 Summary 196
6.2 Conclusion 198

6.3 References 198

List of Figures

Figure 2-1. Occoquan Watershed 9
Figure 2-2. CE-QUAL-W2 Model Inputs for Occoquan Reservoir 12
Figure 3-1. High level architecture of URUNME 23
Figure 3-2. URUNME's graphical user interface: main screen 24
Figure 3-3. Class diagram showing some basic nodes (Due to space limitation, only some selected properties and methods are shown in the diagram) 25
Figure 3-4. Class diagram for a process 26
Figure 3-5. Hierarchical execution path in URUNME 27
Figure 3-6. Class diagram of Parameter and Variable 29
Figure 3-7. 'Output' tab of the Read Excel function Properties Form 34
Figure 3-8. 'Input' tab of the Write Excel function Properties Form 35
Figure 3-9. Low flow analysis in URUNME 42
Figure 3-10. Process panel in URNUME showing periodic downloading and data extraction of NWM 44
Figure 3-11. Auto calibration of CE-QUAL-W2 water level using 'water balance' utility in URUNME 46
Figure 3-12. Sequentially coupled Occoquan watershed model consisting of 7 HSPF and 2 CE-QUAL-W2 models in URUNME 48
Figure 3-13. OpenMI based couple model showing Simple River example from OpenMI v1.4 50
Figure 3-14. Occoquan decision support system showing model calibration results 51
Figure 3-15. Occoquan decision support system showing observed and simulated values of different process parameters at UOSA water reuse plant 52
Figure 4-1. Occoquan Watershed 72
Figure 4-2. Integrated Model Inputs for Occoquan Reservoir 79
Figure 4-3. Data flow diagram for the integrated model 83
Figure 4-4. Execution path of the integrated model 86

Figure 4-5. Calibrated pool elevation, temperature, dissolved oxygen, and nitrate (as nitrogen) (solid lines are simulated and dots are observed values). Temperature, dissolved oxygen and nitrate are bottom values..... 87
Figure 4-6. (a) Linear regression between observed and reforecasted air temperature (b) CDF for observed (dashed line) and reforecasted (solid line) air temperatures 90
Figure 4-7. Low flow frequency analysis for different n-moving averages using 10 year return period..... 92
Figure 4-8. Nitrate profiles for different scenarios at RE02. (D_1 = Projected monthly WRF discharge, D_2 = fixed WRF discharge at 149,524 m^3/d (39.5 mgd), W_1 = WTP withdrawals based on last 5 years of monthly averages, W_2 = fixed at 299,048 m^3/d (79 mgd), N_1, N_2 and N_3 are WRF Effluent nitrate-N set at 7.5, 10 and 12.5 mg/L)..... 92
Figure 4-9. Nitrate profiles for different scenarios at RE02 using 2-m initial drawdown..... 94
Figure 5-1. UOSA-WRF treatment process schematic *(courtesy UOSA)* 155
Figure 5-2. Class diagram of IViewOps model library..... 156
Figure 5-3. IViewOps4 model for UOSA-WRF secondary treatment system. Refer to Table 5-1 for the description of unit-processes and Table 5-2 for flows in different pipes. 157
Figure 5-4. IViewOps4 UOSA-WRF model for chemical P-removal system. Refer to Table 5-1 for the description of unit-processes. 158
Figure 5-5. IViewOps4 model for UOSA-WRF multimedia filters, carbon contactors, and chlorination systems. Refer to Table 5-1 for the description of unit-processes and Table 5-2 for flows in different pipes. 158
Figure 5-6. Primary clarifier TSS removal rating curve 164
Figure 5-7. Isotherm data, provided by UOSA-WRF for new activated carbon, fitted into Equation 5-27 to calculate the isotherm coefficients. (q_{max} = 414 mg/L, a = 0.65, k_{Ads} = 1.5 d^{-1}, k_{Des} = 114 d^{-1})..... 171

Figure A3-1. Class diagram unit conversion in URUNME..... 58
Figure A3-2. Read Excel function Properties Form showing ‘General Tab’ with localized ‘File’ Parameter 58

Figure A3-3. Read Excel function Properties Form showing 'File' parameter ready to be attached to a Variable 59
Figure A3-4. Read Excel function Properties Form showing 'File' parameter attached to a Variable with a dropbox to select the scenario 59
Figure A3-5. SQL function Properties Form showing the 'Query' tab 60
Figure A3-6. R function Properties Form showing the 'Script' tab 60
Figure A3-7. Formula function Properties Form showing the 'Expression' tab 61
Figure A3-8. Execute function Properties Form showing the "External' tab required to run a model 61
Figure A3-9. Execute function Properties Form showing the process 'Low Flows' selected to run in three different scenarios in a batch mode 62
Figure A3-10. Chart wizard in URUNME 62
Figure A3-11. Gauges in URUNME 63
Figure A3-12. Event Manager Properties Form showing how an Event is defined 63
Figure A3-13. Event Manager Panel showing how an Event message is displayed when triggered 64
Figure A3-14. Commands Properties Form for a button showing definition of a 'Run' command 64
Figure A3-15. 'Input' tab showing different Variables in a chart 65
Figure A3-16. Formula function showing the Variables defined for downloading NWM forecast 65
Figure A3-17. Downloader function showing parameters defined to download NWM forecast 66
Figure A3-18. OmiModel function properties form showing output and input exchange items for Simple River model 66
Figure A3-19. OmiInput function properties form showing output exchange item automatically generated for the input variable 'inflows' 67
Figure A3-20. OmiLink properties form showing an OpenMI link between OmiInput function and Simple river model component for 'inflows' 67
Figure A3-21. OmiLink properties form showing an OpenMI link between Omioutput function and Simple river model component for 'inflows' 68

Figure A4-1. Occoquan Reservoir sampling stations 103
Figure A4-2. Occoquan Reservoir CE-QUAL-W2 model braches and segmentation (4 branches, 69 longitudinal segments with an average length of 0.5 km, and 0.5 meter layers) 104
Figure A4-3. Line diffuser system for hypolimnetic oxygenation 105
Figure A4-4. Bottom water temperature profiles for different scenarios at RE02 105

Figure B 4-1. The main screen of the Occoquan Decision Support System. The buttons on the left side are for opening up different sections including historical data, calibration, forecasting, and UOSA WRF process optimization. Buttons on the right side, from top to bottom, are for 1) Home: to go back to the main screen, 2) Back: to go back to the last screen, 3) Save: to save the current settings, 4) Events: to show alarms and warnings, 5) About: to show a brief description of the system, and 6) Exit: to close the application. 106
Figure B 4-2. This screen shows the historical weather data. It is opened by clicking the 'Historical' button from the main screen in Figure B 4-1. The buttons on the left are used to open other historical trends from different rain, stream, and reservoir stations. 107
Figure B 4-3. This screen shows the historical rain data. It is opened by clicking the 'Rain' button from the screen shown in Figure B 4-2. 108
Figure B 4-4. This screen shows the historical stream flow data. It is opened by clicking the 'Streams' button from the screen shown in Figure B 4-3. 109
Figure B 4-5. This screen shows the historical stream temperature and concentrations data. It is opened by clicking the 'Conc' button from the screen shown in Figure B 4-4. The buttons on the bottom left are used to switch between different constituents. 110
Figure B 4-6. This screen shows the monthly stream loads. It is opened by clicking the 'Loads' button from the screen shown in Figure B 4-5. The buttons on the bottom left are used to switch between different constituents. 111

Figure B 4-7. This screen shows the yearly stream loads. It is opened by clicking the 'Yearly' button from the screen shown in Figure B 4-6. The buttons on the bottom left are used to switch between different constituents. 112
Figure B 4-8. This screen shows the historical reservoir concentrations at reservoir stations. It is opened by clicking the 'Reservoir' button from the screen shown in Figure B 4-3. The buttons on the bottom left are used to switch between different constituents. 113
Figure B 4-9. This screen shows depth profiles for temperature, dissolved oxygen and nitrate-nitrogen at different reservoir stations. It is opened by clicking the 'Depth Profile' button from the screen shown in Figure B 4-8. The list to the left of the charts provide all the dates for which the observed data are available. User can click any row on the list to show the depth profile for the selected date. 114
Figure B 4-10. This screen shows the historical pool elevation of the reservoir. It is opened by clicking the 'Pool' button from the screen shown in Figure B 4-9. 115
Figure B 4-11. This screen shows the simulated versus observed time series for the calibration run. It is opened by clicking the 'Calibration' button from the main screen shown in Figure B 4-1. The buttons on the bottom left are used to switch between different constituents. 116
Figure B 4-12. This screen shows the simulated vs observed depth profiles temperature, dissolved oxygen and nitrate nitrogen for the calibration run. It is opened by clicking the 'Depth Profiles' button from the screen shown in Figure B 4-11. The list to the left of the charts provide all the dates for which the observed data are available. User can click any row on the list to show the depth profile for the selected date. 117
Figure B 4-13. This screen shows the simulated vs observed pool elevation for the calibration run. It is opened by clicking the 'Pool' button from the screen shown in Figure B 4-12. 118
Figure B 4-14. This screen shows the forecasted weather data from Climate Forecast System (CFS). It is opened by clicking the 'Forecast' button from the main screen in Figure B 4-1. 119

Figure B 4-15. This screen shows the forecasted stream flows by National Water Model (NWM). The solid line (red) indicates the average of four ensembles while the range shows (green) the maximum and minimum. It is opened by clicking the 'Streams' button from the screen shown in Figure B 4-14. 120
Figure B 4-16. This screen shows the forecasted bottom nitrate-nitrogen as RE02 for 12 future scenarios. It is opened by clicking the 'Reservoir' button from the screen shown in Figure B 4-15. 121
Figure B 4-17. This screen shows the forecasted bottom water temperature as RE02 for 12 future scenarios. It is opened by clicking the 'Temperature' button from the screen shown in Figure B 4-16. 122
Figure B 4-18. This screen shows the forecasted pool elevation of the reservoir. It is opened by clicking the 'Pool' button from the screen shown in Figure B 4-17. 123
Figure B 4-19. This screen shows the process flow for the secondary treatment of UOSA WRF. Observed data from the laboratory are shown as red, field sensors as green, and the optimized results from the IViewOps as blue. It is opened by clicking the 'UOSA WRF' button from the main screen shown in Figure B 4-1. 124

List of Tables

Table 2-1. Input for the CE-QUAL-W2 model 13
Table 3-1. Brief summary of various Functions provided in URUNME 37
Table 4-1. Optimized load distribution 74
Table 4-2. Calibration performance indices 88
Table 5-1. Sizes of different unit operators and unit processes in the plant 159
Table 5-2. Plant flows 161
Table 5-3: Online tanks 162
Table 5-4. Raw influent characteristics 162
Table 5-5. Other influent characteristics 163
Table 5-6. Model calibration results for primary effluent 165
Table 5-7: Dissolved oxygen (DO) setpoints for different zones. 166
Table 5-8: Diffused aeration input parameters 166
Table 5-9. Model calibration results for secondary effluent 167
Table 5-10. Model calibration results for aeration basins 168
Table 5-11. Model calibration results for anaerobic digestion effluent 168
Table 5-12. Chemical dosages 169
Table 5-13. Model calibration results for chemical phosphorus removal process 170
Table 5-14. Simulated sludge production and CO_2 consumption in chemical phosphorus removal process 170
Table 5-15: Design parameters for activated carbon 171
Table 5-16. Model calibration results for final effluent 172

Table A4-1. Summary of CFS variables 101
Table A4-2. Scale factors for each branch and distributed flows 101
Table A4-3. Average monthly WTP withdrawals between 2013-2017 102
Table A 5-1. Existing state variables for SGM and BGM 173
Table A 5-2. New state variables for PCM 173
Table A 5-3. New algebraic variables for PCM 175
Table A 5-4. Model parameters for PCM 175

Table A 5-5. Acidity constants for acids 176
Table A 5-6. Solubility constants for precipitates 176
Table A 5-7. Stability constants for metal complexes 177
Table A 5-8. Algebraic equations for pH calculation 178
Table A 5-9. Process rate equations and stoichiometry for precipitation 179
Table A 5-10. Process rate equations and stoichiometry of oxygen 182
Table A 5-11. Process rate equations and stoichiometry for chlorination 182
Table A 5-12. Process rate equations and stoichiometry of $KMnO_4$ 186
Table A 5-13. Process rate equations and stoichiometry of ClO_2 188
Table A 5-14. Process rate equations and stoichiometry of O_3 190
Table A 5-15. Process rate equations and stoichiometry of H_2O_2 192
Table A 5-16. Process rate equations and stoichiometry of Adsorption 193
Table A 5-17. Process rate equations and stoichiometry of gas transfer 194

Abbreviations and Acronyms

ADM	Anaerobic Digestion Model
ASM	Activated Sludge Model
BGM	Biofilm Growth Model
CE-QUAL-W2	Army Corps of Engineers-Quality-Water 2-Dimensional Model
CFS	Climate Forecast System
CMMS	Computerized Maintenance Management System
COD	Chemical Oxygen Demand
DBP	Disinfection By-Products
DFDI	Data Flow Data Integration
DO	Dissolved Oxygen
DSS	Decision Support System
GEFS	Global Ensemble Forecast System
GIS	Geographical Information System
GUI	Graphical User Interface
HOS	Hypolimnetic Oxygen System
HSPF	Hydrological Simulation Program – Fortran
I/O	Input / Output
IUWM	Integrated Urban Water Management
IWRM	Integrated Water Resource Management
MCRT	Mean Cell Residence Time
MLR	Mixed Liquor Recirculation
NH_3-N	Ammonia / Ammonium Nitrogen
NOAA	National Oceanic and Atmospheric Administration
NOMADS	National Operational Model Achieve and Distribution System
NO_X	Oxidized Nitrogen

NSE	Nash Sutcliffe Efficiency
NWM	National Water Model
OP	Ortho-phosphates
Open-MI	Open Modeling Interface
OWML	Occoquan Watershed Monitoring Laboratory
PBIAS	Percentage bias
PCM	Physicochemical Model
POTW	Publicly Owned Treatment Works
QA/QC	Quality Assurance / Quality Control
RAS	Return Activated Sludge
SCADA	Supervisory Control and Data Acquisition System
SGM	Suspended Growth Model
SKN	Soluble Kjeldahl Nitrogen
SQL	Scripted Query Language
SVI	Sludge Volume Index
TKN	Total Kjeldahl Nitrogen
TN	Total Nitrogen
TP	Total Phosphorus
TSS	Total Suspended Solids
UOSA	Upper Occoquan Service Authority
VSS	Volatile Suspended Solids
WAS	Waste Activated Sludge
WQO	Water Quality Objective
WRF	Water Reclamation Facility
WTP	Water Treatment Plant
WWTP	Wastewater Treatment Plant

Chapter 1 Research Objectives

1.1 Introduction

Integrated solutions and higher-order systems thinking are required to deal with increasingly complex real-world environmental problems (Laniak et al. 2013). Integrated environmental modeling (IEM) provides a comprehensive approach to environmental management by evaluating different components of a system in a holistic manner. Over the years, the interest in IEM and, more specifically, integrated water resource modeling has increased significantly (Kalbacher et al. 2012; Molina et al. 2010). These IEM applications can be used as an effective tool for design, planning, risk assessment, decision-making, and enhancing the transparency and collaboration between stakeholders (Johnston et al. 2011; Peach et al. 2011).

The overarching goal of this research is to develop a futurecasting application based on the integration of various in-house and weather forecast models and historical data sources to simulate the complex interaction of different components of an indirect potable reuse system. The application can provide useful feedback for operators to identify and analyze strategies to manage the plant performance dynamically in response to future reservoir conditions. The following sections provide the motivation and objectives of this study and present the summary of subsequent chapters.

1.2 Study Motivation

1.2.1 A Generic Integrated Environmental Modeling Software

In the past few years, many advancements have been made in integrated environmental modeling (IEM). New component and web-based frameworks have been introduced and the existing ones were improved (Belete et al. 2017; Lloyd et al. 2011; Whelan et al. 2014). While these efforts are vital for addressing the emerging challenges in environmental modeling, they are mostly directed towards advanced applications specific to different science domains (Belete et al. 2017). On the other hand, there is still a need within the modeling community for software programs which focus beyond the various coupling processes and frameworks and specialize in providing advanced pre- and post-processing and runtime capabilities to create a fully automated IEM application.

Even today, many modelers are still hampered by a lack of dedicated tools to handle simple data I/O (Input / Output e.g., reading and writing databases, text files, binary data, etc.) and transformation (e.g. data QA/QC (Quality Assurance / Quality Control), timeseries aggregation, de-aggregation, missing data infilling, joining, unit conversions, etc.). Modelers have to use a number of different software programs for data storage, downloads, analysis, statistics, visualization, etc. In many cases where models are required to run multiple scenarios using different initial and boundary conditions, manual update of input and saving of outputs are required for each run (Belete et al. 2017; Buahin and Horsburgh 2018; Knapen et al. 2013).

Manual operation of integrated models is a tedious process which requires a significant amount of time and effort (Bergez et al. 2013). It is not feasible for applications which are operated on a regular basis and run multiple scenarios. IEM applications based on loose sequentially coupling are less complex and often do not require advanced modeling protocols. However, even such an application requires a large number of different operations to run the integrated models. Specialized software which can provide built-in functionality for such a loose coupling arrangement has not been available in the IEM software domain. Framework-based coupling, on the other hand, also presents similar challenges. Many frameworks lack advanced software support to perform the necessary pre- and post-processing and runtime operations.

There is a need for generic software that can handle both loose and framework based coupling and provide all the necessary “bells and whistles” required for integrated environmental modeling. It should be capable of developing fully automated modeling applications, which can be operated by the click of a button - dynamically creating inputs from different data sources, managing scenarios, running the models, reading outputs, analyzing data, making statistical inferences and ultimately showing results in a visually-aesthetic and interactive way. In essence, it should be able to provide a one-stop solution for fully automated IEM.

1.2.2 Nitrate Regulation in Occoquan Reservoir

The Occoquan Reservoir is located in northern Virginia and is one of the two major water supply sources (the other being the Potomac River) for several municipalities in the region. The Upper Occoquan Service Authority (UOSA) water reclamation facility (WRF) discharges nitrified water into the Bull Run Arm of the reservoir resulting in indirect water reuse of reclaimed water.

Among many operational challenges at UOSA, one is to regulate the nitrate concentration in its reclaimed water, based on the denitrifying capacity of the reservoir. Its operating permit limits the total annual nitrogen load to 6.0×10^5 kg (1.316×10^6 lb). More than 90% of this load is discharged in the form of oxidized nitrogen, mainly as nitrate (NO_3). Although the MCL (Maximum Contaminant Level) for nitrate in drinking water is 10 mg/L as nitrogen, the Occoquan Policy (VSWCB 1971) specifies a Water Quality Objective (WQO) of 5 mg/L at the dam. The WRF is therefore required by permit to reduce its nitrate discharge concentration when the nitrate concentrations at the drinking water intakes rises above 5 mg/L.

During thermal stratification and extremely low hypolimnetic oxygen concentrations in the summer, the supply of nitrate from UOSA actually benefits the reservoir. Under these conditions, microbes in the sediment utilize nitrate as an electron acceptor in the absence of oxygen, advancing the denitrification process. A nitrate discharge optimization study (Bartlett 2013) concluded that the total nitrogen load delivered into the reservoir by the WRF could be more effectively distributed each month based on the reservoir's denitrification capacity. Based on these recommendations, UOSA changed its operational strategy by reducing the degree of denitrification in summer to ensure a higher concentration of nitrate in the effluent and then transitioning back to increased denitrification just before reservoir turnover, generally in early fall. However, last five years of data indicate that the WRF was unable to meet the low nitrate loads recommended by the study during winters mostly due to various operational constraints, including limited organic carbon and low water temperatures which hinder denitrification.

The effect of any change in the discharged load from the WRF on the nitrate concentrations at the dam is based on the hydraulic retention time of the reservoir, which may vary from a few days to months, depending on the inflows. Many factors including the pool elevation, volume and quality (temperature, background nitrate concentration, etc.) of stream inflows, withdrawal by Griffith WTP (Water Treatment Plant), and weather forecast can all affect the future conditions of the reservoir, and consequently its denitrifying capacity. Hence, selecting the desired monthly nitrate concentration for the effluent is still a trial and error process, largely based on the operator's judgment.

The growing water demand caused by urbanization complicates this process further. The safe yield of drinking water from the Occoquan Reservoir, including the reclaimed water, is 3.0×10^6

m^3/d (79 mgd). UOSA's contribution to the inflows has been steadily increasing over the years and, based on the current projections, will exceed 50% of the safe yield after 2025. This would require an effluent nitrate concentration of around 5 mg/L for winters, which is unachievable based on the existing operational capability of the plant. Moreover, WRF plants are always subject to perturbation due to maintenance issues and/or system outages which can temporarily compromise plant performance. UOSA's operation is regulated by the Occoquan Policy which requires increasing the plant's standby capacity and engineered storage to address worst-case scenarios which results in significant financial obligations.

1.2.3 Advanced Physicochemical Modeling

Activated Sludge Models (ASMs) are the most widely applied standardized models (Batstone et al. 2012) and serve as the basis for modeling the suspended growth processes in most of the commercial and noncommercial wastewater treatment plants (WWTP) simulators. The main purpose of these models is to simulate biochemical processes for conventional WWTP. However, treatment processes in WRFs are generally much more complicated and employ a large number of physicochemical processes including acid/base reactions, adsorption, spontaneous or chemical precipitation, redox, gas transfer, etc. Although there is a large amount of information available on the fundamentals of these processes, their use in wastewater process modeling in still limited, either due to the complexity or its diverse sources (originating from many different water and process environments) (Batstone 2009; Batstone et al. 2012). ASMs include some physicochemical processes, but those are either very basic or empirical in nature. Some published and commercially available models have been able to overcome a few of these limitations for specific applications. Fairlamb et al. (2003), Serralta et al. (2004), and Sötemann et al. (2005) have used acid/base reactions and gas transfer for explicitly calculating pH in reactors. De Haas et al. (2001), Martin (2005), Mbamba et al. (2015), and Rittmann et al. (2002) have discussed modeling techniques for chemical precipitation using somewhat similar underlying methodology. However, other processes including adsorption, oxidation, thermal hydrolysis, etc. have not been widely adopted by the different models.

1.3 Study Objectives

1.3.1 URUNME 'You Run Models Easily'

This first study presents the development of URUNME 'You Run Models Easily', a generic software product that provides out-of-the-box functionality for integrated modeling. It explains the software architecture, its features and capabilities, and discusses some real-world examples to demonstrate its applicability in environmental systems modeling.

1.3.2 Occoquan Decision Support System

The second study presents a futurecasting application based on the integration of various in-house and weather forecast models and historical data sources. It discusses the development and implementation of the integrated model and demonstrates its effectiveness as a decision support system (DSS) to improve the operation of the IPR system.

1.3.3 IViewOps4 Physicochemical Model

The third study discusses the development and implementation of a new physicochemical model for version 4.0 of IViewOps. It presents the setup and the calibration for the UOSA-WRF in the model. In addition, it explains the new architecture of IViewOps4 which decouples the mathematical model from the rest of the software and allow users complete access to the model's code.

1.4 Document Organization

The remainder of this document is organized as follows:

Chapter 2 provides the background information regarding the Occoquan watershed, the water reservoir, climate forecast system, national water model, and discusses the reservoir and process models used in this study.

Chapter 3 is a research paper regarding the development of URUNME.

Chapter 4 is research paper about the Occoquan decision support system.

Chapter 5 is research paper regarding the new physicochemical model for IViewOps

Chapter 6 contains the summary of the research and the key conclusions.

1.5 References

Bartlett, J. A. (2013). "Heuristic Optimization of Water Reclamation Facility Nitrate Loads for Enhanced Reservoir Water Quality." Doctor of Philosophy In Civil Engineering, Virginia Polytechnic Institute and State University.

Batstone, D. (2009). "Towards a generalised physicochemical modelling framework." *Reviews in Environmental Science and Bio/Technology*, 8(2), 113-114.

Batstone, D. J., Amerlinck, Y., Ekama, G., Goel, R., Grau, P., Johnson, B., Kaya, I., Steyer, J.-P., Tait, S., and Takács, I. (2012). "Towards a generalized physicochemical framework." *Water Science and Technology*, 66(6), 1147-1161.

Belete, G. F., Voinov, A., and Laniak, G. F. (2017). "An overview of the model integration process: From pre-integration assessment to testing." *Environmental Modelling & Software*, 87, 49-63.

Bergez, J.-E., Chabrier, P., Gary, C., Jeuffroy, M. H., Makowski, D., Quesnel, G., Ramat, E., Raynal, H., Rousse, N., and Wallach, D. (2013). "An open platform to build, evaluate and simulate integrated models of farming and agro-ecosystems." *Environmental Modelling & Software*, 39, 39-49.

Buahin, C. A., and Horsburgh, J. S. (2018). "Advancing the Open Modeling Interface (OpenMI) for integrated water resources modeling." *Environmental Modelling & Software*, 108, 133-153.

De Haas, D., Wentzel, M., and Ekama, G. (2001). "The use of simultaneous chemical precipitation in modified activated sludge systems exhibiting biological excess phosphate removal: Part 6: Modelling of simultaneous chemical-biological P removal-review of existing models." *WaterSA*, 27(2), 135-150.

Fairlamb, M., Jones, R., Takács, I., and Bye, C. (2003). "Formulation of a general model for simulation of pH in wastewater treatment processes." *Proceedings of the Water Environment Federation*, 2003(7), 511-528.

Henze, M., Gujer, W., Mino, T., and Loosdrecht, M. (2000). *Activated sludge models ASM1, ASM2, ASM2d and ASM3*, IWA Pub., London.

Johnston, J. M., McGarvey, D. J., Barber, M. C., Laniak, G., Babendreier, J., Parmar, R., Wolfe, K., Kraemer, S. R., Cyterski, M., and Knightes, C. (2011). "An integrated modeling framework for performing environmental assessments: Application to ecosystem services

in the Albemarle-Pamlico basins (NC and VA, USA)." *Ecological Modelling*, 222(14), 2471-2484.

Kalbacher, T., Delfs, J.-O., Shao, H., Wang, W., Walther, M., Samaniego, L., Schneider, C., Kumar, R., Musolff, A., and Centler, F. (2012). "The IWAS-ToolBox: software coupling for an integrated water resources management." *Environmental Earth Sciences*, 65(5), 1367-1380.

Knapen, R., Janssen, S., Roosenschoon, O., Verweij, P., De Winter, W., Uiterwijk, M., and Wien, J.-E. (2013). "Evaluating OpenMI as a model integration platform across disciplines." *Environmental Modelling & Software*, 39, 274-282.

Laniak, G. F., Olchin, G., Goodall, J., Voinov, A., Hill, M., Glynn, P., Whelan, G., Geller, G., Quinn, N., and Blind, M. (2013). "Integrated environmental modeling: a vision and roadmap for the future." *Environmental Modelling & Software*, 39, 3-23.

Lloyd, W., David, O., Ascough II, J. C., Rojas, K. W., Carlson, J. R., Leavesley, G. H., Krause, P., Green, T. R., and Ahuja, L. R. (2011). "Environmental modeling framework invasiveness: Analysis and implications." *Environmental Modelling & Software*, 26(10), 1240-1250.

Martin, S. T. (2005). "Precipitation and dissolution of iron and manganese oxides." *Environmental Catalysis*, 61-81.

Mbamba, C. K., Batstone, D. J., Flores-Alsina, X., and Tait, S. (2015). "A generalised chemical precipitation modelling approach in wastewater treatment applied to calcite." *Water Research*, 68, 342-353.

Molina, J., Bromley, J., García-Aróstegui, J., Sullivan, C., and Benavente, J. (2010). "Integrated water resources management of overexploited hydrogeological systems using Object-Oriented Bayesian Networks." *Environmental Modelling & Software*, 25(4), 383-397.

Peach, D., Hughes, A., Kessler, H., Mathers, S., and Giles, J. (2011). "Integrated environmental modeling: the new DREAM for Geological Surveys."*Archaean to Anthropocene: GSA Annual Meeting and Exposition, Minnesota, USA, 9-12 Oct 2011*. 1-4.

Rittmann, B. E., Banaszak, J. E., VanBriesen, J. M., and Reed, D. T. (2002). "Mathematical modeling of precipitationand dissolution reactions in microbiological systems." *Biodegradation*, 13(4), 239-250.

Serralta, J., Ferrer, J., Borrás, L., and Seco, A. (2004). "An extension of ASM2d including pH calculation." *Water Research*, 38(19), 4029-4038.

Sötemann, S., Musvoto, E., Wentzel, M., and Ekama, G. (2005). "Integrated biological, chemical and physical processes kinetic modelling Part 1–Anoxic-aerobic C and N removal in the activated sludge system." *WaterSA*, 31(4), 529-544.

VSWCB (1971). "A Policy for Waste Treatment and Water Quality Management in the Occoquan Watershed, §9VAC25-410-10." Virginia State Water Control Board, Richmond, Virginia.

Whelan, G., Kim, K., Pelton, M. A., Castleton, K. J., Laniak, G. F., Wolfe, K., Parmar, R., Babendreier, J., and Galvin, M. (2014). "Design of a component-based integrated environmental modeling framework." *Environmental Modelling & Software*, 55, 1-24.

Chapter 2 Background Information

2.1 Occoquan Watershed

The Occoquan Reservoir is located in Northern Virginia and is one of two major water supply sources (the other being the Potomac River) for Fairfax County. The reservoir spreads over an area of 6.9 km^2 with its drainage basin, the Occoquan watershed (Figure 2-1), spanning 1,484 km^2 (573 square miles). The reservoir has a full pool volume of 3.1 x 10^7 m^3, an average water depth of 5.1 m and a maximum depth of approximately 19 m close to the dam. The reservoir's mean hydraulic residence time is approximately 20 days (Xu et al. 2007).

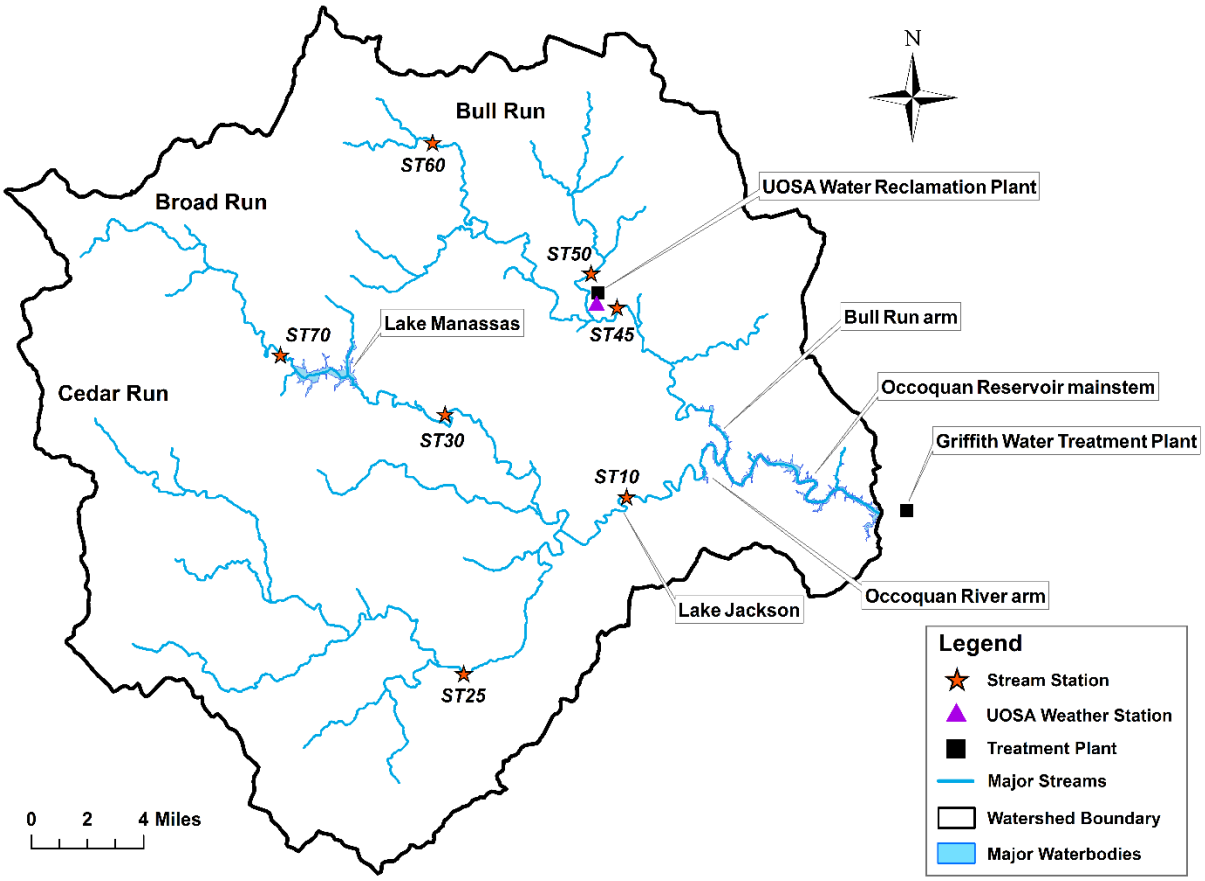

Figure 2-1. Occoquan Watershed

The mainstream of the Occoquan Reservoir is formed by the confluence of the Occoquan River and Bull Run tributaries, 14 km upstream of the Occoquan dam. The headwaters of the reservoir extend well up into these two arms of the reservoir which are called the Occoquan River Arm and the Bull Run Arm, respectively. The Occoquan Reservoir can be classified as a warm

monomictic lake, which undergoes thermal stratification once a year, which is common to North American coastal regions (Wetzel 1983). During summer, the density difference between the epilimnion and hypolimnion waters prevents the Reservoir from mixing, resulting in a thermal gradient. Sometime during early fall, the surface water cools to a temperature equal to the bottom water, causing the lake to mix or overturn.

2.2 Upper Occoquan Service Authority

During the 1960s, eleven small municipal wastewater treatment plants (referred to as Publicly-Owned Treatment Works - POTW) were discharging their effluent in the Occoquan Reservoir. Poor quality of treated water from these POTWs contributed to high pollutant loads in the reservoir. Consequently, the water quality in the reservoir was reduced to undesirable levels with severe eutrophic conditions and algal blooms. To mitigate the situation, the Virginia State Water Control Board (VSWCB) commissioned a study by Metcalf & Eddy Inc., to identify the primary cause of the problem and offer recommendations. Based on this study, the VSWCB enacted a policy in 1971 to manage the wastewater treatment facilities and water quality within the Occoquan Watershed. This policy is known as "A Policy for Waste Treatment and Water Quality Management in the Occoquan Watershed", commonly called as the "Occoquan Policy". A new entity known as the Upper Occoquan Service Authority (UOSA) was created under this policy to provide advanced wastewater treatment for the entire watershed. Later in 1978, UOSA commissioned a new Water Reclamation Facility (WRF) to replace the outdated POTWs.

Fairfax Water's Griffith water treatment plant (WTP) withdraws water from the tail end of the reservoir close to the dam, resulting in indirect potable reuse of the reclaimed water. The WRF discharges into the Bull Run Arm upstream of the reservoir (Figure 2-1). The total design capacity of the plant is 204,412 m^3/d (54 mgd) and it is currently operating at an average of 121,133 m^3/d (32 mgd). Over the years, UOSA's contribution to the inflows of the reservoir has steadily increased. It routinely goes up to 50% of the total inflow during the late summers and early fall (Cubas Suazo 2012) and, in some cases, up to 80% (Van Den Bos 2003), becoming a significant portion of the safe yield of the reservoir.

Among the operational challenges at UOSA is the regulation of the nitrate concentration in reclaimed water throughout the year, based on the denitrifying capacity of the reservoir. During the thermal stratification and extremely low hypolimnetic oxygen concentrations in summer, the

supply of nitrates from UOSA benefits the reservoir (Bartlett 2013). Under extremely low oxygen concentrations, microbes in the sediment utilize these nitrates as electron acceptors, which inhibits the release of phosphorus (P) and other less preferential electron acceptors, Mn^{2+} and Fe^{2+}, into the water column (Banchuen 2002; Cubas Suazo 2012). UOSA, therefore, stops denitrification in summer to ensure a high concentration of nitrates in the effluent. The reservoir overturns at the beginning of fall and remains well-mixed throughout the winter and early spring. The mixing redistributes oxygen across the entire water column and restores the aerobic conditions in the hypolimnion. Given that oxygen is a preferred terminal electron acceptor compared to nitrates, the reservoir loses its denitrification capacity and the WRF switches back to the denitrification process.

2.3 Occoquan Watershed Monitoring

Under the Occoquan Policy, the Occoquan Watershed Monitoring Laboratory (OWML) was established in 1972 by the Department of Civil Engineering of Virginia Polytechnic Institute. OWML was mandated to monitor the Occoquan Reservoir water quality. Over the years, OWML has established monitoring stations throughout the watershed to measure the flow and water quality in different streams. Flows are calculated at each station using a pressure transducer to measure water depth and a predetermined stage-discharge rating curve. At some stations, acoustic velocity/flow meters are also used for direct flow measurement. In all cases, flow is recorded using data loggers and is transmitted to OWML on an hourly basis. To monitor the water quality, grab samples are taken from each station at different frequencies ranging from once a month to four times a month. However, during storm events, flow-weighted composite samples are collected using autosamplers to evaluate the event-mean concentration of different constituents (Kumar et al. 2013). In addition, grab samples are collected from seven different locations at the Occoquan Reservoir for quality monitoring. These samples are collected at different frequencies ranging from once a month to three times a month at different water depths, usually in 5ft intervals.

2.4 Occoquan Reservoir Model

The Occoquan reservoir is simulated using the U.S. Army Corps of Engineers software CE-QUAL-W2, a two-dimensional longitudinal/vertical hydrodynamic and water quantity model (Cole and Wells 2011). It simulates the water quality in a waterbody, using longitudinal

segments and vertical layers while assuming complete lateral mixing. The Occoquan Reservoir is modeled using 4 branches and 69 longitudinal segments in CE-QUAL-W2. Branch-1 is the mainstream of the reservoir, starting from Occoquan River close to Lake Jackson and extends all the way up to the dam. Branch-2 is the Bull Run Arm, discharging Bull Run watershed and UOSA-WRF to the mainstream of the reservoir. Branch-3 and Branch-4 are Sandy and Hooes Run, respectively, which are small tributaries. All the major input parameters required for the CE-QUAL-W2 model run are shown in Figure 2-2

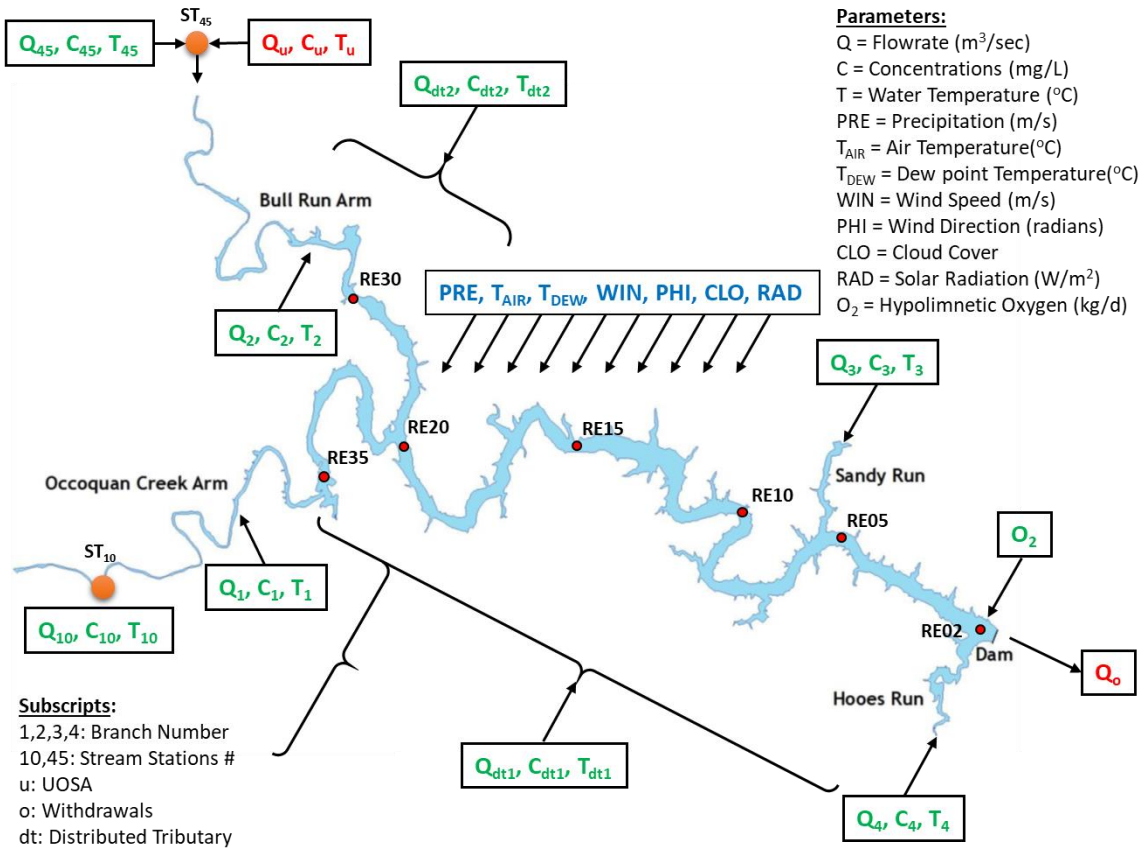

Figure 2-2. CE-QUAL-W2 Model Inputs for Occoquan Reservoir

Time series for these parameters are entered in various fixed-width text files using Julian days (Table 2-1). Each branch in the model requires separate input for flows (m^3/s), constituent concentrations (TSS, OP, NH_3-N, NO_X-N and DO) (mg/L), and water temperature (°C). Additional precipitation data are required for each branch including rainfall intensity (m/s), constituent concentrations (mg/L), and temperature (°C). To simulate the inflows entering the

reservoir around its periphery, distributed flows are added for Branch-1 & 2 only. Branch-3 & 4 are neglected due to small size and flow. At the start of each model run, initial water level and constituent concentration are also required. met.npt text file is used to input the meteorological variables for the entire waterbody including air temperature (^oC), dew point temperature (^oC), wind speed (m/s), wind direction (rad), cloud cover, and radiation (W/m^2).

Table 2-1. Input for the CE-QUAL-W2 model

#	**Parameters**	**File**	**Unit**
1	Branch inflows	qin_brX.prn	m^3/s
2	Branch inflow concentrations	cin_brX.prn	mg/L
3	Branch inflow water temperature	tin_brX.prn	^oC
4	Branch precipitation intensity	pre_brX.prn	m/s
5	Branch precipitation concentrations	cpr_brX.prn	mg/L
6	Branch precipitation temperature	tpr_brX.prn	^oC
7	Distributed inflows	qdt_brX.prn	m^3/s
8	Distributed inflow concentrations	cdt_brX.prn	mg/L
9	Distributed inflow water temperature	tdt_brX.prn	^oC
11	Initial water elevation	bth.npt	m
12	Initial nitrate concentration in each segment and layer	lpr_1.npt	mg/L
13	Meteorological input	met.npt	various

Note: X in filenames denotes the branch number

2.5 IViewOps

IViewOps "Intelligent View of Operations" is an intelligent biochemical process simulator. The software is written in C#.NET and implemented at several BNR and ENR plants (Lodhi et al. 2011; Sen et al. 2012). The model expands from several biochemical models including IWA ASM2d Model (Henze et al. 2000), IWA Anaerobic Digestion Model ADM1 (Batstone et al. 2002), and the Semi-Empirical Biofilm Model (Sen and Randall 2008). It is an asset-based model with an integrated asset management system based on the International Infrastructure Management Manual (National Asset Management Steering Group 2015). Scenario manager in IViewOps can run multiple configurations of the plant using either steadystate or time dynamic simulation.

IViewOps is a multi-layer model that analyzes the plant on three levels: (1) biochemical process modeling (2) assets, their condition and capacity, (3) hydraulic configuration and bottlenecks in each possible operating configuration (Sen et al. 2015). It can be directly linked to a plant's information system to acquire the current operating data on a periodic basis. On the process side, IViewOps imports data from the supervisory control and data acquisition system (SCADA) and laboratory information management system (LIMS) to keep track of the current mixed liquor suspended solids (MLSS), temperature, dissolved oxygen (DO), return activated sludge (RAS) flow, waste activated sludge (WAS) flow, mixed liquor recirculation (MLR) flow, sludge volume index (SVI), etc. On the asset side, the online (ON or OFF) status is obtained from the SCADA. On the other hand, the asset availability (in service or taken out for maintenance) and actual de-rated capacity (based on physical condition and years of service) are imported from the computerized maintenance management system (CMMS).

2.6 Climate Forecast System

NOAA (National Oceanic and Atmospheric Administration) climate forecast system or coupled (atmosphere-ocean-land) forecast system (CFS) is a climate model which provides medium to long range numerical weather prediction and is run by NCEP (National Center for Environmental Prediction). Operational since August 2004, this model has demonstrated a skill level in forecasting precipitation and surface temperature that is comparable to the skill of the statistical methods used by NCEP (Saha et al. 2006). The second version of the model (CFSv2) was launched in March 2011 with some major improvements. The atmospheric component of the model has a horizontal spectral triangular truncation of 126 waves (T126), equivalent to ~100 km grid resolution and 64 sigma-pressure hybrid vertical resolution. The real-time operational forecast consists of 16 CFSv2 runs every day. The long range (~9 months) hourly forecast consists of four cycles per day at 0000, 0600, 1200 and 1800 UTC out to 9 months (Saha et al. 2014). Reforecast data are generated running the same model retrospectively using historical data. It can then be used for the training of calibration methods by comparing it with observed data from the same time period. CSFv2 reforecast data are created for 29 years (1982-2010), for every 5th day from January 1 out to 9 months on the same horizontal and vertical resolution as the operational configuration. The total number of 9-month forecasts is 73 x 4 for each year.

2.7 National Water Model

National Water Model (NWM) is a hydrological model that forecasts stream flows across the continental United States and has been operational since Aug. 16, 2016, on the NOAA Weather and Climate Operational Supercomputing System (WCOSS). A long-range 16-member ensemble forecast is produced every day going out to 30 days in the future. There are 4 ensemble members in each cycle, each forced with a downscaled and biased corrected CFS model. The core component of NWM is the Weather Research and Forecasting Hydrologic model (WRF-Hydro) by the National Center for Atmospheric Research (NCAR). WRF-Hydro is both a stand-alone hydrological model as well as a framework for coupling hydrological models with atmospheric models. WRF-Hydro is configured to use Noah-MP Land Surface Model (LSM) to simulate land surface processes in NWM (Niu et al. 2011; Yang et al. 2011).

2.8 References

Banchuen, T. (2002). "A Microcosm-Based Investigation into Oxidized Nitrogen Removal in the Hypolimnetic Waters of the Occoquan Reservoir of Northern Virginia.", MS Thesis, Virginia Polytechnic Institute and State University.

Bartlett, J. A. (2013). "Heuristic Optimization of Water Reclamation Facility Nitrate Loads for Enhanced Reservoir Water Quality.", PhD Dissertation, Virginia Polytechnic Institute and State University.

Batstone, D. J., Keller, J., Angelidaki, I., Kalyuzhnyi, S., Pavlostathis, S., Rozzi, A., Sanders, W., Siegrist, H., and Vavilin, V. (2002). "The IWA anaerobic digestion model no 1 (ADM1)." *Water Science and Technology*, 45(10), 65-73.

Cole, T. M., and Wells, S. A. (2011). "CE-QUAL-W2: A Two-Dimensional, Laterally Averaged, Hydrodynamic and Water Quality Model, Version 3.71." *U.S. Army Corps of Engineers, Washington, D.C.*

Cubas Suazo, F. J. (2012). "An investigation into the effects of an external electron acceptor on nutrient cycling at the sediment-water interface of the Occoquan Reservoir.", PhD Dissertation, Virginia Polytechnic Institute and State University.

Group, N. A. M. S. (2015). *International infrastructure management manual*, Johnsonville, Wellington.

Hamill, T. M., Bates, G. T., Whitaker, J. S., Murray, D. R., Fiorino, M., Galarneau Jr, T. J., Zhu, Y., and Lapenta, W. (2013). "NOAA's second-generation global medium-range ensemble reforecast dataset." *Bulletin of the American Meteorological Society*, 94(10), 1553-1565.

Henze, M., Gujer, W., Mino, T., and Loosdrecht, M. (2000). *Activated sludge models ASM1, ASM2, ASM2d and ASM3*, IWA Pub., London.

Kumar, S., Godrej, A. N., and Grizzard, T. J. (2013). "Watershed size effects on applicability of regression-based methods for fluvial loads estimation." *Water Resources Research*, 49(11), 7698-7710.

Lodhi, A., Sen, D., Rawlings, J., Kundamal, J., Abbott, D., Wahibi, O., Mende, U., and Gold, L. (2011). "Simultaneous Optimization of Plants for Nitrogen and Phosphorus Removal, Reuse, Energy and Emissions through a Real Time Operations Controller in Middle-East-Asia and Chesapeake Bay Region of US." *Proceedings of the Water Environment Federation*, 2011(14), 3069-3092.

Niu, G. Y., Yang, Z. L., Mitchell, K. E., Chen, F., Ek, M. B., Barlage, M., Kumar, A., Manning, K., Niyogi, D., and Rosero, E. (2011). "The community Noah land surface model with multiparameterization options (Noah-MP): 1. Model description and evaluation with local-scale measurements." *Journal of Geophysical Research: Atmospheres*, 116(D12).

Saha, S., Moorthi, S., Wu, X., Wang, J., Nadiga, S., Tripp, P., Behringer, D., Hou, Y.-T., Chuang, H.-y., and Iredell, M. (2014). "The NCEP climate forecast system version 2." *Journal of Climate*, 27(6), 2185-2208.

Saha, S., Nadiga, S., Thiaw, C., Wang, J., Wang, W., Zhang, Q., Van den Dool, H., Pan, H.-L., Moorthi, S., and Behringer, D. (2006). "The NCEP climate forecast system." *Journal of Climate*, 19(15), 3483-3517.

Sen, D., Lodhi, A., Brooks, M., Angelotti, R., and Godrej, A. (2015). "Integration of Asset Management with Real Time Simulation to Improve Reliability, Preventive and Corrective Maintenance and Reduce Life Cycle Cost in Wastewater Treatment for Reuse." *Proceedings of the Water Environment Federation*, 2015(10), 5152-5178.

Sen, D., Lodhi, A., Gold, L., Abbott, D., Rawligns, J., Mellendick, M., Sedlack, D., Copithorn, R., Pehrson, R., and McCall, C. (2012). "Implementing an Intelligent Operations and Asset Management System that Integrates DCS, SCADA, CMMS and Process Models for Activated Sludge, IFAS and Biofilms to Improve Compliance and Optimize ENR

Plants in Real Time." *Proceedings of the Water Environment Federation*, 2012(15), 1468-1487.

Sen, D., and Randall, C. W. (2008). "Improved computational model (AQUIFAS) for activated sludge, integrated fixed-film activated sludge, and moving-bed biofilm reactor systems, Part I: Semi-empirical model development." *Water environment research*, 80(5), 439-453.

Shah, R., and Mishra, V. (2014). "Evaluation of the reanalysis products for the monsoon season droughts in India." *Journal of Hydrometeorology*, 15(4), 1575-1591.

Shah, R., Sahai, A. K., and Mishra, V. (2017). "Short to sub-seasonal hydrologic forecast to manage water and agricultural resources in India." *Hydrology and Earth System Sciences*, 21(2), 707.

Shah, R. D., and Mishra, V. (2015). "Development of an experimental near-real-time drought monitor for India." *Journal of Hydrometeorology*, 16(1), 327-345.

Shah, R. D., and Mishra, V. (2016). "Utility of Global Ensemble Forecast System (GEFS) Reforecast for Medium-Range Drought Prediction in India." *Journal of Hydrometeorology*, 17(6), 1781-1800.

Tian, D., Martinez, C. J., and Asefa, T. (2016). "Improving Short-Term Urban Water Demand Forecasts with Reforecast Analog Ensembles." *Journal of Water Resources Planning and Management*, 142(6), 04016008.

Van Den Bos, A. C. (2003). "A water quality assessment of the Occoquan Reservoir and its tributary watershed: 1973-2002.", MS Thesis, Virginia Polytechnic Institute and State University.

Wetzel, R. G. (1983). *Limnology*, Saunders, Philadelphia.

Xu, Z., Godrej, A. N., and Grizzard, T. J. (2007). "The hydrological calibration and validation of a complexly-linked watershed–reservoir model for the Occoquan watershed, Virginia." *Journal of Hydrology*, 345(3), 167-183.

Yang, Z. L., Niu, G. Y., Mitchell, K. E., Chen, F., Ek, M. B., Barlage, M., Longuevergne, L., Manning, K., Niyogi, D., and Tewari, M. (2011). "The community Noah land surface model with multiparameterization options (Noah-MP): 2. Evaluation over global river basins." *Journal of Geophysical Research: Atmospheres*, 116(D12).

Chapter 3 URUNME: A Generic Software for Integrated Environmental Modeling

Adnan G. Lodhi[1*], Adil N. Godrej[1], Dipankar Sen[1,2], Ayden A. Baran[1]

[1] Occoquan Watershed Monitoring Laboratory. Virginia Tech. 9408 Prince William Street, Manassas, Virginia, 20110

[2] Santa Clara Valley Water District, San Jose, California 95118

[*] Corresponding Author. Email: adlodhi@vt.edu

Keywords: Integrated modeling; model coupling; decision support system; data analysis; data visualization; scenario management

3.1 Abstract

A new software application, called URUNME, was developed in C#.NET for integrated environmental modeling. URUNME provides out-of-the-box functionality for model coupling, data storage, analysis, visualization, scenario management, and decision support systems. The software features a user-friendly graphical user interface based on drag-and-drop and flowchart type diagrams for easy configuration of modeling projects. Visual functions are provided to automate various pre- and post-processing tasks including reading and writing different databases and file formats, web uploads and downloads, data analysis, timeseries transformation, file management, etc. Data is stored in the embedded SQLite database and is represented as visual variables. Interactive dashboards can be created using multiple screens and visual elements. The built-in scenario management feature provides the capability of running multiple scenarios of a model using different inputs. This paper presents URUNME's architecture and describes how it can be utilized for creating fully automated integrated modeling applications.

3.2 Introduction

Integrated solutions and higher-order systems thinking are required to deal with increasingly complex real-world environmental problems (Laniak et al., 2013). Integrated environmental modeling (IEM) provides a comprehensive approach to environmental management by evaluating different components of a system in a holistic manner. According to Johnston (2010) "Integrated modeling encompasses a broad range of approaches and configurations of models, data and assessment methods to describe and analyze complex environmental problems, often in a multi-media and multi-disciplinary manner." Over the years, the interest in IEM and, more specifically, integrated water resource modeling has increased significantly (Kalbacher et al., 2012; Molina et al., 2010). These IEM applications can be used as an effective tool for design,

planning, risk assessment, decision-making, and enhancing the transparency and collaboration between stakeholders (Johnston et al., 2011; Peach et al., 2011).

Knapen et al. (2013) noted five approaches for the model integration: (1) soft linking, (2) scripts, (3) proprietary one large monolithic model, (4) proprietary loosely link models and (5) standard modeling framework. However, the integrated modeling applications can be broadly categorized into (1) Built-In Integrated Models and (2) Coupled Integrated Models.

3.2.1 Built-In Integrated Models

The first category provides built-in integration to simulate a complex environmental system. In this method, the model integration is generally achieved by using two different approaches: (1) Models for the different sub-systems are contained within a single software (2) Various models developed by the same organization can coupled to each other based on some proprietary linking mechanism. One example of approach-1 is a software called WEAP (Water Evaluation And Planning) which was developed by the Stockholm Environment Institute's US Center (SEI-US) to assist policymakers in evaluating water supply policies and suitable water resources plans (Yates et al., 2005).

3.2.2 Coupled Integrated Models

Coupled applications, on the other hand, are based on linking different standalone models to simulate various components of a targeted environmental system. These models are linked together based on two different approaches: (1) Loose coupling (2) Framework based coupling

3.2.2.1 Loose Coupling

Loose or soft coupling is a sequential approach where data flow paths are unidirectional and configured in a tree-like cascade structure (Rauch et al., 2002). The individual models are linked together such that the output of one model is used as an input to the other. The models used in such applications are mostly open source or at least provide readable input and output in a standard data format (Malard et al., 2017; Xu et al., 2007).

3.2.2.2 Framework Based Coupling

In contrast, tight coupling generally involves linking different standalone models using standardized data transfer protocols based on some commonly accepted standard framework.

Common frameworks used in environmental modeling are generally categorized into either (1) Component-based modeling and (2) Service-Oriented Architecture (SOA)-based modeling (Belete et al., 2017). In component-based modeling, each model is run as an independent component and data exchange between different models at the runtime is achieved using a standard interface (Goodall and Peckham, 2016). Over the past years, a number of component-based frameworks and interface standards have been formulated and applied in various domains including water resources (Buahin and Horsburgh, 2018). For instance, Earth Systems Modeling Framework (ESMF) was developed with the focus on weather, climate, and related Earth science applications (Hill et al., 2004). The Community Surface Dynamics Modeling System (CSDMS) is another example of component-based framework which was developed with the goal of modeling Earth's surface processes and dynamics (Peckham et al., 2013). Another such framework is Object Modeling System (OMS) with currently more than 200 model components that mostly focuses on agro-environmental models (David et al., 2013). In the water resources domain, a more well-known component-based framework is Open Modeling Interface (OpenMI) (Moore and Tindall, 2005). On the other hand, in SOA-based frameworks, models are turned into web services and linked using standard text-based protocols creating plug-and-play autonomous components. Python Network Simulation (Pynsim) Framework is an example of applying such framework (Knox et al., 2018). Other examples of SOA based frameworks include WEEZARD for geoanalysis which is a web service for debris-flow hazard assessment and visualization (Zhang et al., 2018), and EMELI-Web that applies a Basic Model Interface (BMI) for modeling a set of spatially distributed hydrologic models (Jiang et al., 2017).

3.2.3 Need for a Generic IEM Software

In the past few years, many advancements in IEM are made- new component and web-based frameworks have been introduced and the existing ones were improved (Belete et al., 2017; Lloyd et al., 2011; Whelan et al., 2014). While these efforts are vital for addressing the emerging challenges in environmental modeling, they are mostly directed towards advanced applications specific to different science domains (Belete et al., 2017). On the other hand, there is still a need within the modeling community for software programs which focus beyond the various coupling processes and frameworks and specialize in providing advanced pre- and post-processing and runtime capabilities to create a fully automated IEM application.

Even today, many modelers are still hampered by a lack of dedicated tools to handle simple data I/O (e.g., reading and writing databases, text files, binary data, etc.) and transformation (e.g. data QA/QC, timeseries aggregation, deaggregation, missing data infilling, joining, unit conversions, etc.). Additionally, modelers have to use a number of different software programs for data storage, downloads, analysis, statistics, visualization, etc. In many cases where models are required to run multiple scenarios using different initial and boundary conditions, manual update of input and saving of outputs are required for each run (Belete et al., 2017; Buahin and Horsburgh, 2018; Knapen et al., 2013).

Performing all these tasks manually is a tedious process which requires a significant amount of time and effort (Bergez et al., 2013). It is not feasible for models which are operated on a regular basis and run multiple scenarios. For instance, there has been a lot of interest recently in developing decision support systems based on integrated modeling of natural and engineered environmental systems (e.g., watershed, reservoir, treatment plants, etc.) (Lodhi et al., 2018). Most of these applications require constant updates of input data obtained from different dynamic sources (e.g., flow measuring stations, weather stations, weather forecasting models, water quality monitoring labs, online probes, etc.) to run the models on a periodic basis. Although, coding/scripting can be used to automate these tasks, it requires a considerable level of programming skills and in-depth knowledge of different model structure and data formats (Buahin and Horsburgh, 2018).

IEM applications based on loose sequentially coupling are less complex and often do not require advanced modeling protocols. However, even such an application requires a large number of different operations to run the integrated models. A specialized software which can provide built-in functionality for such a loose coupling arrangement has not been available in the IEM software domain. Framework based coupling, on the other hand, also presents similar challenges. Many frameworks lack advanced software support to perform the necessary pre- and post-processing and runtime operations. For instance, most of the software programs developed to run OpenMI compliant models lack the feature-set for creating a fully automated modeling application. In addition, these software programs do not provide any data I/O capabilities for exchanging inputs and outputs from the model components at the runtime.

There is a need for a generic software that can handle both loose and framework based coupling and provide all the necessary bells and whistles required for integrated environmental modeling. It should be capable of developing fully automated modeling applications, which can be operated by a click of a button - dynamically creating inputs from different data sources, managing scenarios, running the models, reading outputs, analyzing data, making statistical inferences and ultimately showing results in a visually-aesthetic and interactive way. In essence, it should be able to provide a one-stop solution for fully automated IEM. In the author's opinion, such software should include but not limited to the following features:

- Easy-to-use graphical user interface.
- Multiple views for creating dashboard type applications.
- Simple flowchart type diagrams to create modeling configurations.
- Advanced data visualization.
- Reading and writing different data formats.
- Embedded database for data storage and querying.
- Advanced data analysis and transformation.
- Advanced statistical modeling.
- Download data from different web servers.
- Run multiple scenarios of the model.
- Represent data using visual vector and scalar variables.
- Allow multi-thread execution of different processes.
- Support for multi-user advanced decision support systems.
- Scheduling capabilities for performing periodic automatic runs

This paper presents URUNME 'You Run Models Easily', a generic software that provides out-of-the-box functionality for integrated modeling. The paper will explain the software architecture, its features and capabilities, and will discuss some real-world examples to demonstrate its applicability in environmental systems modeling.

3.3 Software Architecture

URUNME is programmed in C# using .NET framework. It is developed using a three tiered architecture arranged by presentation, business, and data (Figure 3-1). The user interface (UI) is developed using various third-party libraries, which provides a comprehensive suite of various visual components. Several helper classes are written to wrap the third-party controls for added functionality, which is otherwise not available out-of-the-box.

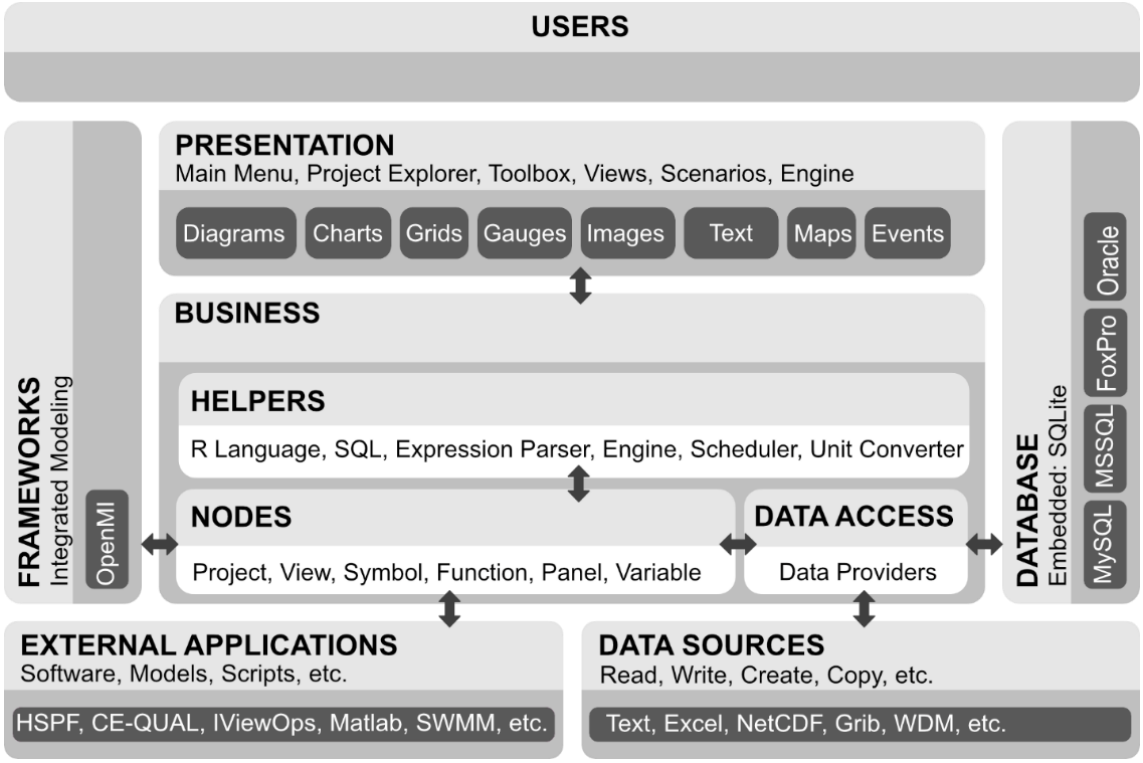

Figure 3-1. High level architecture of URUNME

The business side of the software is programmed as a standalone dynamic link library (DLL), which is accessed by the presentation layer using a strict one-way association. No commercial component is used to develop this DLL, allowing for the option of making it open-sourced in the future, if desired. The business tier is further decomposed into multiple layers, each responsible for implementing different aspects of the logic. The core layer of the business tier is called ‘Nodes’, which contains all the classes that are visually exposed to the users in a project. The remaining classes are contained in the ‘Helper’ layer, which provides various support functions. Classes in data access layer are essentially wrappers on .NET data providers to access different types of databases including SQLite, MySQL, SQL Server,Oracle, etc. In addition, the data

access layer also contains custom classes to read and write different file formats, such as text (comma, space, tab, or custom delimiter and fixed width), Excel, netCDF, Grib2, WDM, etc.

3.3.1 User Interface

The default UI consists of a ribbon type main menu on the top, a project-explorer and toolbox on the left, engine and scheduler windows on the bottom, and a workspace in the remaining area containing scenarios and views (Figure 3-2).

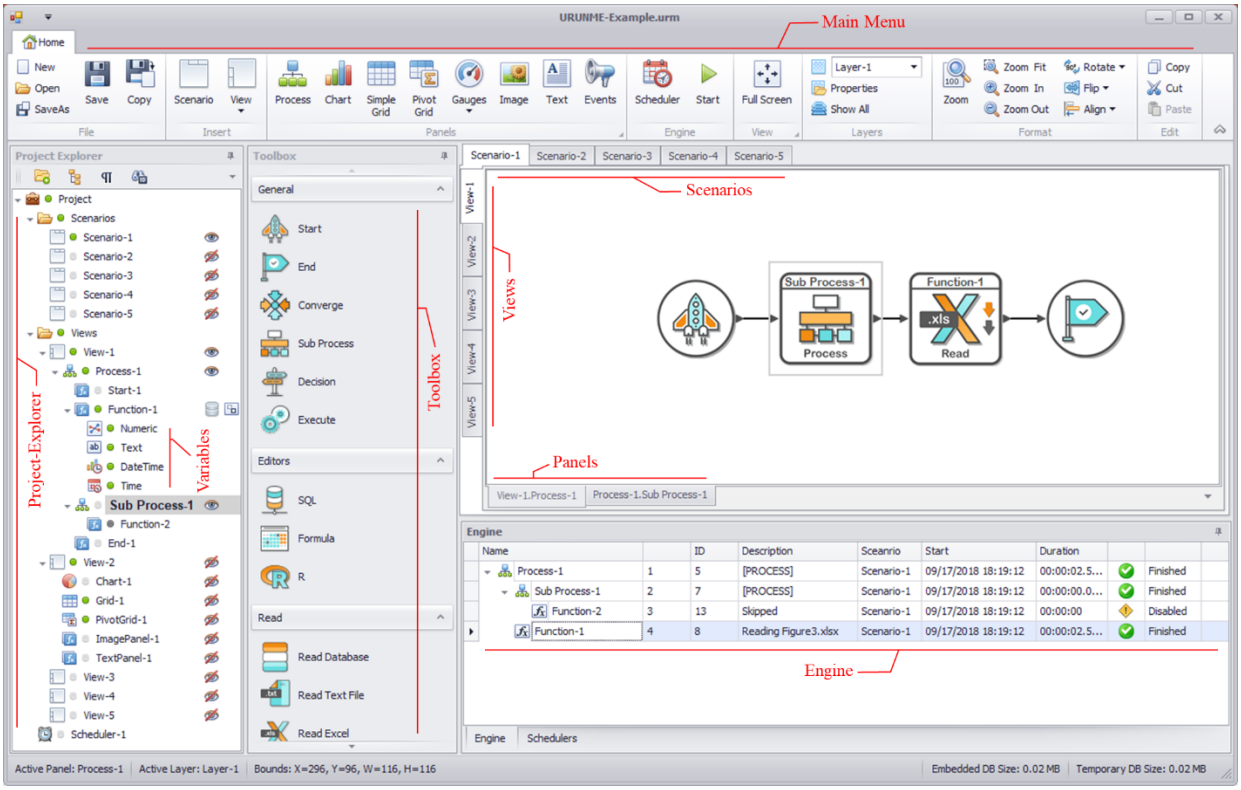

Figure 3-2. URUNME's graphical user interface: main screen

A project in URUNME consist of visual nodes which are shown in the project-explorer as a tree-list. The Node abstract class provides the logic for the hierarchical parent-child structure (Figure 3-3). Each node in a project is derived from the abstract Node class and requires a parent with any number of children. A project is shown as the root node in the project-explorer and is implemented using a singleton Project class. It provides a one-point access to the presentation tier by exposing a number of properties and methods. A project is stored as a binary file with a '.urm' extension using data contract serialization in .NET.

A Scenario class is used to implement all the scenarios in a project. They are stacked on the top of the workspace so that only one can be selected at a time (deemed ‘the active scenario’). A View class represents a standalone window within the workspace that contains visual elements called panels (e.g., diagrams, charts, etc.). The views are stacked as tabs on the left side of the workspace so that only one is visible at a time (deemed ‘the active view’). A panel is a window inside a view containing a visual control (e.g., diagram, chart, grid, etc.). All panels derive directly from Node class and implement the IPanel interface. This interface provides the logic for storing the layout and visual attributes of the panels in a view.

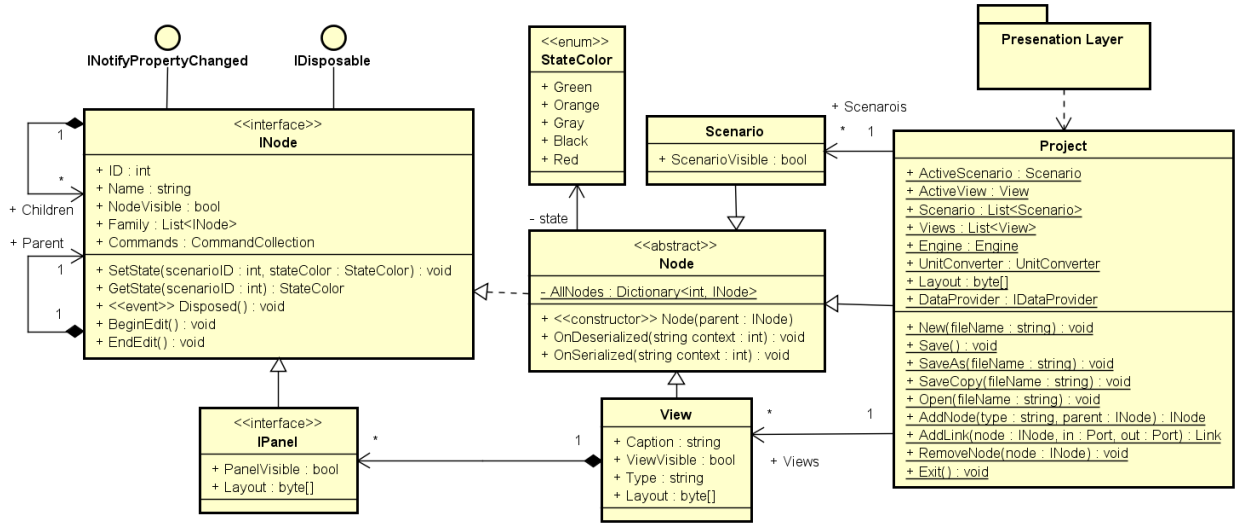

Figure 3-3. Class diagram showing some basic nodes (Due to space limitation, only some selected properties and methods are shown in the diagram)

3.3.2 Process and Functions

One of the core components in URUNME is the diagram panel which is implemented by the Process class as shown in Figure 3-4 (The term diagram and process is used interchangeably throughout the manuscript). This component works as a canvas to create visual objects and implement all the diagram settings, including properties for grid, scroll, size, layers, etc. These visual objects are implemented by the Symbol base class, which exposes properties and methods for visual manipulation. Some concrete classes that are inherited from the Symbol base class (e.g., Textbox, Label, Image, Shape, etc.) are only used as visualization objects in a diagram, as opposed to the functions. The Function abstract class, on the other hand, provides the base for implementing different tasks e.g., data reading, writing, analytics, etc. Each class that is derived

from the Function implements its own business logic by overriding the ‘Run’ method, which is called by the Engine when the user commits a run. Link and Port classes are used for creating any type of connector between two symbols in a diagram.

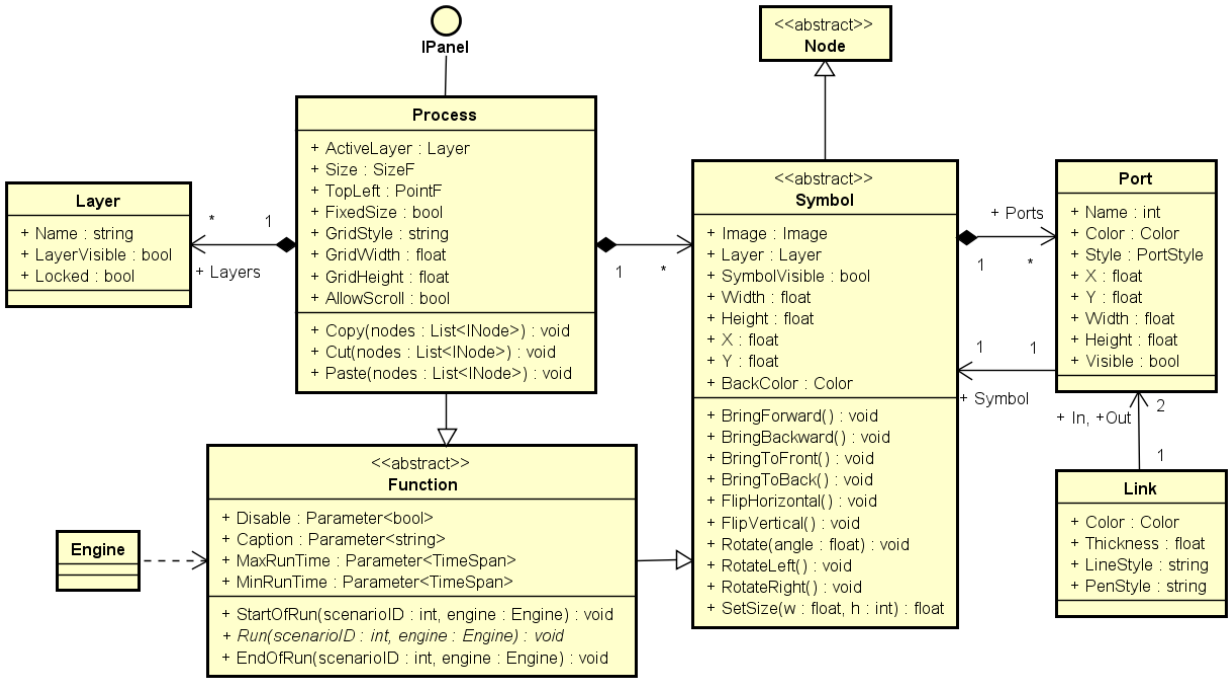

Figure 3-4. Class diagram for a process

The Process class is also inherited from the Function class but implements the IPanel interface as well. Therefore, it is shown both as a symbol in a diagram and a drawing panel in a view. A Process does not have any specific business logic of its own and only runs its child functions when its ‘Run’ method is called. Processes can be either ‘standalone’ or ‘sub-process’, as depicted in the hierarchical structure (Figure 3-5). A standalone process, like Process-1, has no parent. However, it can contain many other sub-processes and functions. A sub-process, on the other hand, can have its own child sub-processes and functions. For instance, in Figure 3-5, when Process-1 is run, it first runs Process-2, which essentially runs all members of Process-3, before running its own functions and then returns the execution back to its standalone process. This structure allows the organization of a large project into smaller manageable processes, which can be run independently or as a part of the parent process.

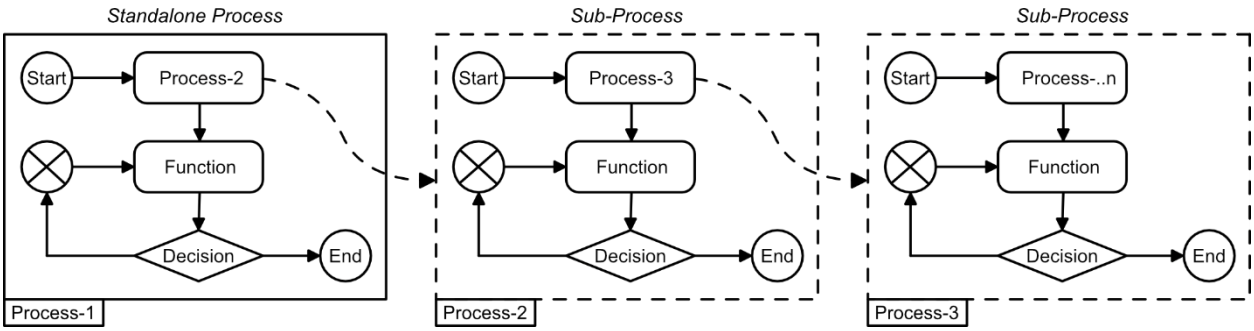

Figure 3-5. Hierarchical execution path in URUNME

3.3.3 Open Modeling Interface

URUNME provides out-of-the-box functionality for running Open Modeling Interface (OMI) v1.4 complaint models. The standard was seamlessly integrated into the software by creating new classes derived from existing Process and Function classes (Figure 3-4). The coupling logic is implemented by reusing the code provided in the standard development kit (SDK) of the OMI framework. The setup is similar to the default model configuration editor provided with the SDK. The coupled models are configured using a sub-process, called OmiProcess, located in the toolbox under 'OpenMI' group. The OmiProcess is inherited from the Process class and implements the diagram editor to drag-and-drop any number of OMI models from the toolbox. An OmiModel is essentially a function that runs an OMI model based on the *.omi file provided as an input. OmiTrigger function provides the trigger to run the models. OmiLink contains the settings for data linkage and is derived from the Link class to represent the model connections.

In addition, two more functions, OmiInput and OmiOutput, are provided to exchange data between URUNME and different OMI model components. Both these function implements OpenMI's Oatc.OpenMI.Sdk.Wrapper.IEngine interface and therefore essentially expose a linkable components. Any existing variable can be dragged and dropped onto a OmiInput function to create an output exchange item based on variable name and quantity. This output exchange item can then be linked to any model to provide input data at the runtime. Similarly, OmiOutput function can be used to create new variables which can be linked to any model as input exchange items. These variables can then be used to read output data from a model component at the runtime. Ability to read and write data directly from different OMI model components at runtime can be useful for any pre- and post-processing operation.

3.3.4 Parameters and Variables

The Parameter class is the building block of the scenario management logic in URUNME (Figure 3-6). It is used as a custom data type in other classes to specify the user-defined attributes/properties. For example, in a read Excel function class, properties like file path, name of the worksheet, cell address, number of rows to be read, etc. are all defined as parameters. To run multiple scenarios in a project, a parameter should be able to store a different value of an attribute for each scenario, if required. For instance, an Excel read function might be required to read data from two separate files in two scenarios. This is implemented by providing an option of storing a value in both global and local contexts within the parameter class. The global value is essentially the default value of a parameter (Value property) which is used in all of the scenarios. A local value, on the other hand, is scenario-specific and defined by a generic directory (values field) in the parameter class. Say a user selects a particular scenario, called 'S1', from the tabs at the top of the workspace, makes a parameter local in a function, and enters a new value. Consequently, whenever the function is run in the selected scenario ('S1'), it will only use the local value of the parameter. In all other scenarios where the parameter is not localized, the function will continue to use the global value of the said parameter. This logic allows any parameter to be made local for any number of scenarios to enter different values for an attribute.

All the data in a project are represented by scalar and vector variables shown as visual nodes in the project-explorer. Variable class is inherited from the Node to represent the data associated with a function. Data transfer in the software is carried out by a simple drag-and-drop of variables onto different functions or panels as inputs. Each variable contains a Field class, which defines all its attributes, including variable type (vector or scalar), data type (Numeric, Text, DateTime, Time), Quantity (Length, Area, Volume, Flow, Flux, etc.), Unit, Format, etc. For example, in order to read tabular data from an Excel file, the user is required to create the variables for each column in the 'Input' tab of the function. Once defined, the function automatically creates its variables corresponding to the number of columns, which are displayed in the project-explorer.

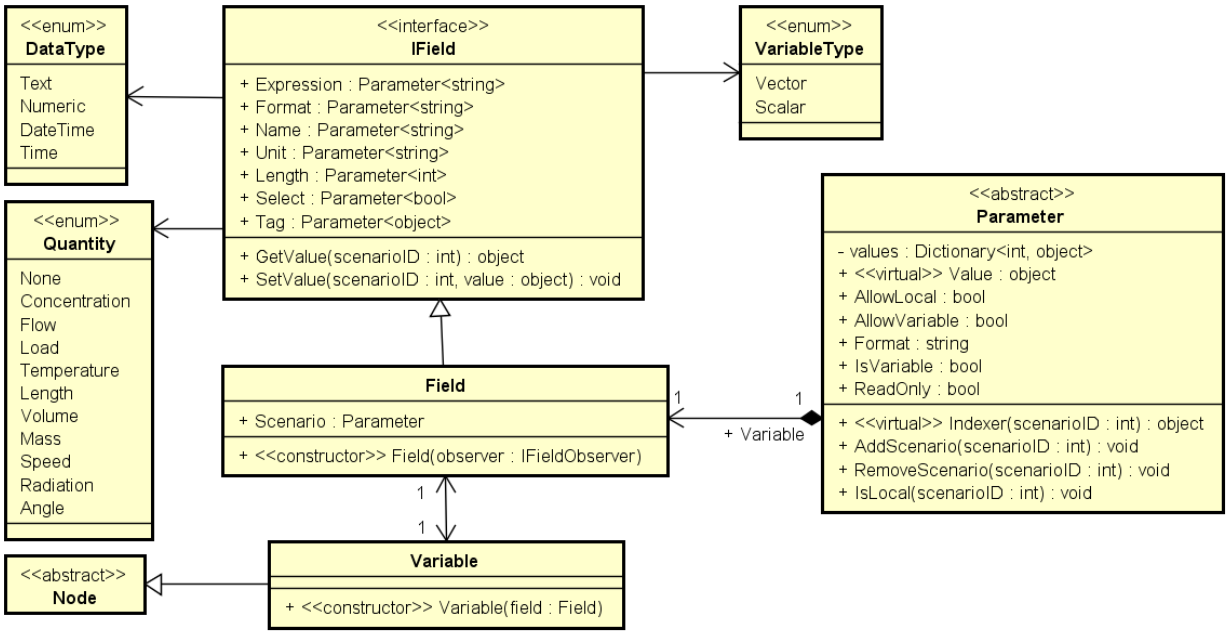

Figure 3-6. Class diagram of Parameter and Variable

In some functions, however, variables are created automatically by deriving their attributes from the input variable. For example, the DataInfilling function provides different built-in methods for generating missing data and creates an output vector variable for each input vector variable. The output variables generated by this function have the same attributes as the associated input variable, including the variable type, data type, quantity, and units. Therefore, the output variable keeps a reference of the input variable. When many different functions are created in a project, this logic creates a chain between one variable derived from another and so on. This provides a very useful mechanism to keep track of changes happening in different chains of connected variables. The state of each variable is defined by the State property (Figure 3-3) using different colors and is shown as bullets alongside each node in the project-explorer. For instance, when a single function is run in a particular scenario, the state of its child variables changes to green or red to indicate success or error, respectively. Consequently, all the variables down the data chain are set to orange to indicate that a source has been changed and an update is required. Also, when any variable changes its state, all the parents up the tree in the project-explorer will show the same state. It must be noted that the state of any variable is scenario-specific and may vary across scenarios, depending upon the status of the data. The state color coding is summarized below:

1) Black : Variables is disabled

2) Gray : Not run yet. Data are unavailable

3) Red : Run error. Data are unavailable

4) Green : Run success. Data are available and up-to-date

5) Orange : Update required. Data are available but may not be up-to-date

Another feature in URUNME is the ability to specify a parameter's value dynamically using a variable. A parameter can use any scalar variable as an input, which overrides the user specified input value. For example, a file path of an Excel read function can be directly defined by a scalar text variable which can then be dynamically changed to read a different Excel file if required.

3.3.5 Embedded Database

URUNME packages SQLite as its default embedded database. A new project automatically creates a single .db file in addition to the .urm. For every function created by the user, a new table is added to the embedded database using the function id with the 'tb' prefix (e.g., tb100, where 100 is the built-in id of function) as table name. By default, the new table only contains two integer columns: 'id' (as the primary key) and 'scenario_id' (to identify data stored for different scenarios). The remaining columns are created at runtime by the function, one for each variable, using its associated field name. All scalar variables in a project, however, are stored in a single table called 'tbscalar' created by default for every project.

The main benefits of SQLite are portability and speed, compared to a conventional server database. With an on-disk format, data are stored as a single ordinary disk file as opposed to a server database which requires dedicated server. This database can be easily shared among different URUNME projects or external software. An important requirement for URUNME is to sift and sort lots of data in diverse ways before permanently storing the essential information into the database. This is achieved by using the in-memory temporary database provided by SQLite. Each function provides the option to either store the data directly in the project's permanent database file or to keep it in the temporary database for analysis. This feature is beneficial in cases where a large amount of data must be queried prior to storage in the database file. The

temporary database in SQLite remains in memory until it comes under memory limitations when it flushes some data to the disk as a temporary file.

One of the downsides of using SQLite is its maximum allowable size. Theoretically, the SQLite database can store up to 140 TB of data, but, in practice, this storage capacity is seldom achieved due to the limitation of the file size in the Windows operating system. In addition, the SQLite database cannot be used for concurrent writing by multiple users, though simultaneous reading is allowed. The advantages and disadvantages were considered during the design stage of the software and ultimately, the decision was made to choose simplicity, speed, and portability of SQLite over a larger data size of a server database.

3.3.6 Unit Converter

Another valuable feature of URUNME is the built-in unit converter. There are a number of different quantities defined in the software (e.g., Length, Area, Volume, Speed, Flow, Flux, Radiation, etc.) using Quantity enum (Figure A3-1). For each quantity, A QuantityDef class can contain a number of units (e.g., m, ft, etc. for Length quantity) implemented by the Unit class, which specifies the relevant conversion factors. All numeric variables contain user-defined Quantity and Unit parameters and calls the associated QuantityDef in the UnitConverter class for unit conversion.

3.4 Features and Capabilities

To create a new project in URUNME, the user has to specify the project directory. The purpose is to ensure that all the data used in a project are contained in one directory (and its sub-directories) for easier exchange between different computers (a user can override this restriction). Folders in a project can be created using the toolbar in the project-explorer to group different types of nodes. A new view or scenario can be added by the ‘Insert’ group in the main menu and is shown in the Project-Explorer under the ‘Views’ and ‘Scenarios’ folders, respectively. Any view or scenario can be made invisible to the workspace by using ‘Show/Hide’ button in the associated context menu. Two types of views are provided in the software: Tabbed and Widget. Tabbed view displays panels as tabs, and only one panel can be shown at a time in a view (similar to worksheets in MS Excel). Widget view, on the other hand, allows the panels to

be docked on the screen in any layout, which may be more suitable for dashboard-like presentations.

3.4.1 Diagram / Process Panel

A new standalone process can be added from the main menu and shown in the project-explorer under the active view. Sub-processes can be added to a process diagram using the ‘General’ group in the toolbox and are shown as the children of the parent process in the project-explorer. To view the Process panel, the ‘Show/Hide’ button can be used in its context menu.

3.4.2 Symbols

The main menu contains a number of items for visual manipulation of symbols in an active diagram, which are divided into different groups: Layers, Format, Edit, and Size. Different layers can be used to group different symbols in a diagram, which can then be made either invisible or locked. Every symbol has a context menu that can be displayed by either right-clicking on it or its corresponding node in the project-explorer. Some objects derived from the Symbol class are used purely for visualization purposes in a diagram and are available in the ‘Miscellaneous’ group in the toolbox. The ‘Label’ symbol is used to write text on a diagram. The ‘Shape’ symbol provides hundreds of built-in figures which can be used to create different shapes. The ‘Button’ symbol is used to create interactive applications as explained in section 3.4. The ‘Image’ symbol is used to insert an image in a diagram. Any number of ports, of various shapes and sizes, can be created for the Image symbols by using the ‘Port’ button in its context menu. The ‘Textbox’ symbol is similar to a Label but used for scalar variables. It can be created by dragging and dropping a scalar variable from the project-explorer to a diagram and automatically updates itself if the input variable changes its state.

3.4.3 Functions

URUNME uses simple flowchart type diagrams to set up a process. Basic functions such as Start, End, Converge, and Decision are used to define the execution path. The Decision function, for instance, is used to run desired functions in a loop until designated criteria are met. Advanced functions are used to perform more dedicated tasks and are available in different groups in the toolbox. Links can be used to connect functions to create an execution flow path for the Engine.

By default, the Ports on a new function are hidden and every process runs its children sequentially based on their order in the project-explorer.

The inputs for any function can be specified in the Properties Form, shown by clicking the 'Properties' button in the context menu of the function. As previously explained, each input parameter in a function can have different values for different scenarios. A parameter can be made local by right-clicking on its associated editor (e.g. textbox, checkbox, combobox, etc.) and clicking 'Use Local Value' in its context menu. This will change the backcolor of the editor to blue and an icon will appear right next to it (Figure A3-2). Now, any value entered by the user will only be applicable for that specific scenario, while the rest of the scenarios will continue to use the global values. A variable can be used as an input to a parameter by right-clicking on its editor and selecting 'Use Variable' in the context menu. It will show an icon next to the editor, indicating that this parameter is now attached to a variable (Figure A3-3). Any scalar variable can then be dragged and dropped onto the editor from the project-explorer. It must be noted that the default value of a variable is always based on the active scenario. Hence, when a variable is attached to a parameter, a combobox (or dropbox) appears next to the parameter editor and sets *Active* as the default Scenario (Figure A3-4). However, if the variable is desired to have a fixed value from a specific scenario, regardless of whichever scenario is active, that scenario should be selected from the drop-down instead (combobox contains the list of all scenarios in the project).

For all functions that create user-defined variables, the 'Output' tab in the Properties Form of the function is used to define the required attributes (Figure 3-7). For example, to read an Excel file, a user is required to define the Name, Variable Type, Data Type, and cell Reference for each variable to be read (These attributes may vary from function to function). Quantity and Unit are also required, in cases where the variable is numeric.

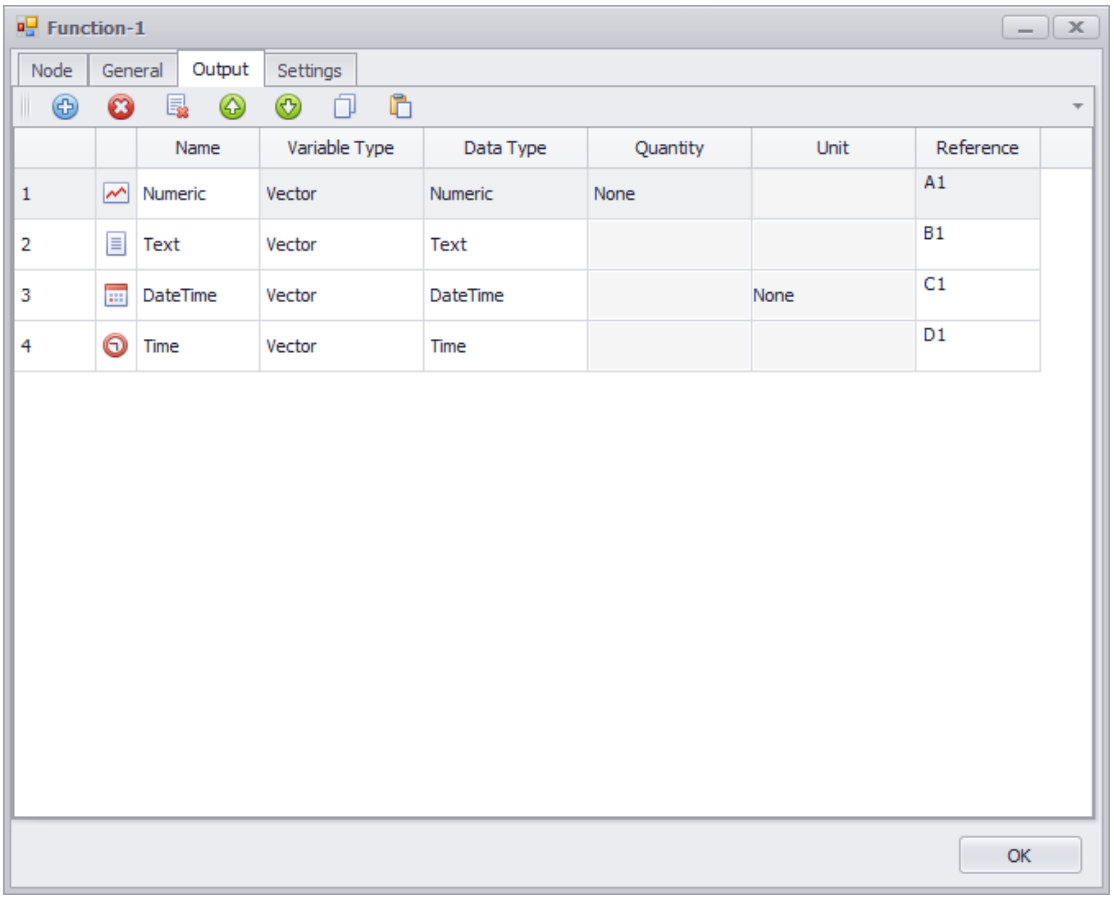

Figure 3-7. ‘Output’ tab of the Read Excel function Properties Form

In functions (e.g., write Excel file) or panels (e.g., charts) where variables need to be added as inputs, a user is required to simply drag-and-drop the desired variable from the project-explorer on the ‘Input’ tab in the Properties Form (Figure 3-8) and then set the Name, Unit (if required), and Scenario (as explained in the above paragraph) attributes. Each function also has a ‘Settings’ tab in its Properties Form, which contains a parameter to disable the function so that it cannot be run by the engine. In addition, it contains two more parameters for the functions that handle data. The ‘Cache’ parameter is used to set whether the data are kept in the temporary or file database and the ‘Insert Mode’ parameter defines how data are added to a table. For ‘Insert Mode’, selecting *Replace* deletes all the existing rows for the given scenario before adding new data while *Append* just adds new data rows after existing data.

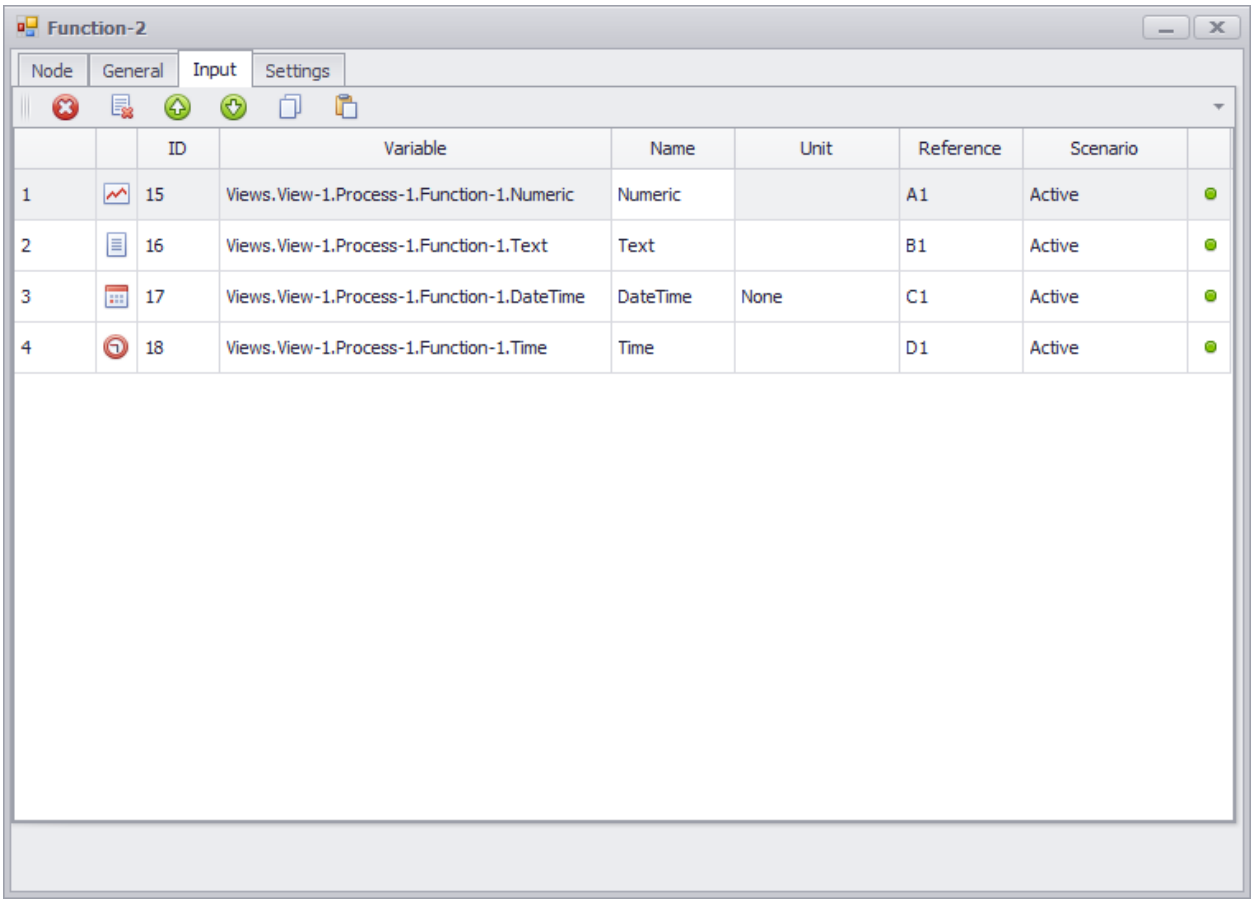

Figure 3-8. 'Input' tab of the Write Excel function Properties Form

Three analysis functions (SQL, R, and Formula) are provided under the 'Editors' group in the toolbox. The SQL function is used to query the embedded database as shown in Figure A3-5 (external databases can also be directly queried using the Read Database function described in Table 3-1). For example, '*Select * From tb100*' will query the table created for a function having an id = 100. Queried columns can be used to create new variables in the 'Output' tab by using the same names in the name attribute as used in the query. Each time the SQL function is run, it executes the query and updates its variables. By default, every query is automatically run only on the active scenario. However, the user can uncheck the 'Use Active Scenario' parameter in the 'General' tab of the SQL function to query the entire table. In addition to querying values, the user can also write non-queries (queries that do not return any data and performs an action e.g. deleting some rows) by checking 'Execute Non Query'. One of the features in the SQL function is the option of using other scalar variables in the query text. For instance, any scalar variable, say a date variable named 'x', can be added to a SQL function by using the 'Input' tab. If there is

a ‘date’ column in a table, say ‘tb100’, it can be queried using ‘*SELECT * FROM tb100 WHERE date > x*’ to get all the rows having a date greater than x. This feature essentially makes a query dynamic in nature and every time it runs, the data are queried based on the current values of the variables embedded in the query text.

The R function has an embedded R engine which is a widely used statistical language with a host of third-party libraries and functions (Figure A3-6). R combined with SQL can provide a powerful data analysis and statistical platform in URUNME. Similar to SQL, any variable can be used in the R script by adding it to the ‘Input’ tab. Output variables are defined to use the return values from the R engine with the same names as defined in the R script. In addition, a separate Formula function is provided to write mathematical and logical expressions on the variables (Figure A3-7). This function incorporates a large number of Excel-style formulas e.g. Abs, Cos, Sin, etc. The reason for including this function in URUNME is to provide additional built-in formulas which are not readily available in SQL or R. Furthermore, due to internal processing, these formulas are generally faster in performance compared to SQL and R which require external engines to run. More formulas will be added to this function in the future based on user feedback.

The Execute function is used to run the external applications (e.g. models, utilities, software, etc.). The path of an executable file is required as an input including any command line arguments accepted by the file (Figure A3-8). A check box is used to tell the function if it should wait until the external application exists before handing back the control to the URUNME engine. A ‘maximum runtime’ parameter is also provided to terminate the execution if the external application is taking more time than specified (in case the external application has stopped working due to error). Execute can also be used to run different scenarios of a project in batch mode by setting the ‘Scope’ attribute to *Internal* in the ‘General’ tab of the function. Any number of processes and functions can then be dragged-and-dropped on the ‘Internal’ tab and the run scenario can then be specified for each of them using the associated drop-down menu (Figure A3-9). By running Execute, these functions are run one by one in the specified scenarios.

In addition to the above, URUNME contains a number of other functions to perform various tasks pertaining to data read and write, file management, timeseries manipulation, statistics, etc.

Due to space limitation, however, only a brief description of each function is provided in Table 3-1. More functions will be added in the future based on user requirements and feedback.

Table 3-1. Brief summary of various Functions provided in URUNME

No.	Function	Description
1	Read Database	Read/Write data from different popular database types including FoxPro, SQL Server, MySQL, ORACLE, SQLite, etc.
2	Write Database	
3	Read Text File	Read/Write data from text files (Comma Separated Values, Space Delimited, Tab Delimited, Custom Delimited and Fixed Width).
4	Write Text File	
5	Read Spreadsheet	Read/Write data from an Excel spreadsheet.
6	Write Spreadsheet	
7	Read WDM	Read/Write timeseries from Watershed Data Management (WDM) format used in HSPF.
8	Write WDM	
9	Read NETCDF	Read netCDF, a multidimensional array-oriented binary format, generally used for meteorological data.
10	Read GRIB2	Read Grib2, a concise binary data format generally used for meteorological data.
11	Read Blob	Read BLOBS (Binary Large Objects) e.g. images, media files, etc.
12	Write Template	Write scalar variables to different text files using tags. This feature is used to automatically change input parameter for models which use text files as input
13	Execute	Run any external executable file or internal processes under different scenarios.
14	SQL	Write queries on the embedded SQLite database using SQL
15	R	Write R code using the embedded R engine.
16	Formula	Write mathematical and logical expressions using built-in formulas
17	File IO	Provides file IO functionality e.g. creating, copying and deleting files and folders.
18	Downloader	Provides a range of features for downloading files from a web server
19	Uploader	Provides a range of features for uploading files to a web server
20	Emailer	Provides a simple way for emailing.
21	Data Infilling	Fill missing data using different methods and/or de-aggregate timeseries
22	Aggregate	Aggregate timeseries using average, sum, time-weighted average and time-weighted sum.
23	Match	Match two different timeseries
24	OmiModel	Run an OpenMI compliant model
25	OmiTrigger	Provides an OpenMI trigger
26	OmiInput	To input data directly to an OpenMI model component at the runtime
27	OmiOutput	To output data directly from an OpenMI model component at the runtime

3.4.4 Run Engine

The Engine is responsible for running different functions and displaying the run status in the window at the bottom of the UI. Any process or function can be run by selecting the ‘Run’ button in the ‘Engine’ group in the main menu, or from its context menu in the diagram, or project-explorer. Moreover, automatic runs can be configured for a given date and time or on a periodic basis using ‘Scheduler’, which can be added to a project from the ‘Engine' group in the main menu. Details for next scheduled run and remaining time for each scheduler are constantly updated in the scheduler window located next to the Engine tab. The Engine runs different functions of a process sequentially. However, different functions can be run in parallel on separate threads, if more than one execution path is available, by checking the ‘Allow Parallel Processing’ parameter in the ‘General’ tab of a process Properties Form.

3.4.5 Panels

Different panels can be added to a View by using ‘Panel’ group in the main menu. A variety of charts are provided with extensive customization features (Figure A3-10), including the option for creating multiple series, panels (built-in panels in a chart), legends, axis, annotations, point labels, etc. In addition, charts provide various built-in data analysis tools including linear regression, error bars, summaries, moving averages, etc. Data can be added to the chart by dragging and dropping any number of vector variables on the chart itself or the ‘Input’ tab in its Properties Form. One of the key features of the chart is its ability to dynamically update its different text properties, e.g., titles, axes, legends etc., using scalar variables as input. For example, a text variable can be used as a chart title using the ‘Annotation’ tab in its property Form. Each time the variable state is changed, the chart title will be updated automatically. Grid panel is used to show data in tabular form. It provides a rich set of built-in sorting, grouping, filtering, and data searching tools. In addition to a simple grid, pivot grid panel is also provided to create pivot tables for multidimensional data analysis. All of these panels update automatically if there is any change in the underlying data.

Gauges can be used to show scalar variables on the screen for a higher level of data visualization. Different types of customizable elements are provided to imitate real gauges including circular,

angular, linear, thermometers, digital, etc. (Figure A3-11). Gauges are very useful for creating dashboard type applications to mimic screens used in supervisory control systems.

Image panel is used to display an image on the screen. URUNME provides the option of reading and storing Blobs (binary large object, e.g. images, media files, etc.) which can be read using the 'Read Blob' function. These blobs are similar to variables and can be dragged and dropped onto an image panel or as symbols in a diagram. Any time the 'Read Blob' function is run, the associated images are updated in the database and the panel or symbol automatically updates its image. This functionality can be really useful in applications where externally created outputs (e.g. charts and diagrams from different models) from other software programs are shown as images on a dashboard in URUNME.

When a large amount of data are processed in a simulation, it is very difficult to monitor the changes in different variables. The Event Manager panel provides a very simple mechanism of data monitoring and can display any message, warning, or alarm. Any number of events can be specified in the Event Manager, where each event contains a scalar variable, user-defined message, and a logical expression as a trigger (Figure A3-12). The logical expression is evaluated every time its associated variable changes its state and, if true, the message is displayed on the event manager screen (Figure A3-13). For example, this feature can be used for indicating a need for model calibration if certain performance indices are above or below a certain threshold.

3.4.6 Commands

A useful feature of URUNME is its ability to create interactive dashboards where different actions can be defined in response to user initiated triggers (e.g., mouse click, key press, etc.). This is accomplished by adding different commands to any visual element in the software (panels, symbols, functions, etc.). Commands can be configured by using the 'Commands' button in the context menu and specifying the different attributes (Figure A3-14). Any predefined action (e.g., Run a function, show or hide a view or panel, change size, move or rotate an image, create some animation, etc.) can be defined in a command in response to a trigger (e.g., mouse click, key press, etc.) for a target visual element. In addition, a logical expression

can be specified in a command using a scalar variable, to override the trigger if specific criteria are not met.

3.5 Case Studies

This section describes different projects created in URUNME ranging from simple data analysis to advanced model coupling and interactive dashboards. Most of the examples discussed here are from real-world projects involving different applications of integrated models in watershed analysis, forecasting in potable reuse systems, and climate change (project files for some of the case studies are available for download at https://www.urunme.com/resources/). The first case is described in more detail to illustrate how different processes are set up in a URUNME project. The remaining project examples are described more concisely and include only the pertinent details.

3.5.1 Data Analysis

URUNME can be used for in-depth data analysis owing to the embedded SQL and R language support and other built-in functions. A case in point is the low-flow frequency analysis carried out on a stream (called ST10) in the Occoquan watershed (located in northern Virginia, USA) in an attempt to calculate drought conditions under different return periods. In this method, first, annual minima are derived from daily flow by selecting the lowest flow every year using different averaging durations (e.g., 1, 7, 10, etc. days). An n-day moving average is progressed through the daily data to calculate the timeseries for each duration and then yearly minima are calculated (Gustard and Demuth, 2009). A cumulative distribution function (CDF) is developed using the yearly minimum flows. Low flow for any return period (T) can then be calculated by selecting the desired exceeding probability (p) on the CDF where ($T = 1/p$). For instance, a commonly used standard called 7Q10 represents the minimum 7-day flow expected to occur every 10 years. The following example illustrates how a different set of features in URUNME can be used to calculate the low flows in real time using online flow data from a stream station.

Figure 3-9 shows the process for low flow frequency analysis for the duration of 7, 15, 30, 60, 90 and 180 days over a return period of 2, 5, and 10 years ($p = 0.5$, 0.25 and 0.1 respectively). This example demonstrates that once low flows are calculated for any given return period, different scenarios can be created to calculate other return periods by simply localizing one variable. A

formula function called ‘Global’ is used to create one variable called p which is kept local for each scenario to define the return period. Flow data are obtained from three different sources. The ‘Historical’ function reads a text file obtained from a USGS (United States Geological Survey) website containing the daily flows for this location from 1968 to 1980. ‘Read ST 25, 30’ reads daily flows from a Visual FoxPro database for stream stations ST25 and ST30, located upstream of ST10, for a time period between 1980 and 2003 (before ST10 was commissioned). The ‘Fill 25,30’ function uses interpolation to fill in any missing data in the timeseries. The ‘Compute ST10’ function contains a simple formula to extrapolate missing ST10 data between 1980 and 2003 using flows from ST25 and ST30 based on the drainage area of each station (ST10 = ST25 * 2.166 + ST30). The ‘ST10’ function reads the data for the remaining time period from the database for the online stream station ST10. The ‘QAQC’ function contains a simple SQL statement to remove any duplicates and also sort the data by date, in case there is any discrepancy. The ‘Daily Flow’ function aggregates the data from ST10 to daily flows by using a time-weighted average. ‘Fill ST10’ infills any missing data using interpolation. ‘All Flow’ contains a SQL statement using ‘UNION’ to add the three different sources of data and create one single timeseries from 1968 to present date (Figure A3-5). The ‘Moving Avg’ formula function creates moving averages from the final timeseries for each time duration (Figure A3-7). ‘Yearly Min’ aggregates the moving averages for each duration to get yearly minima. Finally, ‘Low Flow’ uses an R script to create a CDF for each duration and returns low flow for a given p, using inverse CDF (Figure A3-6). Once this Process is created and tested, any number of scenarios can be created to get values from different return periods by changing the value of variable p in each scenario. ‘Run All’, which is an ‘Execute’ function, is used to conveniently run all the scenarios sequentially (Figure A3-9). A button can be added in the diagram to run the Execute function if a more dashboard type application is desired.

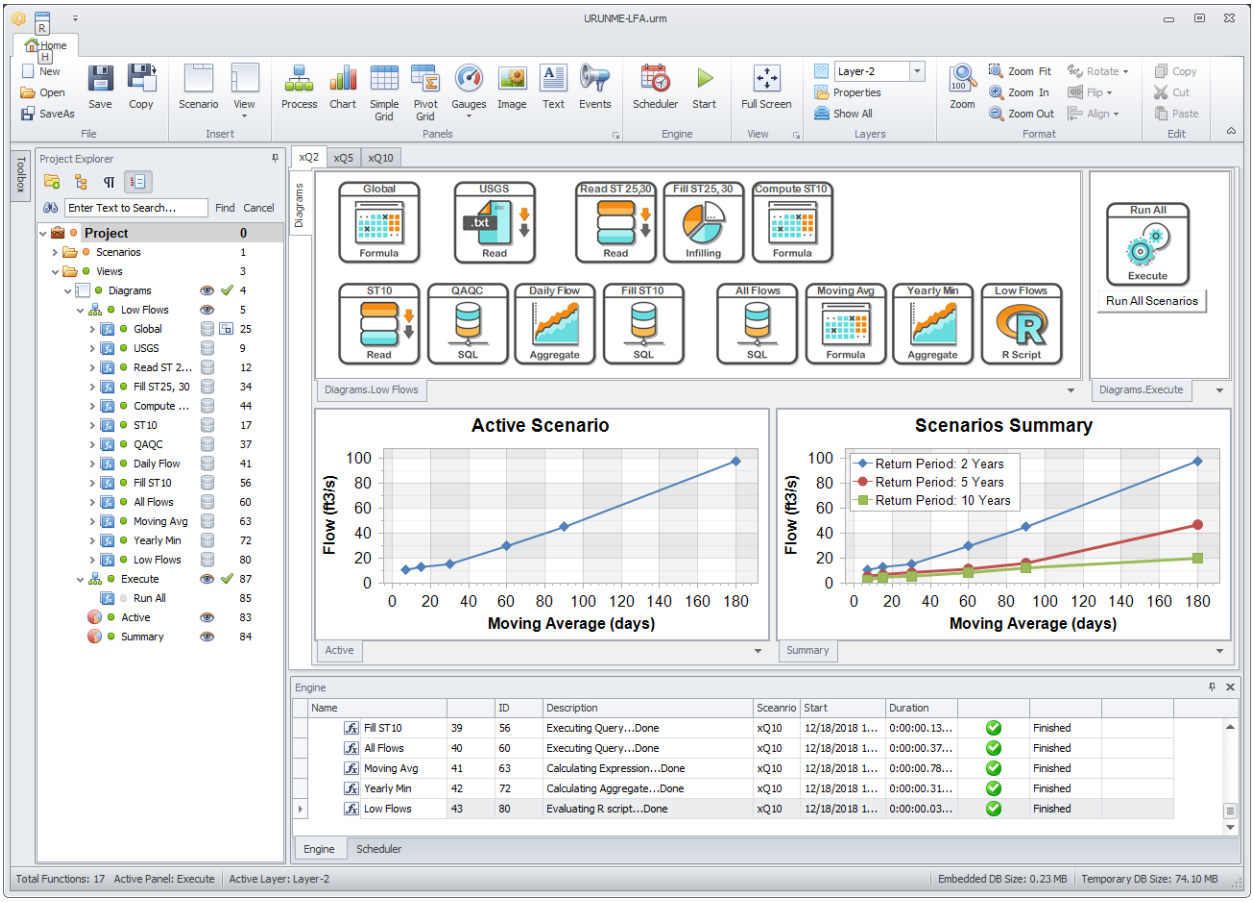

Figure 3-9. Low flow analysis in URUNME

The two charts shown in Figure 3-9 precisely show how scenario management is implemented in URUNME. The ‘Low flow’ function produces two vector variables, ‘x’ for return periods and ‘xQy’ for low flows. If the variable xQy is attached to the chart using an ‘Active’ scenario attribute, each time the user changes the scenario, the chart will update itself using the values from the active scenario (Left chart in Figure 3-9). However, in order to compare values from all the three scenarios at the same time, the variable xQy should be dropped three times on the right chart, each with its own ‘Scenario’ name attribute (Figure A3-15). This will create three different timeseries, each for one scenario. This particular chart will not update every time the active scenario is changed by the user. This case study shows a very simple example of data analysis and how different scenarios can be used in URUNME. More sophisticated analytics can be performed using similar techniques.

3.5.2 Web Data Download

URUNME can be used to download data from different websites using various file transfer protocols on a periodic basis for real-time modeling, analysis, and visualization. The following example is adopted from a futurecasting project where forecasted streamflow data are downloaded from National Water Model (NWM) FTP (File transfer protocol) server on a daily basis. NWM is a hydrological model that forecasts stream flows across the continental United States and has been in operation since Aug. 16, 2016, on the National Oceanographic and Atmospheric Administration (NOAA) supercomputing system. A long-range 16-member ensemble forecast is produced every day going out 30 days in the future with 4 ensemble members in each cycle at 00, 06, 12, and 18 UTC. Figure 3-10 shows the process created in URUNME used to download and query the 4 ensemble members produced at 1800 hours. Each day, a new directory is created in the NWM FTP URL (ftp://ftpprd.ncep.noaa.gov/pub/data/nccf/com/nwm/prod) named based on the production date with a 'nwm.' prefix, e.g. 'nwm.20180805'.

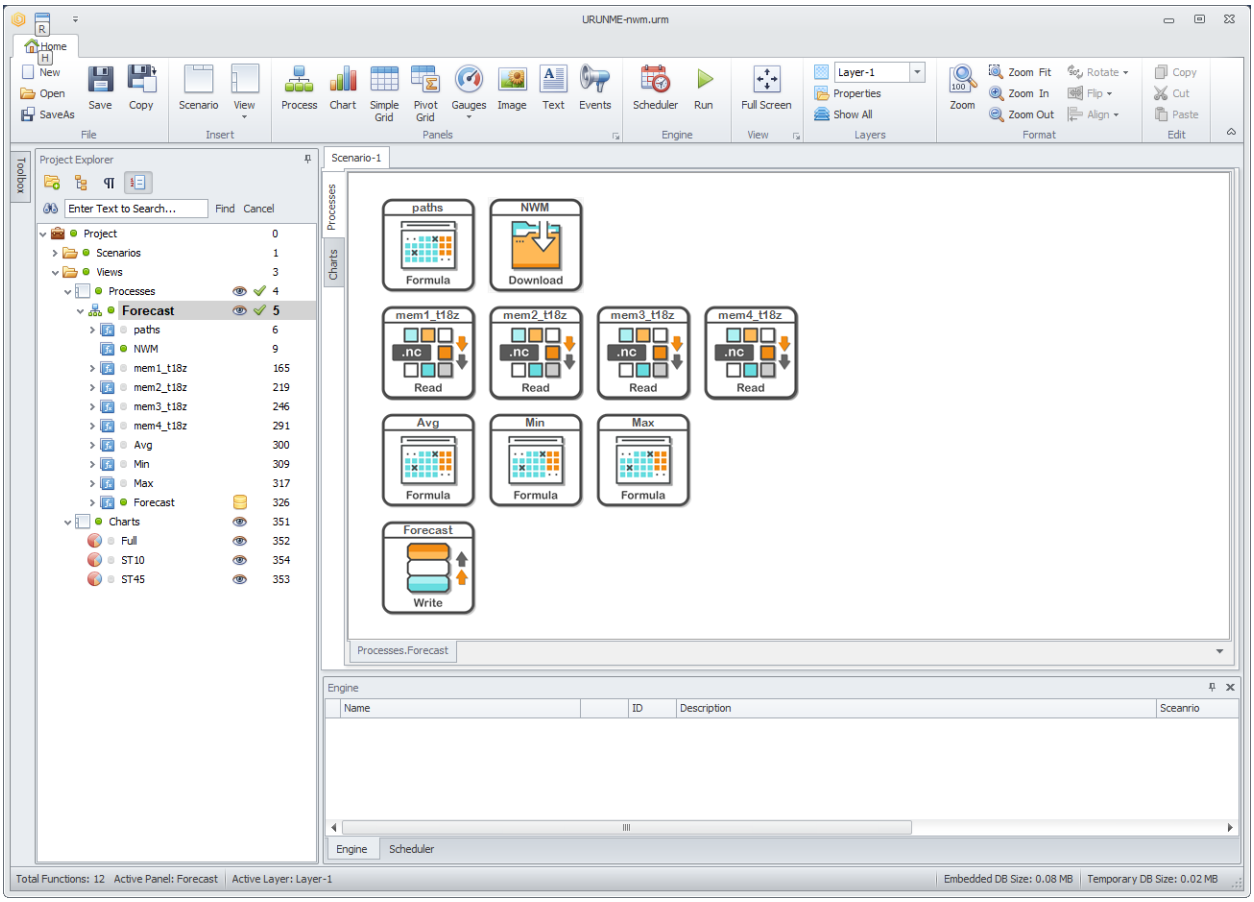

Figure 3-10. Process panel in URNUME showing periodic downloading and data extraction of NWM

A ‘Formula’ function is used to create the URL and local paths shown, using the following expressions (Figure A3-16):

todate = ***Now****();*

startdate = ***Sub****(todate,* ***TimeSpan****(1, 0, 0, 0));*

todatetext = ***Text****(startdate, 'yyyyMMdd');*

remotepath = ***Concatenate****('/pub/data/nccf/com/nwm/prod/nwm.', todatetext);*

localpath = ***Concatenate****('\\Forecast\\', todatetext);*

mem1path = ***Concatenate****(localpath, '\\long_range_mem1');*

mem2path = ***Concatenate****(localpath, '\\long_range_mem2');*

mem3path = ***Concatenate****(localpath, '\\long_range_mem3');*

mem4path = ***Concatenate****(localpath, '\\long_range_mem4');*

Now() formula gets the current date and ***Sub***(*datetime, timespan*) subtracts a day from it. ***Text***(*datetime, format*) converts the date to text using the given format. The ***Concatenate***(*text1, text2, ...*) function is then used to create the remote path (FTP URL) and local directories where each ensemble is stored.

The ‘Downloader’ function is used to download each ensemble in netCDF format and store them into their respective directories using the parameters shown in Figure A3-17. A total of 120 netCDF files are downloaded for each ensemble. The parameters ‘remotepath’ and ‘localpath’ in the downloader function are set to ‘Use Variables’ and the corresponding variables from the function ‘paths’ are used as inputs. Simple masks are used to include or exclude files or folders from the download. Four ‘Read netCDF’ functions, one for each ensemble, are used to read the downloaded files. The ‘Read netCDF’ function has the option of reading either a single file or an entire directory of multiple files and then combining the data to create a single timeseries. Flow data for the required stream are extracted from these netCDF files by providing the stream identification numbers, as defined by NWM. Once the data are read into the temporary database, ‘Formula’ functions are used to calculate min, max, and means of the four ensembles before storing that information into the permanent embedded database using the ‘Write Database’ function. A ‘Scheduler’ is used to run this process automatically on a daily basis.

3.5.3 Auto Calibration

URUNME can be used to automatically calibrate models based on user defined criteria. Although very sophisticated auto-calibration techniques can be used, a very simple example is shown here from a reservoir modeling project to elaborate the basic concept. CE-QUAL-W2 is a two-dimensional hydrodynamic and water quantity model developed by the U.S. Army Corps of Engineers to simulate the water quantity and quality in a waterbody (Cole and Wells, 2011). The simulated water elevation from the model is often not well calibrated (the model does not account for water loss due to seepage, etc.) and requires external calculations to create artificial tributary inflows/outflows for water balance. A water balance utility is provided in the CE-QUAL-W2 package, which requires a text file 'el_obs.npt' containing observed water elevation as an input for the simulated time period. The model is required to be run multiple times, and each iteration must be followed by running the utility to calibrate the water elevation. A looped process is created in URUNME to run the model and water balance utility successively (Figure 3-11), which automatically calibrates the model until a desired performance is achieved.

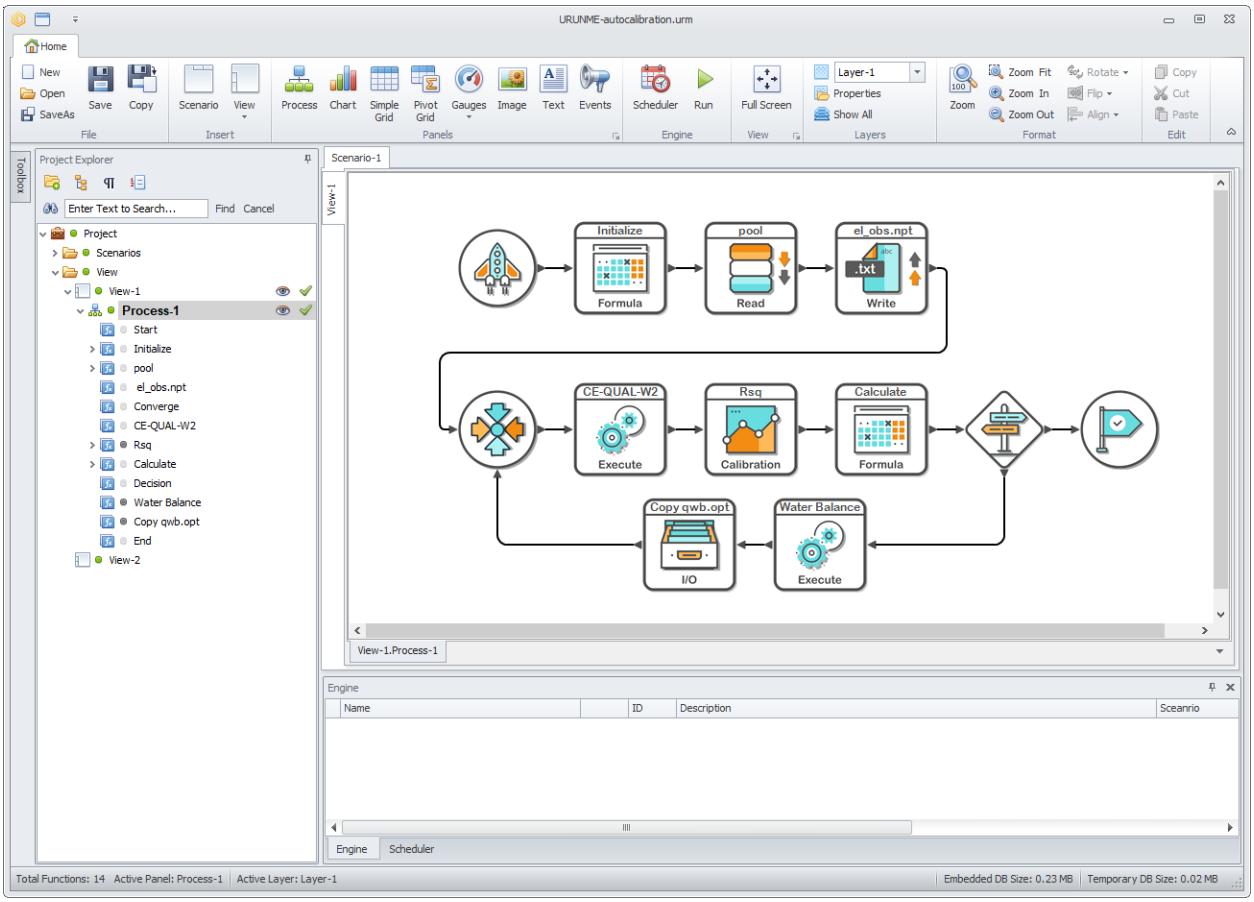

Figure 3-11. Auto calibration of CE-QUAL-W2 water level using ‘water balance’ utility in URUNME

The process starts with a ‘Formula’ function to initialize a variable called ‘count’ to keep track of the number of times the model is run. Observed water elevation is read from the Visual FoxPro file ‘pool.db’ for the given time period by a ‘Read Database’ function and is then written to the ‘el_obs.npt’ file by a ‘Write Text File’ function in the desired format. The CE-QUAL-W2 model is run by ‘Execute’ (Figure A3-8) and then followed by ‘Calibration’ function to calculate different calibration performance indices as scalar variables, such as r-squared (Rsq). Rsq variable is used by the ‘Calculate’ formula function to evaluate the following two expressions:

count = count + 1;

stop = if (count > 10 OR Rsq > 0.9, 1, 0)

The ‘count’ is incremented and an if statement is used to calculate a scalar variable ‘stop’ (the condition shown above is just for demonstration purposes, any logical statement can be used instead) to be used by the ‘Decision’ function to break the loop and go to the ‘End’. This is achieved by dragging and dropping the ‘stop’ variable in the ‘Decision’ Properties Form (when variable is 1, the loop breaks). In case the criterion is not met, the process goes into the loop and executes the water balance utility. A similar technique can be used for calibrating models by using any optimization routine or objective function.

3.5.4 Loose Model Coupling

The Occoquan model is a set of computer models linked together to simulate the watershed’s hydrology and water quality (Xu et al., 2007). It consists of seven watershed models (HSPF) and two reservoir models (CE-QUAL-W2). The coupling of these models is achieved by using the output from the upstream model as input for the downstream model. In the past, the entire modeling process was carried out manually, which required a huge amount of time and effort to carry out the simulation process which took days, if not weeks, to complete. In 2017, the entire Occoquan model was migrated to URUNME, which could automate the simulation process and run the application automatically. A dashboard was created for visualization of different inputs and outputs using multiple views and panels.

Due to the complex nature of the coupled model, each task is accomplished through a dedicated process. There are two main standalone processes in the Project: ‘Observed’ and ‘Models’. The

‘Observed’ process contains multiple processes that use hundreds of functions for reading data from different sources (database, text, excel, wdm, etc.). These data sources include meteorological data from different weather stations, flow and water quality data from stream stations, water elevation and water quality data from reservoir stations, water quality data from a water reuse plant, oxygen flow rates form the hypolimnetic oxygenation system, and water withdrawals from a water treatment plant. Various data analyses and manipulation operations are performed in these processes to develop the required input for each model. That includes QAQC of data, infilling missing data, timeseries aggregation, unit conversions, load calculations, etc. To keep the database size small, most functions use the temporary database and only processed information is stored in the embedded database.

The ‘Model’ process is used to run all nine models sequentially, as shown in Figure 3-12. Each sub-process in the diagram runs one model and consists of multiple other sub-processes and functions. Output data from one model is transferred to the downstream model and saved in the embedded database to create outputs for the dashboard. Unit conversion between the two models, HSPF (English units) and CE-QUAL-W2 (SI units), are also carried out automatically. The entire simulation process is run with the click of a button and takes less than two hours to complete.

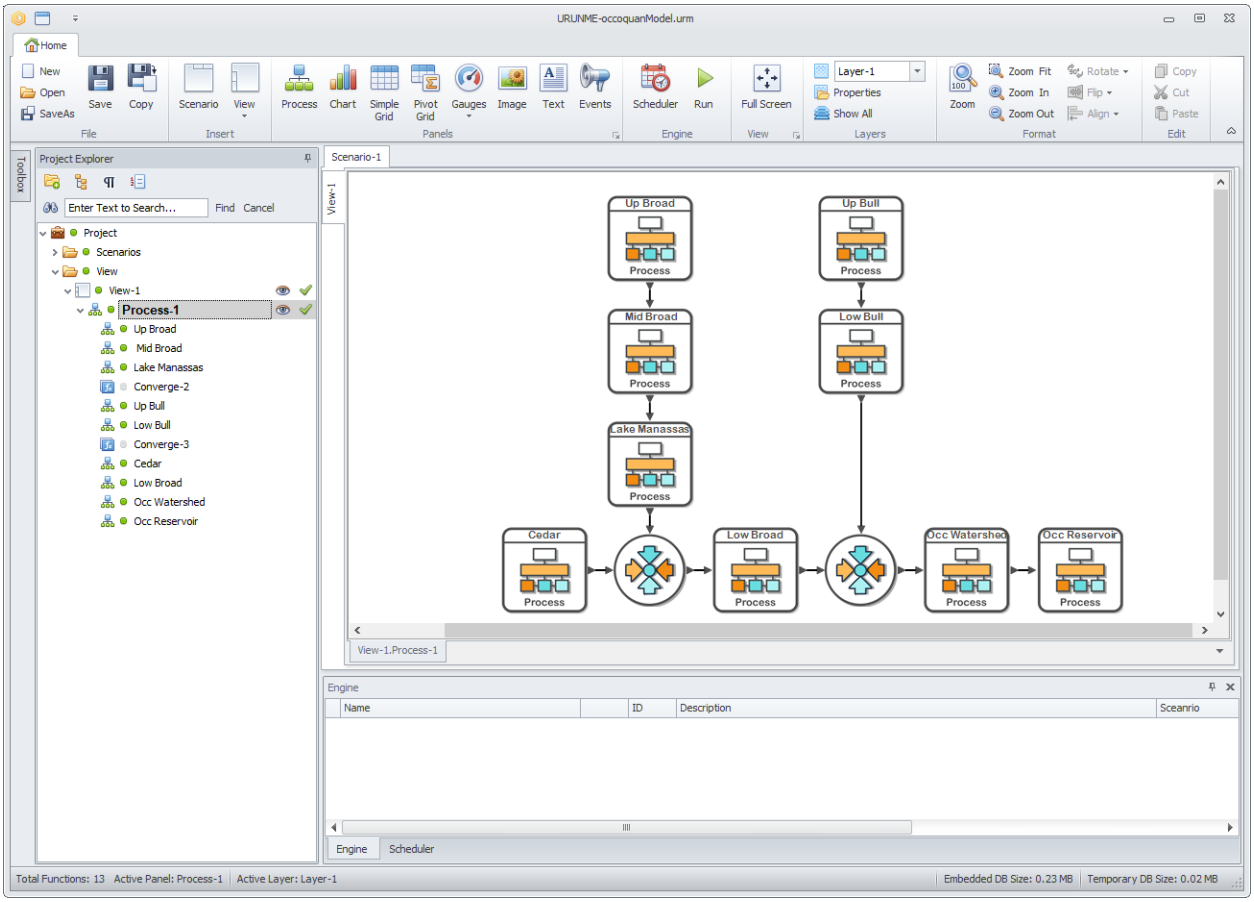

Figure 3-12. Sequentially coupled Occoquan watershed model consisting of 7 HSPF and 2 CE-QUAL-W2 models in URUNME

3.5.5 OpenMI based Coupling

This case study is presented primarily to illustrate how easy it is to use the OpenMI framework within URUNME application. It also explains the mechanism for direct data exchange with the OpenMI component.

This case study is based on the Simple River model provided with OpenMI v1.4 and shown in Figure 3-13. The left panel on the screen shows the parent process which has two functions to read and write data from two separate Excel files. The 'OMI Process' sub-process is shown in the right panel with the OpenMI model composition. The 'OmiModel' Function simply requires the path of Simple River model's .omi file to load the linkable engine DLL (Figure A3-18). The two variables, 'date' and 'inflows' read by the 'ReadExcel' function are dragged and dropped on the 'OmiInput' function. That automatically creates an output data exchange item 'inflows'

within ‘OmiInput’ ‘Input’ tab (Figure A3-19), which can then be linked to branch ‘inflow’ item of the model component using a Link (Figure A3-20). Similarly, in the ‘OmiOutput, function, a variable called ‘outflow’ is created using ‘output’ tab in the properties Form which essentially works as an input data exchange item. This variable is then linked to the required branch ‘Flow’ item of model components (Figure A3-21). The lists of available input and output data exchange items for a component are shown in the properties Form of the function (Figure A3-18). The data exchange linkages between different Omi functions can be created in the properties Form of the visual Link.

At runtime, the Simple River component directly read inflows from the ‘OmiInput’ function and ‘OmiOuput’ pulls outflows from the model component. This example shows how the OpenMI framework is seamlessly embedded in URUNME as a sub-process (in future similar sub-processes can be created for other frameworks) and can be executed with any pre- and post-processing operations. This architecture even allows different OpenMI sub-processes to be run and exchange data sequentially, if required.

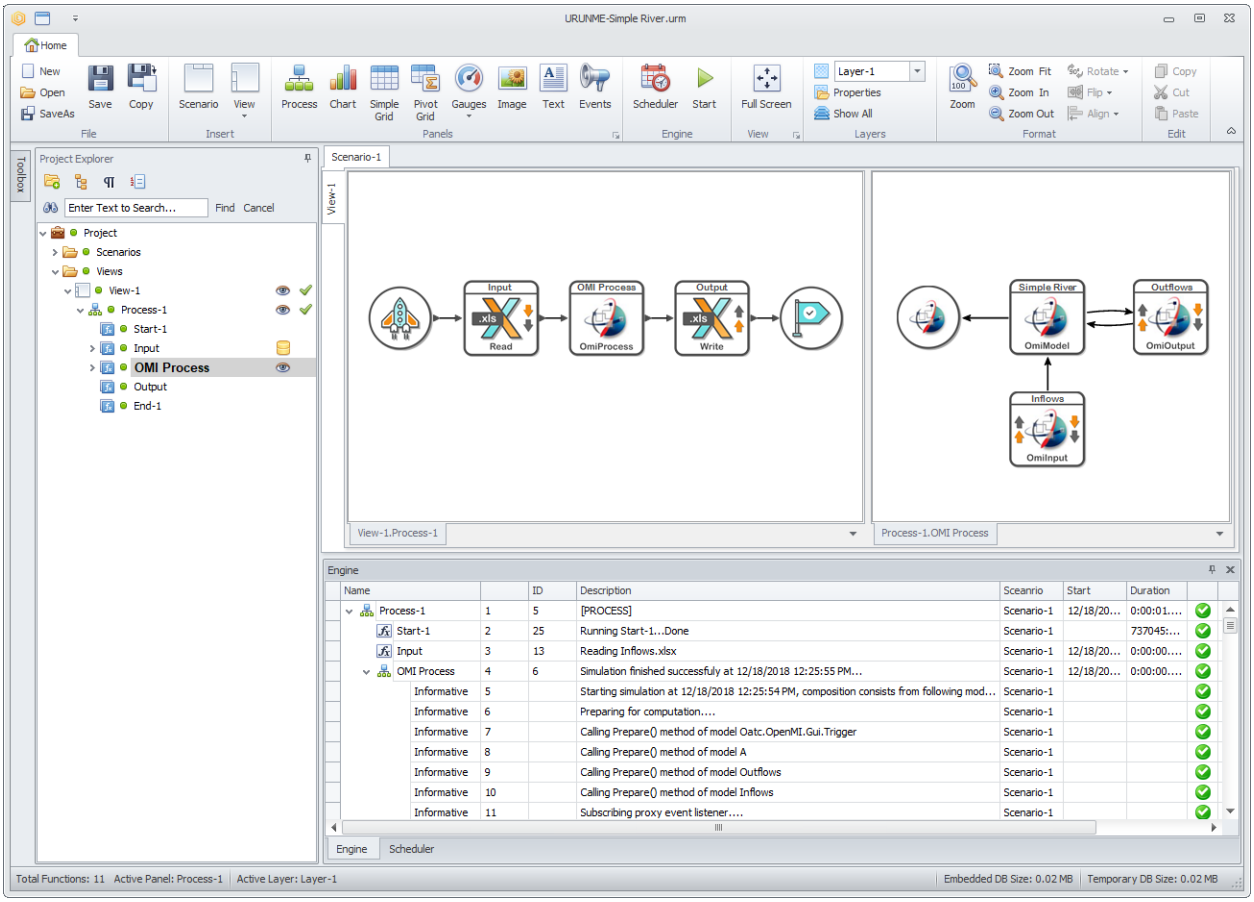

Figure 3-13. OpenMI based couple model showing Simple River example from OpenMI v1.4

3.5.6 Scenario Management

Scenario management plays a key role in developing decision support systems, particularly for future projection and planning. Baran et al. (2018) used URUNME to model climate change and land use change impact by using the coupled model described in 3.5.4. For that study, 68 different scenarios of climate change and land use change projections were created for two periods, the mid and late-21st centuries, using various iterations of two emission scenarios, four GCM (General Circulation Model), and two downscaling methods. Different functions in URUNME were used to read GCM files in NetCDF format, query the required data, downscale using built-in statistical tools, and then feed the resulting inputs into the hydrological models for each scenario. Scenario management in URUNME provided the capability to model large amounts of data (about 2.5 GB for each scenario) and compare the results for each of these projections.

3.5.7 Decision Support Systems

URUNME provides built-in capability for creating interactive dashboards using different views and panels with a large number of customizable options. Different Commands can be used for any visual element (views, panels, symbol, function, buttons, etc.) to perform different actions. This feature can be extremely helpful in creating a full interactive dashboard where the user can interact with visual elements to perform any number of tasks.

This case study presents a decision support system (DSS) developed in URUNME for the Upper Occoquan Service Authority (UOSA) water reuse plant location in northern Virginia (Lodhi et al., 2018). The DSS is based on an integrated reservoir model that uses real-time Climate Forecast System (CFS) and NWM data to predict future reservoir conditions. The resulting application provides valuable feedback to IViewOps (Sen et al., 2018), a process simulator used at the plant as a day-to-day operational tool. The Figure 3-14 shows one of the many views created in a dashboard application for the DSS. Buttons on the left are used to open a specific view. When clicked, each of the buttons executes a command using ‘Mouse Click’ as a trigger, ‘Open’ as an action, and the desired View as a target. The charts shown in the figure compare the observed and simulated temperatures at the surface and bottom of the Occoquan reservoir for

model calibration. There are various buttons on the bottom left menu to show results each constituent. By clicking the ‘Temp’ button, for example, multiple commands are run sequentially. The first command changes the value of a scalar text variable to ‘temperature’. This variable is used in multiple SQL functions to query data for a particular constituent from various tables in the embedded database. The second command executes all the SQL functions to read the temperature data. The vector variables from these SQL functions are used as inputs for the charts. This change in the variable state forces all the charts to update automatically. The third command changes the value of another text variable to ‘^{o}C’ which is used in the y-axis title for all charts.

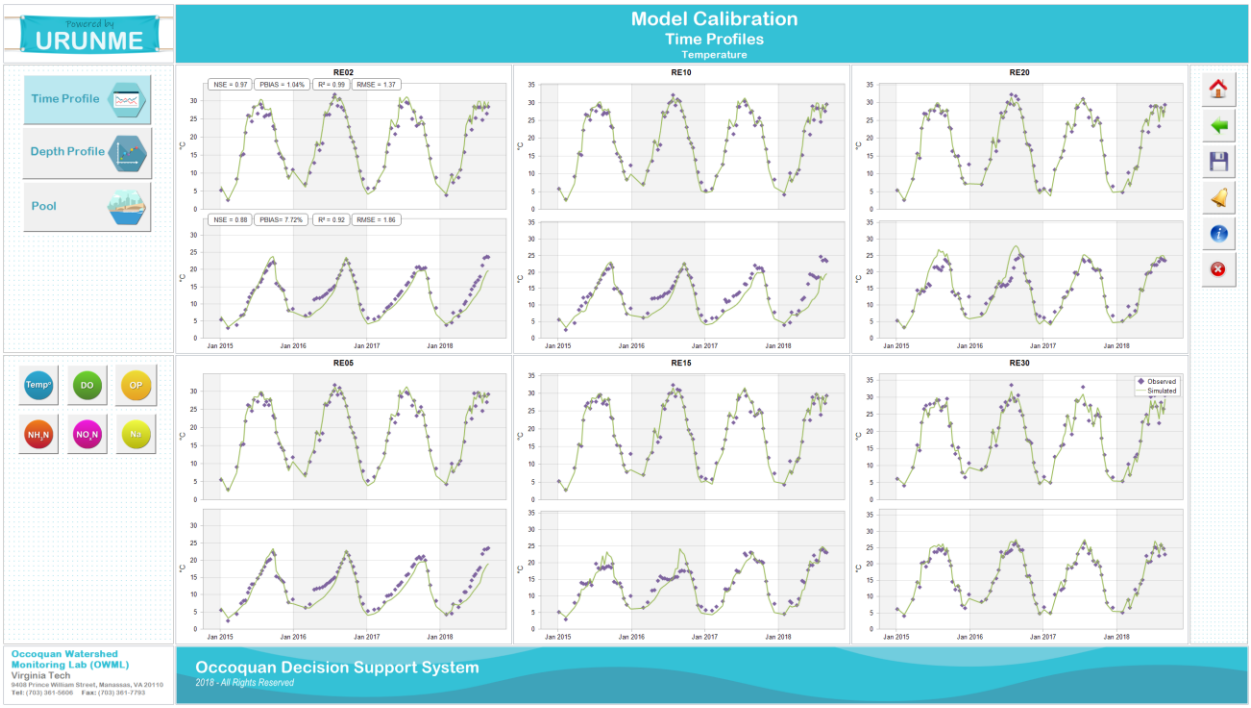

Figure 3-14. Occoquan decision support system showing model calibration results

Another view from the same application shows the output from the process simulator (Figure 3-15). IViewOps reads online data directly from SCADA (Supervisory Control and Data Acquisition System) and the laboratory to optimize the plant using different predefined combinations of process configuration (tanks in service), mixed liquor recycle, dissolved oxygen, wasting, supplemental carbon, etc. while specifying certain constraints on the effluent quality. In Figure 3-15, observed data from the laboratory are shown as red, field sensors as green, and the optimized results from the biochemical simulator as blue.

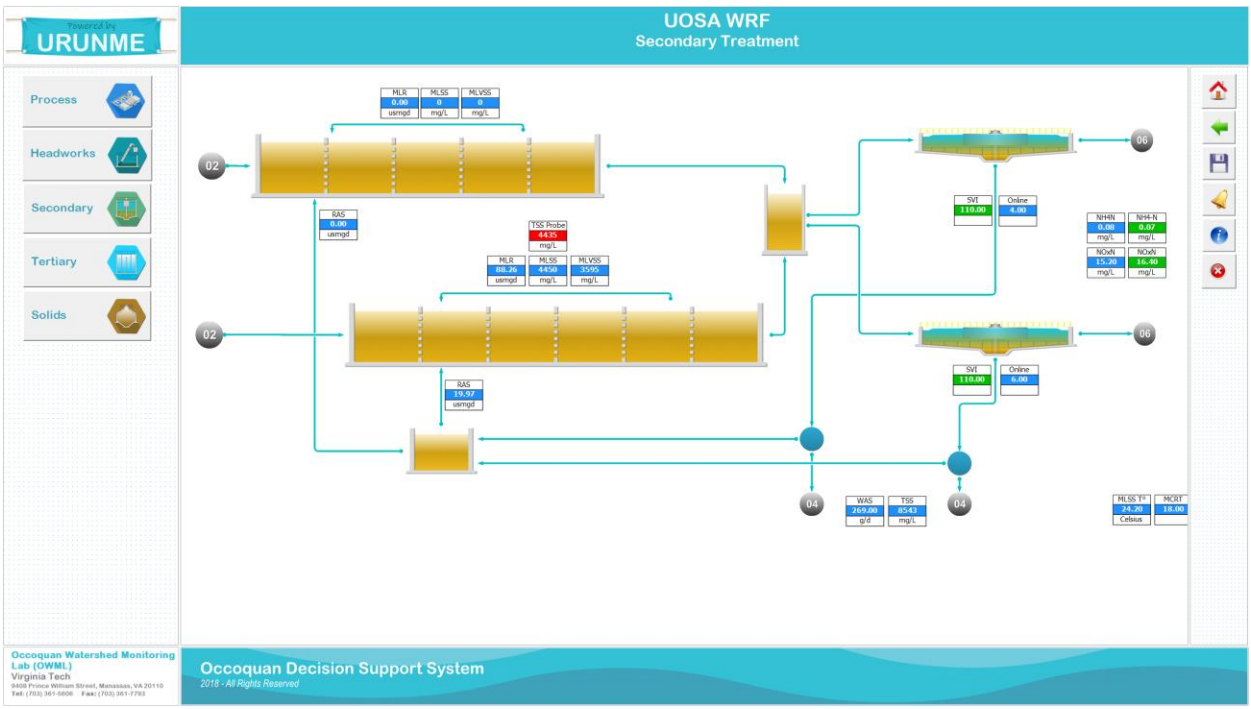

Figure 3-15. Occoquan decision support system showing observed and simulated values of different process parameters at UOSA water reuse plant

3.6 Summary

Commonly, the term integrated modeling only refers to the coupling mechanism used to automate the data exchange between different linked models. However, most such applications require extensive pre- and post-processing for developing a fully automated integrated model. URUNME is developed with the goal to not only facilitate the model coupling, but to automate the entire simulation process - creating inputs from different data sources, reading outputs, analyzing data, making statistical inferences and ultimately showing results in a visually-aesthetic and interactive way. It serves as an intelligent layer between the users, models, and data sources, practically hiding the underlying mechanics of the complex simulation process. The core functionality of URUNME can be categorized into six components as discussed below:

- **Automation:** Out-of-the-box support for sequential and framework based coupling and advanced pre- and post-processing capabilities for creating fully automated IEM applications.
- **Data:** Embedded SQLite database for storing data locally on a temporary or permanent basis. Support reading and writing of various database types and file formats. Represented data using

visual vector and scalar variables for simple drag and drop data transfer between different functions.

- **Analysis:** Advanced data analytics and statistics using Excel-type formulas, embedded R-language, SQL, timeseries transformation functions, etc.
- **Visualization:** Powerful graphics engine to create insightful and information-rich data visualization. Support multiple views and various visual elements (diagrams, chart, pivot table, gauge, grid, image, text, event manager, etc.)
- **Scenario:** Advanced scenario management to run a model multiple times using different initial and boundary conditions and store output data separately for each scenario.
- **Decision:** Tools for creating intelligent decision support systems using interactive dashboards. Provides a platform for informed planning and decision-making based on advanced data analysis, scenario-based modeling, forecasting, and risk assessments.

This paper has demonstrated how URUNME can be used for performing different modeling tasks using real world examples ranging from simple data analysis to complex model integration. With the increasing need to model and analyze complex environmental problems that are both multimedia and multidisciplinary (Laniak et al., 2013), a software platform such as URUNME can provide a one-stop solution. More functionality and features will be added to URUNME based on user feedback. Support for several new data formats, implementation of other modeling frameworks, upgdrade to OpenMI 2.0, and integration of Geographic Information System (GIS) mapping features are also part of the future software development plan.

3.7 Acknowledgments

The authors acknowledge the support of UOSA and OWML for supporting and funding this research. We would also like to honor the memory of the late Dr. Thomas J. Grizzard for his unwavering commitment in the establishment and operation of the Occoquan program and the OWML for over 40 years.

3.8 References

Baran, A. A., Moglen, G. E., and Godrej, A. N. (2018). "An integrated system modeling for studying the individual and combined impact of climate change and land use changes on Occquan watershed streamflows in Northern Virginia." *Unpublished Manuscript*, Virginia Tech.

Belete, G. F., Voinov, A., and Laniak, G. F. (2017). "An overview of the model integration process: From pre-integration assessment to testing." *Environmental Modelling & Software*, 87, 49-63.

Bergez, J.-E., Chabrier, P., Gary, C., Jeuffroy, M. H., Makowski, D., Quesnel, G., Ramat, E., Raynal, H., Rousse, N., and Wallach, D. (2013). "An open platform to build, evaluate and simulate integrated models of farming and agro-ecosystems." *Environmental Modelling & Software*, 39, 39-49.

Buahin, C. A., and Horsburgh, J. S. (2018). "Advancing the Open Modeling Interface (OpenMI) for integrated water resources modeling." *Environmental Modelling & Software*, 108, 133-153.

Cole, T. M., and Wells, S. A. (2011). "CE-QUAL-W2: A Two-Dimensional, Laterally Averaged, Hydrodynamic and Water Quality Model, Version 3.71." *U.S. Army Corps of Engineers, Washington, D.C.*

David, O., Ascough II, J. C., Lloyd, W., Green, T. R., Rojas, K., Leavesley, G. H., and Ahuja, L. R. (2013). "A software engineering perspective on environmental modeling framework design: The Object Modeling System." *Environmental Modelling & Software*, 39, 201-213.

Goodall, J. L., and Peckham, S. D. (2016). "Interoperability between the Basic Modeling Interface (BMI) and the Open Modeling Interface (OpenMI): a step toward building the earth system bridge for modeling framework interoperability.", *International Environmental Modelling & Software Society, Conference, Toulouse, France (2016).*

Gustard, A., and Demuth, S. (2009). "Manual on low-flow estimation and prediction." *World Meteorological Organization*, WMO-No.1029.

Hill, C., DeLuca, C., Balaji, Suarez, M., and Silva, A. d. (2004). "The architecture of the earth system modeling framework." *Computing in Science & Engineering*, 6(1), 18-28.

Jiang, P., Elag, M., Kumar, P., Peckham, S. D., Marini, L., and Rui, L. (2017). "A service-oriented architecture for coupling web service models using the Basic Model Interface (BMI)." *Environmental Modelling & Software*, 92, 107-118.

Johnston, J. M. "CIEM: Community of Practice for Integrated Environmental Modeling." *Proc., 2010 Open-MI Meeting*

Johnston, J. M., McGarvey, D. J., Barber, M. C., Laniak, G., Babendreier, J., Parmar, R., Wolfe, K., Kraemer, S. R., Cyterski, M., and Knightes, C. (2011). "An integrated modeling framework for performing environmental assessments: Application to ecosystem services in the Albemarle-Pamlico basins (NC and VA, USA)." *Ecological Modelling*, 222(14), 2471-2484.

Kalbacher, T., Delfs, J.-O., Shao, H., Wang, W., Walther, M., Samaniego, L., Schneider, C., Kumar, R., Musolff, A., and Centler, F. (2012). "The IWAS-ToolBox: software coupling for an integrated water resources management." *Environmental Earth Sciences*, 65(5), 1367-1380.

Knapen, R., Janssen, S., Roosenschoon, O., Verweij, P., De Winter, W., Uiterwijk, M., and Wien, J.-E. (2013). "Evaluating OpenMI as a model integration platform across disciplines." *Environmental Modelling & Software*, 39, 274-282.

Knox, S., Meier, P., Yoon, J., and Harou, J. J. (2018). "A python framework for multi-agent simulation of networked resource systems." *Environmental Modelling & Software*, 103, 16-28.

Laniak, G. F., Olchin, G., Goodall, J., Voinov, A., Hill, M., Glynn, P., Whelan, G., Geller, G., Quinn, N., and Blind, M. (2013). "Integrated environmental modeling: a vision and roadmap for the future." *Environmental Modelling & Software*, 39, 3-23.

Lloyd, W., David, O., Ascough II, J. C., Rojas, K. W., Carlson, J. R., Leavesley, G. H., Krause, P., Green, T. R., and Ahuja, L. R. (2011). "Environmental modeling framework invasiveness: Analysis and implications." *Environmental modelling & software*, 26(10), 1240-1250.

Lodhi, A., Godrej, A. N., Angelotti, R., and Sen, D. (2018). "A decision support system for indirect potable reuse based on integrated modeling and futurecasting.", *Journal of Water Reuse and Desalination*.

Malard, J., Inam, A., Hassanzadeh, E., Adamowski, J., Tuy, H., and Melgar-Quiñonez, H. (2017). "Development of a software tool for rapid, reproducible, and stakeholder-friendly dynamic coupling of system dynamics and physically-based models." *Environmental modelling & software*, 96, 410-420.

Molina, J., Bromley, J., García-Aróstegui, J., Sullivan, C., and Benavente, J. (2010). "Integrated water resources management of overexploited hydrogeological systems using Object-Oriented Bayesian Networks." *Environmental Modelling & Software*, 25(4), 383-397.

Moore, R. V., and Tindall, C. I. (2005). "An overview of the open modelling interface and environment (the OpenMI)." *Environmental Science & Policy*, 8(3), 279-286.

Peach, D., Hughes, A., Kessler, H., Mathers, S., and Giles, J. (2011). "Integrated environmental modeling: the new DREAM for Geological Surveys."

Peckham, S. D., Hutton, E. W., and Norris, B. (2013). "A component-based approach to integrated modeling in the geosciences: The design of CSDMS." *Computers & Geosciences*, 53, 3-12.

Rauch, W., Bertrand-Krajewski, J.-L., Krebs, P., Mark, O., Schilling, W., Schütze, M., and Vanrolleghem, P. A. (2002). "Deterministic modelling of integrated urban drainage systems." *Water science and technology*, 45(3), 81-94.

Sen, D., Fashokun, A., Angelotti, R., Brooks, M., Bhaumik, H., Card, C., Lodhi, A., Godrej, A., and Chung, C. (2018). "An Artificial Intelligence Platform for Asset Management Contributes to Better Decision-making Tools for Operations, Maintenance, and Utility Management." *Water Environment Research*, 90(4), 355-375.

Whelan, G., Kim, K., Pelton, M. A., Castleton, K. J., Laniak, G. F., Wolfe, K., Parmar, R., Babendreier, J., and Galvin, M. (2014). "Design of a component-based integrated environmental modeling framework." *Environmental Modelling & Software*, 55, 1-24.

Xu, Z., Godrej, A. N., and Grizzard, T. J. (2007). "The hydrological calibration and validation of a complexly-linked watershed–reservoir model for the Occoquan watershed, Virginia." *Journal of Hydrology*, 345(3), 167-183.

Yates, D., Sieber, J., Purkey, D., and Huber-Lee, A. (2005). "WEAP21—A demand-, priority-, and preference-driven water planning model: part 1: model characteristics." *Water International*, 30(4), 487-500.

Zhang, F., Chen, M., Ames, D. P., Shen, C., Yue, S., Wen, Y., and Lü, G. (2018). "Design and Development of a Service-oriented Wrapper System for Sharing and Reusing Distributed Geoanalysis Models on the Web." *Environmental Modelling & Software*, *111*, pp.498-509.

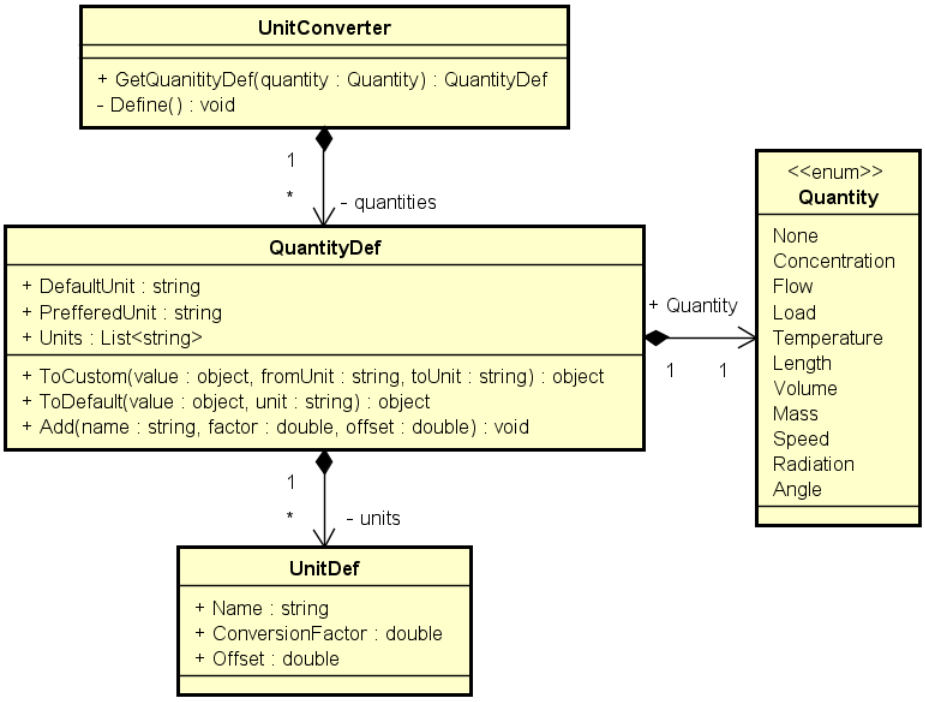

Figure A3-1. Class diagram unit conversion in URUNME

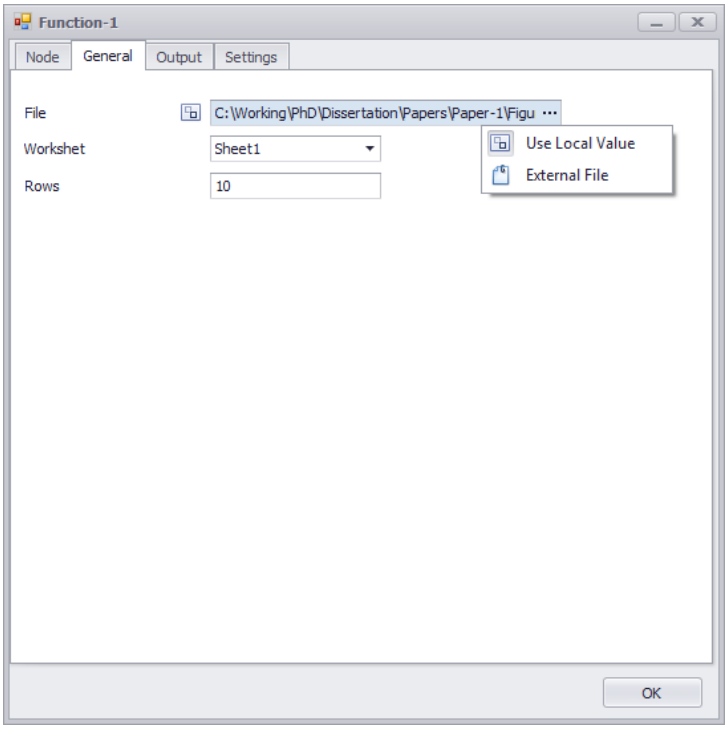

Figure A3-2. Read Excel function Properties Form showing ‘General Tab’ with localized ‘File’ Parameter

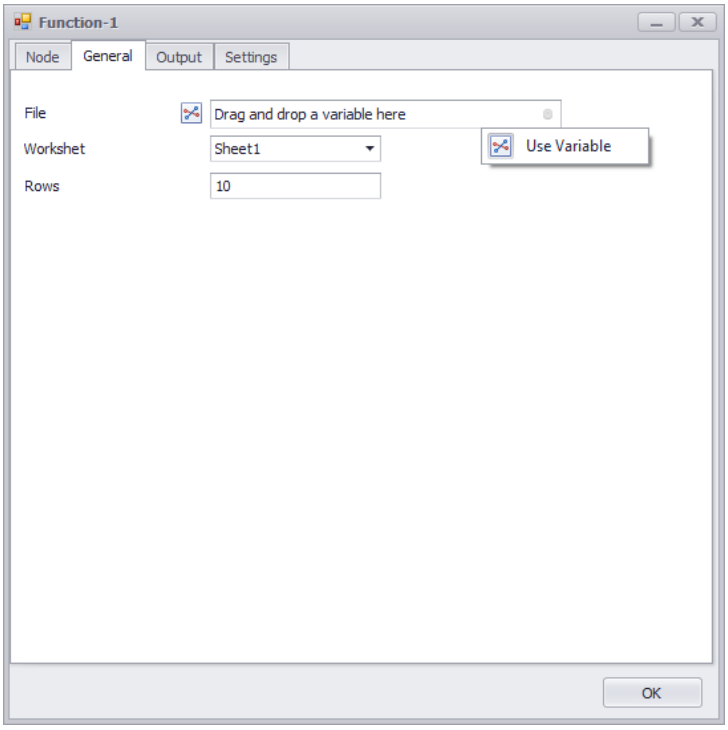

Figure A3-3. Read Excel function Properties Form showing ‘File’ parameter ready to be attached to a Variable

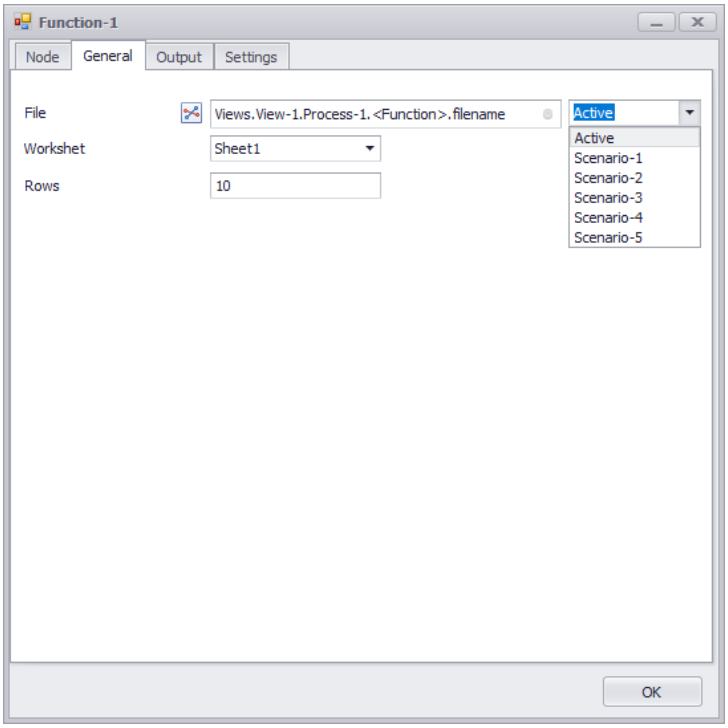

Figure A3-4. Read Excel function Properties Form showing ‘File’ parameter attached to a Variable with a dropbox to select the scenario

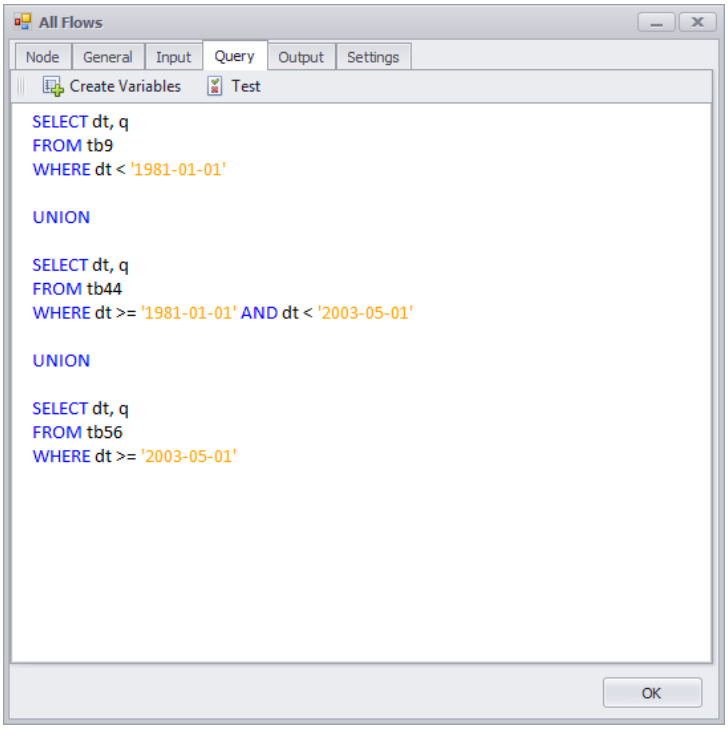

Figure A3-5. SQL function Properties Form showing the ‘Query’ tab

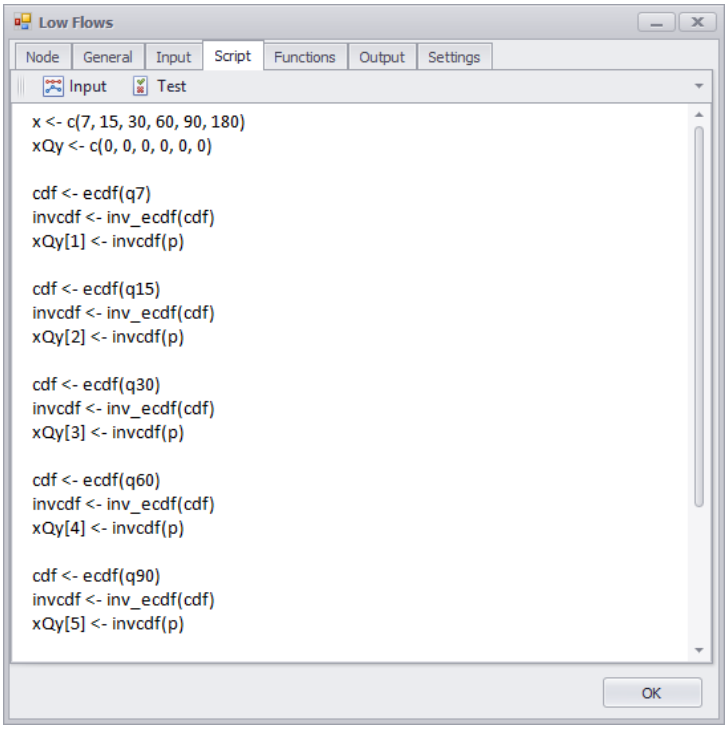

Figure A3-6. R function Properties Form showing the ‘Script’ tab

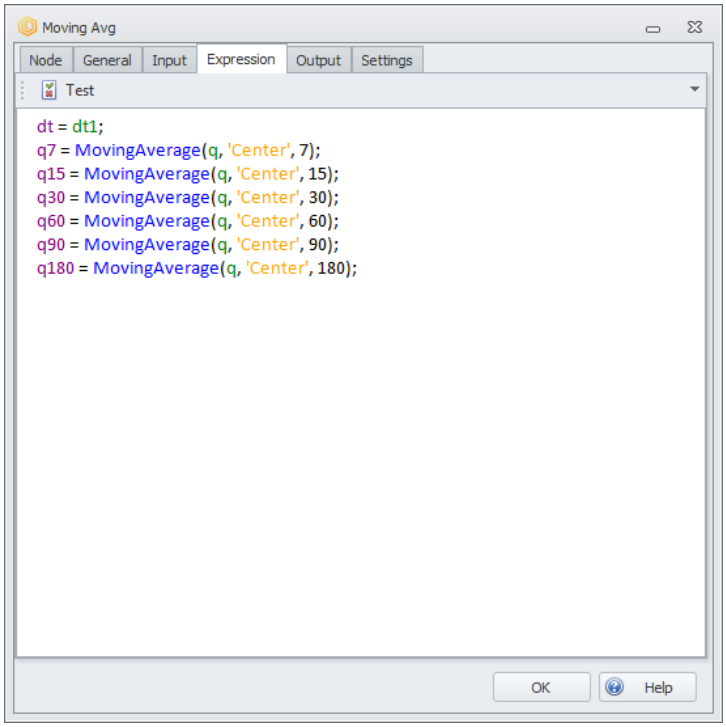

Figure A3-7. Formula function Properties Form showing the ‘Expression’ tab

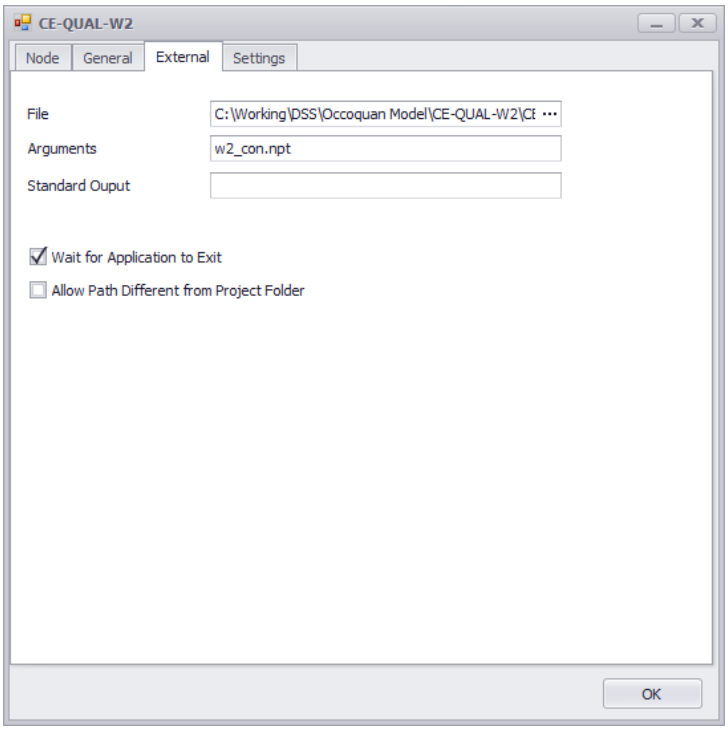

Figure A3-8. Execute function Properties Form showing the “External’ tab required to run a model

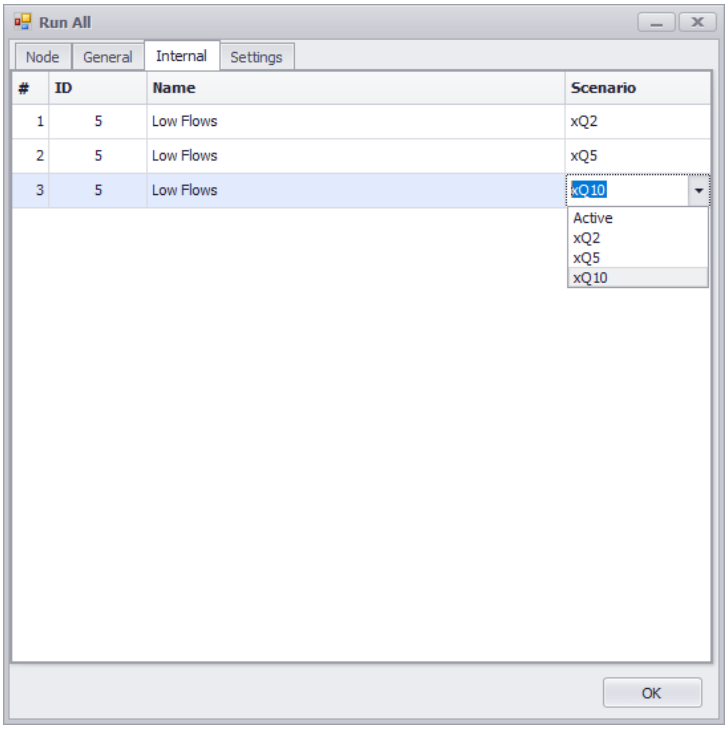

Figure A3-9. Execute function Properties Form showing the process 'Low Flows' selected to run in three different scenarios in a batch mode

Figure A3-10. Chart wizard in URUNME

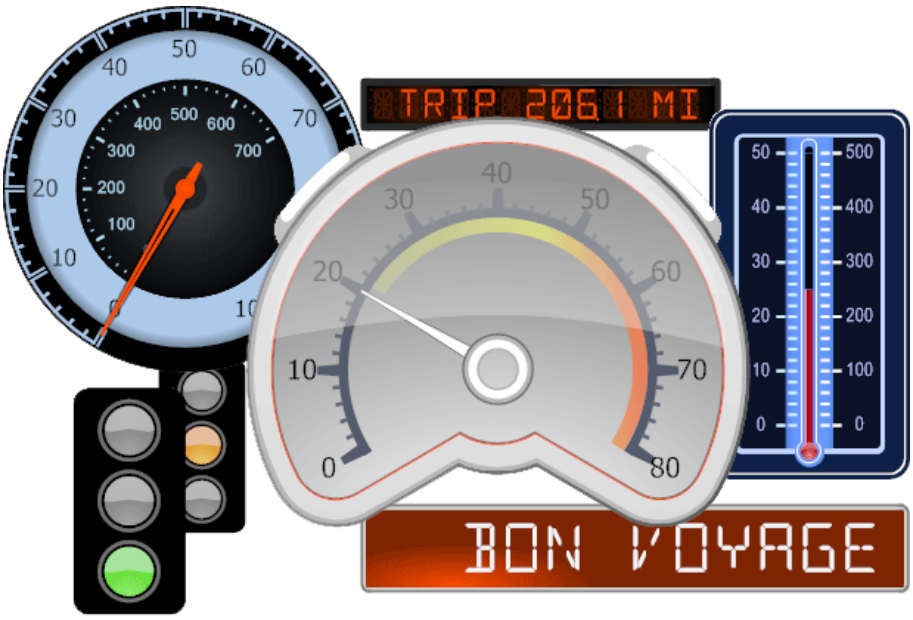

Figure A3-11. Gauges in URUNME

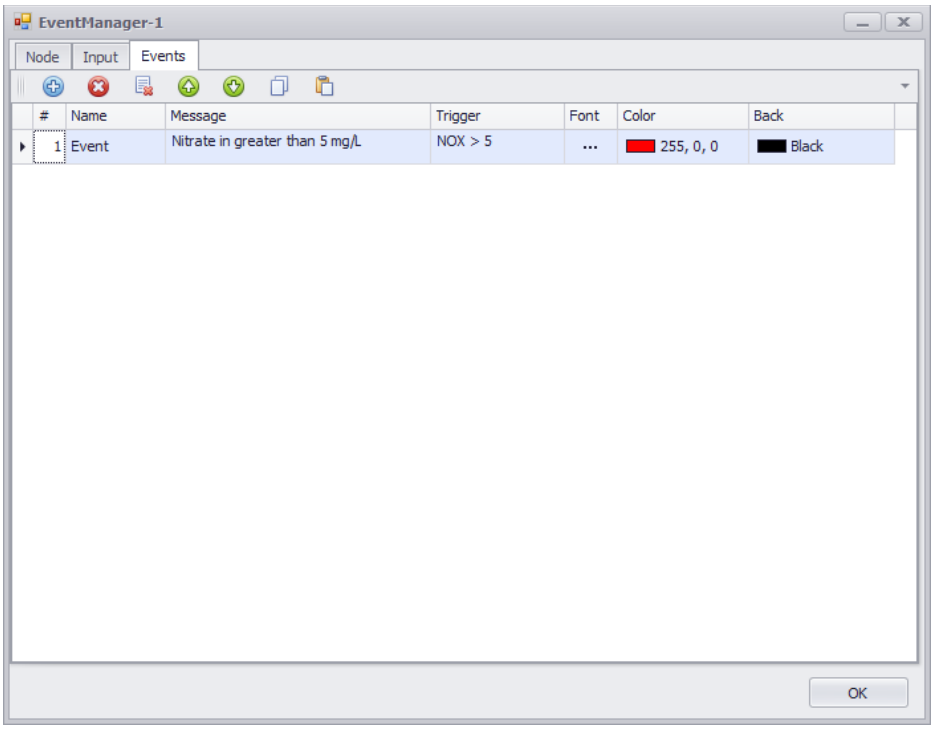

Figure A3-12. Event Manager Properties Form showing how an Event is defined

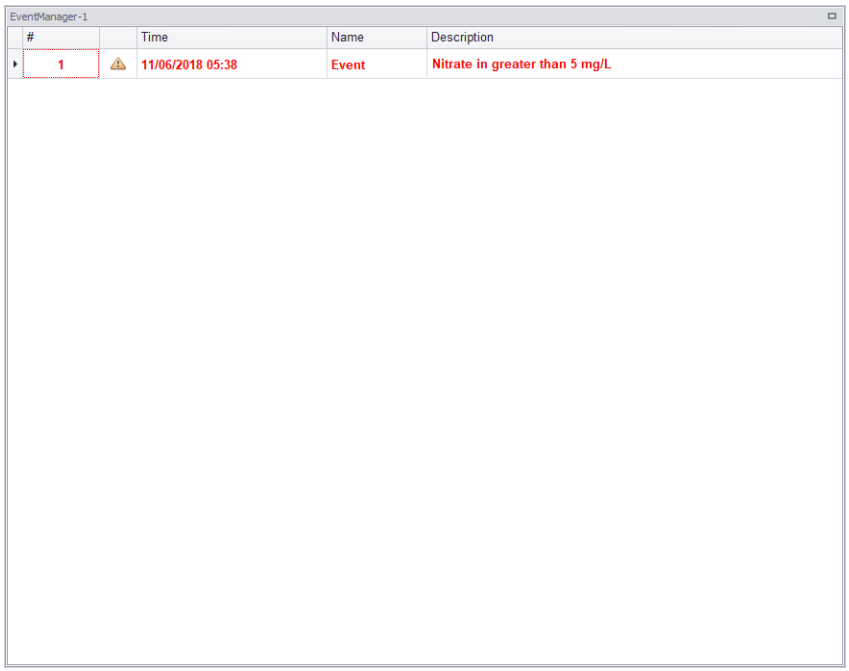

Figure A3-13. Event Manager Panel showing how an Event message is displayed when triggered

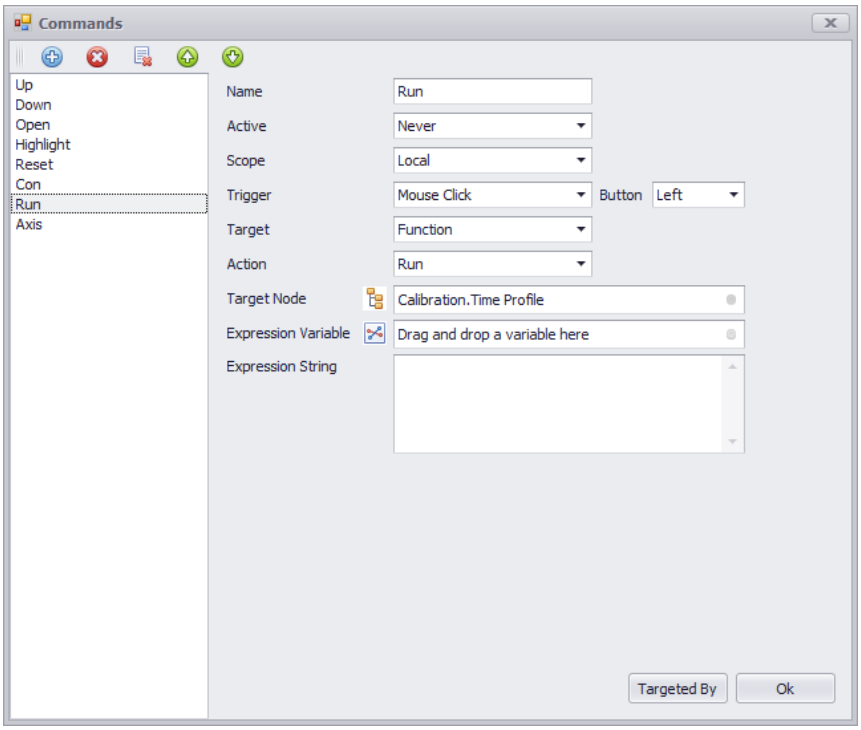

Figure A3-14. Commands Properties Form for a button showing definition of a ‘Run’ command

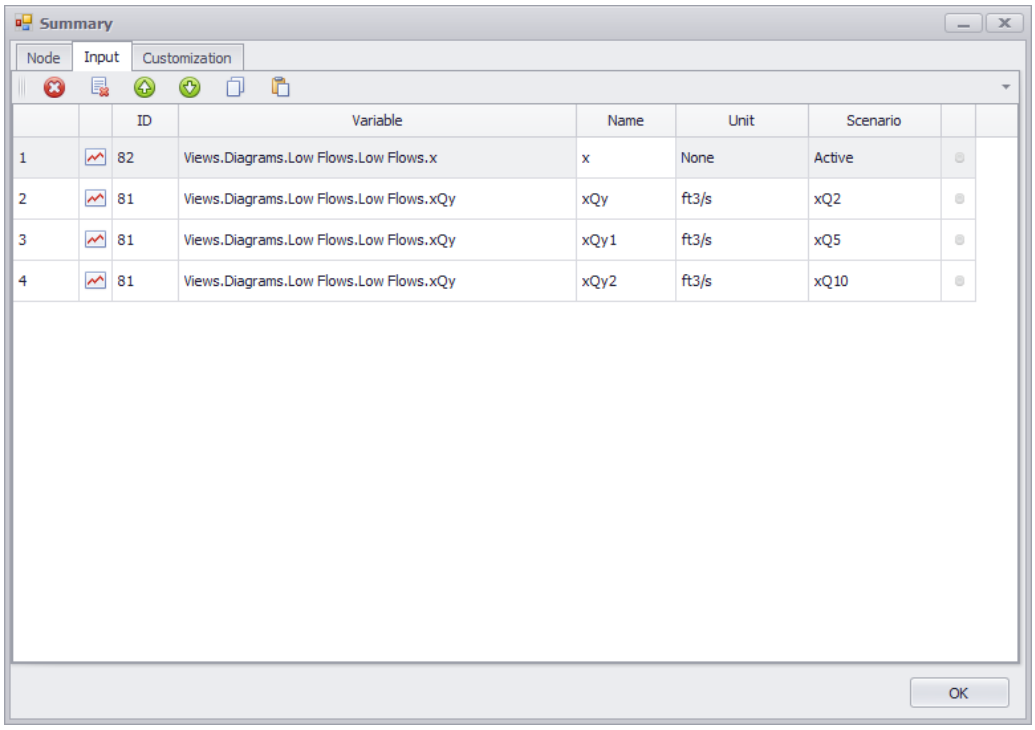

	ID	Variable	Name	Unit	Scenario
1	82	Views.Diagrams.Low Flows.Low Flows.x	x	None	Active
2	81	Views.Diagrams.Low Flows.Low Flows.xQy	xQy	ft3/s	xQ2
3	81	Views.Diagrams.Low Flows.Low Flows.xQy	xQy1	ft3/s	xQ5
4	81	Views.Diagrams.Low Flows.Low Flows.xQy	xQy2	ft3/s	xQ10

Figure A3-15. ‘Input’ tab showing different Variables in a chart

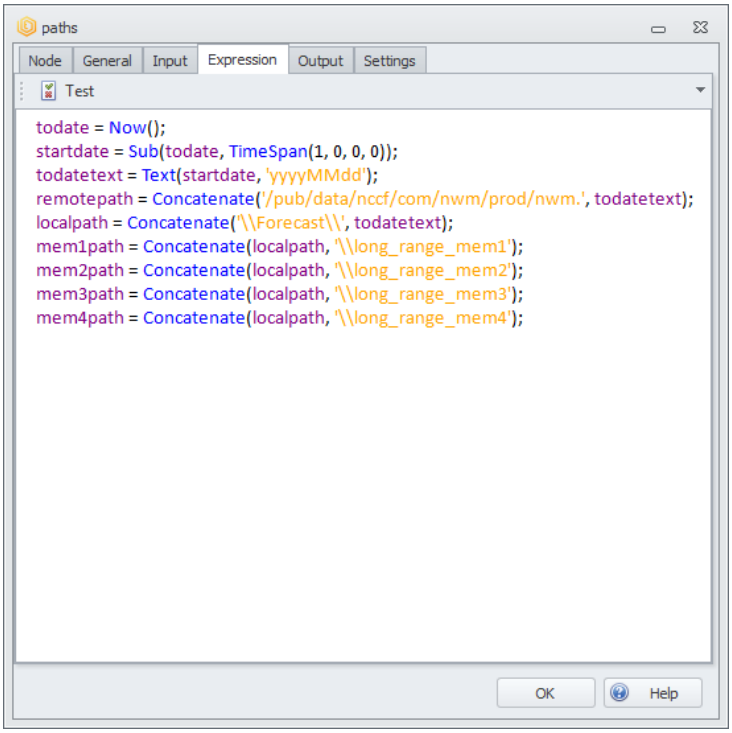

Figure A3-16. Formula function showing the Variables defined for downloading NWM forecast

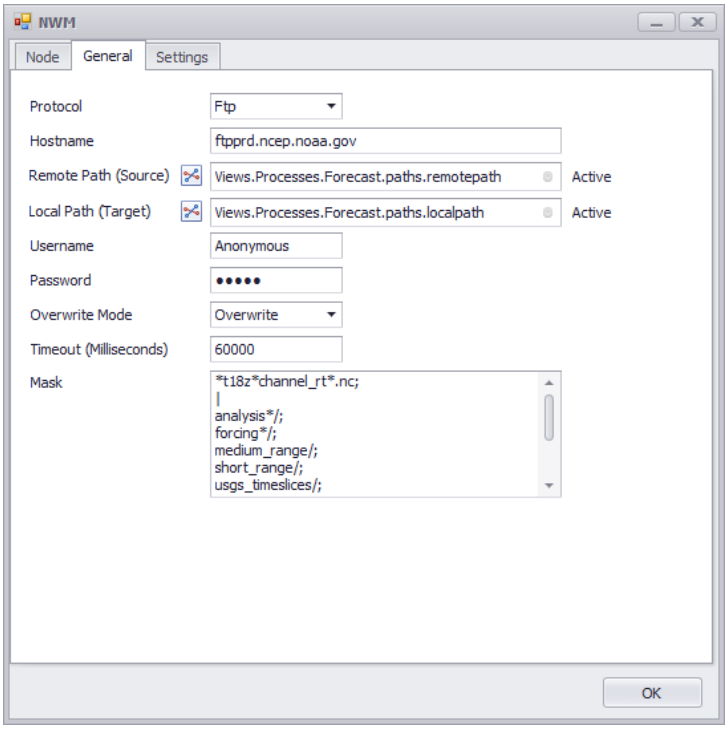

Figure A3-17. Downloader function showing parameters defined to download NWM forecast

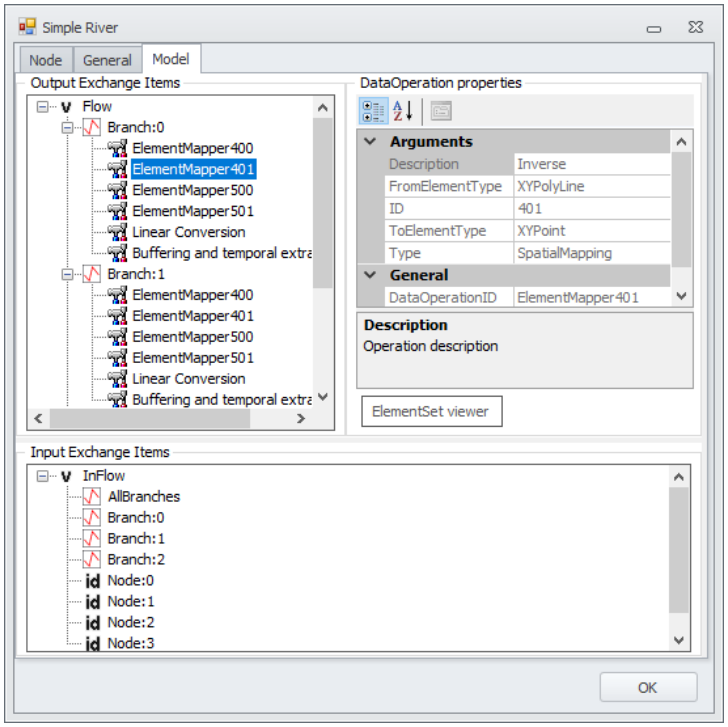

Figure A3-18. OmiModel function properties form showing output and input exchange items for Simple River model

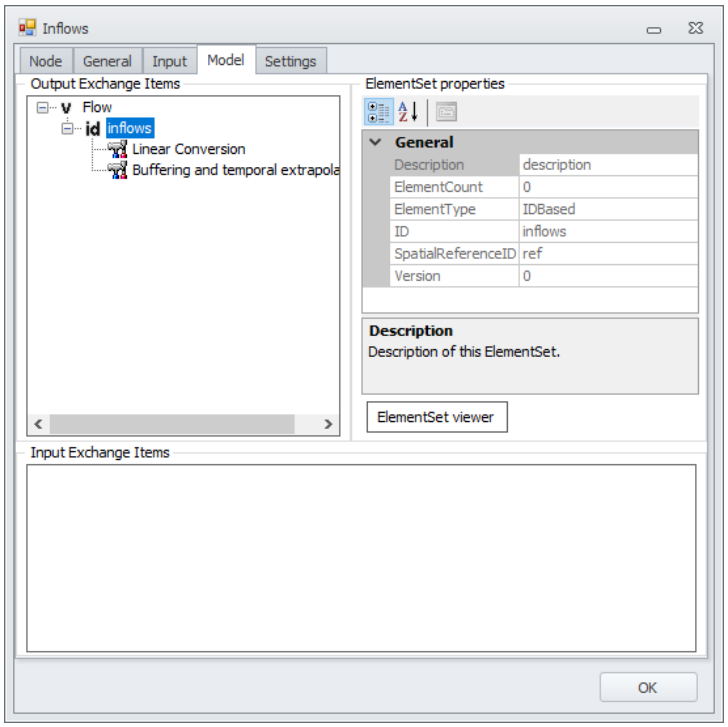

Figure A3-19. OmiInput function properties form showing output exchange item automatically generated for the input variable ‘inflows’

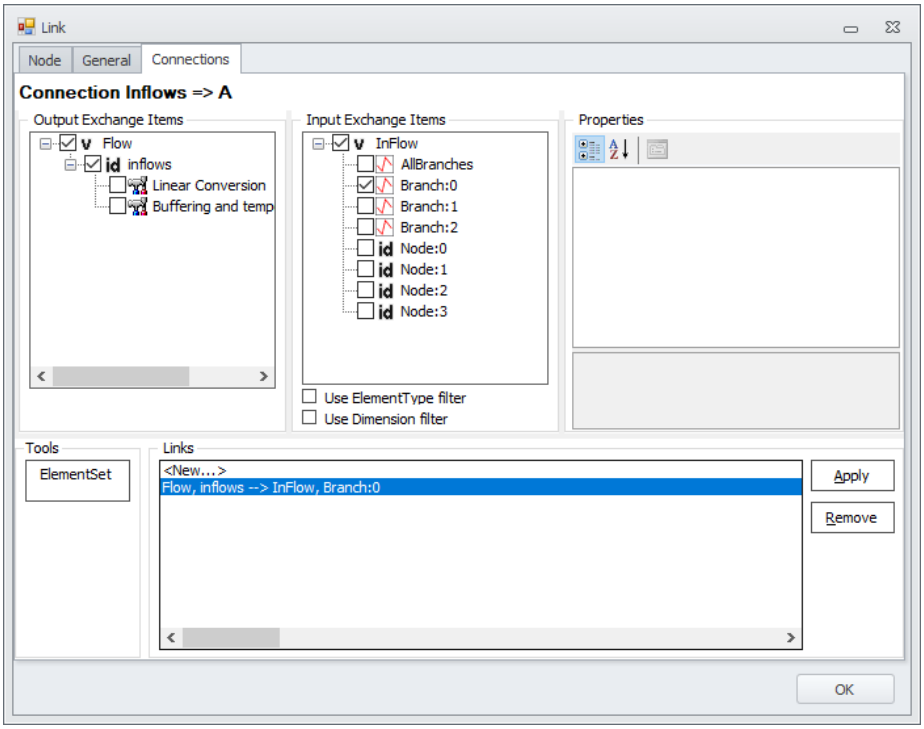

Figure A3-20. OmiLink properties form showing an OpenMI link between OmiInput function and Simple river model component for ‘inflows’

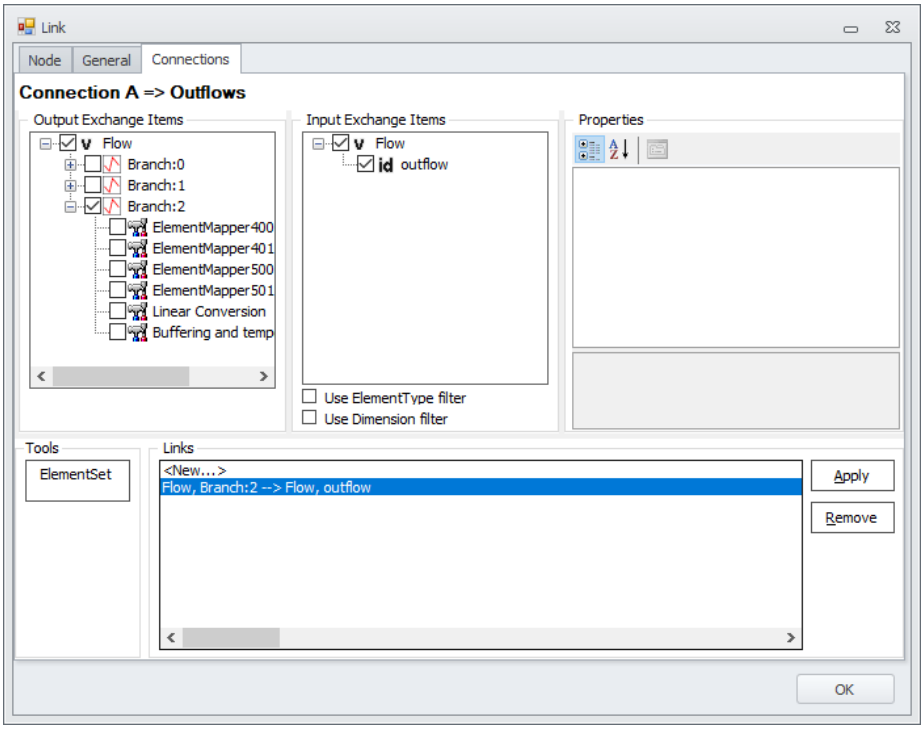

Figure A3-21. OmiLink properties form showing an OpenMI link between Omioutput function and Simple river model component for ‘inflows’

Chapter 4 A decision support system for indirect potable reuse based on integrated modeling and futurecasting

A. G. Lodhi[1, *], A. N. Godrej[1], D. Sen[1,2], R. Angelotti[3], M. Brooks[3]

[1] Occoquan Watershed Monitoring Laboratory. Virginia Tech. 9408 Prince William Street, Manassas, Virginia, 20110

[2] Santa Clara Valley Water District, San Jose, California 95118

[3] Upper Occoquan Service Authority, Centreville, Virginia 20121

[*] Corresponding Author. Email: adlodhi@vt.edu

Keywords: Decision Support System; Futurecasting; Integrated Modeling Indirect Potable Reuse; National Water Model; Wastewater Treatment

Published in 2019 in Journal of Water Reuse and Desalination

4.1 Abstract

Optimal operation of water reclamation facilities (WRFs) is critical for an indirect potable reuse system (IPR), especially when the reclaimed water constitutes a major portion of the safe yield, as in the case of the Occoquan reservoir located in Northern Virginia. This paper presents how a reservoir model is used for predicting future reservoir conditions based on the weather and stream flow forecasts obtained from the Climate Forecast System and the National Water Model. The resulting model predictions provide valuable feedback to the operators for correctly targeting the effluent nitrates using a plant operations and optimization model called IViewOps. The integrated models are run through URUNME, a newly developed integrated modeling software, and form a Decision Support System (DSS). The system captures the dynamic transformations in the nutrient loadings in the streams, withdrawals by the water treatment plant, WRF effluent flows, and the plant operations to manage nutrient levels based on the nitrate assimilative capacity of the reservoir. The DSS can provide multiple stakeholders with a holistic view for design, planning, risk assessments, and potential improvements in various components of the water supply chain, not just in the Occoquan but in any reservoir augmentation type IPR system.

4.2 Introduction

Reliable and optimal operation of a water reclamation facility (WRF) is a fundamental risk management component for an indirect potable reuse (IPR) system. It requires timely and informed decision-making in response to fluctuating operational conditions, *e.g.* weather

patterns, plant performance, water demand, etc. Futurecasting of IPR systems consists of modeling different near-term future scenarios supplemented by medium to long-range weather forecasts, which provides useful feedback to decision-makers. Such predictive analyses can aid in alleviating future risks associated with water availability and quality without the need to install and maintain large standby capacities.

Over the years, the interest in integrated water resource management (IWRM) has increased significantly. IWRM takes a comprehensive approach to water management by viewing the water supply, drainage, and sanitation systems holistically. To develop design and management tools for a better understanding of these integrated systems and their complex behaviors, an integrated modeling approach is required. According to Rauch et al. (2002), the concept of integrated modeling was proposed as far back as 1970. The first integrated urban drainage model was applied in 1980, though the concept did not become widely adopted until the 1990s (Mitchell et al. 2007). Since then, there have been many applications of IWRM modeling focused on the simulation of entire urban water systems (Coombes and Kuczera 2002; Schütze et al. 1996). Similar approaches have also been used in integrated watershed management. Wu et al. (2006) implemented a watershed runoff model HSPF (Hydrological Simulation Program - Fortran) coupled with a reservoir model CE-QUAL-W2 for the Swift Creek watershed in Virginia. A more complex model of seven HSPF and two CE-QUAL-W2 applications has been used for the Occoquan watershed in northern Virginia (Xu et al. 2007). Integration of different models to simulate an IPR system, however, has not been reported in the literature to the best of the author's knowledge.

There are several approaches to integrated modeling. Some software applications provide built-in integration to simulate a coupled system, where the models for different sub-systems are either contained within the software or are linked automatically. Coupled models are based on integrating different standalone models that simulate various components of the target system individually (e.g. watershed, reservoir, treatment plants, etc.). Integration of such models is carried out using different levels of sophistication: from manual coupling to fully automated systems. Coupled models are commonly operated sequentially (Rauch et al. 2002; Schütze et al. 1996; Xu et al. 2007). This loosely coupled modeling approach is unidirectional and flow paths are configured as a tree-like structure. Although this approach seems relatively simple, there is

voluminous data input, output, and transfer between the models (Azmi and Heidarzadeh 2013). In addition, some of these models are not very user-friendly, take a significant amount of time to run, and require a significant level of familiarity with the model structure to operate. A more advanced coupling approach called iterative coupling, on the other hand, relies on the tight coupling of sub-systems to create model synchronization based on back-and-forth data transfer for each time-step using either a standard or custom protocol. An example of one such standard framework is Open MI (Open Modeling Interface) (Moore and Tindall 2005).

Futurecasting involves strategic planning by evaluating system dynamics, predictive analysis, and a variety of other strategies to help develop an insightful vision of the future. Shah et al. (2017) examined short to medium-range forecast data (7-45 days) to study water and agriculture resource management in India using GEFS (Global Ensemble Forecast System) and CFS v2 (Climate Forecast System). By using forecast data as an input to simulate forecasted runoff and soil moisture, they were able to show that their methodology could provide timely information in decision-making for farmers and water managers. A near real-time drought monitor was also developed to estimate the severity and extent of agricultural and hydrologic droughts (Shah and Mishra 2015).

The overarching goal of this research is to develop a futurecasting application based on the integration of various in-house and weather forecast models and historical data sources. The outputs can provide useful feedback for plant operators to identify and analyze strategies to manage the WRF performance dynamically in response to future reservoir conditions. This paper will discuss the development and implementation of the integrated modeling application and will demonstrate its effectiveness as a decision support system (DSS) to inform and improve the reliable operation of the IPR system.

4.2.1 Study Area

The Occoquan Reservoir is located in northern Virginia and is one of the two major water supply sources (the other being the Potomac River) for several municipalities in the region. The reservoir spreads over an area of 6.9 km^2 and its drainage basin, the Occoquan watershed (Figure 4-1), spans across 1,484 km^2 (573 square miles). The reservoir has a full pool volume of 3.1 x 10^7 m^3, an average water depth of 5.1 m, and a maximum water depth of approximately 19 m

close to the dam. The reservoir has a full pool elevation of around 37 meters above mean sea level (m MSL) and mean hydraulic residence time is approximately 20 days (Xu et al. 2007). The mainstream of the Occoquan Reservoir is formed by the confluence of the Occoquan River and Bull Run tributaries, 14 km upstream of the Occoquan dam. The headwaters of the reservoir extend well up into these two arms of the reservoir which are called the Occoquan River Arm and the Bull Run Arm, respectively. The Upper Occoquan Service Authority (UOSA) WRF discharges into the free flowing stream above the Bull Run Arm, upstream of stream station ST45. The WRF has a total design capacity of 204,412 m^3/d (54 mgd) and currently operates at an average of 121,133 m^3/d (32 mgd). The contribution of the WRF to the reservoir's inflow routinely varies throughout the year, usually going up to 50% of the total inflow during the late summers and early fall and, in some extreme cases, comprises up to 80% of the reservoir inflow. Fairfax Water's Griffith Water Treatment Plant (WTP) withdraws water from the tail end of the reservoir close to the dam, resulting in indirect potable reuse of the reclaimed water.

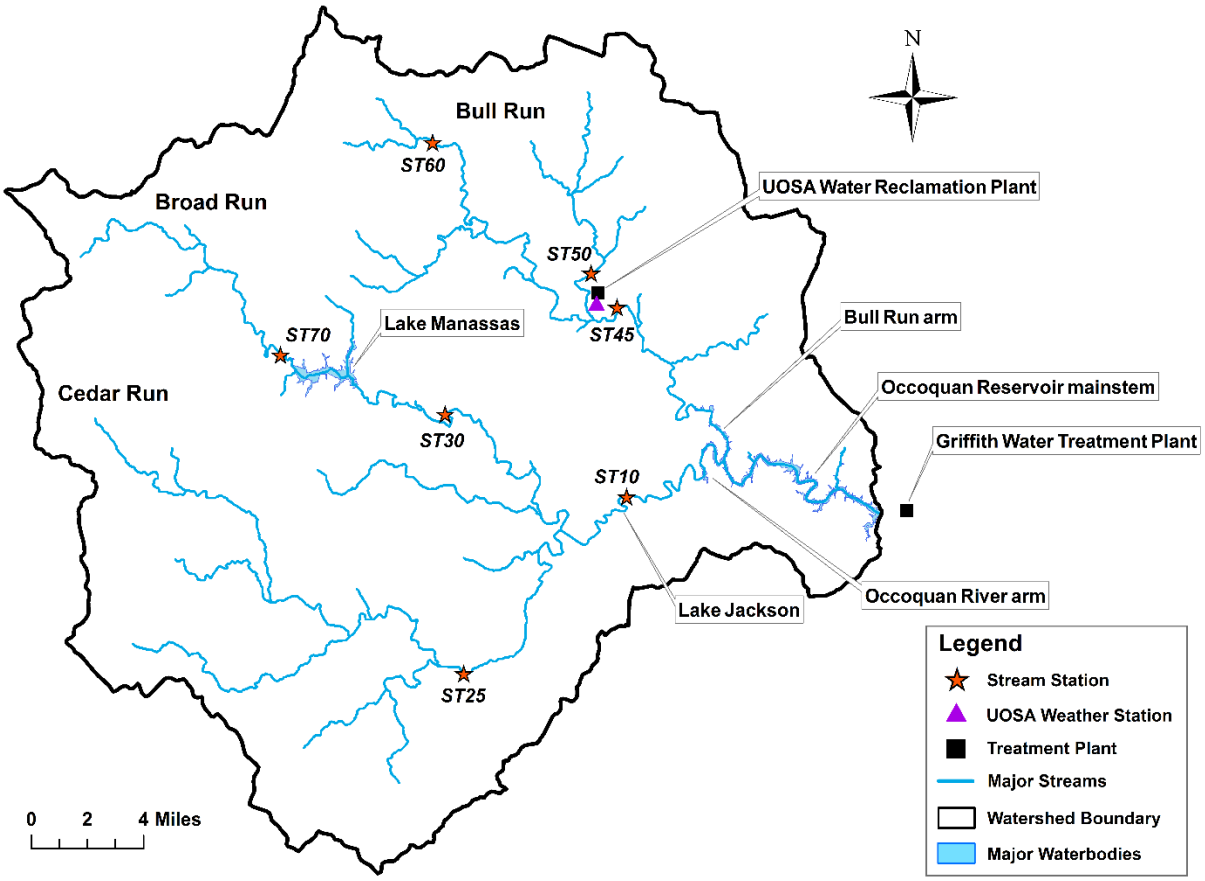

Figure 4-1. Occoquan Watershed

The Occoquan Watershed Monitoring Laboratory (OWML) is responsible for monitoring the watershed water quality. Over the years, OWML has established monitoring stations throughout the watershed to measure the flow and water quality in different streams (Currently operational: ST00/01, ST10, ST25, ST30, ST45, ST50, ST60, and ST70). Continuous flow measurements are carried out at all the stations and data are logged and transmitted to the OWML's database servers on an hourly basis. To monitor the water quality, grab samples are taken from each station at different frequencies ranging from once a month to four times a month. During storm events, flow-weighted composite samples are collected using autosamplers to evaluate the average concentration of different constituents. Grab samples are also collected from seven locations (RE02, RE05, RE10, RE15, RE20, RE30, and RE35) on the Occoquan Reservoir for quality monitoring (Figure A4-1). Temperature, dissolved oxygen, nitrate, pH, oxidation-reduction potential (ORP), and conductivity data are collected in situ at different water depths (usually at 1.5 m intervals, starting at 0.3 m from the surface) at frequencies ranging from once a month to three times a month. Many other constituents (such as nitrogen and phosphorus forms, total organic carbon, etc., are measured, via sample retrieval and transport to the laboratory for analysis, at the top and bottom of the reservoir stations. OWML also operates a weather station located close to the WRF (called OWML weather station at UOSA) which measures different meteorological parameters including rainfall, air temperature, solar radiation, wind speed and direction, humidity, etc., which are transmitted on an hourly basis to OWML's database servers.

4.3 Methods

Regulation of nitrate in reclaimed water throughout the year is a unique operational challenge at UOSA. Its operating permit limits the total annual nitrogen load to 6.0×10^5 kg (1.316×10^6 lb). More than 90% of this load is discharged in the form of oxidized nitrogen, mainly as nitrate (NO_3). Although the MCL (Maximum Contaminant Level) for nitrate in drinking water is 10 mg/L as nitrogen, the Occoquan Policy (VSWCB 1971) specifies a Water Quality Objective (WQO) of 5 mg/L at the dam. The WRF is therefore required by permit to reduce its nitrate discharge concentration when the nitrate concentrations at the drinking water intakes rise above 5 mg/L.

It has been observed that during thermal stratification and extremely low hypolimnetic oxygen concentrations in the summer, the supply of nitrate from UOSA actually benefits the reservoir.

Under these conditions, microbes in the sediment utilize nitrate as an electron acceptor in the absence of oxygen, advancing the denitrification process. As a result, the release of phosphorus (P) and other less preferential electron acceptors, Mn^{2+} and Fe^{2+}, into the water column is inhibited. The reservoir overturns at the beginning of fall and remains well-mixed throughout the winter and early spring. The mixing redistributes oxygen across the entire water column and restores the aerobic conditions, thereby diminishing the denitrification capacity of the reservoir.

A nitrate discharge optimization study (Bartlett 2013) concluded that the total nitrogen load delivered into the reservoir by the WRF can be more effectively distributed each month based on the reservoir's denitrification capacity. Based on these recommendations, UOSA changed its operational strategy by reducing the degree of denitrification in summer to ensure a higher concentration of nitrate in the effluent and then transitioning back to increased denitrification just before reservoir turnover, generally in early fall. Using the optimized load distribution provided in that study, average monthly concentrations were calculated using the average monthly flows from the last five years (2013-2017) compared to the observed average monthly concentrations during the same time period, as shown in Table 4-1. The results indicated that the WRF is unable to meet the low nitrate loads recommended during winters mostly due to various operational constraints, including limited organic carbon and low water temperatures which hinders denitrification. During at least one winter drought in the past, UOSA reportedly had to add methanol under emergency conditions to improve the denitrification process when exceedance of the WQO was imminent. On the other hand, in the summer months, there is insufficient TKN in the raw influent to generate desired nitrate loads. Although there is underutilized Occoquan reservoir denitrification capacity in the summer, several in-house studies have shown that certain storm events at low pool elevations may still briefly increase nitrate concentrations to levels above the WQO due to high nitrate loads from the WRF.

Table 4-1. Optimized load distribution

Month	**Average Monthly Flows**		**Optimized Loads**	**Optimized Concentrations**	**Actual Concentrations**	**%Diff**
	mgd	m^3/d	kg	mg/L	mg/L	
Jan	33.6	127080	21000	6.9	9.0	23.3
Feb	34.9	132073	21000	6.6	9.2	27.9
Mar	35.6	134677	21000	6.5	7.7	16.0

Apr	33.6	127334	21000	6.9	6.9	0.0
May	36.2	137039	93000	28.3	13.9	-103.7
Jun	36.1	136510	93000	28.4	15.2	-86.5
Jul	34.1	129086	93000	30.0	16.3	-84.2
Aug	33.1	125112	89000	29.6	17.7	-67.2
Sep	33.1	125305	89000	29.6	14.6	-102.7
Oct	34.7	131483	21000	6.7	10.4	36.0
Nov	34.3	129658	21000	6.7	9.1	25.9
Dec	37.7	142805	21000	6.1	8.0	23.1
Total			**604000**			

As also noted by Bartlett et al. (2013), these optimized loads cannot be used as a fixed allocation schedule for the WRF due to the dynamic nature of the system. In winter months, the optimized nitrate load distribution is quite conservative, as it is calculated based on the worst-case scenario using extremely low natural stream flows (winter drought). The effect of any change in the discharged load from the WRF on the nitrate concentrations at the dam is based on the hydraulic retention time of the reservoir, which may vary from a few days to months, depending on the inflows. Therefore, many factors including the pool elevation, volume and quality (temperature, background nitrate concentration, etc.) of stream inflows, withdrawal by Griffith WTP, and weather forecast can all affect the future conditions of the reservoir, and consequently its denitrifying capacity. Hence, selecting the desired monthly nitrate concentration for the effluent is still a trial and error process, largely based on the operator's judgment.

The growing water demand caused by urbanization complicates this process further. The safe yield of drinking water from the Occoquan Reservoir, including the reclaimed water, is 3.0 x 10^6 m^3/d (79 mgd). UOSA's contribution to the inflows has been steadily increasing over the years and, based on the current projections, will exceed 50% of the safe yield after 2025. In reference to Table 4-1, this corresponds to an optimized effluent nitrate concentration of around 5 mg/L for winters, which is unachievable based on the existing operational capability. Moreover, WRF plants are always subject to perturbation due to maintenance issues and/or system outages which can temporarily compromise plant performance. UOSA's operation is regulated by the Occoquan Policy which requires increasing the plant's standby capacity and engineered storage to address worst-case scenarios which results in significant financial obligations.

Various models have been used by stakeholders to understand and improve the water quality of the Occoquan watershed.

4.3.1 IViewOps (Intelligent View of Operations) Model

UOSA is currently using a wastewater and reuse process simulation software IViewOps as a day-to-day tool for simulating changes to operation and effect of assets out of service for maintenance (Sen et al. 2015). IViewOps is a multi-layer model that analyzes and optimizes the plant on three levels: (1) biochemical process modeling (2) asset's condition and capacity, (3) hydraulic configuration and bottlenecks in each possible operating configuration. It reads data directly from SCADA (Supervisory Control and Data Acquisition system), LIMS (Laboratory Information Management System) and CMMS (Computerized Maintenance Management System) to run the most recent operational configuration. Although IViewOps is a very helpful tool for plant operators, a more comprehensive methodology is needed to understand the effect of various nitrate concentrations on the current and future reservoir conditions in order to reevaluate the operational strategy if required. For instance, it would be helpful to know: (1) the target effluent nitrate concentration, (2) the effect of higher WRF contribution during droughts, (3) the length of time available before the WQO is exceeded, if the WRF effluent nitrate concentration increases due to any operational constraint, (4) the effect of an expected rain event, especially after a long dry period.

4.3.2 Climate Forecast System – Weather Model

The National Oceanic and Atmospheric Administration (NOAA) Climate Forecast System (CFS) is a climate model which provides medium- to long-range numerical weather predictions. The atmospheric component of the model has a horizontal spectral triangular truncation of 126 waves (T126), equivalent to ~100 km grid resolution. The long-range (~9 months) hourly forecast consists of four cycles per day at 0000, 0600, 1200 and 1800 UTC (Saha et al. 2014). Forecasts for a specific location can be extracted from the model output by either simply using the value from the nearest grid point or using some form of interpolation between the surrounding grid points (WMO 2012).

CFSv2 reforecast data are available for 29 years (1982-2010), from every January 5th, on the same horizontal and vertical resolution as the operational configuration. Bias correction is used

to calibrate the raw forecast data from CFS. This method assumes that model error stays constant in time, i.e., the relationship between the distributions X_{OBS} (Historical observed) and X_{REF} (CFS reforecast) is the same as the relationship between distributions X_{FOR} (CFS raw forecast) and X_{CAL} (Calibrated forecast) (Ho et al. 2012). Assuming the exact distribution of X_{OBS} and X_{FOR} are unknown, quantile mapping can be used to match the statistical moments of the observed to simulated data. In this method, Cumulative Distributive Functions (CDF) of X_{OBS} and X_{FOR} are generated, for each meteorological parameter, using Weibull plotting position X_{CAL} and is calculated by:

$$X_{CAL} = F_{OBS}^{-1}\left[F_{REF}\left(X_{FOR}\right)\right]$$

Where F_{REF} is the CDF for X_{REF} and F_{OBS}^{-1} is the inversed CDF for $X_{OBS.}$

4.3.3 National Water Model

The NOAA National Water Model (NWM) is a hydrological model that forecasts stream flows across the continental United States and has been operational since Aug. 16, 2016. A long-range 16-member ensemble forecast is produced every day going out to 30 days in the future. There are 4 ensemble members in each cycle, each forced with a downscaled and biased corrected CFS model. The core component of NWM is the Weather Research and Forecasting Hydrologic model (WRF-Hydro) by the National Center for Atmospheric Research (NCAR). WRF-Hydro is configured to use Noah-MP Land Surface Model (LSM) to simulate land surface processes in NWM (Niu et al. 2011). At present, NWM provides reforecast data and there is no archive available for old forecasts (only two days of forecast data are maintained on the FTP server at any point in time). Therefore, the raw forecast is used without any calibration in this model. It must, however, be noted that the current version of the NWM does not include the operation and management of lakes and reservoirs within the model.

4.3.4 Occoquan Reservoir Model

The Occoquan Reservoir is modeled using the U.S. Army Corps of Engineers software CE-QUAL-W2, a two-dimensional longitudinal/vertical hydrodynamic and water quantity model (Cole and Wells 2011). It is an open-source model written in Fortran which simulates the water quality in a waterbody, using longitudinal segments and vertical layers while assuming complete

lateral mixing (appropriate for long, narrow, riverine reservoirs such as the Occoquan). The reservoir is modeled using 4 branches and 69 longitudinal segments (Figure A4-2). Branch-1 is the mainstream of the reservoir, starting from the Occoquan River and extending up to the dam. Branch-2 is the Bull Run Arm, discharging from the northern part of the watershed and the WRF to Branch-1. Branch-3 and Branch-4 are Sandy and Hooes Run, respectively, which are relatively small tributaries.

The major boundary conditions for CE-QUAL-W2 are (1) flow and water quality parameters for each branch and the reservoir periphery (i.e. distributed flows), (2) meteorological data, and (3) any water withdrawals (e.g. Griffith WTP). Time series for these parameters are entered for a simulated time period in various fixed-width text files using Julian days. Each branch and distributed flow in the model requires a separate input for flows (m^3/s), constituent concentrations (TSS, OP, NH_3-N, NO_X-N and DO) (mg/L), and water temperatures (^oC). Additional precipitation data are required for each branch including rainfall intensity (m/s), constituent concentrations (mg/L), and temperature (^oC). A separate text file is used to input the meteorological variables for the entire waterbody including air temperature (^oC), dew point temperature (^oC), wind speed (m/s), wind direction (radian), cloud cover (0-10), and radiation (W/m^2). The discharge from the WRF is modeled as a point source to Branch-2. Water withdrawal from the Griffith WTP is inputted as Branch-1 outlet flows using a separate file. At the start of each model run, initial water level and constituent concentrations are also required. All the major input parameters required for the CE-QUAL-W2 model run are summarized in Figure 4-2.

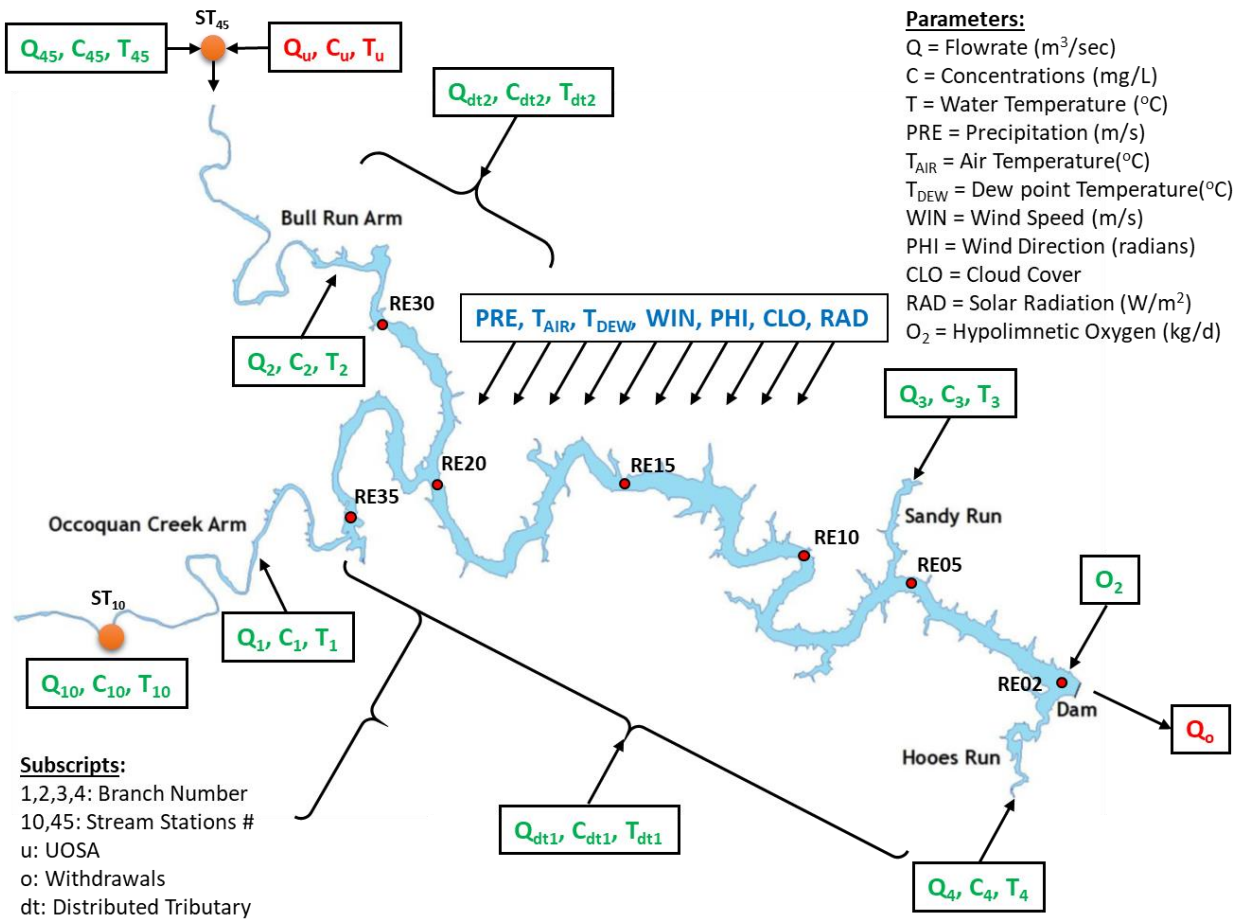

Figure 4-2. Integrated Model Inputs for Occoquan Reservoir

4.3.5 Hypolimnetic Oxygenation System Model

A Hypolimnetic Oxygenation System (HOS) has been operational in the Occoquan Reservoir since 2012. It primarily consists of a line diffuser (Figure A4-3) that runs from the dam to the deepest section of the reservoir along the original stream channel, almost equally divided between segment 47 and 48 of the model. The system is generally started at the end of spring, gradually increases the oxygen flow rate to its maximum during August and September, throttles back to its minimal flow, and then is stopped sometime during fall.

Since CE-QUAL-W2 cannot simulate complex bubble-plume dynamics, oxygen mass rate (kg/day) must be individually inputted for each layer and mixing must be simulated using a vertical mixing coefficient. This method is an oversimplification of complex bubble-plume dynamics and therefore is usually unable to predict the correct oxygen concentrations and

temperatures caused by mixing in the water column. A dedicated line diffuser model was proposed by Singleton (2008) to simulate a linear two-dimensional or planar bubble plume governed by the differential equations for mass, momentum, and heat. This linear plume model (LPM) uses the discrete bubble approach to simulate the oxygen distribution and mixing in the vertical layers of the water column. It requires the boundary conditions, such as temperature and oxygen distribution, along the water column to compute oxygen transfer rates and mixing flows.

An iterative coupling approach is required to apply LPM to the reservoir model. By default, CE-QUAL-W2 is compiled into an executable file which cannot be accessed by any external software. It was therefore reprogrammed into a Dynamic Link Library (DLL) (W2Model.dll). A number of new subroutines were added to the existing code that can be accessed externally to (1) initialize the model, (2) run a single timestep, and (3) read and write different configurational and simulated data. A new software, called W2Coupler, was developed in C#.NET to iteratively solve the plume model and transfer data back and forth between the reservoir model and LPM at each timestep. A new graphical user interface (GUI) was developed in W2Coupler, which replaced the default CE-QUAL-W2 Form (screen showing the run progress) and incorporated additional information including depth of maximum plume rise (DMPR) and oxygen mass rates and entrainment flows for each layer. The GUI contains options for entering LPM parameters and setting properties of the oxygenated segments. The time series for the oxygen flow rate (N-m/min) of each segment is inputted into W2Coupler using a separate text file, oin_x.npt, where postfix ‘x’ is the segment number.

The coupler first runs the reservoir model for each user-defined timestep and reads the simulated boundary conditions, including the temperature and oxygen depth profiles, for each oxygenated segment in the reservoir. It then solves the LPM’s nonlinear differential equations using the fourth-order Range-Kutta method to calculate the oxygen transfer and entrainment flow for each layer, as well as the depth of maximum plume rise (DMPR). To simulate mixing, W2Coupler automatically adds dynamic pumps (A feature in CE-QUAL-W2 to model pumps in the reservoir) to the reservoir model equivalent to the number of layers in each of the oxygenated segments. Each pump is set to withdraw water from its associated layer, equal to the entrainment flow, and discharge it at the DMPR layer. The calculated parameters are then inputted back into the reservoir model for the next timestep. This iterative process is carried out throughout the

simulation until the end of the run. The source code for W2Coupler and the modification in CE-QUAL-W2 is provided in the supplement material of this paper for free distribution and reuse.

4.3.6 Decision Support System

4.3.6.1 URUNME Software Application

A new software application, called URUNME, is developed in C# language for model integration and automation (Lodhi et al. 2018). This application works as a thin layer between the users, models, and data sources, practically hiding the mechanics of the modeling process. It provides a user-friendly GUI based on drag-and-drop functionality and uses simple flow chart type diagrams for Project configuration (saved as a .urm file). A single diagram is called a process, which consists of different functions and/or sub-processes interconnected through links. Each function is used to accomplish different tasks including running external models, reading and writing data from different formats (database, text files, excel, netCDF, WDM, etc.), uploading and downloading from web servers, statistics (Built-in R support, etc.), time series transformation (aggregation, missing data infilling, etc.), querying database (SQL), expression evaluator (Excel style built-in formulas), etc. URUNME contains an embedded SQLite database for storing data (saved as a .db file). Data generated by functions is saved in the embedded database and is represented as vector and scalar variables, shown as nodes in the project explorer. These variables support various engineering units and conversions and can be dragged and dropped onto other functions as an input (e.g. writing to a file) or onto other GUI items for data visualization. URUNME employs a powerful graphics engine for creating insightful and information-rich dashboards for data visualization. Multiple views can be used in the application to create different screens for users. Creating a dashboard is as simple as adding a GUI element (chart, pivot table, gauge, map, grid, image, text, event manager, etc.) on the screen and dragging and dropping variables onto these panels for data binding. These GUI elements are automatically updated in case of any change to the underlying data (e.g. after a model run). One of the key features of URUNME is the capability of creating and running multiple scenarios of the model using different inputs. Any function parameter (e.g. file name) can be made local (specific to that scenario) to run a different condition (e.g. input different meteorological data). Furthermore, different scenarios and processes can be run in a batch mode manually or by using the Scheduler feature, which allows runs to be scheduled at different times or on a periodic basis.

4.3.6.2 Operational Configuration

The DSS was setup using two separate projects in URUNME. The first project (model.urm) is responsible for running the integrated model and stores all the simulated and observed data in its embedded database (model.db). The database file is automatically uploaded to a dedicated FTP server after every model run. The second project (dashboard.urm) is created as an interactive dashboard, containing various menus and visual elements (charts, tables, diagrams, etc.) to show the most up-to-date futurecasting results and historical trends (Figure B 4-1 to Figure B 4-19). The dashboard project updates its elements directly from the model.db file. URUNME, installed on the computer of different users, uses the dashboard project to download the most recent data from the server to update the outputs on a periodic basis. This structure allows multiple users to run the DSS dashboard application independent of the model implementation.

URUNME reads from various data sources dynamically (data being continuously updated in different database) and performs extensive data analysis and manipulation before feeding it to the model as inputs or storing it as historical trends. All the operations carried out during the entire simulation process are fully automated and use hundreds of functions in various process flow diagrams. The overall data flow path to operate the model is shown in Figure 4-3.

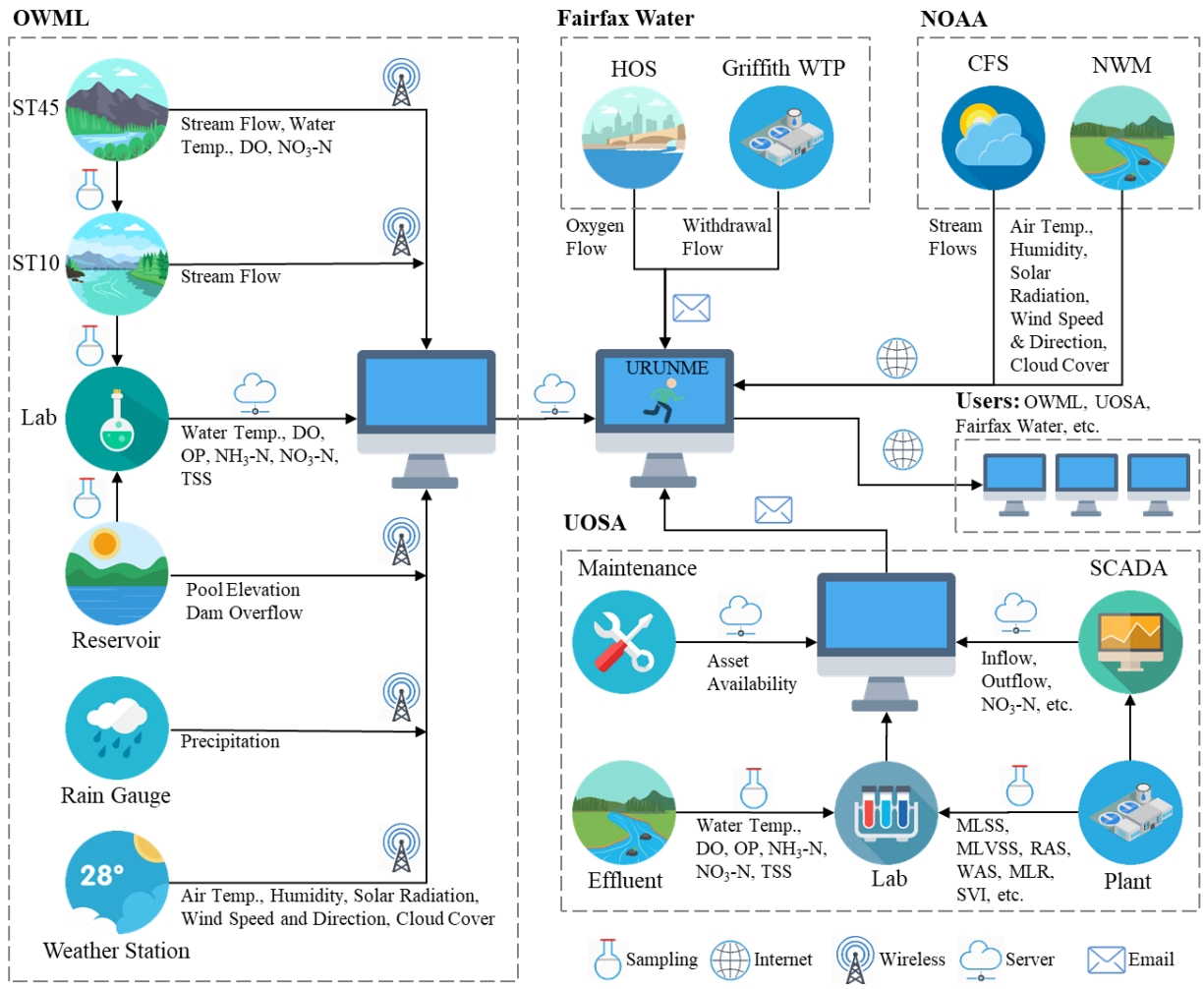

Figure 4-3. Data flow diagram for the integrated model

4.3.6.3 Calibration Scenario

The calibration scenario, called ‘base’, is used to evaluate the current model calibration using the last three years of observed data. Please note that for the Occoquan case described in this paper, these choices on data and simulation length are those taken for the Occoquan model application, and are not limitations imposed by URUNME. As long as there is sufficient storage space and memory available, URUNME has no documented limits on the size of the problem it is called upon to run. For this Occoquan run, inflows for all the branches and distributed areas were calculated from observed flows at ST10 and ST45. These flows are converted to model branch inputs by scale factors (Table A4-2) obtained by dividing the drainage area of each branch by the drainage area of the associated stream station. Water quality data for these stations are read separately for base and storm flows from the laboratory database. Base flow concentrations,

measured intermittently at these stations, are interpolated to create a time series for each input constituent and water temperature. The constituent values are then replaced by storm flow concentrations for the duration of each storm event. The meteorological data from the UOSA weather station is read from a text file updated hourly. HOS oxygen flow rates and water withdrawal by the WTP are provided by Fairfax Water through email and read into the embedded database. All the data are formatted and written to different model input text files.

The first step after the base run is to validate whether the simulated pool elevations, temperature, and different constituents are consistent with the values observed during the calibration period. In case of unsatisfactory calibration performance for any water quality parameter, recalibration has to be done manually before running the remaining forecast scenarios. It must, however, be noted that after successful initial calibration, frequent changes in model performance are not expected. Both graphical and statistical techniques are employed to keep track of the model's calibration performance. After every model run, timeseries plots of observed vs. simulated data are created by the DSS to provide an overview of the calibration and to identify the differences in time and magnitude of the data visually. Generally, an agreement between observed and simulated frequencies indicates an adequate model performance (Moriasi et al., 2007). Four different statistical indices are used for evaluating the model calibration including (1) Nash-Sutcliffe Efficiency (NSE), (2) Percentage BIAS (PBIAS), (3) Root Mean Square Error, and the (4) Coefficient of determination (R^2). NSE is a dimensionless normalized statistic that determines the relative magnitude of residuals compared to the measured data variance (Nash and Sutcliff, 1970). It ranges between $-\infty$ to 1, with NSE = 1 as optimal. Moriasi et al. (2007) has recommended some guidelines for acceptable NSE values for water quality calibration where NSE > (0.5, 0.65] is considered 'satisfactory', NSE > (0.65, 0.75] as 'good', and NSE > 0.75 as 'very good'. Although these recommendations are based on monthly means, the thresholds can still provide a reasonable basis for comparison for daily data. PBIAS is an error index, which measures the average tendency of the simulated data in comparison to the observed values (Gupta et al., 1999). The optimal value of PBIAS is 0. It can be either positive or negative, indicating under or overestimation bias respectively. Similar to NSE, Moriasi et al. (2007) has recommended guidelines for acceptable PBIAS for water quality based on a monthly timestep, where PBIAS < $\pm$ (70%, 40%] is considered 'satisfactory', PBIAS < $\pm$ (40%, 25%] as 'good', and PBIAS < 25% as 'very good'. RMSE is also an error index which is the average magnitude

of calibration error. Moriasi et al. (2007) have provided guidelines only for RMSE normalized by standard deviation but not for standalone RMSE values. R^2 describes the proportion of variation in observed data explained by the model. It ranges from 0 to 1, with 1 being optimal. It is very commonly used for model evaluation. Similar to the RMSE, no accepted guidelines are available for R^2.

4.3.6.4 Forecast Scenarios

To run the forecast scenarios, the latest CFS operational forecast GRIB2 files are automatically downloaded from the NOAA website for the four selected grid points closest to the UOSA weather station (Table A4-1). The data are first interpolated for the UOSA weather station using the Inverse Distance Method (Flitter et al. 2016) and then bias corrected before storing into the embedded database. To estimate stream flows, the four most recent ensembles are downloaded from the NWM website. There are a total of 120 netCDF files in every ensemble, each containing data for one timestep of six hours. Forecasted flows are read from these files as a 'streamflow' variable (m^3/s) using a feature_id key to identify the required stream's reach. Files for each ensemble are combined and flowrates for ST10 (feature_id: 22339083) and ST45 (feature_id: 22339527) are extracted from each ensemble using a scale factor of 0.01 (as indicated in the metadata of the netCDF files).

A total of 24 forecast scenarios were created using various combinations of boundary conditions including (1) Natural stream flows, (2) WRF discharge, (3) WRF effluent nitrate concentrations, and (4) WTP withdrawal. These user-defined timeseries include two possible natural stream flows (Q_1 and Q_2 [m^3/d]), two possible UOSA discharge flowrates (D_1 and D_2 [m^3/d]), three possible UOSA effluent nitrate concentrations (N_1, N_2, and N_3 [mg/L Nitrate-N]), and two possible WTP's withdrawal flowrates (W_1 and W_2 [m^3/d]). Future stream temperatures and water quality constituents are calculated using historical trends. Monthly averages for the base (C_b) and storm flow (C_s) concentrations are calculated from the last five years for ST10 and ST45. In addition, average monthly base flows (Q_b) are also calculated for the same period to identify any storm events in the forecasted flows. Timeseries for stream concentrations are created using C_b, unless forecasted flow for a given day is greater than Q_b, in which case C_s is used.

Two different forecasts are produced by the DSS. A 30-day forecast is based on NWM stream flows going out 30 days in the future. Q_1 and Q_2 are calculated using the average and either of

the maximum or minimum flows for each day in the four ensembles for ST10 and ST45. Long-range 90-day forecast, on the other hand, is used as a What-If-Analysis to simulate any worst-case scenario. For winter months, this forecast is generally used to simulate an extended drought period and its effect on the reservoir. Such droughts have been observed in the past, during both winter and summer, the worst of which lasted for around nine months in 1977. Such a scenario potentially increases the WRF's contribution to the inflows of the reservoir, which may lead to high nitrate concentrations, especially during winters. 90-day forecast is simulated after the first 30-day forecast for all the 24 scenarios. The expected stream flows during a drought condition for these 90 days are calculated using low flow frequency analysis (discussed later).

The overall execution flow path of the model is shown in Figure 4-4. First, the base scenario is run for the last three years. Using the restart feature in CE-QUAL-W2 v4.1, the boundary conditions are saved in a file at the end of the run for the last day of simulation. Data for each of the forecast scenarios are created and inputted to the model by URUNME before it is run, from the present day to 120 days in the future. All 24 scenarios are run sequentially using the present day boundary conditions from the saved file and the output data are saved into the embedded database.

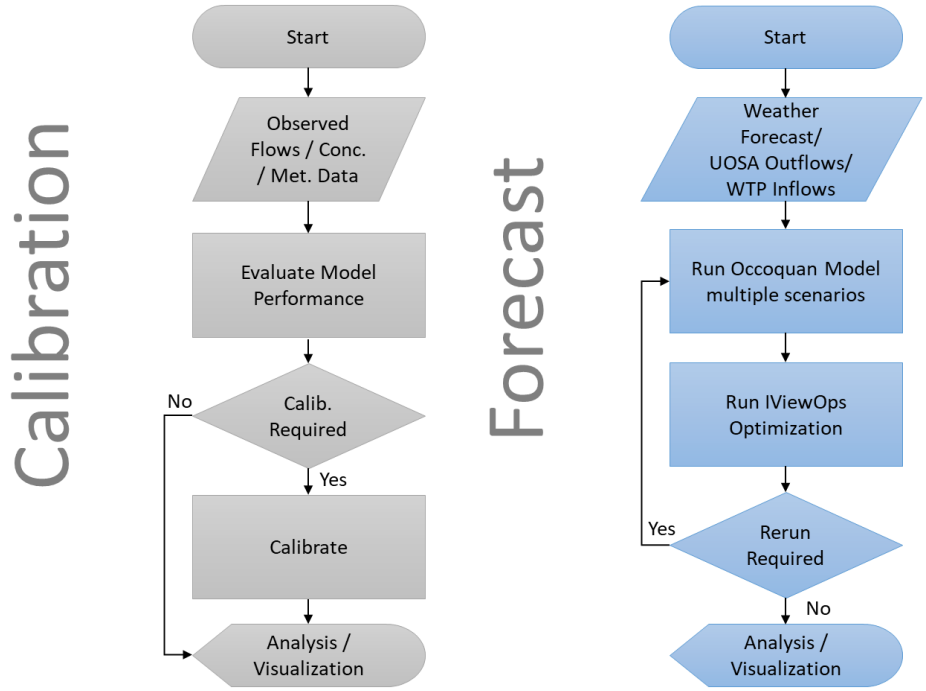

Figure 4-4. Execution path of the integrated model

4.4 Results and Discussion

The results presented in this section are for RE02, extracted from the DSS output generated on October 10, 2018. RE02 is located at around 0.5 km from the dam and is the closest sampling station to the WTP intakes (Figure 2).

4.4.1 Calibration of the Coupled Model

The base scenario was run for the last three years starting from January 1, 2015 to October 10, 2018. Observed and simulated timeseries plots of pool elevation, temperature, dissolved oxygen and nitrate concentrations are shown in Figure 4-5. The temperature and concentration plots contain the actual data collected from the reservoir bottom (shown as dots) along with the simulated model output (shown as solid lines) from the bottom-most layer. The calibration indices for all the reservoir stations, as calculated by the DSS are shown in Table 4-2.

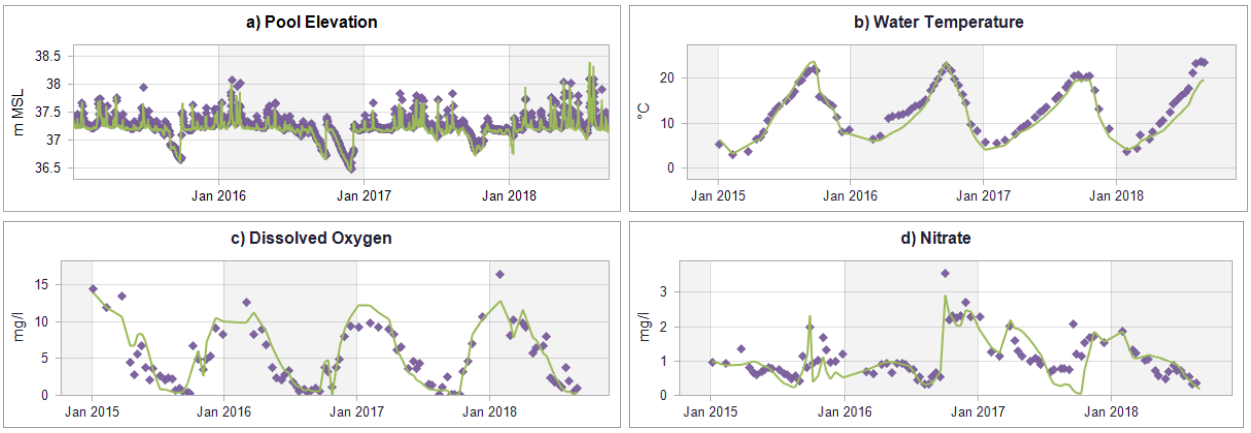

Figure 4-5. Calibrated pool elevation, temperature, dissolved oxygen, and nitrate (as nitrogen) (solid lines are simulated and dots are observed values). Temperature, dissolved oxygen and nitrate are bottom values.

4.4.1.1 Temperature

Due to inadequate hypolimnetic mixing, initial runs of the model under-predicted the bottom water temperatures at RE02. The poorer mixing was caused by a lower value of plume rise (DMPR) computed by the linear plume model (LPM) than the observed value of plume rise caused by hypolimnetic aeration.

The DMPR is most influenced by the initial bubble radius and entrainment coefficient (α) in addition to the oxygen flowrate (Singleton, 2008). The value of α was decreased from the

recommended value of 0.11 to 0.05. An initial bubble radius of 0.75 mm was used (which is the average of the manufacturer specified bubble radius of 0.5 to 1 mm). This fine-tuning increased the average DMPR and consequently the bottom water temperatures at RE02. The final calibration results for water temperature show NSE values between 0.73 to 0.97 for the bottom layer at all the reservoir stations. The PBIAS for all the reservoir stations remained within ± 10%. RMSE values remained between 1.0 and 2.8 ^{o}C, while R^2 ranged from 0.85 to 0.98.

Table 4-2. Calibration performance indices

Parameter	**Calibration**		**Reservoir Stations**						
	Index	***Unit***	***RE02***	***RE05***	***RE10***	***RE15***	***RE20***	***RE30***	***RE35***
Temperature	*NSE*		0.88	0.84	0.73	0.86	0.83	0.97	0.80
	PBIAS	%	7.7	9.8	12.6	2.2	-3.6	-2.0	-5.6
	RMSE	^{o}C	1.9	2.1	2.8	2.0	2.4	1.0	2.7
	R^2		0.92	0.90	0.85	0.90	0.92	0.98	0.91
Dissolved Oxygen	*NSE*		0.80	0.76	0.8	0.71	0.79	0.63	0.7
	PBIAS	%	-6.3	-13.5	-9.5	1.1	-14.5	9.1	-4.7
	RMSE	mg/L	1.7	1.8	1.8	2.1	2.1	2.37	2.5
	R^2		0.83	0.87	0.86	0.78	0.82	0.7	0.73
Nitrate Nitrogen	*NSE*		0.54	0.55	0.51	0.5	0.48	0.76	-0.92
	PBIAS	%	7.1	6.3	6.2	18.7	26.9	8.1	-27.0
	RMSE	mg/L	0.4	0.46	0.63	0.93	1.26	1.2	0.59
	R^2		0.62	0.65	0.51	0.53	0.57	0.78	0.02

4.4.1.2 Dissolved Oxygen

The initial calibration runs showed higher DO concentrations in the oxygenated segments of the model than those observed. Bryant et al. (2011) have demonstrated that the mixing induced by hypolimnetic oxygenation at the sediment-water interface increases the sediment oxygen demand (SOD). However, the reservoir model was setup with a constant zero-order SOD for each segment and provides no built-in mechanism to increase the SOD dynamically during a simulation. Therefore, modifications were made in the CE-QUAL-W2 code to enable the W2Coupler to read the current SOD from the reservoir model at each timestep and rewrite it back to the model after correction. A new option was created in the W2Coupler to enable the user to modify the SOD dynamically by entering any empirical equation as a function of SOD

and oxygen flowrate. A text editor is provided to separately enter the equation for each segment using SOD and Q with segment id as postfix (e.g. Q47 and S47 represents the current oxygen flow rate and SOD for segment 47). With this new capability, the model was run a number of times with different empirical formulations. Finally, the following equation provided the best calibration performance at $f = 0.07$ for both segments 47 and 48:

$$SOD_{new} = (1 + f_i \times Q_i) \times SOD_i$$

Where f_i is a calibration factor, SOD_i is the temperature-corrected SOD, and Q_i is the oxygen flow rate in N-m^3/hr for segment i at the current timestep. An f value of 0.07 corresponds to a 6.6 times increase in SOD at a maximum oxygen flowrate of 80 N-m^3/hr for each segment. NSE values shown in Table 4-2 indicates 'good' to 'very good' performance for dissolved oxygen with the exception of RE30, where NSE for dissolved oxygen is 0.63 ('satisfactory'). The PBIAS for all the reservoir stations remained within $\pm$ 15% which is considered "very good". RMSE values remained between 1.7 to 2.5 mg/L and R^2 between 0.7 to 0.87.

4.4.1.3 Nitrates

The nitrate calibration has shown mostly 'satisfactory' NSE values with the exception of RE20 and RE35 which are 'unsatisfactory'. Bartlett (2013) observed similar results due to high nitrate spikes at RE35 during low flows caused by the backflow from Branch-2 (Bull Run arm) to the Branch-1 (Occoquan River arm) of the model. This phenomenon is known to occur in the reservoir during summer and is poorly predicted by the model due to its inability to simulate an extended period of continuous bottom-layer anoxia upstream of RE35. This condition also affected the calibration of RE20 where NSE is slightly below 0.5. The PBIAS, however, has 'good' to 'very good' for all the stations. RMSE values remained within 0.4 to 1.26, where higher values are for stations close to Branch-2 (i.e. RE20 and RE30) due to higher inflow nitrate-nitrogen concentration from WRF. R^2 ranged from 0.51 to 0.78 excluding RE35.

4.4.2 Bias Correction for CFS

To determine the effectiveness of the bias correction in improving the forecasting skill, the method was first trained for ten years, between 2006 to 2015, and then applied to the raw forecast data for 2016 and 2017 for validation. Figure 4-6a indicates a good correlation between

observed and reforecasted air temperatures in the training period (R^2=0.73, NSE = 0.67 and PBIAS = 11.5%,). However, the CDF of these datasets plotted together in Figure 4-6b shows a significant bias, where the reforecast air temperatures are under-predicted in the entire range in general and at lower values in particular. After applying the bias correction to the validation period, the R^2, NSE, and PBIAS between observed and reforecast data improved from 0.72, 0.63, and 15.5% to 0.73, 0.71 and 3.6% respectively. Other parameters were also tested using the same method (not shown), although the improvements in the forecasting skill were not significant for some parameters.

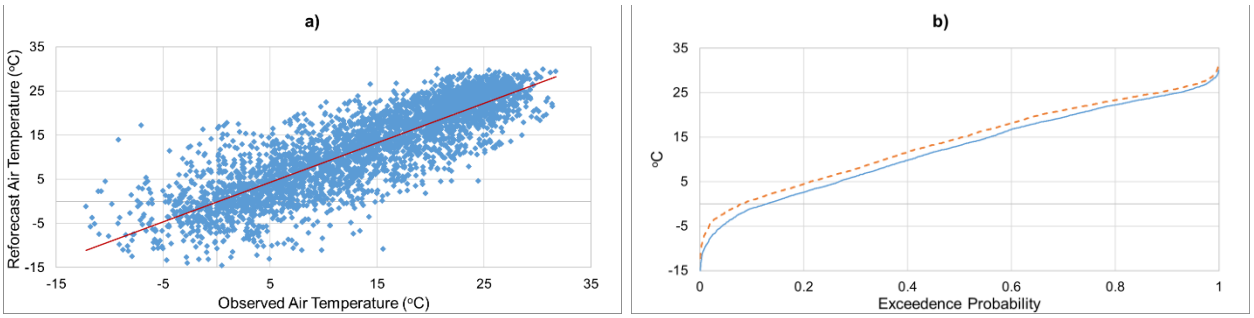

Figure 4-6. (a) Linear regression between observed and reforecasted air temperature (b) CDF for observed (dashed line) and reforecasted (solid line) air temperatures

4.4.3 Futurecasting

As explained earlier, different combinations of boundary conditions (Q, N, D, and W) are used to create forecasting scenarios. Most of these scenarios are selected in consultation with the stakeholders and are reviewed periodically based on different factors including time of the year, plant performance, water demand, etc.

For the 30-day forecast, the natural stream flows, Q_1 and Q_2 at ST10 and ST45 were obtained using the average and minimum of the four ensembles in the NWM forecast, respectively. The plant's effluent Nitrate-N concentration was set to 13.6 mg/L as N (N_2), the last 7-day average from the date of model run. Upper and lower values for the effluent nitrate concentrations, i.e. N_1 and N_3, were set to 0.75 and 1.25 of N_2, respectively. The WRF effluent discharge D_1 was taken from the projections for September and October (Table 4-1). To simulate higher than projected discharge conditions, D_2 was set to 149,524 m^3/d (39.5 mgd) which is approximately 15% higher than average D_1 for the year. Due to unavailability of the projected withdrawals from the WTP

for 2018, W_1 for the forecast was taken from the average monthly withdrawals in the last 5 years i.e. 2013-2017 (

Table A4-3). Finally, W_2 was set to the safe yield of the reservoir i.e. 299,048 m^3/d (79 mgd), to simulate the highest possible withdrawals from the reservoir.

Low-flow frequency analysis (Gustard and Demuth 2009) was carried out to develop the stream flows during the drought conditions simulated in the 90-day forecast. A 10-year return period (T) is used for this analysis, which is considered as an acceptable standard to calculate drought conditions. For instance, a commonly used term '7Q10' in low flow analysis represents the minimum 7-day flow expected to occur every 10 years. Historical daily flow data from USGS (US Geological Survey) and OWML databases were obtained for ST10 and ST45 from 1968 and 1973 onwards, respectively. First, an n-day (where n = duration) centered moving average is passed through the daily data to calculate the timeseries for the duration of 7, 15, 30, 60, 90 and 180 days. Annual minima were then derived for each duration by selecting the lowest flow every year. A cumulative distribution function (CDF) was developed using the yearly minimum flows and low flows were then calculated by selecting the exceedance probability (p) of 0.1 (T = 1/p) on the CDF (Figure 4-7). Low flows for 90Q10 were selected corresponding to the forecast duration of 90 days. Using these flows, UOSA contribution for 90-days forecast would remain close to 62.5% of the total reservoir inflows. For effluent nitrates, N_2 was set to 10 mg/L based on the average effluent nitrate concentration from October to January (Table 4-1). N_2 and N_3 were set at 7.5 mg/L and 12.5 mg/L respectively. Discharge and withdrawal scenarios were set similar to 30-days forecast.

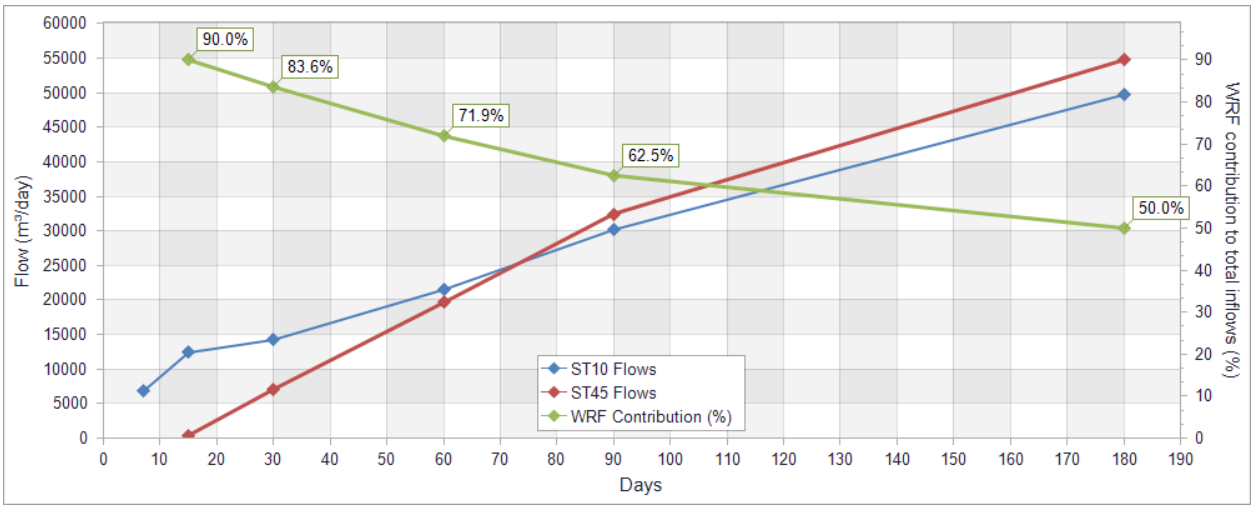

Figure 4-7. Low flow frequency analysis for different n-moving averages using 10 year return period

The forecasted bottom-layer water temperature profiles are shown in Figure A4-4. The predicted values are consistent with the observed water temperatures during the forecasted months and therefore indicate an acceptable model performance. The nitrate profiles were outputted for the middle layer (Figure 4-8), which is around the same level from where most of the water is withdrawn by the WTP. These results are for the stream flows in Q_1 scenario followed by 90Q10 drought flows (there was no significant difference between the output from Q_1 and Q_2). The model run showed no significant change in the nitrate during the 30-days forecast (shown with green background) and concentrations remained well below 1 mg/L. NWM predicted relatively higher stream flow for the 30 days which reduced the UOSA contribution to the total inflows to the reservoir to around 11% on average. The dilution caused by the higher stream flows kept the nitrate levels below 3 mg/L at ST45 during all the N scenarios. Additionally, the reservoir denitrification capacity remained significantly high during September due to relatively higher water temperatures causing low nitrate concentrations.

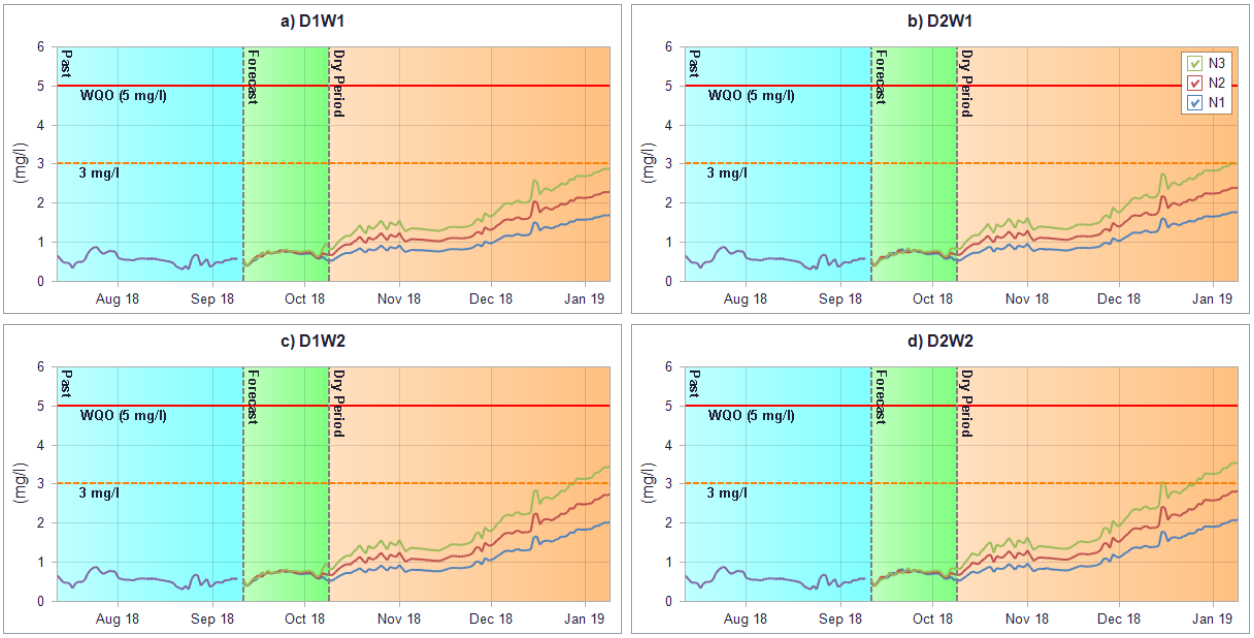

Figure 4-8. Nitrate profiles for different scenarios at RE02. (D_1 = Projected monthly WRF discharge, D_2 = fixed WRF discharge at 149,524 m^3/d (39.5 mgd), W_1 = WTP withdrawals based on last 5 years of monthly averages, W_2 = fixed at 299,048 m^3/d (79 mgd), N_1, N_2 and N_3 are WRF Effluent nitrate-N set at 7.5, 10 and 12.5 mg/L)

For D_1W_1 (Figure 4-8a), the nitrate concentrations at RE02 reached a maximum of 1.7, 2.3, and 2.9 mg/L for N_1, N_2, and N_3, respectively, at the end the forecast. A drawdown of 0.63 meters (2.1 ft) in the pool elevation was simulated by the model due to higher WTP withdrawals compared to the total inflows to the reservoir on average. Although D_2W_1 (Figure 4-8b) scenarios were simulated with higher effluent discharge corresponding to 15% additional Nitrate-N load to the reservoir, the results did not show any significant changes in nitrate concentrations compared to D_1W_1. This can be attributed to the lower drawdown in this scenario (0.4 meters) due to higher WRF contribution. The relatively higher HRT in this scenario is counteracting the effect of higher nitrate loads. This signifies that in severe drought conditions, the higher WRF effluent flows would actually be beneficial for the reservoir, delaying the increase in nitrate levels at RE02 due to higher HRT. In both D_1W_2 and D_2W_2 scenarios (Figure 4-8c and Figure 4-8d respectively), the nitrates at RE02 increased faster when the withdrawal was increased from W_1 to W_2 (299,048 m^3/d). A higher effluent nitrate-N from UOSA (N_3 = 12.5 mg/L Nitrate-N) resulted in 3 mg/L nitrates at RE02 after approximately 79 days. Again the main reason was higher drawdowns, 1.5 meters and 1.25 meter for D_1W_2 and D_2W_2 respectively, which essentially lowered the capacity of the reservoir to resist change.

The nitrate levels shown in the above results remained under the WQO limit in all the twelve (12) scenarios. This would indicate that an extended winter drought based on 90Q10 is not going to adversely affect the reservoir. However, it must be noted that these results are based on a single model output where the boundary conditions were highly conducive for such favorable results. Due to higher than average precipitation in summer and early fall of 2018, the reservoir was already at full pool at the start of the 90-day forecast. The starting HRT of the reservoir was calculated to be approximately 120 days based on the withdrawal at the time. In addition, the background concentrations were significantly low (~0.5 mg/L). Even at the lower denitrifying capacities of the reservoir during the winter months, the higher HRT provided better resiliency against any abrupt increase in nitrate at RE02. The relatively higher simulated nitrate concentrations for scenarios involving W_2 are only because of the reduction in HRT due to higher drawdown caused by more withdrawals.

As elaborated in the above discussion, the initial pool elevation and hence the HRT of the reservoir plays a crucial role in the outcome of the forecast. To understand the effect of how

lower pool elevations can affect the nitrate concentrations in the reservoir, a hypothetical condition was considered where an already existing drought condition in the fall was extended into winter (the simulation was only done for this study and is not a part of regular DSS forecast). All the 12 scenarios were rerun by creating an artificial drawdown of 2 meters just before the start of the 90-day forecast, which corresponds to a reduction of 33% in the reservoir volume (Figure 4-9). It can be seen that in all the scenarios, the higher effluent nitrate concentration of 12.5 mg/L (N_3) will eventually push the nitrates to the WQO limit in the forecasted period. The worst case scenario remains D1W2 where the nitrates reaches 5 mg/L at RE02 in around 77 days.

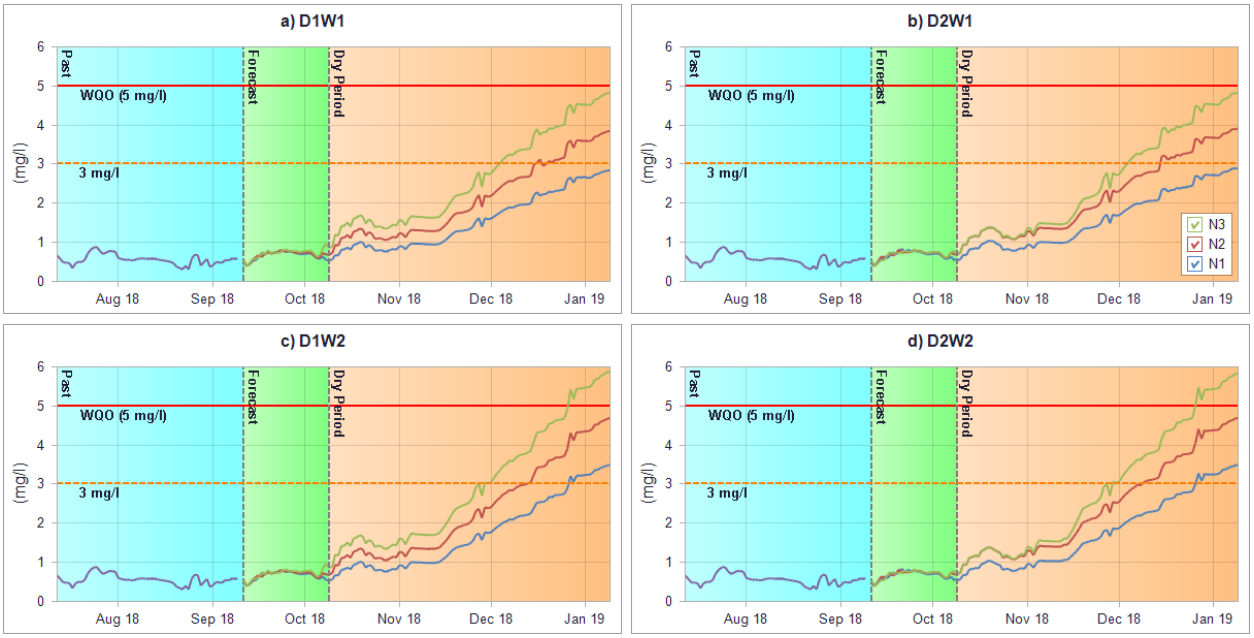

Figure 4-9. Nitrate profiles for different scenarios at RE02 using 2-m initial drawdown

The above results presented how the dynamic nature of the system can affect the reservoir based on different boundary conditions. Different meteorological parameters can also have significant effects on the outcome. For instance, colder than the normal air temperature in fall or winter can also increase the nitrate concentration at RE02 by reducing the denitrification capacity of the reservoir. On the contrary, any significant rain event can washout the entire reservoir diluting the nitrate concentrations to much lower levels.

4.4.4 Process Optimization

Every week, the DSS moves forward in time by predicting the reservoir water quality based on the most recent initial and future boundary conditions. When the forecasted water quality going out 30 to 60 days is above the 3 mg/L Nitrate-N threshold, the DSS automatically runs an optimization routine on IViewOps to determine means to reduce the nutrient discharge from the UOSA plant by simultaneously adjusting asset availability (changing maintenance schedules to bring unavailable assets such as reactors, clarifiers and pumps back online) and operational setpoints. Sen et al. (2016) have discussed the nitrate optimization in detail for winter by using different combinations of process configuration (tanks in service), mixed liquor recycle, DO setpoints, wasting, supplement carbon, etc., while specifying the constraints on the effluent quality.

The DSS can help the plant operators to decide the extent of denitrification, especially during the winter months. Instead of running the plant at full throttle to maximize denitrification, the operators can target a more realistic effluent nitrate concentration based on the existing condition of the reservoir. Less denitrification means potential cost savings due to:

- Reduced amount of carbon required for denitrification and therefore more BOD (Biochemical Oxygen Demand) available for the digesters to increase biogas production for heating and electricity generation.
- Less supplemental carbon (methanol, MicroC, etc.) required for denitrification.
- Less anoxic zone mixing requirements and reduce nitrate recycle pumping rates.
- Lower anoxic volumes reduce undesired luxury bio-P uptake resulting in less soluble phosphate release and consequently lower struvite formation in digesters. This reduces the potential cost of descaling of the centrifuge system and struvite control chemical feed.

4.5 Conclusion

This paper presented the development and implementation of a DSS for the Occoquan IPR system to forecast and regulate the nitrate concentrations in the augmented reservoir. The entire DSS application is powered by newly-developed software, called URUNME, to fully automate the operation of the integrated reservoir and process models, forecasting products, and various data sources. URUNME was also used to develop information-rich and user-friendly interactive dashboards to output the updated historical data and forecasting results for the stakeholders.

The reservoir model is operated once every week, running multiple future scenarios based on different combination of natural stream inflows, plant effluent flows and nitrate concentrations, and water withdrawal by the WTP. The future weather conditions are simulated using the forecasts obtained from the CFS. A 30-day forecast predicted the reservoir conditions based on the NWM stream flow forecast going out 30 days. A 90-day forecast, on the other hand, is used as a what-if analysis to simulate the effects of any possible future winter drought.

The forecasted nitrate-N concentrations under different scenarios can be used by the WRF to identify and analyze operational strategies dynamically in response to the reservoir future conditions. In case nitrates going out 30 to 60 days exceeds 3 mg/L, the DSS can be used to run different optimization routines on IViewOps to determine the means to reduce the nutrient discharge. Even when the target nitrates effluent concentrations are difficult to achieve due to operational constraint, the DSS output provides a fair estimate of the time it would take for the reservoir to reach unacceptable nitrate levels. This provides valuable feedback to the plant managers for contingency planning e.g. rescheduling maintenance of certain assets, adding supplemental carbon chemicals, changing plant configuration, etc., to avoid any future emergency conditions. As the DSS progresses forward in time, the optimization of the WRF is revisited every 7 days with updated outputs due to the dynamic nature of the system. For instance, any significant rain event can partially or completely washout the entire reservoir, diluting the nitrate concentrations to much lower levels.

The file transfer system makes it easier for the WRF to run the simulations based on reservoir model runs done at OWML. Each week, URUNME is run to generate a database file that is sent to the WRF via FTP. The plant uses the URUNME interface to run this together with IViewOps and populate relevant data in a screen that is a sister screen to SCADA. The operations and maintenance staff can then make decisions about how to optimize the plant and what the future conditions would be with optimization.

4.5.1 Future Applications of URUNME based DSS

Integrated modeling using the URUNME system provides a comprehensive approach to environmental management by evaluating different components of a system in a holistic manner. It can be used as an effective tool for design, planning, and risk assessments and can facilitate

informed decision-making, enhancing the transparency and collaboration between different stakeholders. Moreover, it can be used for simulating, understanding and managing a combination of wastewater, drinking water and groundwater interaction such as:

1. IPR applications in Southern California (Orange County).
2. Wastewater treatment, discharge to a reservoir, extraction for drinking water supply, and drinking water treatment (IPR, Wichita Falls, Texas);
3. Raw water supply from a reservoir, water treatment, and sludge disposal to the wastewater treatment plant (WSSC [Washington Suburban Sanitary Commission], Maryland).

Although developing a reservoir model from scratch is a major undertaking that requires a significant amount of data for setting up and calibrating the model. However, there are certain components of this DSS which can be reused for similar applications without any major modification:

- Downloading the data, reading the binary file formats (GRIB2, NetCDF), and calibrating the forecasts from the CFS and NWM.
- Obtaining data from different data sources (stream stations, reservoir stations, weather stations, etc.), manipulating and transforming data, and writing the boundary conditions and input parameters to the reservoir model.
- Open source HOS model developed for CE-QUAL-W2.
- Different screens created as part of the DSS dashboard.

The use of a DSS driven by URUNME can be used in various systems in addition to water resources. These can include chemical and biological engineering systems and their models, manufacturing and supply chain management systems and their models. URUNME is available free of cost for academic use (www.urunme.com).

4.6 Acknowledgment

The authors acknowledge the support of UOSA and OWML for supporting and funding this research. We would also like to honor the memory of the late Dr. Thomas J. Grizzard for his unwavering commitment in the establishment and operation of the Occoquan program and the OWML for over 40 years.

4.7 References

Azmi, M., and Heidarzadeh, N (2013). "Dynamic modelling of integrated water resources quality management." *Proc., Proceedings of the Institution of Civil Engineers-Water Management*, Thomas Telford Ltd, 357-366.

Bartlett, J. A. (2013). "Heuristic Optimization of Water Reclamation Facility Nitrate Loads for Enhanced Reservoir Water Quality." PhD Dissertation, Virginia Polytechnic Institute and State University.

Bryant, L. D., Gantzer, P. A., and Little, J. C. (2011). "Increased sediment oxygen uptake caused by oxygenation-induced hypolimnetic mixing." *Water Research*, 45(12), 3692-3703.

Cole, T. M., and Wells, S. A. (2011). "CE-QUAL-W2: A Two-Dimensional, Laterally Averaged, Hydrodynamic and Water Quality Model, Version 3.71." *U.S. Army Corps of Engineers, Washington, D.C.*

Coombes, P. J., and Kuczera, G (2002). "Integrated urban water cycle management: Moving towards systems understanding." *Proc., Proceedings of the 2nd National Conference on Water Sensitive Urban Design, Engineers Australia*, 2-4.

Flitter, H., Weckenbrock, P., Weibel, R., and Wiesmann, S. (2016). "Continuous spatial variables." Geographic Information Technology Training Alliance (GITTA).

Gupta, H. V., Sorooshian, S., and Yapo, P. O. (1999). "Status of automatic calibration for hydrologic models: Comparison with multilevel expert calibration." *Journal of Hydrologic Engineering*, 4(2), 135-143.

Gustard, A., and Demuth, S. (2009). "Manual on low-flow estimation and prediction." *World Meteorological Organization*, WMO-No.1029.

Ho, C. K., Stephenson, D. B., Collins, M., Ferro, C. A., and Brown, S. J. (2012). "Calibration strategies: a source of additional uncertainty in climate change projections." *Bulletin of the American Meteorological Society*, 93(1), 21-26.

Lodhi, A., Godrej, A., Sen, D., and Baran, A. (2018). "URUNME: A Generic Software for Integrated Environmental Modeling to Help 'You Run Models Easily'." *Manuscript in preparation*.

Mitchell, V., Duncan, H., Inman, M., Rahilly, M., Stewart, J., Vieritz, A., Holt, P., Grant, A., Fletcher, T., and Coleman, J. (2007). "Integrated urban water modelling-past, present, and future." *Rainwater and Urban Design 2007*, 806.

Moore, R. V., and Tindall, C. I. (2005). "An overview of the open modelling interface and environment (the OpenMI)." *Environmental Science & Policy*, 8(3), 279-286.

Moriasi, D. N., Arnold, J. G., Van Liew, M. W., Bingner, R. L., Harmel, R. D., and Veith, T. L. (2007). "Model evaluation guidelines for systematic quantification of accuracy in watershed simulations." *Trans. Asabe*, 50(3), 885-900.

Nash, J. E., and Sutcliffe, J. V. (1970). "River flow forecasting through conceptual models part I—A discussion of principles." *Journal of hydrology*, 10(3), 282-290.

Niu, G. Y., Yang, Z. L., Mitchell, K. E., Chen, F., Ek, M. B., Barlage, M., Kumar, A., Manning, K., Niyogi, D., and Rosero, E. (2011). "The community Noah land surface model with multiparameterization options (Noah-MP): 1. Model description and evaluation with local-scale measurements." *Journal of Geophysical Research: Atmospheres*, 116 (D12109).

Rauch, W., Bertrand-Krajewski, J.-L., Krebs, P., Mark, O., Schilling, W., Schütze, M., and Vanrolleghem, P. A. (2002). "Deterministic modelling of integrated urban drainage systems." *Water science and technology*, 45(3), 81-94.

Saha, S., Moorthi, S., Wu, X., Wang, J., Nadiga, S., Tripp, P., Behringer, D., Hou, Y.-T., Chuang, H.-y., and Iredell, M. (2014). "The NCEP climate forecast system version 2." *Journal of Climate*, 27(6), 2185-2208.

Schütze, M., Butler, D., and Beck, M (1996). "Development of a framework for the optimisation of runoff, treatment and receiving waters." *Proc., 7th International Conference on Storm Drainage, Hanover, Germany*, 9-13.

Sen, D., Brooks, M., Lodhi, A., Angelotti, R., Hall, A., and Chung, C. (2016). "Improvements to Sensor Recalibration, Scheduling Maintenance and Planning by Implementing an Asset Based Process Model Connecting to SCADA and Lab-Experiences from Plants for Treatment, Nutrient Removal and Reuse." *Proceedings of the Water Environment Federation*, 2016(9), 627-655.

Sen, D., Lodhi, A., Brooks, M., Angelotti, R., and Godrej, A. (2015). "Integration of Asset Management with Real Time Simulation to Improve Reliability, Preventive and Corrective Maintenance and Reduce Life Cycle Cost in Wastewater Treatment for Reuse." *Proceedings of the Water Environment Federation*, 2015(10), 5152-5178.

Shah, R., Sahai, A. K., and Mishra, V. (2017). "Short to sub-seasonal hydrologic forecast to manage water and agricultural resources in India." *Hydrology and Earth System Sciences*, 21(2), 707.

Shah, R. D., and Mishra, V. (2015). "Development of an experimental near-real-time drought monitor for India." *Journal of Hydrometeorology*, 16(1), 327-345.

Singleton, V. L. (2008). "Hypolimnetic Oxygenation: Coupling Bubble-Plume and Reservoir Models." PhD Dissertation, Virginia Polytechnic Institute and State University.

VSWCB (1971). "A Policy for Waste Treatment and Water Quality Management in the Occoquan Watershed, §9VAC25-410-10." Virginia State Water Control Board, Richmond, Virginia.

WMO (2012). "Guidelines on Ensemble Prediction Systems and Forecasting." World Meteorological Organization, Switzerland.

Wu, J., Yu, S. L., and Zou, R. (2006). "A Water Quality-Based Approach for Watershed Wide Bmp Strategies 1." *JAWRA Journal of the American Water Resources Association*, 42(5), 1193-1204.

Xu, Z., Godrej, A. N., and Grizzard, T. J. (2007). "The hydrological calibration and validation of a complexly-linked watershed–reservoir model for the Occoquan watershed, Virginia." *Journal of Hydrology*, 345(3), 167-183.

Table A4-1. Summary of CFS variables

#	Variable	Description	File Name	Unit	Level
1	TMP_2maboveground	Air temperature	tmp2m.01.yyyymmddhh.daily.grb2	ºK	2 m above ground
2	SPFH_2maboveground	Specific humidity	q2m.01.yyyymmddhh.daily.grb2	kg/kg	2 m above ground
3	PRATE_surface	Precipitation	prate.01.yyyymmddhh.daily.grb2	$kg/m^2/s$	Surface
4	VGRD_10mabovegroupd	V-Component of wind	wnd10m.01.yyyymmddhh.daily.grb2	m/s	10 m above ground
5	UGRD_10mabovegroupd	U-Component of wind	wnd10m.01.yyyymmddhh.daily.grb2	m/s	10 m above ground
6	DSWRF_surface	Downward short-wave radiation flux	dsw.01.yyyymmddhh.daily.grb2	W/m^2	Surface
7	TCDC_entireatmosphere_consideredasasinglelayer_	Total cloud cover	tcdcclm.yyyymmddhh.daily.grb2	percent	Entire atmosphere

where
yyyy: year
mm: month
dd: day
hh: forecast hour (00, 06, 12, or 18)

Table A4-2. Scale factors for each branch and distributed flows

#	Inflow	Equation
1	Branch-1	$Q_1 = 1.05 \times Q_{10}$
2	Branch-2	$Q_2 = 1.26 \times \left(Q_{45} - Q_{UOSA}\right) + Q_{UOSA}$
3	Branch-3	$Q_3 = 0.06 \times (Q_{45} - Q_{UOSA})$
4	Branch-4	$Q_4 = 0.02 \times Q_{10}$
5	Distributed Branch-1	$Q_{dt1} = 0.04 \times Q_{10}$
6	Distributed Branch-2	$Q_{dt2} = 0.10 \times (Q_{45} - Q_{UOSA})$

Table A4-3. Average monthly WTP withdrawals between 2013-2017

#	Month	Withdrawals		% of Safe yield
		m^3/d	mgd	
1	January	240,236	63.5	80.3
2	February	238,326	63.0	79.7
3	March	237,007	62.6	79.3
4	April	239,339	63.2	80.0
5	May	246,113	65.0	82.3
6	June	264,376	69.8	88.4
7	July	271,707	71.8	90.9
8	August	267,055	70.5	89.3
9	September	267,447	70.7	89.4
10	October	260,453	68.8	87.1
11	November	243,407	64.3	81.4
12	December	239,194	63.2	80.0

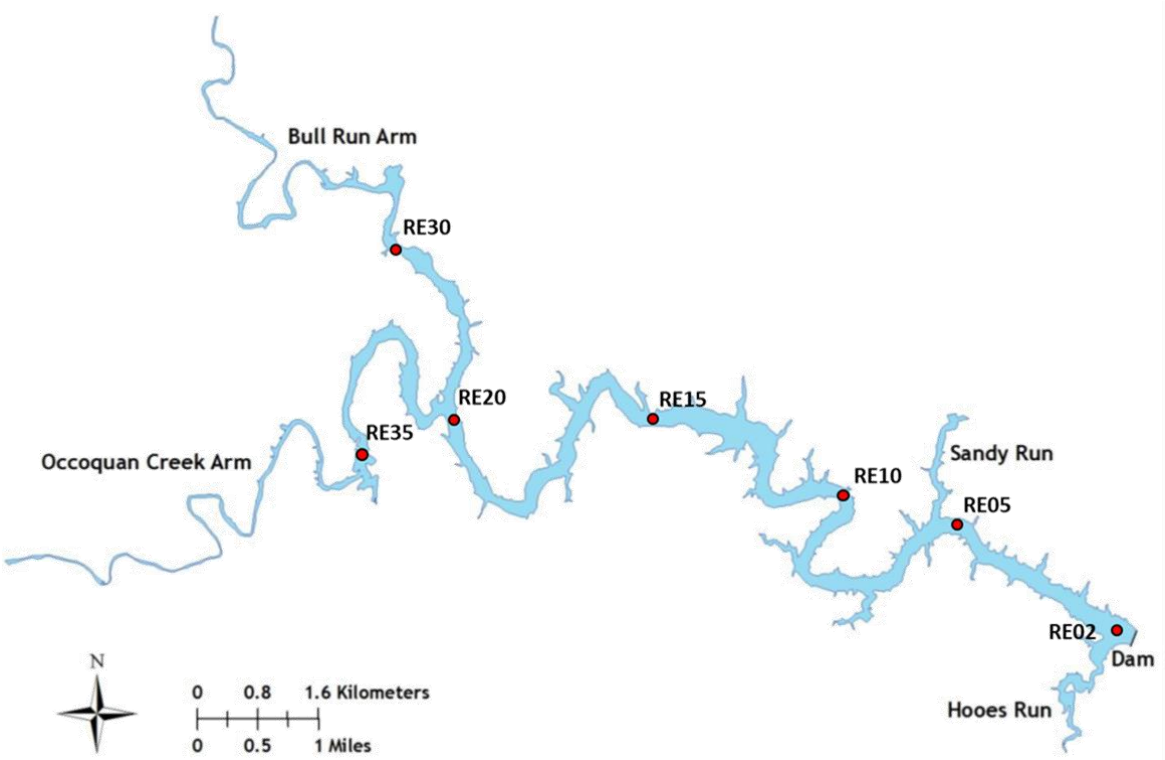

Figure A4-1. Occoquan Reservoir sampling stations

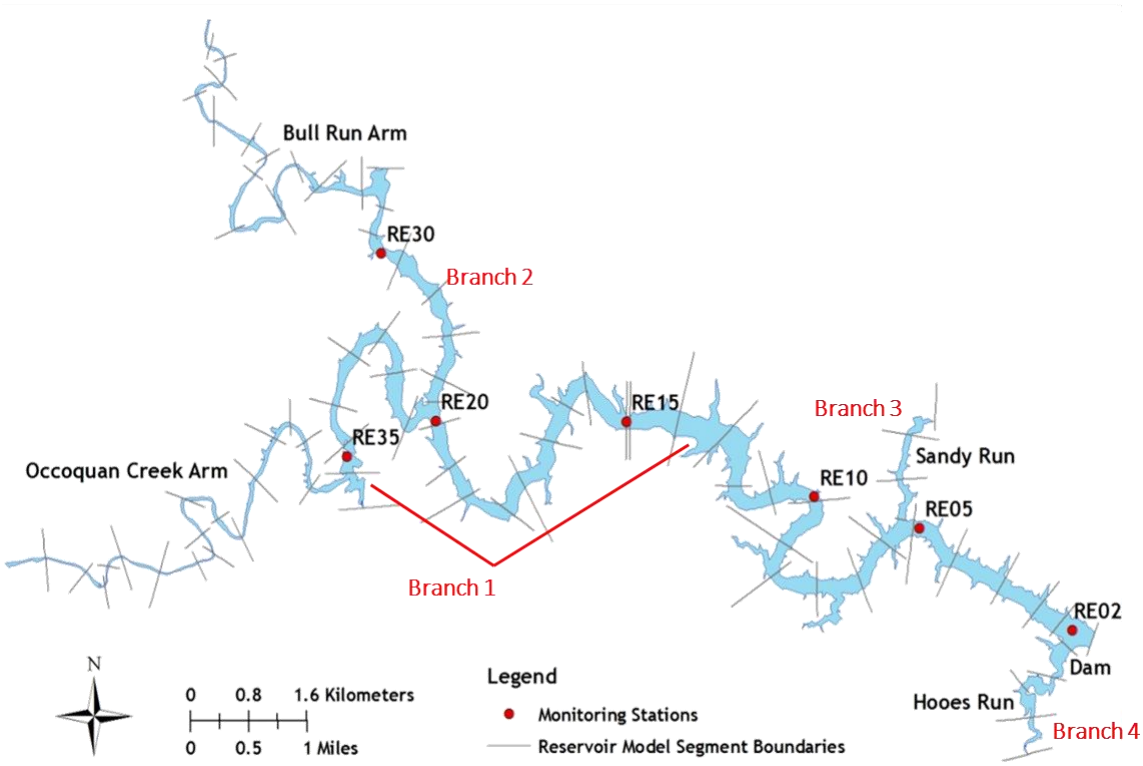

Figure A4-2. Occoquan Reservoir CE-QUAL-W2 model braches and segmentation (4 branches, 69 longitudinal segments with an average length of 0.5 km, and 0.5 meter layers)

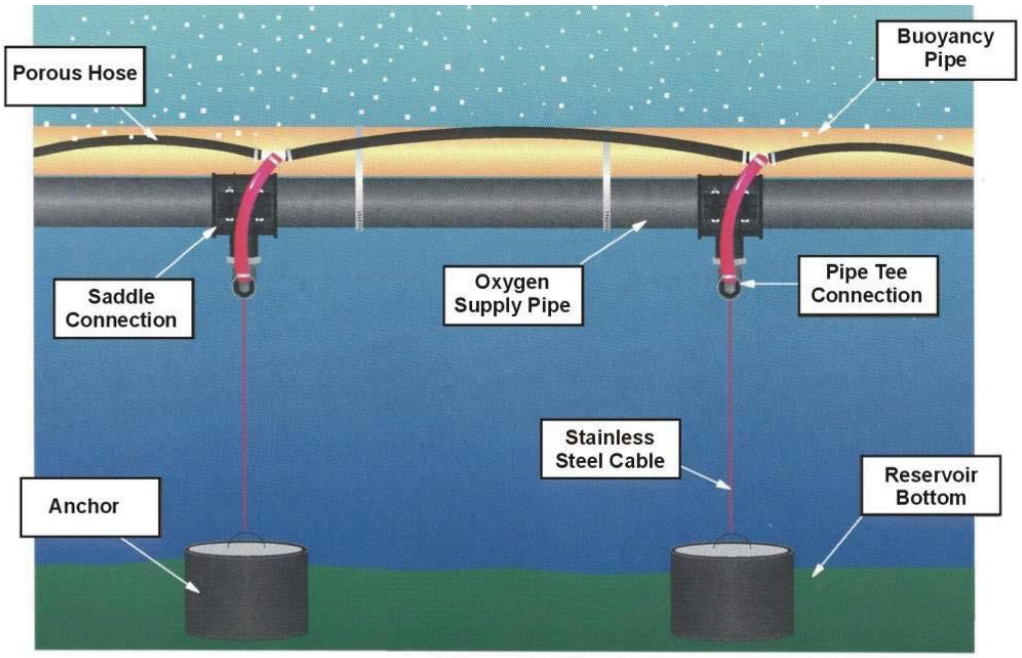

Figure A4-3. Line diffuser system for hypolimnetic oxygenation

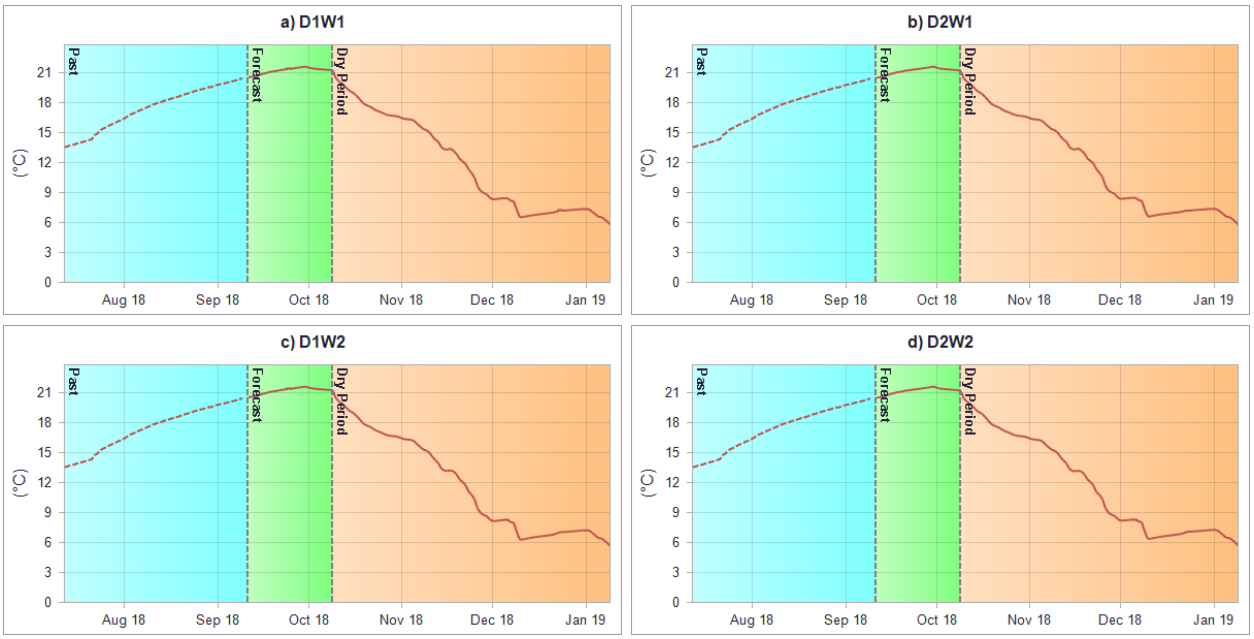

Figure A4-4. Bottom water temperature profiles for different scenarios at RE02

Figure B 4-1. The main screen of the Occoquan Decision Support System. The buttons on the left side are for opening up different sections including historical data, calibration, forecasting, and UOSA WRF process optimization. Buttons on the right side, from top to bottom, are for 1) Home: to go back to the main screen, 2) Back: to go back to the last screen, 3) Save: to save the current settings, 4) Events: to show alarms and warnings, 5) About: to show a brief description of the system, and 6) Exit: to close the application.

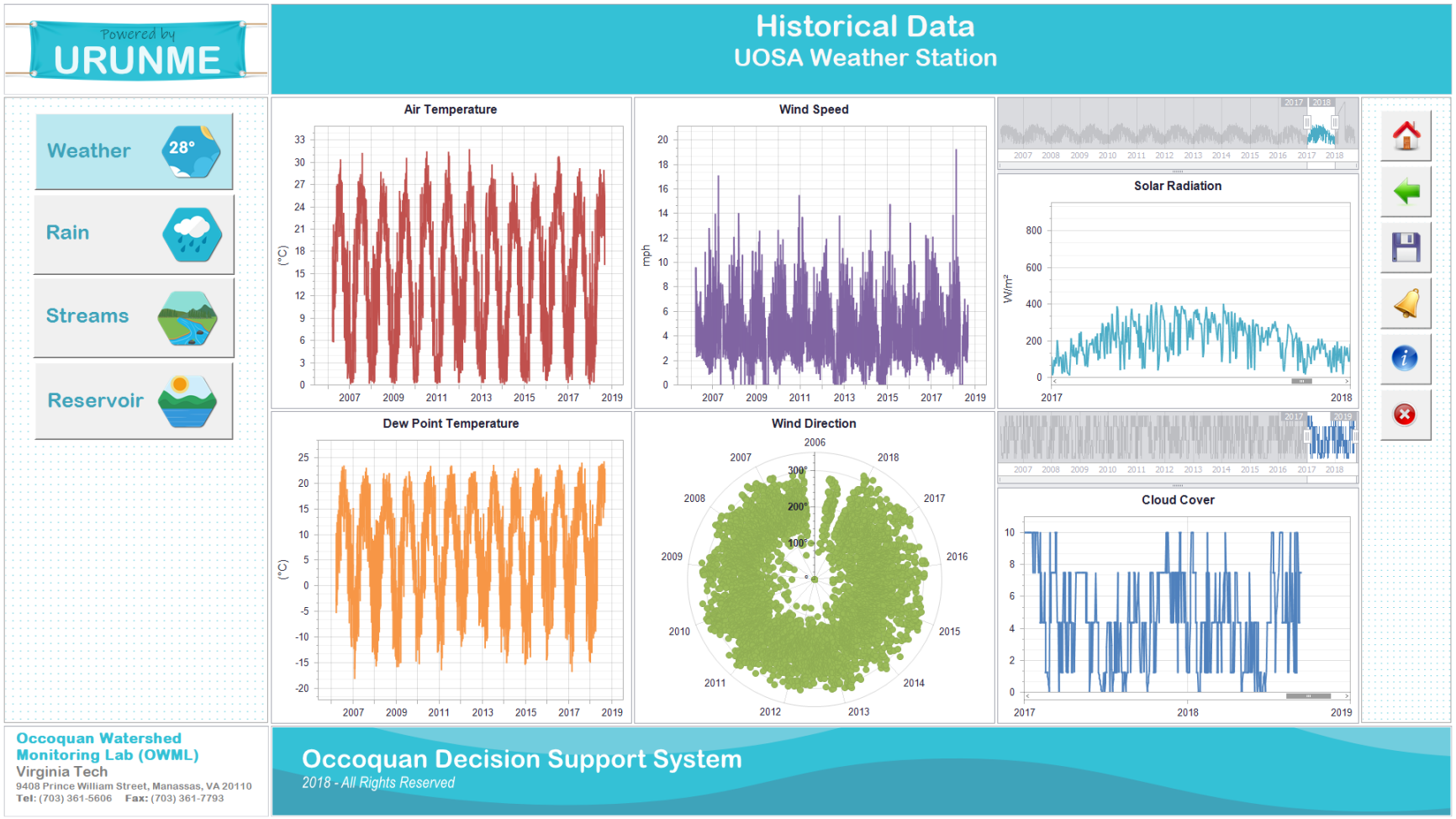

Figure B 4-2. This screen shows the historical weather data. It is opened by clicking the 'Historical' button from the main screen in Figure B 4-1. The buttons on the left are used to open other historical trends from different rain, stream, and reservoir stations.

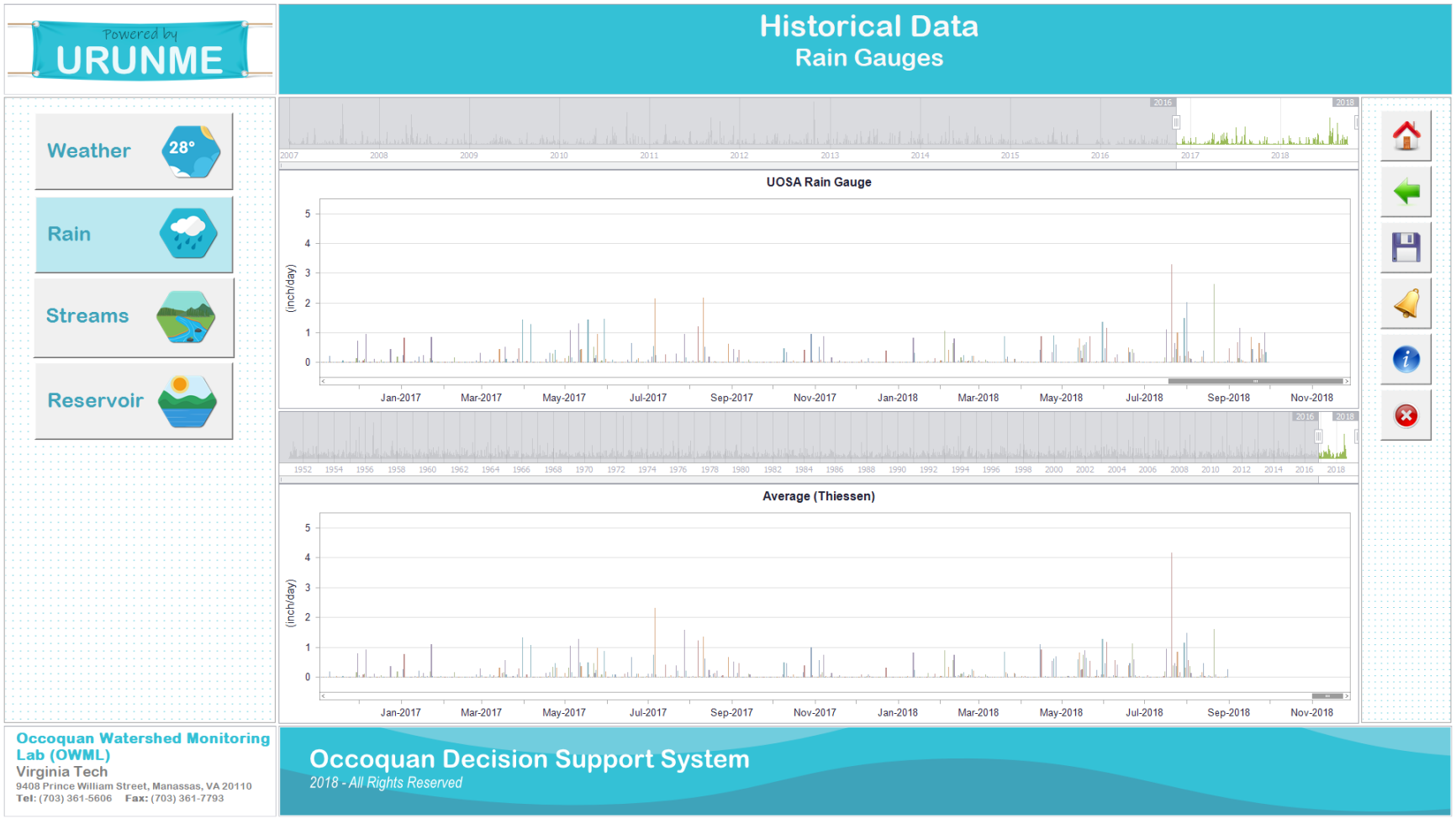

Figure B 4-3. This screen shows the historical rain data. It is opened by clicking the 'Rain' button from the screen shown in Figure B 4-2.

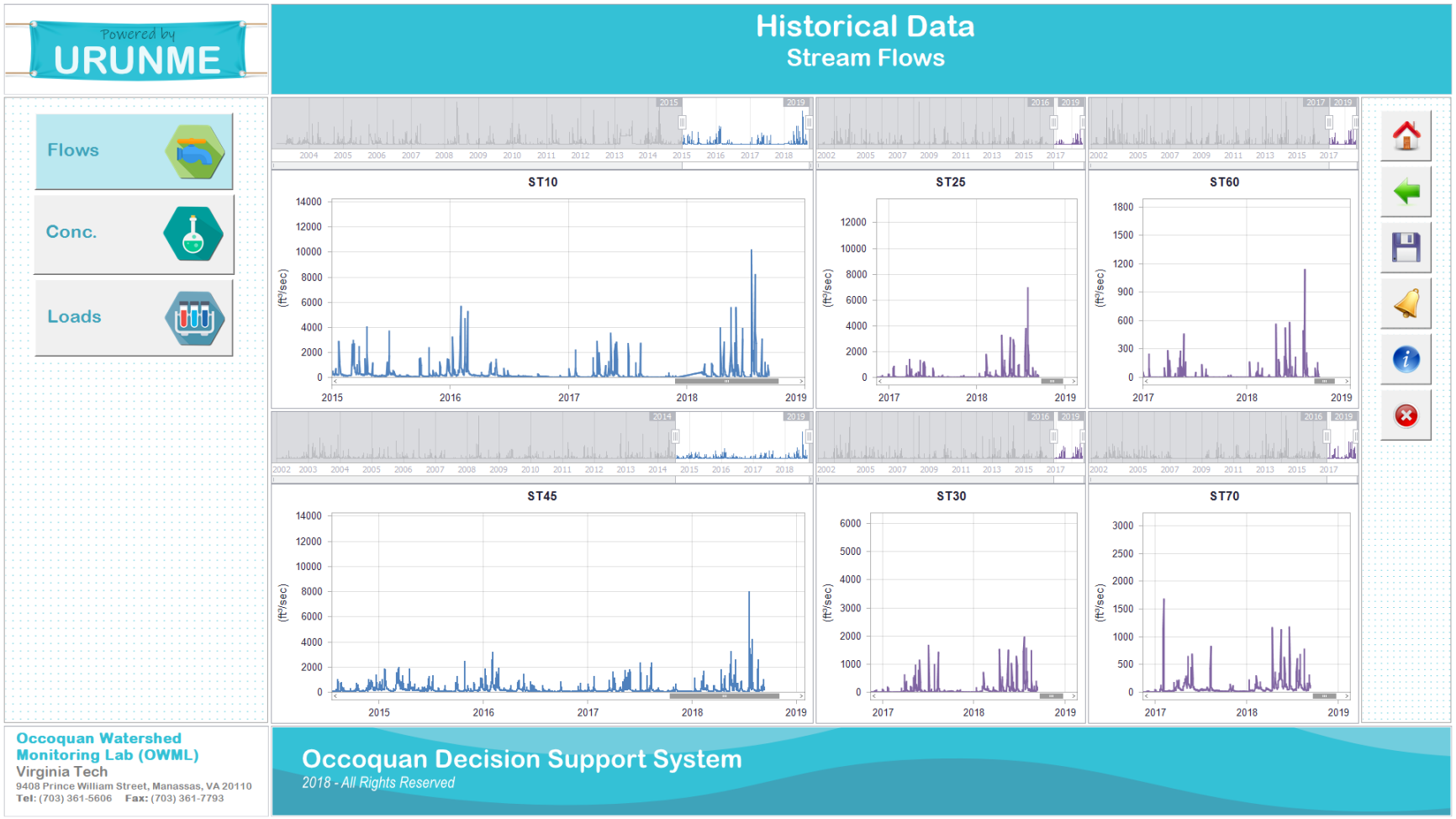

Figure B 4-4. This screen shows the historical stream flow data. It is opened by clicking the 'Streams' button from the screen shown in Figure B 4-3.

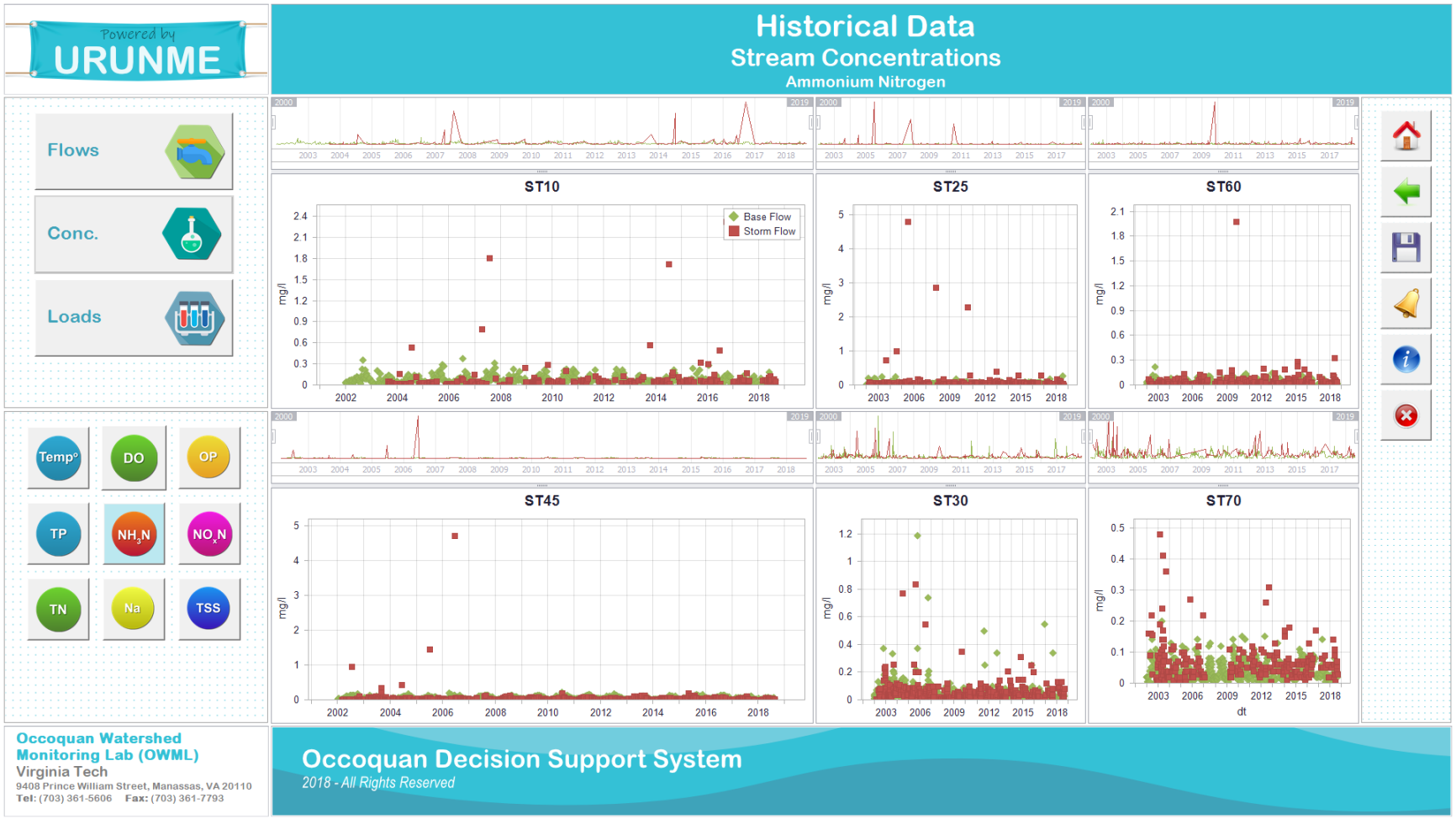

Figure B 4-5. This screen shows the historical stream temperature and concentrations data. It is opened by clicking the 'Conc' button from the screen shown in Figure B 4-4. The buttons on the bottom left are used to switch between different constituents.

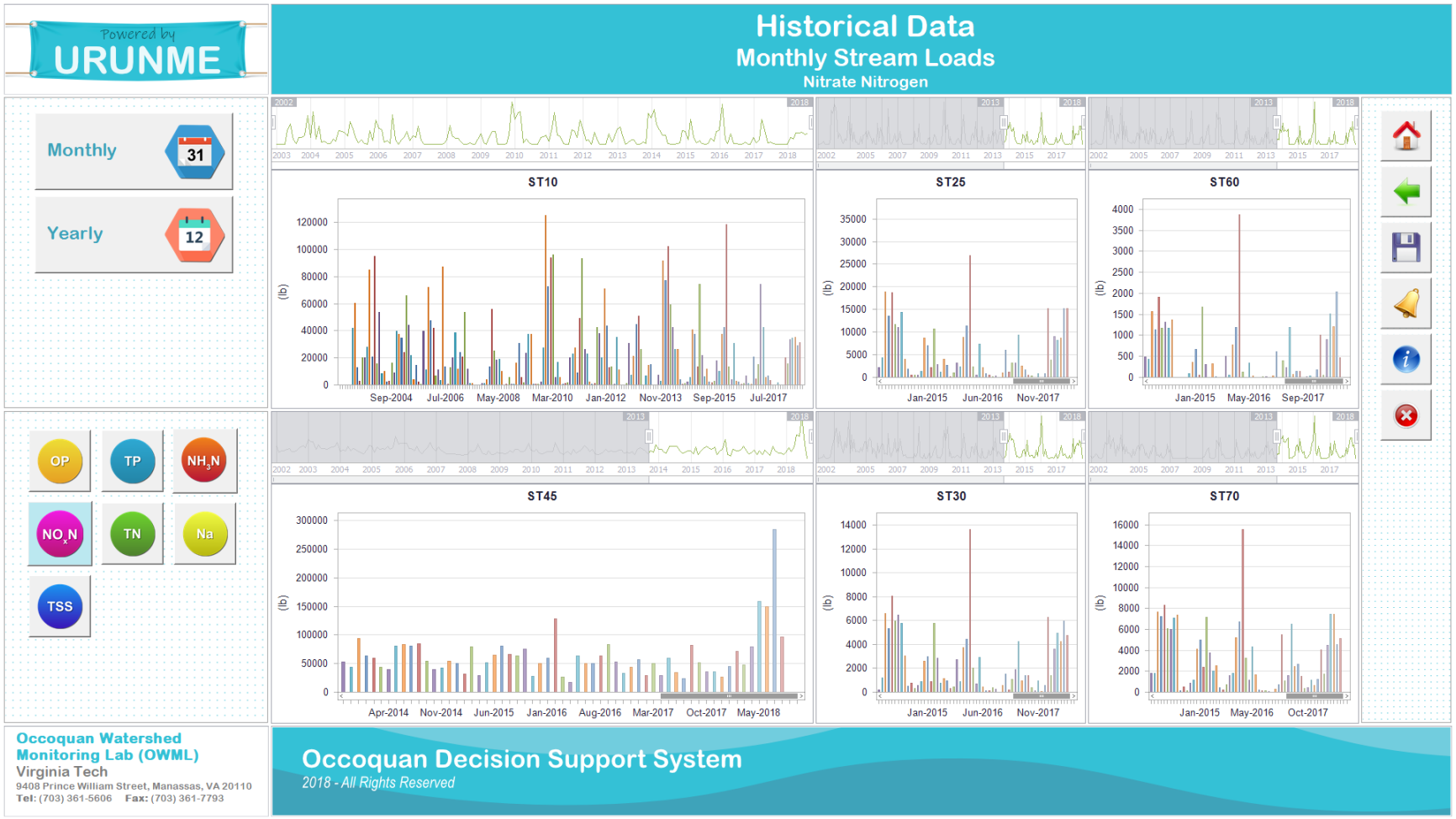

Figure B 4-6. This screen shows the monthly stream loads. It is opened by clicking the 'Loads' button from the screen shown in Figure B 4-5. The buttons on the bottom left are used to switch between different constituents.

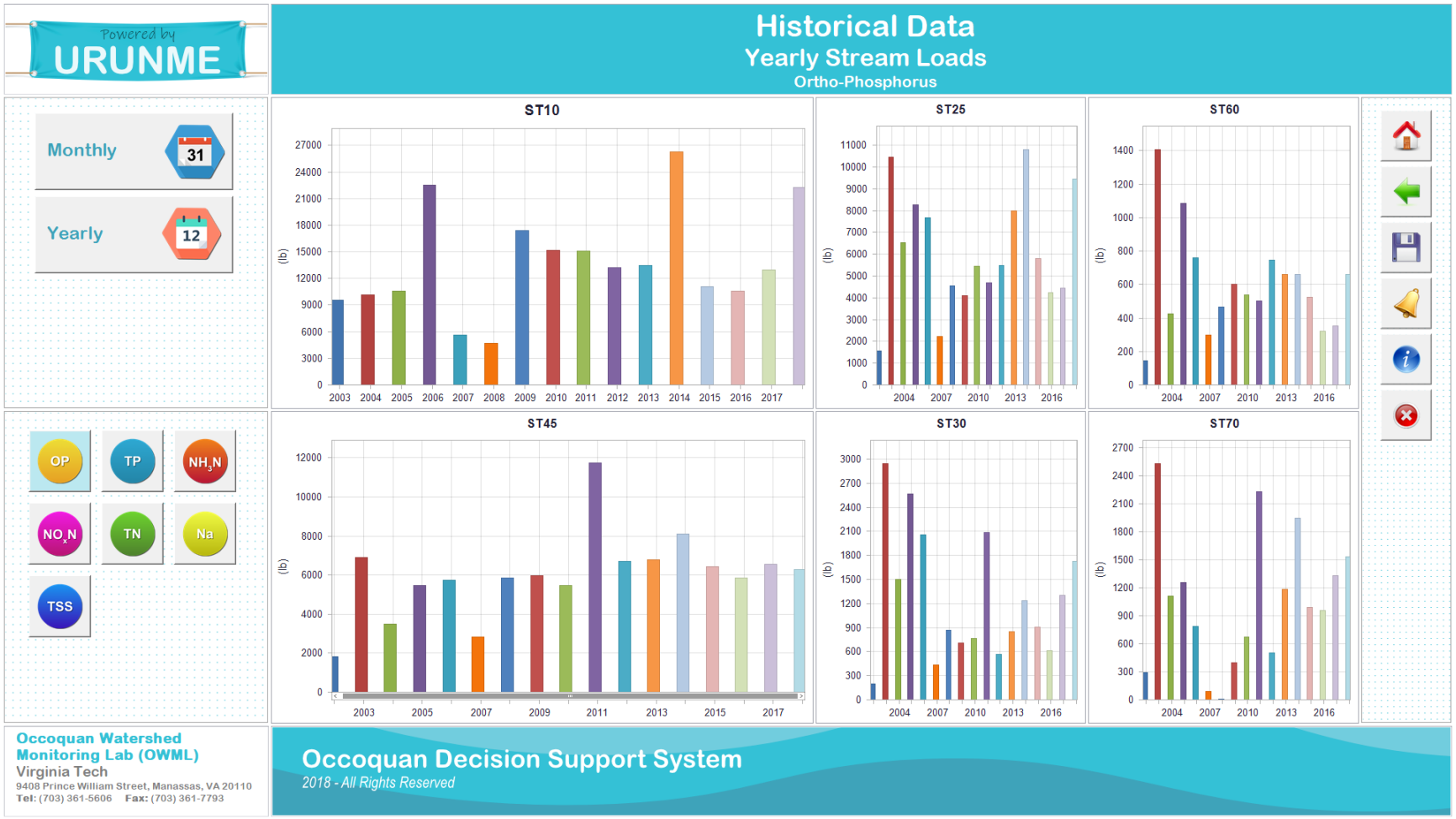

Figure B 4-7. This screen shows the yearly stream loads. It is opened by clicking the 'Yearly' button from the screen shown in Figure B 4-6. The buttons on the bottom left are used to switch between different constituents.

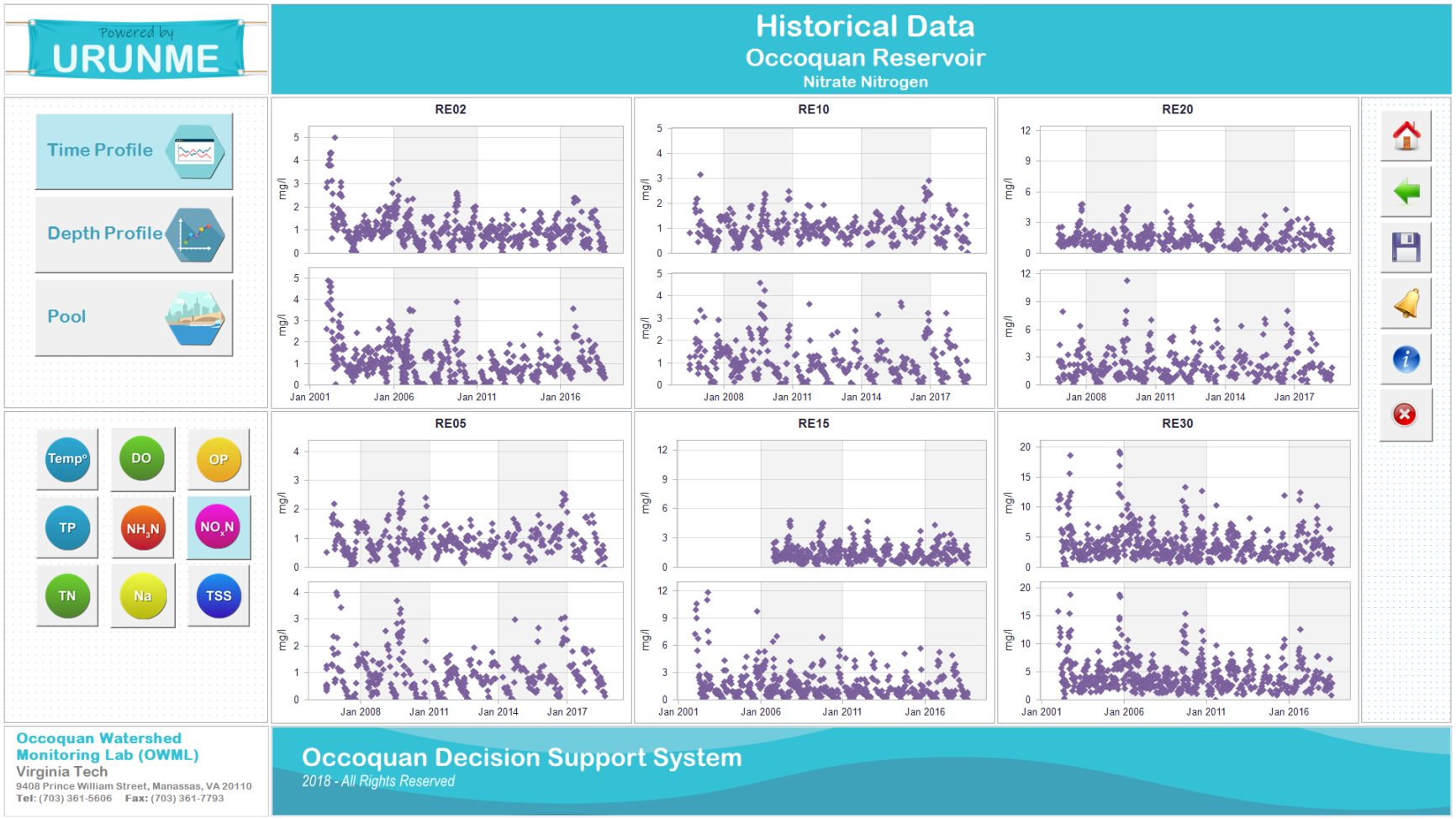

Figure B 4-8. This screen shows the historical reservoir concentrations at reservoir stations. It is opened by clicking the 'Reservoir' button from the screen shown in Figure B 4-3. The buttons on the bottom left are used to switch between different constituents.

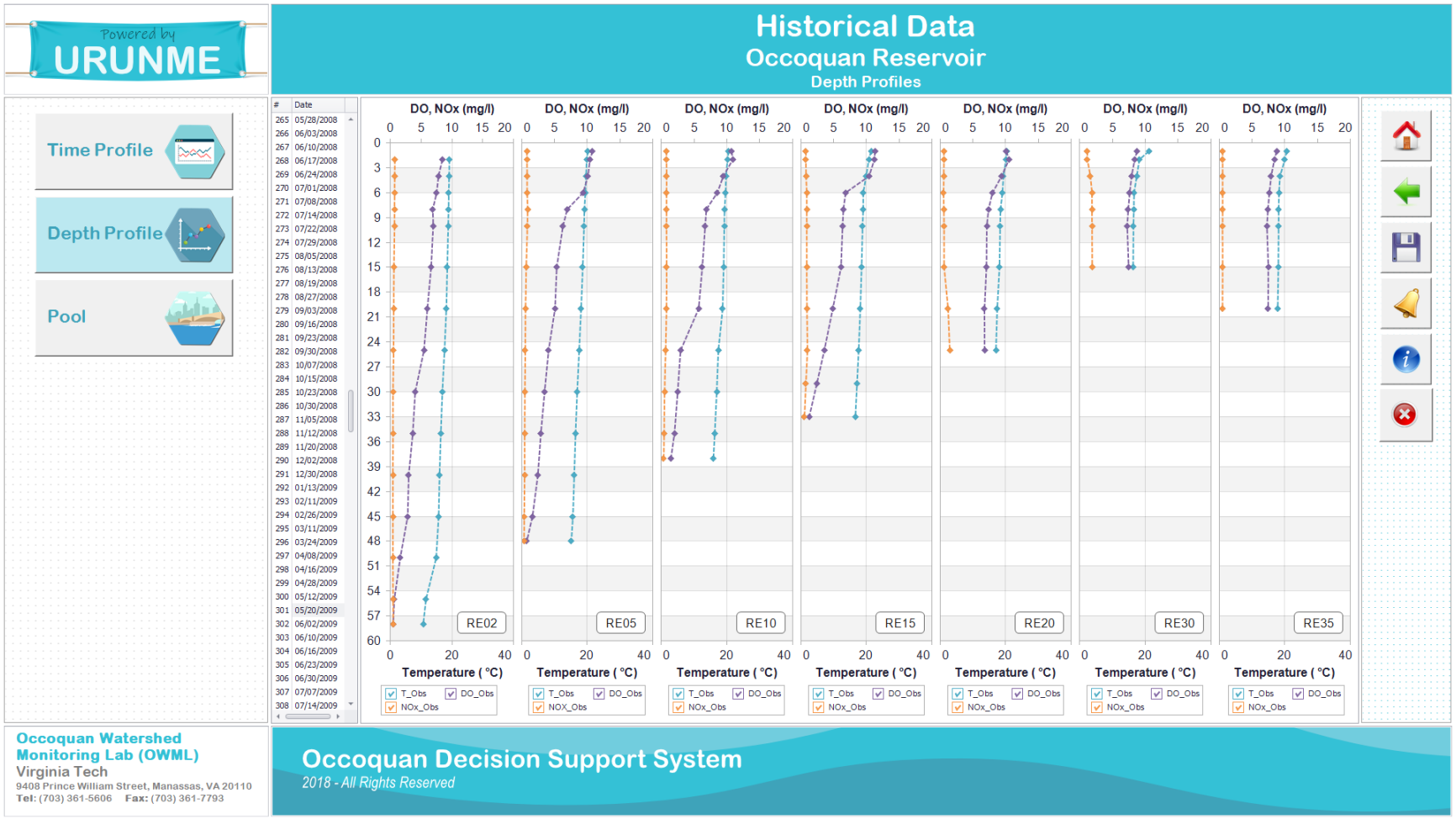

Figure B 4-9. This screen shows depth profiles for temperature, dissolved oxygen and nitrate-nitrogen at different reservoir stations. It is opened by clicking the 'Depth Profile' button from the screen shown in Figure B 4-8. The list to the left of the charts provide all the dates for which the observed data are available. User can click any row on the list to show the depth profile for the selected date.

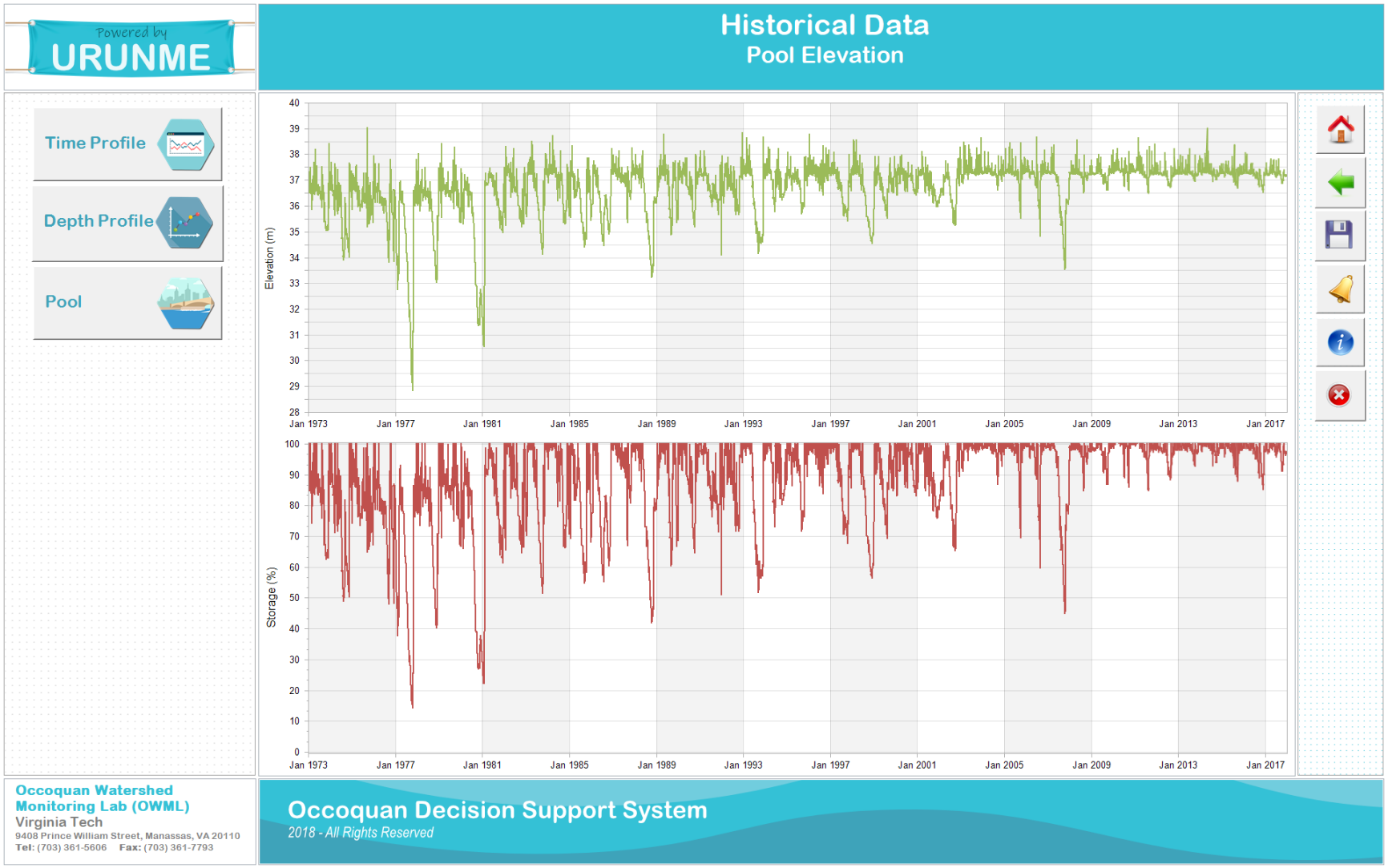

Figure B 4-10. This screen shows the historical pool elevation of the reservoir. It is opened by clicking the 'Pool' button from the screen shown in Figure B 4-9.

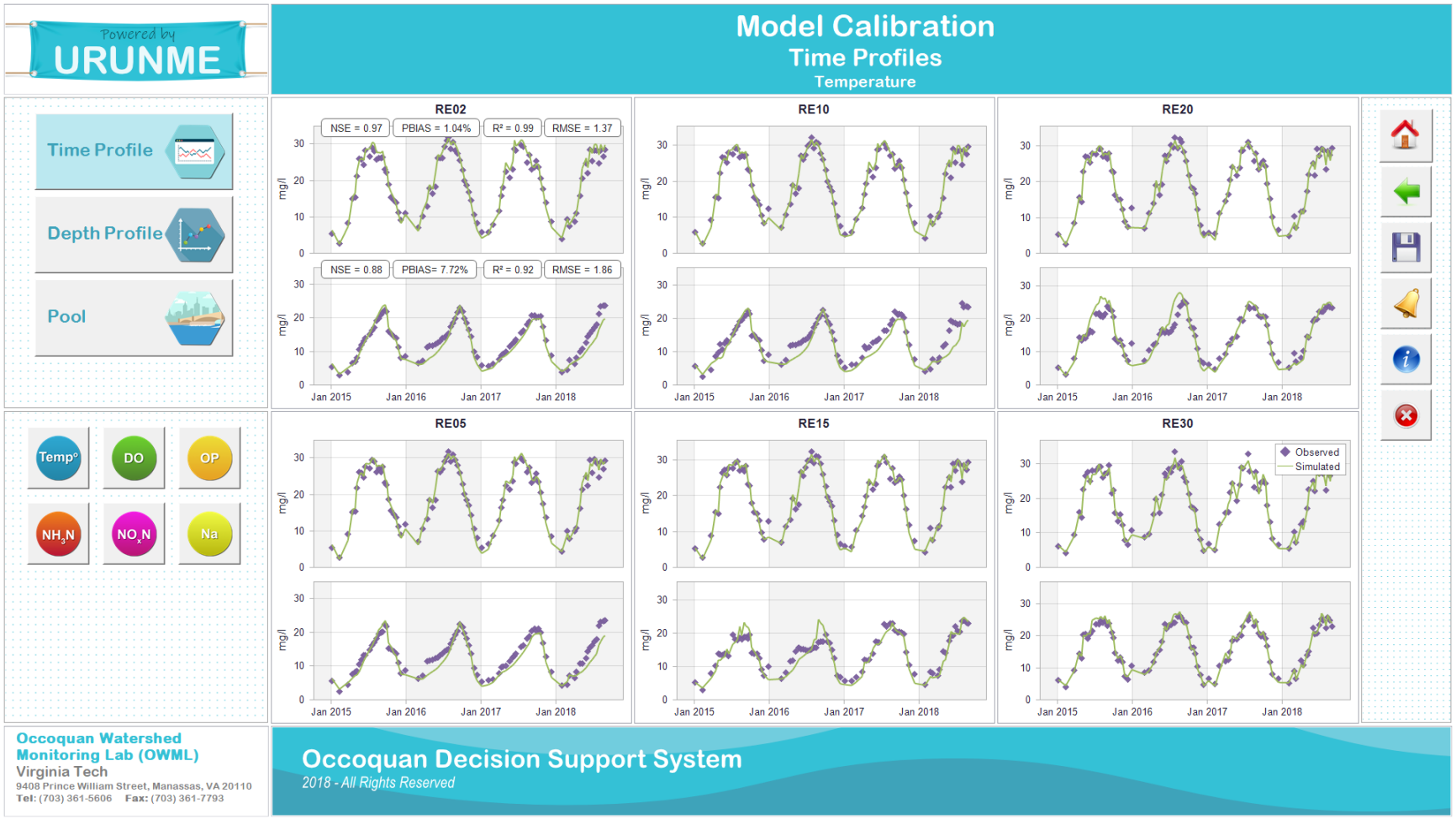

Figure B 4-11. This screen shows the simulated versus observed time series for the calibration run. It is opened by clicking the 'Calibration' button from the main screen shown in Figure B 4-1. The buttons on the bottom left are used to switch between different constituents.

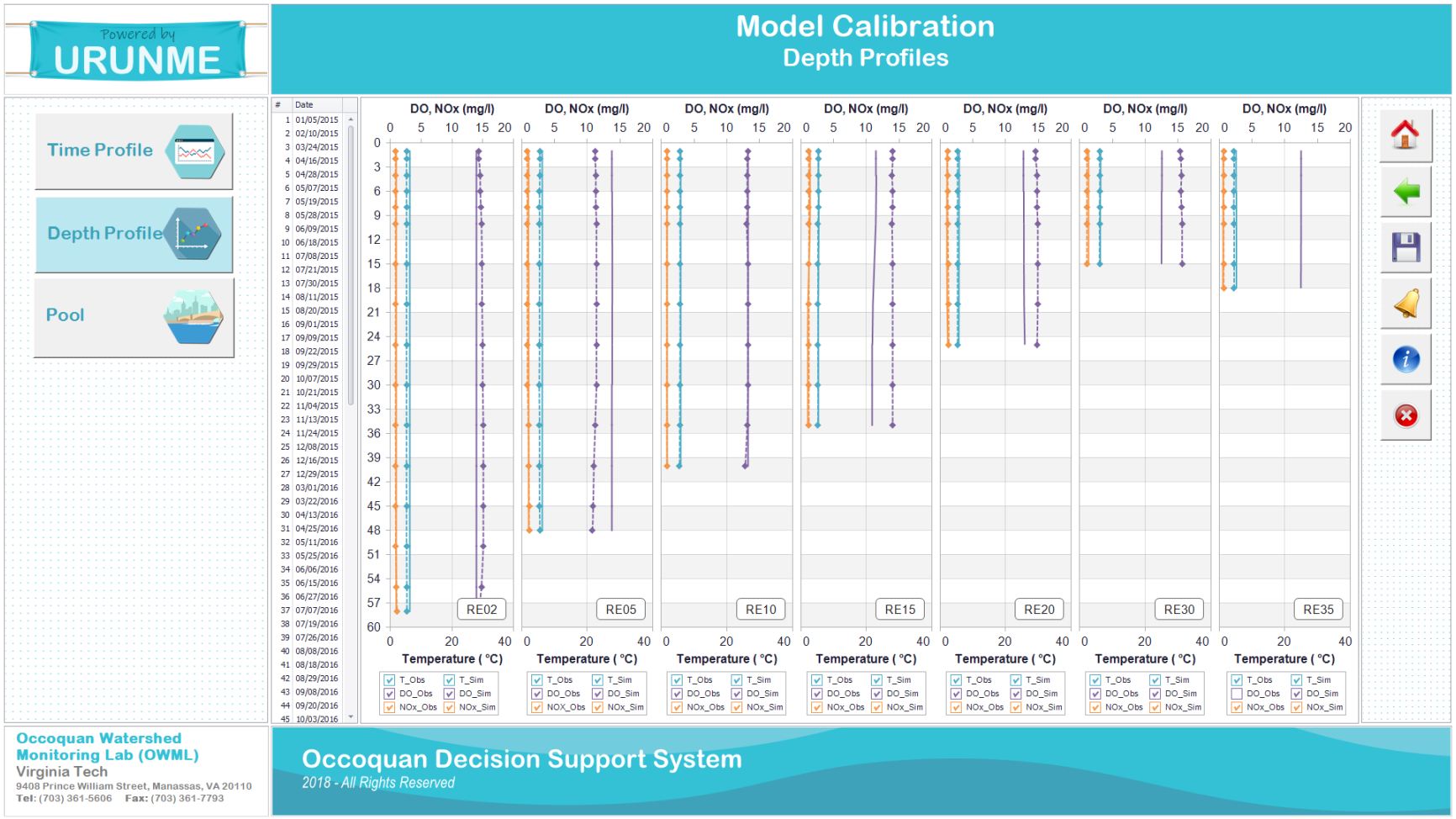

Figure B 4-12. This screen shows the simulated vs observed depth profiles temperature, dissolved oxygen and nitrate nitrogen for the calibration run. It is opened by clicking the 'Depth Profiles' button from the screen shown in Figure B 4-11. The list to the left of the charts provide all the dates for which the observed data are available. User can click any row on the list to show the depth profile for the selected date.

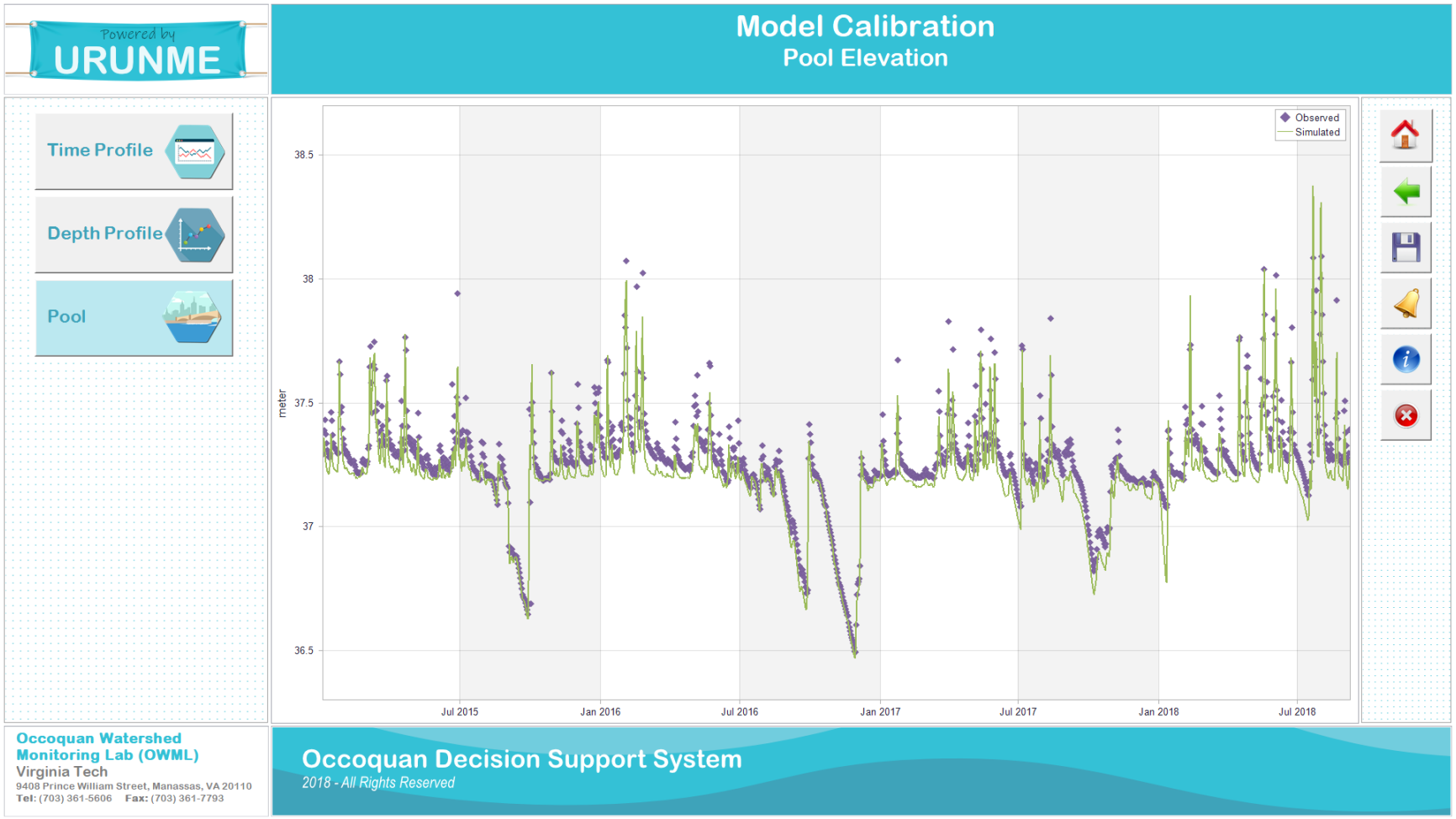

Figure B 4-13. This screen shows the simulated vs observed pool elevation for the calibration run. It is opened by clicking the 'Pool' button from the screen shown in Figure B 4-12.

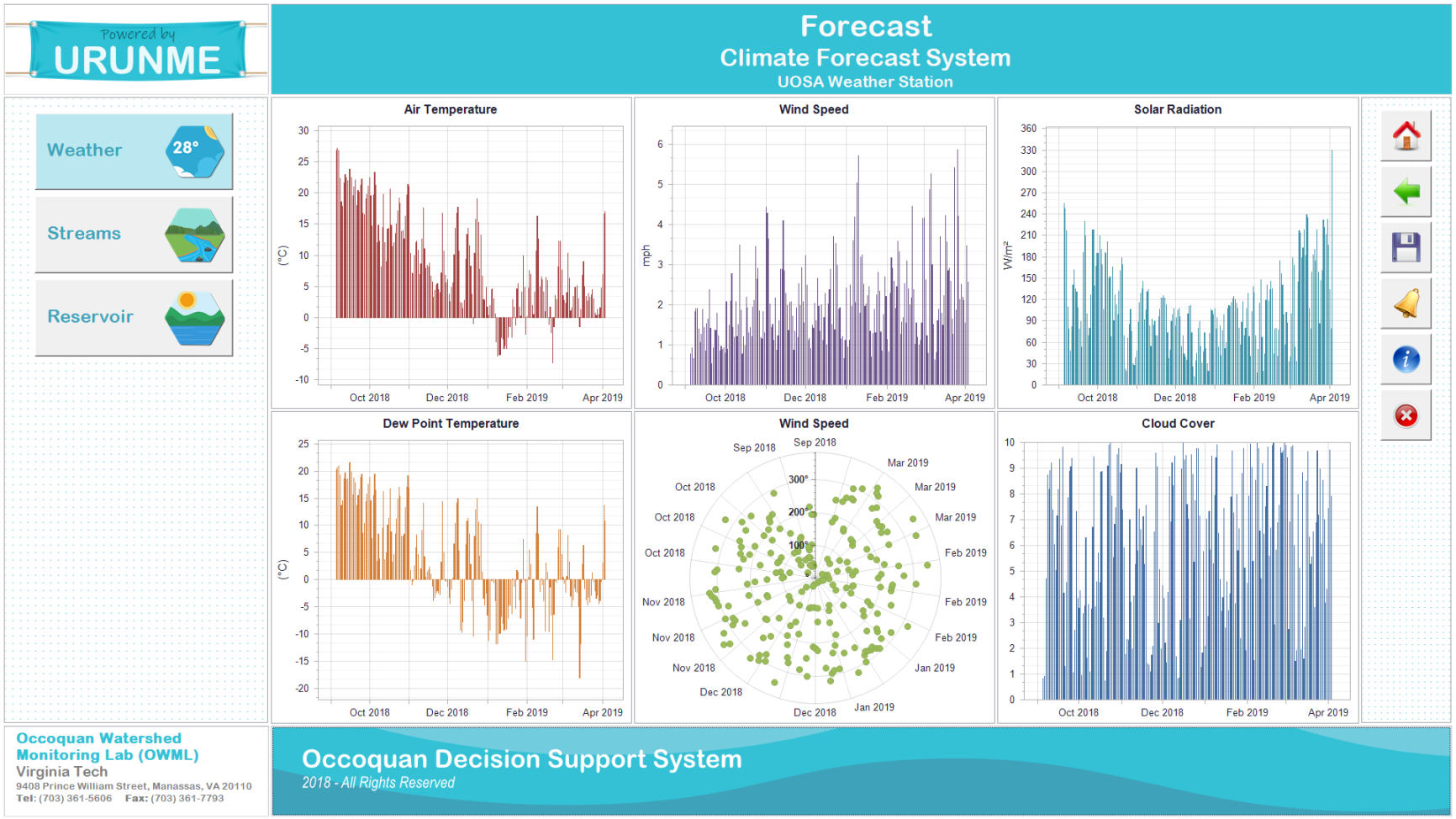

Figure B 4-14. This screen shows the forecasted weather data from Climate Forecast System (CFS). It is opened by clicking the 'Forecast' button from the main screen in Figure B 4-1.

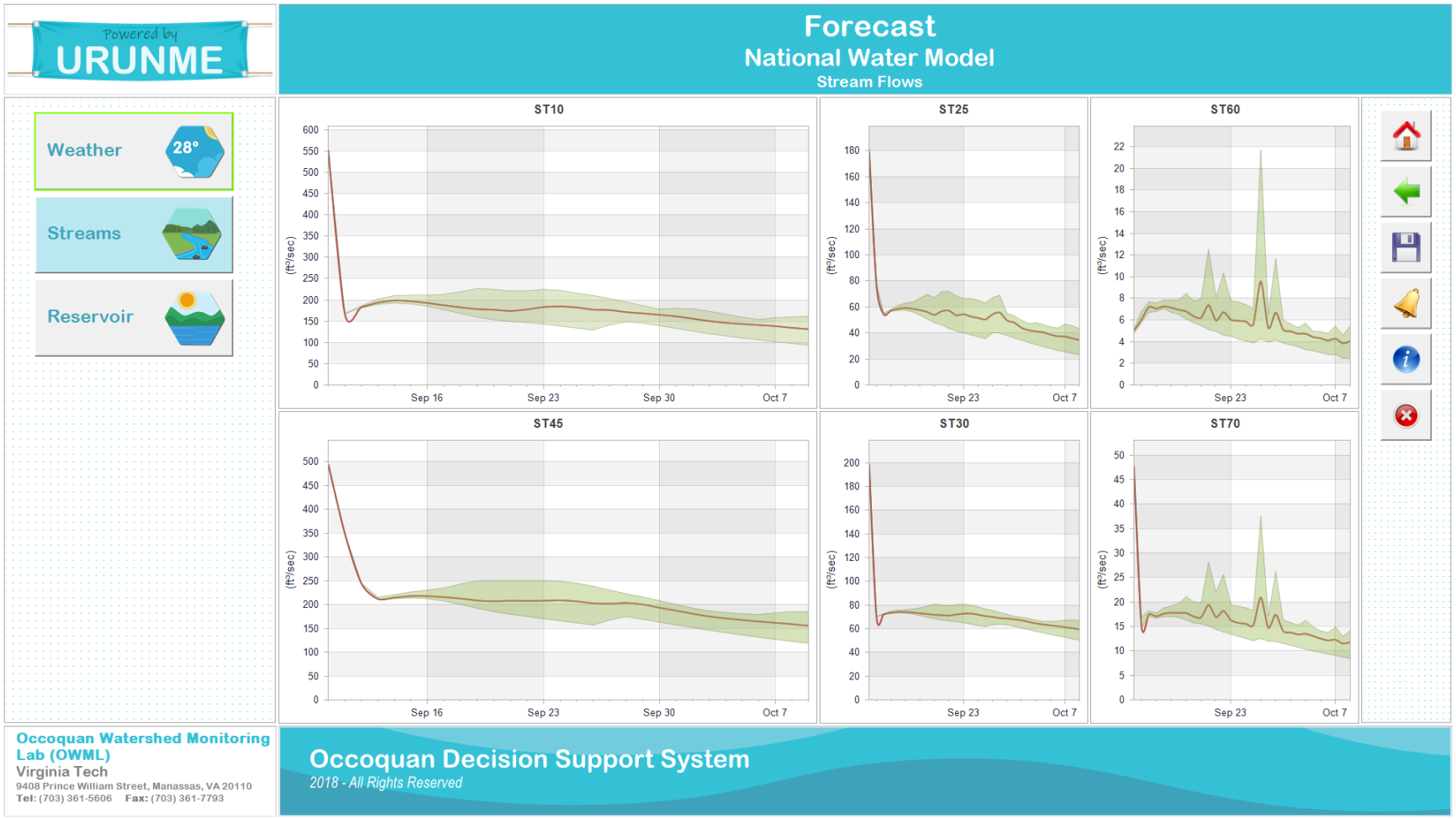

Figure B 4-15. This screen shows the forecasted stream flows by National Water Model (NWM). The solid line (red) indicates the average of four ensembles while the range shows (green) the maximum and minimum. It is opened by clicking the 'Streams' button from the screen shown in Figure B 4-14.

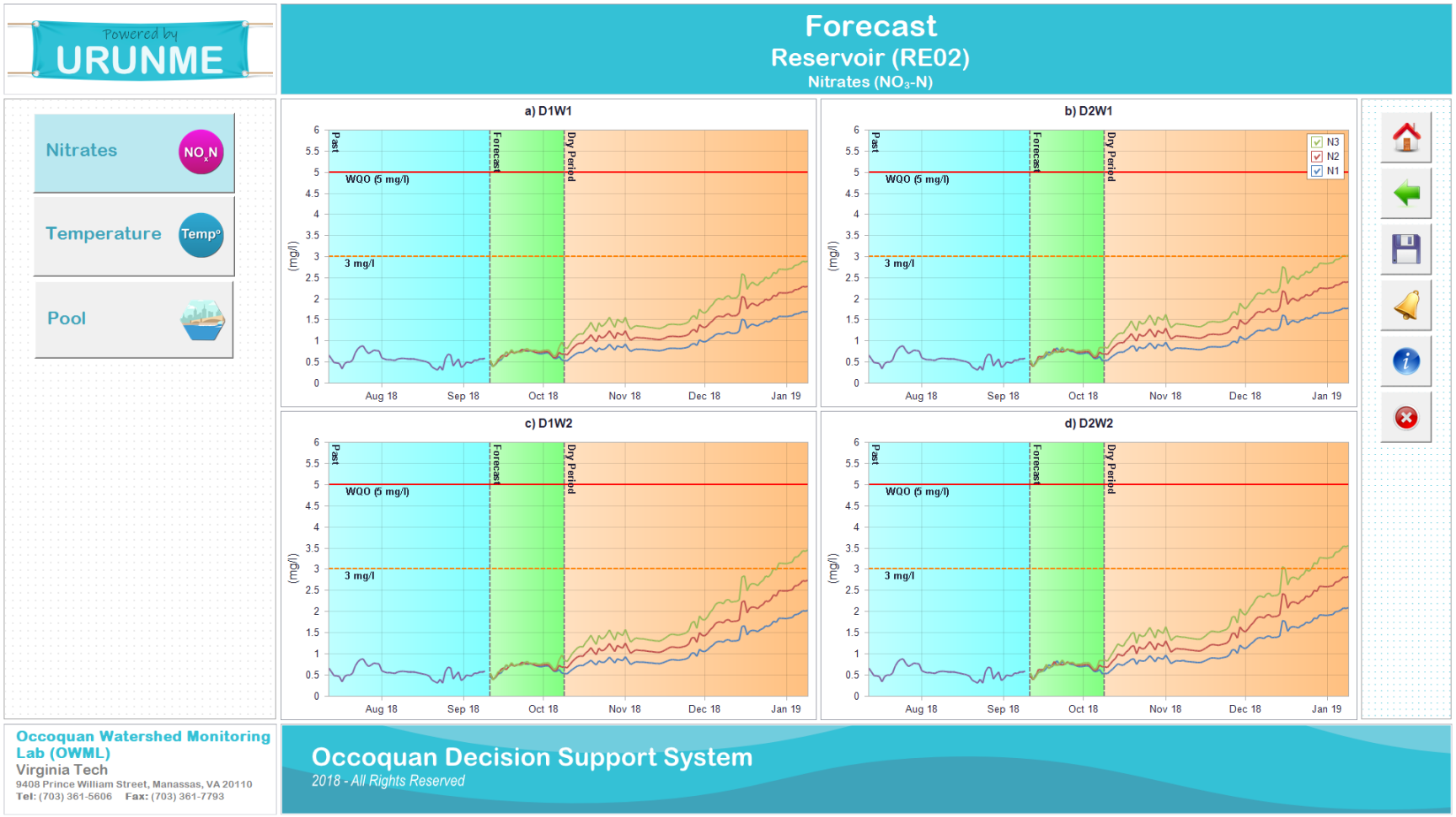

Figure B 4-16. This screen shows the forecasted bottom nitrate-nitrogen as RE02 for 12 future scenarios. It is opened by clicking the 'Reservoir' button from the screen shown in Figure B 4-15.

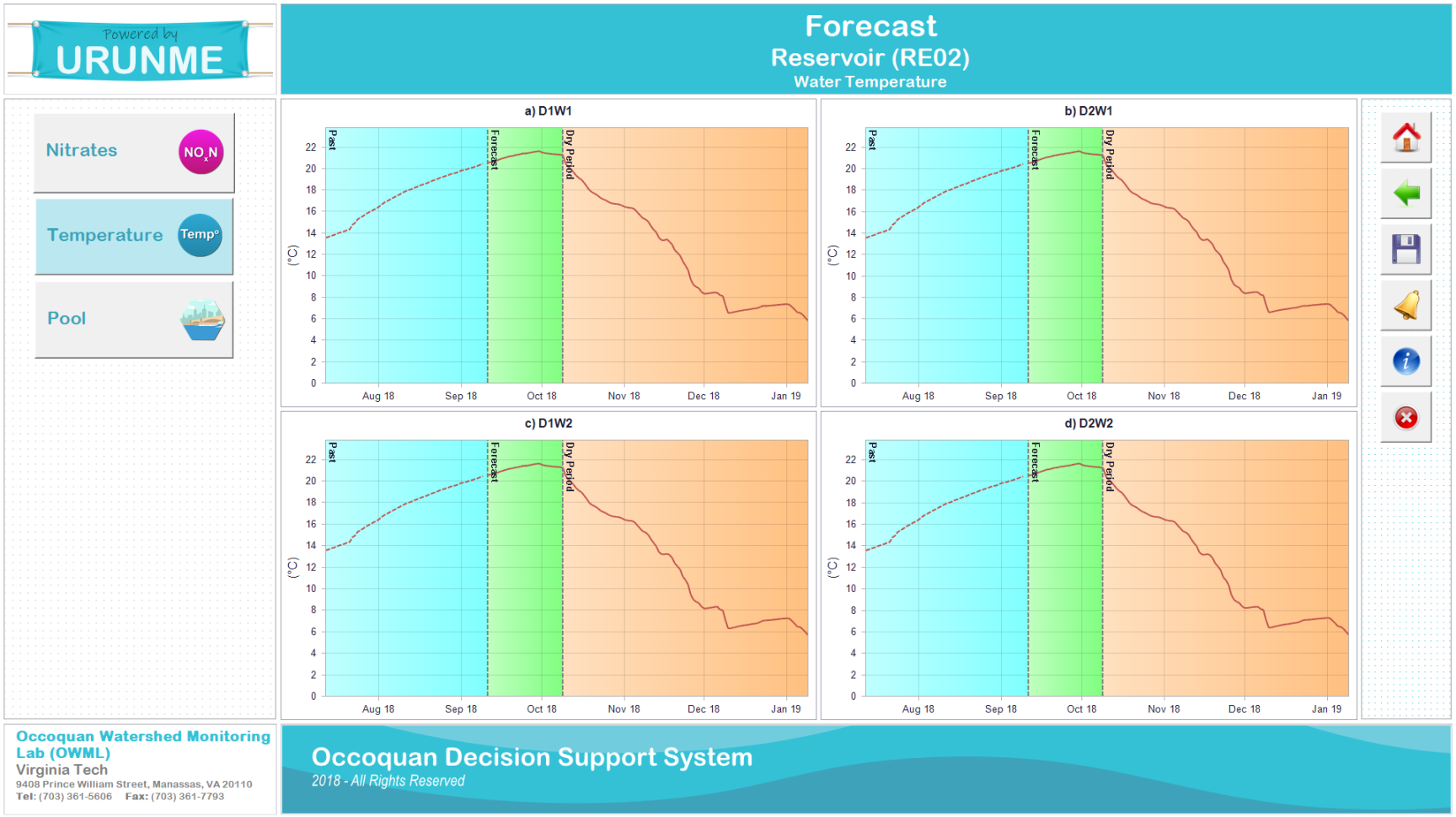

Figure B 4-17. This screen shows the forecasted bottom water temperature as RE02 for 12 future scenarios. It is opened by clicking the 'Temperature' button from the screen shown in Figure B 4-16.

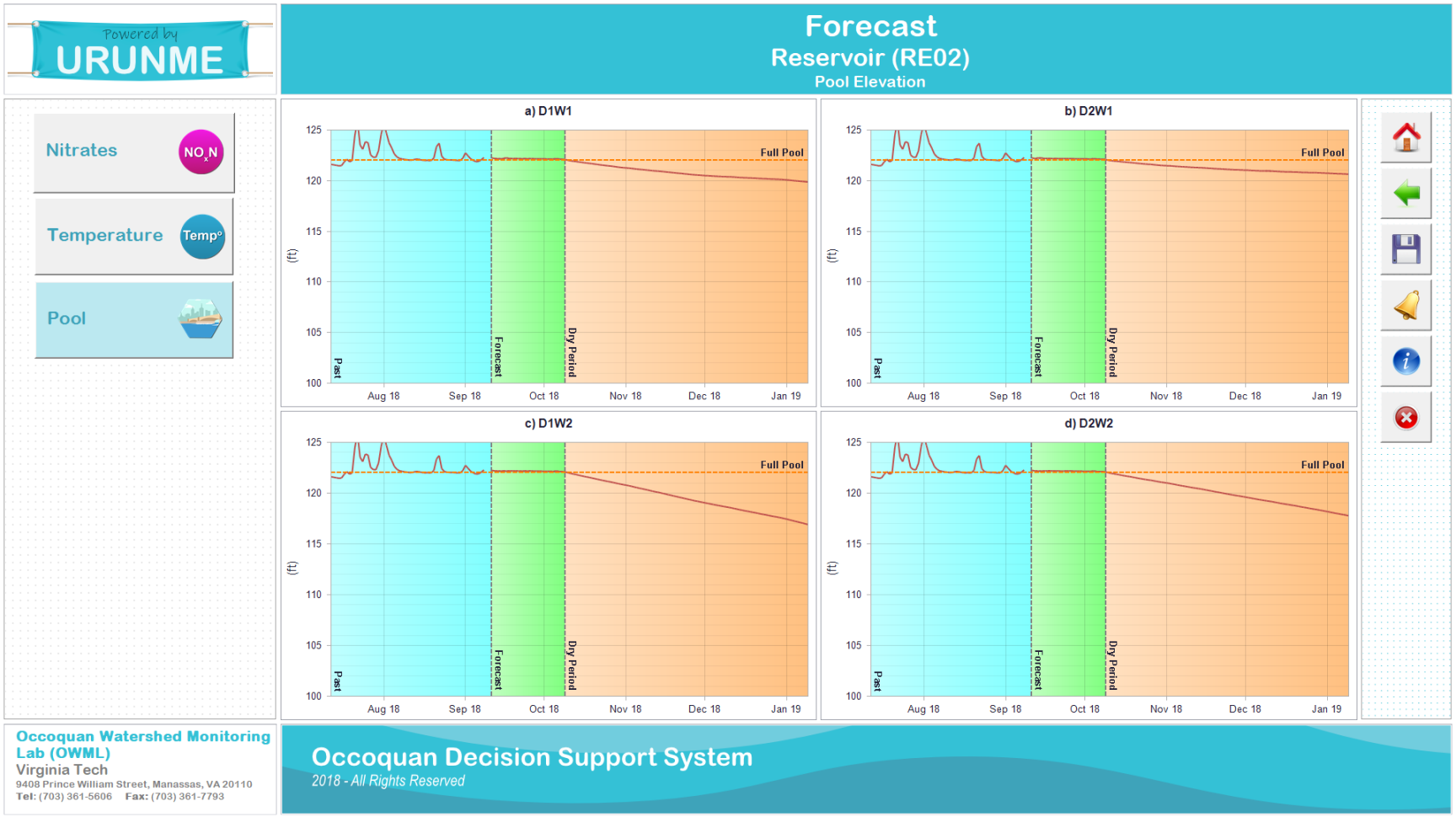

Figure B 4-18. This screen shows the forecasted pool elevation of the reservoir. It is opened by clicking the 'Pool' button from the screen shown in Figure B 4-17.

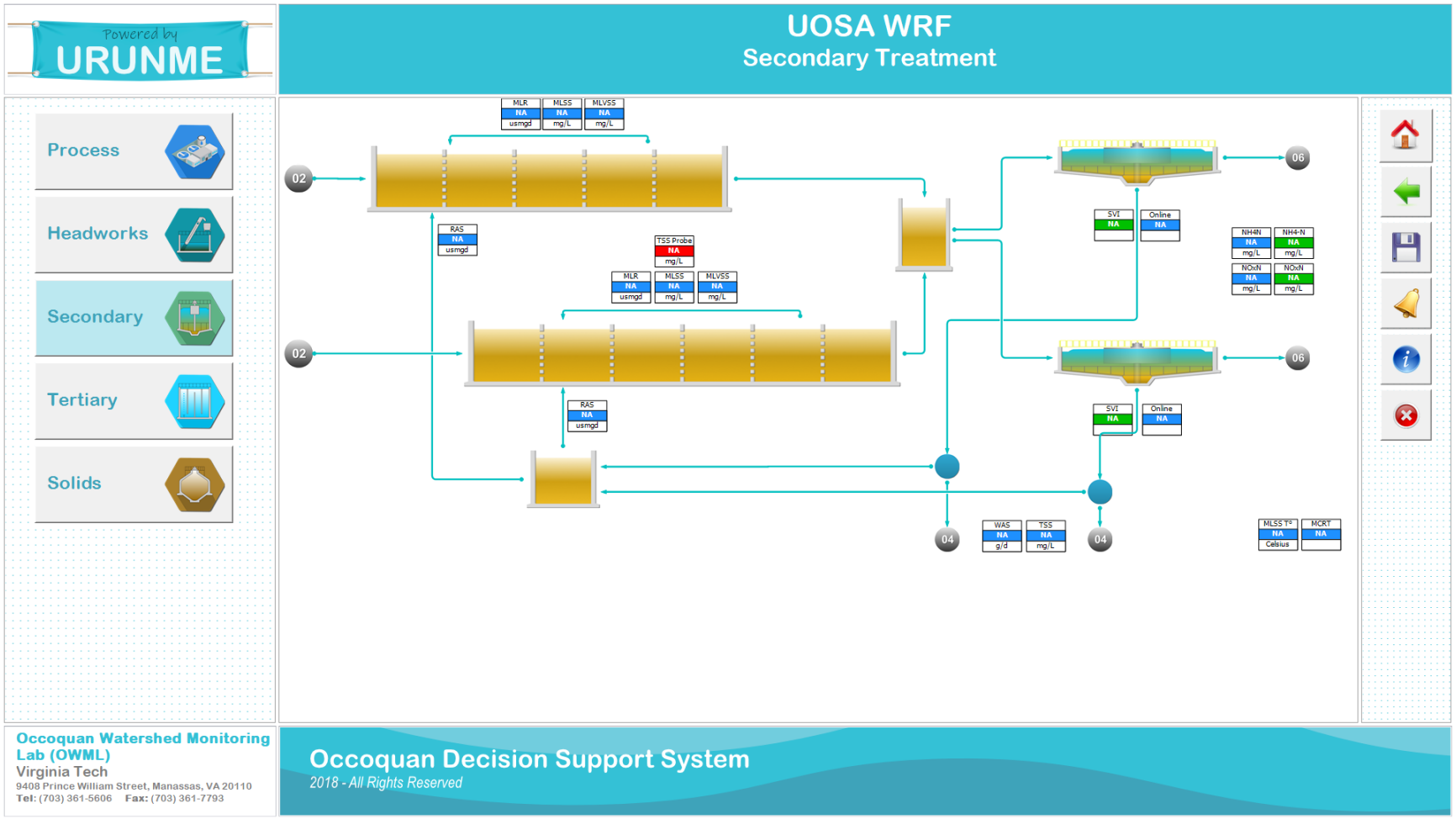

Figure B 4-19. This screen shows the process flow for the secondary treatment of UOSA WRF. Observed data from the laboratory are shown as red, field sensors as green, and the optimized results from the IViewOps as blue. It is opened by clicking the 'UOSA WRF' button from the main screen shown in Figure B 4-1.

Chapter 5 Expansion of the Activated Sludge Model (ASM2d) for simulating advanced processes in water reuse systems

A. G. Lodhi[1, *], A. N. Godrej[1], D. Sen[1,2], R. Angelotti[3], M. Brooks[3]

[1] Occoquan Watershed Monitoring Laboratory. Virginia Tech. 9408 Prince William Street, Manassas, Virginia, 20110

[2] Santa Clara Valley Water District, San Jose, California 95118

[3] Upper Occoquan Service Authority, Centreville, Virginia 20121

[*] Corresponding Author. Email: adlodhi@vt.edu

Keywords: Water and Wastewater Treatment, Activated Sludge Models, Biofilm Models, Physicochemical Models, Modeling Software, Process Simulators

5.1 Abstract

Optimal operation of water reuse systems requires timely and informed decision making in response to fluctuating operational conditions. Advanced process models can be used as day-to-day tools to develop reliable operational strategies. IViewOps3 (version 3.0), an intelligent process simulator, has been used in several wastewater treatment facilities to evaluate and optimize daily plant performance. The process simulator of IViewOps3, however, is based on IWA biochemical models (e.g., ASM, ADM, etc.) and therefore limited to secondary treatment. This paper discusses the development and implementation of a physicochemical model for version 4.0 of IViewOps, capable of simulating advanced processes including pH (acid/base systems), precipitation, oxidation, adsorption, biofiltration, carbonation, chlorination, etc. The full plant model setup and calibration results for the UOSA (Upper Occoquan Service Authority) water reclamation facility in IViewOps4 are presented. How automated data transfer mechanisms are used to obtain current operating conditions from plant information systems (SCADA, LIMS, etc.) to run and calibrate the model on a periodic basis are described. In addition, the paper explains the new architecture of IViewOp4 which decouples the mathematical model from the main software code. The entire model library has been reprogrammed into a new, open-sourced C#.NET DLL (Dynamic Link Library) project, which grants users complete access to the model's code and the ability to modify or add desired parameters and equations.

5.2 Introduction

Mathematical models are essential for the design, optimization, and troubleshooting of wastewater treatment plants (WWTP). Process simulation software uses these models to evaluate

multiple operating conditions and treatment scenarios with greater efficiency. An increasing number of WWTP operators are using these simulators to optimize their operation (Boltz et al. 2010). WWTP simulators consist of modules, representing unit operations and processes, that can be configured and connected by pipes/links to model specific processes. The algorithm used in each module can vary greatly. Some modules include empirical removal rates while others involve complex mathematical models based on detailed equations for substrate removal and biomass growth processes. Examples of the latter include the International Water Association (IWA) Activated Sludge Models (ASMs), namely ASM1, ASM2d, and ASM3 (Henze et al. 2000), and the Anaerobic Digestion Model No. 1 (ADM1) (Batstone et al. 2002). ASMs are among the most widely applied standardized models (Batstone et al. 2012) and serve as the basis for modeling suspended growth processes in most commercial and noncommercial WWTP simulators. These models also serve as the benchmark for new or expanded activated sludge models, both in research and in practice (Morgenroth et al. 2000). Generally speaking, suspended growth simulation results generated from ASM-type models are comparable when given equivalent influent wastewater characteristics and stoichiometric and biokinetic parameter values (Boltz et al. 2010).

The main purpose of these models is to simulate biochemical processes. However, physicochemical processes including acid/base reactions, adsorption, spontaneous or chemical precipitation, redox, and gas transfer, etc., directly or indirectly influence biochemical processes. Although there is a large amount of information available on the fundamentals of these processes, their use in wastewater process modeling is still limited, either due to the complexity or diversity of its sources (i.e., originating from many different water and process environments) (Batstone 2009; Batstone et al. 2012). ASMs and ADM1 include some physicochemical processes, but they are either very basic or empirical in nature. For instance, ASMs use alkalinity to approximate the pH inhibition but lack the mechanism to calculate pH based on acid/base systems. ASM2d provides kinetic rate equations for chemical precipitation without pH dependence (Henze et al. 2000), whereas ADM1 provides an explicit method to calculate pH but doesn’t include processes for spontaneous precipitation in anaerobic digesters. Some published and commercially available models have been able to overcome a few of these limitations for specific applications. Fairlamb et al. (2003), Serralta et al. (2004), and Sötemann et al. (2005) have used acid/base reactions and gas transfer for explicitly calculating pH in reactors. De Haas

et al. (2001), Martin (2005), Mbamba et al. (2015), and Rittmann et al. (2002) have discussed modeling techniques for chemical precipitation using somewhat similar underlying methodology. However, other processes including adsorption, oxidation, thermal hydrolysis, etc. have not been widely adopted by these different models.

5.1.1 Upper Occoquan Service Authority

The Upper Occoquan Service Authority (UOSA) water reclamation facility (WRF) was commissioned in 1978. The plant discharges into the free-flowing stream above the Bull Run Arm of the Occoquan reservoir. Fairfax Water's Griffith Water Treatment Plant (WTP) withdraws water from the tail end of the reservoir close to the dam, resulting in indirect potable reuse of the reclaimed water. The total design capacity of the WRF is 158,987 m^3/d (42 mgd) based on annual average and 204,412 m^3/d (54 mgd) on peak monthly (30 days rolling) flow. It is currently operating at a yearly average of around 121,133 m^3/d (32 mgd). The treatment flow schematic of the WRF is provided in Figure 5-1.

5.1.2 IViewOps3

IViewOps3 "Intelligent View of Operations (version 3.0)" is an intelligent biochemical process simulator. The software was written in C#.NET and implemented at several wastewater treatment plants (WWTP) (Lodhi et al. 2011; Sen et al. 2012). IViewOps's model expands from three biochemical models including IWA ASM2d model (Henze et al. 2000), IWA anaerobic digestion model ADM1 (Batstone et al. 2002), and semi-empirical biofilm model (Sen and Randall 2008). The suspended growth model (SGM) in IViewOps is essentially based on the same set of equations as IWA-ASM2d, with some additional biochemical processes (Lodhi et al. 2010). The number of state variables in SGM has been increased from 19 to 33, as shown in Table A 5-1, and the changes are summarized below:

- To simulate the four-step nitrification and denitrification processes, three new state variables $S_{NO2}, S_{NO}, S_{N_2O}$ are introduced into the model. Nitrifiers have been further divided into two separate groups of microorganisms including ammonium oxidizing bacteria X_{AOB} and nitrite oxidizing bacteria X_{NOB}.

- The fermentable and non-fermentable fractions of the readily biodegradable organic substrate are modeled separately, replacing (S_S) with two new state variables, (S_F) and (S_{nF}). This provides separation of the different COD (chemical oxygen demand) components required in modeling the fermentation process in anaerobic bioreactors. Also, the product of hydrolysis of the slowly biodegradable substrate (X_{CB}) is divided between the fermentable and non-fermentable fraction of the soluble substrate using a new stoichiometric coefficient (f_{SF}).
- The organic nitrogen and phosphorus are modeled as separate state variables in both particulate and soluble forms and are further categorized as biodegradable (X_N, X_P, S_N, S_P) and nonbiodegradable fractions $(X_{NU}, X_{PU}, S_{NU}, S_{PU})$. Hydrolysis of each biodegradable component is modeled as a separate process.
- Two new groups of microorganisms, obligate anaerobic fermenters (X_{AOF}) and obligate anaerobic methanogens (X_{OAM}), were added to the model for simulating the fermentation and methanogenesis processes under anaerobic conditions.
- Methanotrophs (X_{MET}) that use methanol (S_{MET}) as a substrate are tracked separately. This allows the model to determine how much time it will take to establish the required population of methanotrophs in both suspended growth and in biofilm when methanol is added during certain months of the year.

The IViewOps's biofilm model (BGM) is based on the semi-empirical approach outlined by Sen and Randall 2008. Compared to the diffusional model, which is computationally extensive, the semi-empirical method is relatively simpler based on similar structure of the Monod equation as provided in ASMs. A second Monod expression is used in the equations to simulate the changes in biofilm flux rate as based on the COD and ammonium-nitrogen concentrations in the bulk liquid and its effect on biofilm thickness and the fraction of nitrifiers in the biofilm. This model is used with the same set of state variables as SGM.

Application of IViewOps3 has been limited to secondary treatment due to its inability to model advanced physicochemical processes. To simulate a full-scale WRF, a physicochemical model (PCM) has been added to version 4 of IViewOps. This paper will present the new PCM model, its initial setup, and calibration for the UOSA-WRF. The use of automated data transfer

mechanisms to obtain current operating conditions from SCADA (Supervisory Control and Data Acquisition System) and LIMS (Laboratory Information Management System) to run and calibrate the model is discussed. The new architecture of IViewOps4, which allows the decoupling of the mathematical model from the rest of the software code, is also presented.

5.3 Methods

This section provides a brief theoretical background and presents the model equations that are implemented in the PCM. The complete details of the state and algebraic variables, constants, parameters, equations, and stoichiometry of the model are provided in Table A 5-1 to Table A 5-17.

5.3.1 pH (Acid/Base Systems)

ASM models use alkalinity (mol $[HCO_3^-]$/L) as an approximation for the pH for biological reactions. It is assumed that any decrease in alkalinity would indicate a drop in pH, and all biochemical equations are provided with a switch to shut-off the process at low alkalinity. This assumption is generally acceptable for modeling activated sludge and biofilm processes, where wastewater is well-buffered, and a drastic change in pH is not expected (Sötemann et al. 2005). However, physicochemical processes such as precipitation, oxidation, complexation, etc., are directly affected by acid/base systems. For instance, the ionic concentration of PO_4^{3-}, which reacts with different metals to form precipitates, can be significantly less than the state variable for orthophosphates depending upon the pH of the system. Therefore, for most physicochemical processes, calculations of pH and associated concentrations of different ionic species are required to solve the PCM equations.

The pH of a reactor, along with concentration of different acid/base components, can be calculated by solving a set of algebraic equations based on equilibrium, mass balance, and charge balance (Brezonik and Arnold 2011; Stumm and Morgan 1996). Charge balance calculations require concentrations of different cations and anions in the water, which are difficult to obtain. An alternative approach is to use alkalinity in place of charge balance. Although some researchers argue against using alkalinity to calculate pH (Batstone et al. 2012), such methods are commonly used for natural waters (Munhoven 2013). In addition, using alkalinity to calculate pH is advantageous because alkalinity (S_{ALK}) (1) is already a state variable used in

ASM2d and is extensively used in developing the model equations for SGM and BGM in IViewOps, and (2) is more commonly measured in water and wastewater treatment plants compared to different ions required for charge balance.

Based on the above, the following definition of alkalinity is used in the model in place of the charge balance:

$$\left[S_{ALK}\right]+\left[S_{H^+}\right]-\left[S_{OH^-}\right]-\left[S_{HCO^{3-}}\right]-2\left[S_{CO_3^{2-}}\right]-\left[S_{H_2PO_4^-}\right]-2\left[S_{HPO_4^{2-}}\right]-3\left[S_{PO_4^{3-}}\right]$$
$$-0.628\left[S_{CH_3COO^-}\right]-\left[S_{OCl^-}\right]-\left[S_{NH_3}\right]=0 \qquad (5\text{-}1)$$

In addition, a new state variable S_{IC} (total inorganic carbon) is added to the model to keep track of the total inorganic carbon in the system such that:

$$\left[S_{IC}\right]=\left[S_{HCO_3^-}\right]+\left[S_{CO_3^{2-}}\right]+\left[S_{CO_2}\right] \qquad (5\text{-}2)$$

The dissolved carbon dioxide concentration in the water is calculated using the following gas transfer equation:

$$\frac{S_{CO_2}}{dt}=k_L\frac{A_{tank}}{V_{tank}}\left(K_{H_CO_2}P_{CO_2}-S_{CO_2}\right) \qquad (5\text{-}3)$$

The reactions used to simulate the acid-base systems are provided in Table A 5-5. The pH-model equations are summarized in Table A 5-8 (equations related to iron and aluminum in the model are explained in the next section). These equations are solved simultaneously as a system of nonlinear algebraic equations implicitly for each reactor. This essentially means that after each iteration performed by the main solver for calculating the state variables, each reactor calculates its algebraic variables independently, as long as its pH computation option is switched on.

A reactor can be either simulated as open or closed in the pH model. In the case of a closed reactor, the atmospheric transfer of CO_2 is stopped by shutting down Equation 5-3 and keeping S_{IC} constant. On the other hand, an open reactor can be modeled both in equilibrium or nonequilibrium with the atmosphere in terms of CO_2. Nonequilibrium condition is modeled by using Equation 5-3. In case of equilibrium, on the other hand, Equation 5-3 is replaced by Equation 5-4 based on user-defined partial pressure of CO_2:

$$K_{H_CO_2} P_{CO_2} - S_{CO_2} = 0 \tag{5-4}$$

5.3.2 Precipitation

Precipitation occurs when metals ions, with their associated anions, are transferred from liquid to solid phase either due to the addition of certain chemicals or spontaneously due to changes in concentrations, pH, and/or ORP (Oxidation-Reduction Potential) of the water. Chemical precipitation is used extensively in water and wastewater treatment for the removal of colloidal and suspended particles, phosphates, hardness, and heavy metals (Batstone et al. 2012; Metcalf et al. 2003). In addition, spontaneous precipitation can occur in some processes like anaerobic digestion due to metal phosphates (Batstone et al. 2002; Musvoto et al. 2000). Table A 5-6 summarizes the most commonly found precipitates in water and wastewater treatment and their solubility reactions.

Batstone et al. (2012) and De Haas et al. (2001) have discussed different approaches for modeling chemical phosphorus removal. Among the IWA-ASM models, only ASM2d provides equations for modeling phosphorus precipitation using first-order kinetics without pH dependence. Although this approach is much simpler and easier to model, it fails to encompass the complexity of the process by neglecting acid/base systems and metal complexation in water (Mbamba et al. 2015). A more advanced approach is based on chemical equilibrium using a first-order coefficient (Batstone and Keller 2003; Batstone et al. 2012; De Haas et al. 2001; Musvoto et al. 2000; Rittmann et al. 2002). It is essentially based on the assumption that the driving force for precipitation is the excess dissolved species relative to their solubility (Brezonik and Arnold 2011). This model is based on separate kinetic equations for precipitation and dissolution processes (Briggs 1996; De Haas et al. 2001) given as:

$$-\frac{dS_{Me}}{dt} = k_{Pre}\left(Q_{sp} - K_{sp}\right) \;\; if\,(Q_{sp} > K_{sp}) \tag{5-5}$$

$$\frac{dS_{Me}}{dt} = k_{Dis}\left(K_{sp} - Q_{sp}\right)\left(\frac{X_{Me}}{K_{RED} + X_{Me}}\right) if\,(K_{sp} > Q_{sp}) \tag{5-6}$$

where S_{Me} is the metal and X_{Me} is the metal precipitate.

Equation 5-6 includes an additional switch to cease the re-dissolution reaction in case no metal precipitates (X_{Me}) are present in the water. For ferric (Fe^{3+}) and aluminum (Al^{3+}), which readily

complex with ligands such as OH^- and PO_4^{3-}, calculation of each metal's ionic concentration requires additional algebraic equations based on the solution's chemical equilibrium and mass balance (Brezonik and Arnold 2011; Stumm and Morgan 1996). A state variable, with a general form $S_{Me_T^{3+}}$, is required for each of the metals (Fe^3 and Al^{3+}) as a sum of the ionic form and all their hydrolyzed species, as shown in Table A 5-7. Four hydroxyls and one phosphate complex are used to calculate the speciation of ferric ions in water (De Haas et al. 2001). The ionic concentration of the variable $S_{Fe_T^{3+}}$ can be calculated using the following equation:

$$\left[S_{Fe_T^{3+}}\right]-\left[S_{Fe^{3+}}\right]-\beta_{1,Fe^{3+}}\left[S_{Fe^{3+}}\right]\left[S_{OH^-}\right]-\beta_{2,Fe^{3+}}\left[S_{Fe^{3+}}\right]\left[S_{OH^-}\right]^2-\beta_{3,Fe^{3+}}\left[S_{Fe^{3+}}\right]\left[S_{OH^-}\right]^3-\beta_{4,Fe^{3+}}\left[S_{Fe^{3+}}\right]\left[S_{OH^-}\right]^4-\beta_{FeH_2PO_4^{2+}}\left[S_{Fe^{3+}}\right]\left[S_{H^+}\right]^2\left[S_{PO_4^{3-}}\right]=0 \quad (5\text{-}7)$$

The same approach can be used for aluminum species. For other metals, including Ca^{2+}, Mg^{2+}, Mn^{2+}, etc., the complexation is generally neglected and the total metal concentration is considered equal to its ionic concentrations. The complete set of model equations for the precipitation reactions is provided in Table A 5-9.

5.3.3 Oxidation

5.3.3.1 Iron and Manganese

Iron and manganese are among the most important metals involved in physicochemical processes. They are somewhat similar in chemical characteristics and their redox chemistry plays an important part in water and wastewater treatment systems. Iron generally has two important oxidation states, ferric (Fe^{3+}) and ferrous (Fe^{2+}). Manganese, on the other hand, can exist in many oxidation states, (Mn^{4+}), (Mn^{7+}), and (Mn^{2+}). The more reduced state (+2) is relatively more soluble for both metals, especially in the absence of dissolved oxygen and low pH. The oxidized states for these metals, however, have more complicated acid/base systems and complexing and hydrolyzing properties (Brezonik and Arnold 2011). In an oxidizing environment, ferric is the preferred state of iron, and can react with hydroxides, sulfides, and phosphates to form precipitates. This is useful for coagulation, chemical phosphorus removal, etc. On the other hand, reducing conditions favor ferrous ions which are involved in forming precipitates, e.g., vivianite in anaerobic digesters in presence of high phosphorus concentrations.

Elevated concentrations of iron and manganese can cause taste problems or other aesthetic issues such as discoloration of water and staining of laundry and plumbing fixtures.

Oxidation of Fe^{2+}

It can be seen from the pe-pH diagram of iron (Martin 2005) that Fe^{2+} is dominant only at low pH whereas the insoluble $Fe(OH)_{3(s)}$ is dominant over a wide range of pH . Ferrous is therefore more susceptible to oxidation by dissolved oxygen compared to Mn^{2+}. Additionally, ferrous has a low tendency to hydrolyze, except at very low pH, and therefore the hydrolyzed forms can be considered negligible. Although some bacteria can oxide Fe^{2+} at very low pH (< ~4) (Brezonik and Arnold 2011), the primary mechanism of oxidation is abiotic at high pH (pH $\geq$ 5). The oxidation rate is first order with respect to dissolved oxygen and Fe^{2+} and second order with respect to OH^- (Stumm and Morgan 1996), given as:

$$\frac{-dS_{Fe^{2+}}}{dt} = k_{Oxd,Fe^{2+},O_2} S_{O_2} S_{Fe^{2+}} S_{OH^-}^2 \tag{5-8}$$

This indicates a 100-fold increase in the rate of reaction for a unit increase in pH. The oxidation product of this reaction is modeled as $Fe(OH)_{3(s)}$.

Chemical oxidation of iron with other commercially available oxidants (i.e., $KMnO_4$, ClO_2, and O_3) has been studied extensively (Knocke et al. 1991; Reckhow et al. 1991). A general form of equation can be used to model the chemical oxidation of Fe^{2+} by different oxidants with very high kinetic rates given as:

$$\frac{-dS_{Fe^{2+}}}{dt} = k_{Oxd,Fe^{2+},oxidant} S_{Oxd} S_{Fe^{2+}} S_{OH^-}^c \tag{5-9}$$

Although ferrous is readily oxidizable by the oxidants discussed above, it has a very high tendency of making unreactive or less reactive complexes with organic acids (i.e., humic and fulvic acids). Therefore, it can become highly resistant to oxidation in the presence of dissolved organic material (DOM) (Knocke et al. 1991). The inhibition of Fe^{2+} oxidation by organic ligands can be modeled using:

$$Fe^{2+} + L^- \; f \quad FeL^+ \text{ where } K = \frac{[S_{FeL^+}]}{[S_{Fe^{2+}}][S_{L^-}]} \tag{5-10}$$

Due to the non-biodegradable nature of organic ligands (L^-), the complexation of ferrous can be modeled by solving the following two algebraic equations:

$$\left[S_{Fe_T^{2+}}\right]-\left[S_{Fe^{2+}}\right]-\left[S_{FeL^+}\right]=0 \tag{5-11}$$

$$K_{FeL^+}\left[S_{Fe^{2+}}\right]S_U-S_{FeL^+}=0 \tag{5-12}$$

where the ligand L^- is represented by the state variable S_U.

Oxidation of Mn^{2+}

Since Mn^{2+} is more stable towards oxidization, its reaction with O_2 at least 10^6 times slower than Fe^{2+}, it can be considered negligible at neutral pH (Martin 2005). However, at higher pHs (> ~8), the oxidation rate becomes significant. Unlike iron, the manganese oxidation reaction is not stoichiometric and the reaction rate accelerates due to oxidation products (i.e., the reaction is autocatalytic). Therefore, the oxidation of Mn^{2+} is modeled using a two-term rate equation, uncatalyzed and catalyzed, given as under:

$$-\frac{dS_{Mn^{2+}}}{dt}=k_{1,Mn^{2+},O_2}S_{Mn^{2+}}S_{O_2}S_{OH^-}^2+k_{2,Mn^{2+},O_2}S_{Mn^{2+}}S_{MnO_2} \tag{5-13}$$

Oxidation of Mn^{2+} yields a mixture of precipitates that can be represented as MnO_2. Knocke et al. (1991) and Reckhow et al. (1991) have provided the rate constants for the oxidation of Mn^{2+} by some commonly used oxidants, using a general form of the above equation:

$$-\frac{dS_{Mn^{2+}}}{dt}=k_{1,Mn^{2+},Oxd}S_{Mn^{2+}}S_{Oxd}S_{OH^-}^2+k_{2,Mn^{2+},Oxd}S_{Mn^{2+}}S_{MnO_2} \tag{5-14}$$

Presence of DOM can slow down the oxidation of Mn^{2+} but can be neglected since the effect is much less significant compared to Fe^{2+} (Knocke et al. 1991).

Reductive redissolution

Redissolution of manganese precipitates is a very slow process which is not commonly observed in treatment plants and can therefore be neglected. However, iron can undergo reduction in anaerobic processes and needs to be modeled. The literature on the kinetics of reductive redissolution of insoluble iron and manganese is very sparse. The difficulty in studying such reactions is due to the fact that the reactants are solid and the reduction process can be both biotic or abiotic in nature (Brezonik and Arnold 2011). There can be many parallel pathways for

reductive redissolution (Martin 2005). In addition, there may be some inhibitions which can reduce the redissolution process.

One approach is to assume all iron as ferric in aerobic conditions and ferrous under anaerobic conditions. Another more complex method is to model the overall redox reactions and provide redox potential as an output (Batstone et al. 2012). A more middle-of-the-road approach is to use a pure redox rate reaction to convert Fe^{3+} to Fe^{2+}, instead of redissolution, based on a user-defined value of ORP for each reactor. This would eliminate the need of knowing the nature of the reducing mechanism and the reaction rate can thus be approximated using the following Nernst equation:

$$-\frac{dS_{Fe^{3+}}}{dt} = k_{Red,Fe^{3+}}\left(1-\frac{S_{Fe^{2+}}}{S_{Fe^{3+}}}\frac{10^{\frac{ORP}{0.059}}}{K_{eq,Fe^{3+},Fe^{2+}}}\right) \tag{5-15}$$

5.3.3.2 Chlorination

Chlorine is one of the most widely used disinfectants in the world because of its relatively low cost, high rate of pathogen inactivation, and ability to maintain residual in distribution systems (Metcalf et al. 2003). However, the main disadvantage is its non-selectivity (Stumm and Morgan 1996), which results in forming various disinfectant by-products (DBPs).

Free chlorine

Cl_2, HOCl, and OCl^- are collectively known as free chlorine. At high pH (>5), hydrolysis of chlorine gas is almost complete (Brezonik and Arnold 2011) and can be neglected. The acid-base reaction of $HOCl/OCl^-$ is modeled as part of pH calculation. The reaction of chlorine with an organic substrate (S) can be modeled using second-order kinetics (Brezonik and Arnold 2011; Deborde and Von Gunten 2008) :

$$-\frac{dS}{dt} = k_1 S_{HOCl} S + k_2 S_{OCl^-} S \tag{5-16}$$

Chloramines

Chloramines are formed by the reaction of NH_3 with HOCl. Monochloramine (NH_2Cl) is the major product of chlorination in the presence of ammonia. It can be further oxidized to dichloramine ($NHCl_2$) and trichloramine (NCl_3), although at a much lower rate (Stumm and Morgan 1996). The rate of reaction for ammonia, monochloramine, and dichloramine (expressed

generally as S_{N_T}) can be written in the following general form (Brezonik and Arnold 2011; Weil and Morris 1949):

$$-\frac{dS_{N_T}}{dt} = kS_{HOCl}S_{N_T} \tag{5-17}$$

Breakpoint Chlorination

Trichloramine is an unstable compound which can further decompose into Cl^- and N_2, especially at higher Cl_2:N ratios (>7.6: 1) (US-EPA 1999). The rate reaction for the decomposition of trichloramine is independent of free chlorine concentration and given as under (Deborde and Von Gunten 2008; Kumar et al. 1987):

$$-\frac{dS_{NCl_3}}{dt} = 2\left(k_{0,NCl_3} + k_{1,NCl_3}S_{OH^-} + k_{H_2PO_4^-}S_{H_2PO_4^-} + k_{HPO_4^{2-}}S_{HPO_4^{2-}} + k_{HCO_3^-}S_{HCO_3^-} + k_{2,NCl_3}S_{OH^-}^2\right)S_{NCl_3} \tag{5-18}$$

Chlorine decay:

In addition to the above reactions, chlorine demand can also be created by other substances in water including algae, basin walls, or other unknown inorganics (Fisher et al. 2011). To cater to such demand, a first-order reaction is added to the model based on the following equation:

$$-\frac{dS_{Cl_2}}{dt} = kS_{Cl_2} \tag{5-19}$$

where S_{Cl_2} represents the state variable for free chlorine.

5.3.3.3 Ozonation

Ozone is one of the most powerful oxidants used in water treatment and is capable of oxidizing many inorganic and organic compounds. It is used for many applications including disinfection; color, smell, and taste removal; oxidation of manganese; and removal of organics. As a disinfectant, it is more selective towards organic compounds than chlorine and therefore does not contribute to the formation of DBPs. It decomposes spontaneously in water by a complex mechanism forming free radicals (Hoigné and Bader 1983a; Hoigné and Bader 1983b; Stumm and Morgan 1996). Part of the ozone reacts directly with the solutes but this is a highly selective, and often slow, process. However, the hydroxyl free radicals are less selective, fast, and can easily oxidize all types of organic compounds and many inorganic solutes. The kinetic formulation of ozone oxidation is based on the following first-order equations, with respect to

ozone and solute concentration respectively (Hoigné and Bader 1983b; Stumm and Morgan 1996):

$$-\frac{dS}{dt} = kS_{O_3}S \tag{5-20}$$

Although ozone is present in much higher concentrations during the ozonation processes, the $^{\bullet}OH$ radical is still responsible for significant removal of substrate, especially if the substrates are resistant to O_3. Therefore, an additional rate expression is added to Equation 5-20 for direct reaction of $^{\bullet}OH$ with substrate S (Brezonik and Arnold 2011; Von Gunten 2003), given as under:

$$-\frac{dS}{dt} = k_{O3,S}S_{O_3}S + k_{^gOH,S}[^gOH]S \quad \text{where} \quad [^gOH] = S_{O_3}R_c \tag{5-21}$$

Von Gunten (2003) has documented a large number of rate constants for ozone and $^{\bullet}OH$ and recommends $R_c > 10^{-7}$ for the initial phase and $10^{-9} < R_c < 10^{-7}$ for the secondary phase of ozonation. The oxidation products are often hard to predict. In some cases, the ozonation process partially mineralizes the organic matter making the remaining oxidized organic compounds more biodegradable and biologically removable (e.g., through biofiltration).

In addition to ozone, hydrogen peroxide (H_2O_2) is used for the advanced oxidation of organic pollutants involving the production of highly nonselective reactive $^{\bullet}OH$ radicals. An equation similar to 5-21 can also be used to model H_2O_2. The model equations for oxidation using ozone and hydrogen peroxide are provided in Table A 5-14 and Table A 5-15 respectively.

5.3.4 Adsorption

Adsorption is a mass transfer process in which a constituent or solute (i.e., adsorbate) in the liquid phase is partitioned onto a solid surface (i.e., adsorbent). The use of adsorption processes is not very common in conventional wastewater treatment processes (Metcalf et al. 2003). In contrast, water reuse and treatment plants frequently apply adsorption for the removal of trace organics from drinking water. It can also be used as a polishing process for the removal of remaining dissolved organic material after normal biological treatment. The application of activated carbon adsorption is generally employed in two ways: (1) powdered activated carbon (PAC) and (2) granular activated carbon (GAC). PAC can be directly applied to a water stream in slurry form. The application points are generally upstream of the settling basins to allow a

sufficient amount of contact time for adsorption. The exhausted carbon is combined with waste sludge and removed for disposal by gravity settling. In contrast, GAC is typically used as a fixed bed column, where water is applied at the top and withdrawn from the bottom and the carbon is held in place by the underdrain system.

Freundlich and Langmuir are the two most commonly used isotherms in water and wastewater treatment processes. The Freundlich isotherm equation has no kinetic basis and therefore cannot be used in a mass balance problem. The Langmuir model, on the other hand, is directly derived from kinetic principles. It is based on the assumptions that (1) there are a fixed number of accessible sites on the adsorbent surface, and (2) adsorption is reversible. The rate of adsorption in the Langmuir model is proportional to the difference between the maximum amount that can be adsorbed at a given concentration and the amount that has already been adsorbed (i.e., the driving force).

To model the Langmuir adsorption process, separate rate equations are used for simultaneous adsorption and desorption processes as functions of the fluid-phase and the adsorbed concentration of the constituent. Suppose the bulk liquid concentration of organic material is S and the adsorbed concentration on the surface of the adsorbent is X_{AS} (Brezonik and Arnold 2011; Plazinski et al. 2009). Then, the general form of adsorption and desorption equations can be given as:

$$-\frac{dS}{dt} = k_{Ads} S \left\{ q_{max} X_A - X_{AS} \right\} \tag{5-22}$$

$$\frac{dS}{dt} = k_{Des} X_{AS} \tag{5-23}$$

Equations 5-22 and 5-23 are added separately for each of the COD components in the model (Table A 5-16). At steady state, the rate of adsorption is equal to the rate of desorption. Equating equations 5-22 and 5-23 gives the general form of the Langmuir isotherm:

$$q = q_{max} \frac{S}{k+S} \text{ where } q = X_{AS} / X_A \text{ and } k = k_{Des} / k_{Ads} \tag{5-24}$$

For PAC, both X_A and X_{AS} are considered state variables. However, to model a fixed bed GAC contactor, the value of X_A is fixed based on the fill fraction and bulk density of activated carbon where:

$$X_A = Bulk\ density\ of\ AC \times Fill\ Fraction \text{ where } Fill\ Fraction = \frac{Bed\ Volume}{Reactor\ Volume} \quad (5\text{-}25)$$

The adsorption equation used in IViewOps is a modified form of Langmuir isotherm which assumes that the adsorption is fractal rather than linear (Skopp 2009):

$$-\frac{dS}{dt} = k_{Ads} S^a \left\{ q_{max} X_A - X_{AS} \right\} \quad (5\text{-}26)$$

Based on the above, Equation 5-24 can be rewritten as:

$$q = q_{max} \frac{S^a}{k + S^a} \quad (5\text{-}27)$$

One advantage of using the above equation is that when $k >> S^a$, the equation can also be used to model Freundlich isotherm as well:

$$q = \frac{q_{max}}{k} S^a \text{ where } k + S^a \approx k \quad (5\text{-}28)$$

As explained above, for steadystate conditions the Langmuir model will always simulate a fully exhausted carbon with no net removal of the substrate ($S_{in} = S_{out}$). To model the carbon in the adsorptive phase, the following equation is added to the PCM to simulate non-equilibrium conditions (adsorption > desorption) at steadystate.

$$-r_{Sat} = k_{Sat} X_{AS} \quad (5\text{-}29)$$

Equation 5-29 models the removal of some adsorbed organics from the carbon sites without adding it back the bulk liquid in order to simulate only partial saturation of carbon sites. The coefficient k_{Sat} is set to zero for time dynamic simulations.

GAC beds can also be used as biological activated carbon (BAC) reactors, where biofilm growth on the carbon surface biodegrades the organic matter to regenerate the adsorptive sites. One of the key advantages of BAC is the ability of the biofilm to hydrolyze and biodegrade some nonbiodegradable organics (e.g., DOM) (Simpson 2008). As explained before, IViewOps employs a semi-empirical model to simulate the biofilm growth. The biofilm model (BGM), howover, only simulates the oxidation of the biodegradable components of the COD (e.g., S_F, S_{nF}, S_A, etc.). To model the uptake of inert orgainics (S_U) by the BGM, a new equation is added

to the PCM, which simulates the hydrolysis of adsorbed non-biodegradable (X_{AU}) into biodegradable COD (S_F):

$$-\frac{dX_{AU}}{dt} = k_{Hyd} X_{AU} \tag{5-30}$$

5.3.5 Effect of temperature

Temperature has a very strong effect on reaction rates and equilibrium constants. The van't Hoff equation is the most commonly used method to quantify changes in the equilibrium constant (K) for a reaction, with temperature (T), using standard enthalpy ΔH^{o} (Brezonik and Arnold 2011; Stumm and Morgan 1996), given as under:

$$\ln \frac{K_2}{K_1} = \frac{\Delta H^{o}}{R}\left(\frac{1}{T_1} - \frac{1}{T_2}\right) \tag{5-31}$$

Rearranging Equation 5-31, $K_2 = K_1 e^{\frac{\Delta H^{o}}{RT_1T_2}(T_2 - T_1)}$ or

$$K_2 = K_1 \theta^{(T_2 - T_1)} \text{ where } \ln \theta = \frac{\Delta H^{o}}{RT_1T_2} \tag{5-32}$$

Equation 5-32, called the Arrhenius equation, is used to correct all the model parameters for a given temperature based on user-defined θ values in IViewOps.

5.3.6 Effect of ionic strength

In the case of a very dilute solution, the activity of an ionic species and its molar concentration is assumed to be the same. However, under non-ideal conditions, the activity of a component is lower than its concentration and is defined as $a_i = \gamma_i c_i$, where γ_i is the activity coefficient and c_i is the molar concentration of ion i. The simplest method of calculating an activity coefficient is to use the Debye-Hückel equation:

$$\log(\gamma_i) = -Az_i^2\sqrt{I} \text{ where } I = \frac{1}{2}\sum_{i=1} c_i z_i \tag{5-33}$$

where I is the ionic strength, A is a solvent specific constant, and z is the valence number of ion i (Brezonik and Arnold 2011; Stumm and Morgan 1996). This method is applicable for I <

~0.005. For higher ionic strengths (e.g., I < ~0.1), an extended form of the Debye-Hückel equation is used:

$$\log(\gamma_i) = \frac{-AZ_i^2\sqrt{I}}{1+Ba_i\sqrt{I}} \tag{5-34}$$

In IViewOps, the activity coefficient is calculated using a user-defined ionic strength based on the relevant the Debye-Hückel equation.

5.3.7 Open source model library

Most of the commercial water and wastewater process simulation software are black-box models. Although the model equations used in the software may be fully documented, the actual software code is not accessible as in cases of open-sourced models. This is not only because of the proprietary nature of the code but also because the mathematical model is generally buried deep inside the software architecture and cannot be decoupled from the solver, which was the case with IViewsOps3. One of the objectives of this research was to re-architecture IViewOps to decouple the model code from the main software to provide the user a standalone dynamic link library (DLL). This not only allows the user to understand the model structure and equations in detail but also to modify or add new equations to improve the existing processes in the model.

A new DLL was created for IViewOps4 in C#.NET and all the equations were reprogrammed in the new project with strict one-way coupling from the main software to the model. This DLL library is freely available to users and can be accessed using Visual Studio community (free) edition. Changing the model would require the user to recompile the DLL project after the modifications are made and replace it in the installation directory of IViewOps4. The class diagram the new library is shown in Figure 5-2

The generic Component<T> class defines all the state and algebraic variables in the model. The three model classes (SGM, BGM, and PCM) implement the IModel interface, which provides the structure for writing the equations in matrix notation. IModel requires each class to implement three properties (Process, Derivatives and Stoichiometry) and three methods (SetProcesses, SetDerivatives, and SetStoichiometry) in addition to the default coefficients for each model. At the start of the model run, the IViewOps's solver automatically writes the temperature corrected values of the coefficients for each model class. It then calls the SetStoichiometry method to set

the stoichiometric constant for each process. Subsequently, the SetProcesses and SetDerivatives methods are called at each iteration to set processes and derivative properties, respectively, based on the state variables provided as an argument to the methods, until convergence is achieved.

5.4 Results and Discussion

As a part of this research, IViewOps has been setup at UOSA-WRF and is currently being used as a day-to-day operational tool. It retrieves the input data directly from the plant information system and runs the model on a periodic basis to assist the operators. Model inputs are obtained using an Excel linkup file that has been programmed to retrieve data directly from the SCADA system. The linkup file performs various QA/QC operations and calculations on the raw data to create 30-day and 24-hour averages of various input parameters (e.g., flows, dissolved oxygen setpoints, online tank status, etc.). Additionally, laboratory data is obtained from the LIMS and compared with simulated results to validate the model performance on a regular basis.

This section describes the full-plant model setup of UOSA-WRF created in IViewOps4 and discusses the initial calibration of the model. To cover the entire range of operational variations in the plant (e.g., differences in water temperature, plant configuration, etc.), three months from summer (July, August, and September in 2017) and three from winter (January, February, and March in 2018) were selected for the model runs. Due to the complex nature of the plant, the model was setup in three separate configuration files (for the secondary treatment, chemical phosphate removal, and filtration systems) and then sequentially linked together to simulate the entire system (Figure 5-3 to Figure 5-5).

Tank sizing was based on the design specifications provided by the plant (Table 5-1). Input data for the model runs were based on either the last 30-days or 24-hours averages. For instance, the plant flows for each scenario at various key locations (e.g., influent flows, RAS, WAS, digester effluent, etc.) were estimated based on the last 30-day average, which corresponded to 1 to 2 MCRT (mean cell residence time) for the UOSA-WRF to build the correct biomass concentrations in the system. The 30-day averaged flows for each scenario are summarized in Table 5-2.

The plant operational configuration was based on the last 24-hours online status of each tank. IViewOps automatically reads the online status of each process unit (e.g., primary clarifier, secondary clarifier, aerations tanks, digesters, etc.) from the linkup sheet and internally uses the

correct number of tanks to simulate the process. The status of each system for the given scenario is provided in Table 5-3.

5.4.1 Influent

A number of different influents are modeled to simulate flows from different sources (Figure 5-3). The raw influent characteristics are calculated for each month using baseline data generated from yearly averages. Generally, an adequate number of the last 30-day raw influent measurements are not available at most of the WWTPs to properly characterize the influent. Yearly means are therefore used to define the baseline influent flows and concentrations, which depict the average flow conditions at a plant (Table 5-4). It is assumed that, for any given day, if the last 30-day averaged influent flow is higher than the baseline flow by a given margin (e.g., 10%), a wet period is assumed and the influent concentrations must be diluted by the same margin. Similarly, the same logic is applied to lower than baseline flow during the last 30 days, which should be concentrated to depict the dry weather conditions. The following relationship was used to correct the concentration of each influent constituent (e.g., COD, NH_4^+, etc.):

$$Corrected\ Concentration = \frac{Base\ Flow \times Base\ Concentration}{Actual\ Flow} \tag{5-35}$$

The corrected raw influent concentrations for each scenario are shown in Table 5-4. In addition to the above, flow characteristics from other sources including septage, recycle flows from different locations including the emergency retention pond (ERP), multimedia filters, and plant toilets are summarized in Table 5-5.

5.4.2 Headworks

The plant's headwork primarily consists of mechanically cleaned bar screens, vortex grit chambers, and circular primary clarifiers (Figure 5-3). Screens and grit chambers were setup as fixed percentage removal of inert TSS (X_M) by 0.25% and 5.0%, respectively. The percentage removal of TSS in the primary clarifier was modeled using a rating curve based on the hydraulic loading rate ($m^3m^{-2}d^{-1}$) developed using historical data (Figure 5-6).

Calibration of the clarifiers was accomplished by comparing the simulated primary effluent concentrations and the amount of biogas produced in the digesters to the last 30-day averaged

observed values. Results are shown in Table 5-6. It can be seen that the PBIAS (percentage bias) for all the simulated primary effluent variables are less than 5%. The MAE (mean absolute error) and RMSE (root mean square error) for all the variables are also relatively small. It can be noted that the TSS removal efficiency of primary clarifiers varied significantly with the hydraulic loading rates and was worse during two-tank operation, particularly in September 2017. The digester biogas calibration is discussed in Section 5.4.4.

5.4.3 Secondary Treatment

The secondary treatment system of UOSA-WRF is based on the Modified Ludzack-Ettinger (MLE) denitrification process. The system is modeled in two separate trains: East and West (Figure 5-3). The East train is modeled using three parallel tanks, each containing an anaerobic selector, an anoxic zone, and four aerobic zones in series. The West train, on the other hand, has four parallel tanks, each containing an anaerobic selector followed by two swing zones and four aerobic zones. To model the plug flow nature of the aeration tanks, separate reactors are used in the model for each zone (these zones are within the same tank and are not physically separated). Swing and aerobic zones in the tanks are equipped with a diffused aeration system controlled by DO setpoints, which are used as the input to the model. The input design parameters for diffused aeration system are provided in Table 5-8. The combined outflow from the East and West side aeration basins is divided among all the secondary clarifiers (Table 5-2).

DO concentrations in the aeration tanks vary frequently in the aeration tanks. The steady state simulations are therefore run using the last 24-hour averaged DO concentration (Table 5-7). The calibration of the secondary system was accomplished by tweaking the SGM coefficients and using the laboratory data to compare observed vs. simulated values for three key parameters: secondary effluent concentrations, MLSS in different reactors, and total air flow rates to the aeration tanks.

The calibration results for secondary effluent concentrations are provided in Table 5-9. It can be seen that the model was able to simulate all the effluent parameters, with the exception of ammonia-nitrogen, within a PBIAS of 10%. The relatively higher PBIAS of 11.61% for ammonia-nitrogen can be neglected due to very small MAE and RMSE (around 0.02 mg/L). The model was able to accurately capture the variation in effluent nitrate-nitrogen concentrations in

the plant effluent between summer and winter months. In summer, higher nitrate concentrations in the plant effluent benefit the reservoir and therefore denitrification is minimized by shutting off the nitrate recycle flows and bringing more aeration tanks online. In winter, however, the reservoir loses its denitrification capacity and the effluent nitrates are regulated by maximizing the denitrification using more anoxic zones and higher nitrate recycles. The simulated effluent nitrate concentrations in the summer remained between 14.84 mg/L to 15.86 mg/L, which are close to the observed values. By bringing more anoxic volume online in the winters, the model was able to reduce the nitrate concentrations in the range of 7.57 to 8.57 mg/L.

The model was also able to predict the luxury uptake of phosphorus by phosphorous accumulating bacteria (PAOs). Although the UOSA plant was not designed for biological phosphorus removal (BPR), high MCRTs and the availability of sufficient anaerobic and anoxic volumes promoted the growth of PAOs throughout the year. This allows significant phosphorus uptake in the secondary system before tertiary chemical P removal. Nonetheless, the presence of these bacteria presents some operational challenges especially during solids dewatering due to unintended precipitation of brushite and struvite, as explained in Section 5.4.4.

The calibration results for aeration tanks are provided in Table 5-10. The total air flow to the aeration tank was calculated by the model and compared with the observed air flows from the blowers. Since the DO input concentrations were daily averages, simulated airflows were only compared to the last 24-hour averaged observed combined airflow for all the aeration tanks. In addition, the MLSS calculated by the model was compared to both the last 30-day average of laboratory data and the last 24-hour average online probe values from SCADA. The results indicated that the model was able to predict a PBIAS of less than 1% for airflow and less than 5% for MLSS. The outputted MLVSS/MLSS ratios were in the range of 0.8 to 0.85, which are close to the general observed values at the plant.

5.4.4 Digestion and Solids Handling

Waste activated sludge (WAS) is thickened using a dissolved air floatation (DAF) system and then blended with primary sludge, screened, and fed into the anaerobic digesters (Figure 5-3). The DAF system was setup as a percentage removal (95% removal of TSS) module followed by bending tanks. The primary digester system was modeled at a constant operating temperature of

35ºC and fixed CO_2 partial pressure of 0.325 atm, based on the composition of the biogas. The model was able to predict the pH and alkalinity of the digester's effluent with a PBIAS of less than 8.1%, as shown in Table 5-11. The simulated biogas production of the digester was found to have a PBIAS of 5.9%. Calibration of the digesters' effluent ammonia and orthophosphates was accomplished by adjusting the rate of hydrolysis and precipitation of brushite and struvite in the digester. The results indicated a PBIAS of less than 5% for both nutrients.

Due to the high concentration of CO_2 gas in the digester effluent, the pH of the supernatant remains close to neutral even in the presence of the high alkalinity produced during digestion (Table 5-11). However, due to the low pressure caused by centrifugal dewatering, a considerable amount of CO_2 escapes the water causing a sudden increase in pH. This results in further precipitation of brushite and struvite in the system, especially at high orthophosphate concentrations. This causes scaling and blockages of the dewatering system and requires frequent maintenance at the plant. Using the pH solver in IViewOps4, the model was able to successfully predict these precipitations. Currently, the exact increase in the observed pH and the amount of precipitation in the dewatering system are not measured at the plant. The model, however, can be used to simulate these undesirable situations in the future as long as sufficient observed data are available to calibrate the model.

The digested sludge is blended with the DAF sludge in the holding tank and then dewatered using three centrifuges. The centrifuges were modeled using the as a percentage removal module (97% removal of TSS). The centrate from the centrifuges goes through the sludge holding tank before it is mixed with supernatant from the DAF and sent back to the headworks as recycled flow (Figure 5-3).

5.4.5 Chemical Phosphorus (P) Removal

The chemical P removal is achieved by using lime ($CaOH_2$) to increase the pH and promote precipitation. The system consists of rapid mix and flocculation basins followed by chemical clarifiers. To subsequently neutralize the pH, a two-stage recarbonation system is used, with clarifiers after the first stage. Coarse bubble diffusers are used to feed CO_2 into the recarbonation system using the flue gases from different processes in the plant and purchased CO_2.

The lime dosage was simulated by adding a given amount Ca^{2+} ($S_{Ca^{2+}}$) and alkalinity (S_{ALK}) upstream of the rapid mix basin, based on monthly supply rates provided by the plant (Table 5-12). The rapid mix and flocculation were simulated using the chemical reactor modules (Figure 5-4) modeling three precipitates: calcium carbonate ($CaCO_3$), magnesium hydroxide ($Mg(OH)_2$), and hydroxyapatite ($Ca_5(PO_4)_3OH$). Calibration of the precipitates was carried out in two steps. First, hydroxyapatite was calibrated by comparing the simulated effluent orthophosphates with the observed data and then calibrating the other two precipitates using effluent alkalinity (Table 5-13). The rapid mix effluent pH remained within the acceptable setpoint range of 10.8 - 11.1 for all lime dosage rates. The chemical clarifiers were modeled using a percentage removal based on the observed effluent TSS values. The combined chemical sludge production from the chemical and re-carbonation clarifiers is shown in Table 5-14. The average sludge production for all the scenarios was calculated to be 222 kg/1000m^3, which is well within the range of 144 - 419 kg/1000m^3 provided by the plant.

Each recarbonation stage was also modeled as a chemical reactor by adding the desired amount of CO_2 (kg/day) to simulate the carbonation process. The CO_2 supply rates were calibrated using the required effluent pH setpoint of 10.0 - 10.2 and 7.0 - 7.6 for stages 1 and 2, respectively (Table 5-13). The average CO_2 dosage was calculated to be 13.9 kg/1000m^3. The actual monthly dosages based on purchased CO_2 gas for 2017-2018 varied between 0 to 17.49 kg/1000m^3. This wide variation is due to the utilization of flue gases for recarbonation, whenever available, from different combustion in order to save purchased CO_2.

5.4.6 Activated Carbon Contactors

Multimedia filters and biologically active carbon (BAC) contactors are used at the plant to meet the desired permits of TSS below 1 mg/L and COD below 10 mg/L. At any given time, the number of online BAC contactors depends on many factors including the plant flows, COD loading, maintenance, operator's preference, etc. The main objective is to minimize the cost associated with carbon regeneration by maximizing the biological removal. This is achieved by using mostly exhausted contactors (assuming to have no adsorptive capacity at the given effluent concentration) with predominantly biological COD removal. The fresher carbon contactors, which are still in adsorptive phase, are only used during times of high COD loading to ensure permit compliance.

Since effluent flow and quality through each BAC contactor have not been regularly monitored in the plant, there were no data available to establish the adsorptive capacity of various contactor at any given time. However, considering the plant was mostly operating close to baseline flows during the selected dates, it was assumed the COD removal mechanism in most of the operating BAC contactors was primarily biological. Therefore, for this model setup, all of the online BAC contactors were considered in the exhaustive phase and modeled only for biofilm COD removal. Multimedia filters were simply modeled using percentage removal based on the observed TSS values. The GAC contactors, on the other hand, were simulated with the active BGM and adsorption model.

The coefficients for the Langmuir model were estimated by fitting the isotherm data provided by UOSA into 5-27 for fresh activated carbon (Figure 5-7). The general specifications for GAC are provided in Table 5-15. The specific surface are of the activated carbon was calculated to be 1200 m^2/m^3 (Table 5-15) based on the assumption that it is composed of spherical particles. The east and west sides of the BAC contactor were modeling separately with 8 and 32 tanks, respectively. Each BAC module was modeled as 5 bioreactors in series to depict the different layers of the contactor. The biofilm model was calibrated by estimating the hydrolysis coefficient (Equation 5-30) and adjusting different coefficients in the BGM.

5.4.7 Disinfection and Final Effluent

The final step of the process is the disinfection of the effluent using sodium hypochlorite followed by dechlorination using sodium bisulfite. The long narrow chlorination basin was modeled as a multi-reactor module comprising of multiple complete mix reactors in series to simulate plug flow conditions. The chlorination system was calibrated for residual free chlorine of more than 0.6 mg/L after the contact basin and below detectable limit after dechlorination as required by the plant.

The calibration results for the final effluent from the plant are provided in Table 5-16. It can be seen that all the effluent parameters are well calibrated since the PBIAS remained under 10% for all the scenarios, with the exceptions of ammonia and orthophosphates. Higher PBIAS for these nutrients can be neglected due to very small MAE of 0.03 and 0.01 mg/L respectively. The effluent COD was below the permit limit of 10 mg/L and ammonia nitrogen under 0.1 mg/L. The

nitrate levels remained relatively similar to the secondary effluent. The orthophosphates and total phosphorus were also under the permit limit of 0.1 mg/L.

5.5 Recommendations

The assumption that all the BAC contactors are in the exhausted phase was only made due to the unavailability of required operational data for the system and may be revisited in the next upgrade of the model. The BAC setup can be improved in the future by assuming three (or more) phases of BAC based on its adsorptive capacity and biological COD removal (Simpson 2008): (1) exhausted, full biodegradation, (2) partially adsorptive, some biodegradation, (3) adsorptive, no biodegradation. The system can then be modeled using three separate BAC groups in IViewOps, each with all of the 40 contactor tanks. Each group can be calibrated to simulate the desired contribution of carbon adsorption and biological uptake in COD removal. To run the model on a given day, the placement of each online contactor into a particular group could be decided based on its total time in operation, bed volumes turnover, effluent COD, etc. For instance, if, for a given day, 24 exhausted contactors are operated with 4 fresh ones, IViewOps could make an equal number of tanks online from each of the associated groups to run the model. Although this method requires constant monitoring of all the contactors and their conditions, it is expected to produce better results as long as the necessary data are made available.

5.6 Conclusion

The use of mathematical models as decision support tools for both engineered and natural systems has been growing over the years. Particularly in wastewater treatment, an increasing number of operators are now using different process simulators to troubleshoot and optimize the plant operations. However, most of the wastewater simulators are limited to secondary treatment due to their inability to model advanced physicochemical processes. This paper presented a new physicochemical process model (PCM) incorporated into the latest version of IViewOps for simulating processes like pH (acid/base systems), precipitation, oxidation, adsorption, biofiltration, carbonation, chlorination, etc. A total of 70 new state variables, 16 algebraic variables, and 184 kinetic equations were included in the model. A new solver was developed for implicitly solving the pH model for any reactor if desired by the user. This allows users to limit the pH calculation only to select reactors and reduce the computational overhead.

The setup of the full-scale model for UOSA-WRF was discussed in detail and model results were presented. The initial calibration indicated that pH, precipitation, carbonation, biofiltration, and chlorination can be accurately modeled using the new PCM. It was shown that the addition of a pH model is not only essential for modeling processes like chemical P removal, but also for predicting undesired precipitation in the dewatering system. The model was able to accurately predict the primary clarifier, secondary clarifier, and final effluent concentrations with a PBIAS of less than 10% in most cases. Other calibration variables including total airflow, MLSS in the aeration basins, and biogas from the digester were also simulated by the model with a PBIAS of less than 10%. The model was able to accurately capture the different nitrate concentrations during summers and winters caused by changes in plant configurations. It also predicted the presence of phosphorus accumulating bacteria in the system throughout the year promoting biological P uptake. The amount of simulated sludge production by the chemical P removal system was within the range generally observed at the plant. The carbon dioxide dosage for recarbonation was also calculated to be within the acceptable range.

Finally, the new architecture of IViewOps4 was briefly explained. It was discussed how decoupling the model code from the rest of the software and making it open-sourced allows the users to modify and/or add new processes. It is envisaged that the addition of a new open-sourced PCM in IViewOps will not only allow modeling of advanced wastewater and water reuse processes, but also expand into applications for water treatment systems.

5.7 Acknowledgment

The authors acknowledge the support of UOSA and OWML for conducting this research. We would also like to honor the memory of the late Dr. Thomas J. Grizzard for his unwavering commitment in the establishment and operation of the Occoquan program and the OWML for over 40 years.

5.8 References

Batstone, D. (2009). "Towards a generalised physicochemical modelling framework." *Reviews in Environmental Science and Bio/Technology*, 8(2), 113-114.

Batstone, D., and Keller, J. (2003). "Industrial applications of the IWA anaerobic digestion model No. 1 (ADM1)." *Water Science and Technology*, 47(12), 199-206.

Batstone, D. J., Amerlinck, Y., Ekama, G., Goel, R., Grau, P., Johnson, B., Kaya, I., Steyer, J.-P., Tait, S., and Takács, I. (2012). "Towards a generalized physicochemical framework." *Water Science and Technology*, 66(6), 1147-1161.

Batstone, D. J., Keller, J., Angelidaki, I., Kalyuzhnyi, S., Pavlostathis, S., Rozzi, A., Sanders, W., Siegrist, H., and Vavilin, V. (2002). "The IWA anaerobic digestion model no 1 (ADM1)." *Water Science and Technology*, 45(10), 65-73.

Boltz, J., Morgenroth, E., and Sen, D. (2010). "Mathematical modelling of biofilms and biofilm reactors for engineering design." *Water Science and Technology*, 62(8), 1821-1836.

Brezonik, P., and Arnold, W. (2011). *Water chemistry: an introduction to the chemistry of natural and engineered aquatic systems*, OUP USA.

Briggs, T. A. (1996). "Dynamic modelling of chemical phosphorus removal in the activated sludge process.", MS Thesis, McMaster University.

De Haas, D., Wentzel, M., and Ekama, G. (2001). "The use of simultaneous chemical precipitation in modified activated sludge systems exhibiting biological excess phosphate removal: Part 6: Modelling of simultaneous chemical-biological P removal-review of existing models." *Water Sa*, 27(2), 135-150.

Deborde, M., and Von Gunten, U. (2008). "Reactions of chlorine with inorganic and organic compounds during water treatment—kinetics and mechanisms: a critical review." *Water research*, 42(1), 13-51.

Fairlamb, M., Jones, R., Takács, I., and Bye, C. (2003). "Formulation of a general model for simulation of pH in wastewater treatment processes." *Proceedings of the Water Environment Federation*, 2003(7), 511-528.

Fisher, I., Kastl, G., Sathasivan, A., and Jegatheesan, V. (2011). "Suitability of chlorine bulk decay models for planning and management of water distribution systems." *Critical reviews in environmental science and technology*, 41(20), 1843-1882.

Henze, M., Gujer, W., Mino, T., and Loosdrecht, M. (2000). *Activated sludge models ASM1, ASM2, ASM2d and ASM3*, IWA Pub., London.

Hoigné, J., and Bader, H. (1983). "Rate constants of reactions of ozone with organic and inorganic compounds in water—I: non-dissociating organic compounds." *Water Research*, 17(2), 173-183.

Hoigné, J., and Bader, H. (1983). "Rate constants of reactions of ozone with organic and inorganic compounds in water—II: dissociating organic compounds." *Water research*, 17(2), 185-194.

Knocke, W. R., Van Benschoten, J. E., Kearney, M. J., Soborski, A. W., and Reckhow, D. A. (1991). "Kinetics of manganese and iron oxidation by potassium permanganate and chlorine dioxide." *Journal of the American Water Works Association*, 83(6), 80-87.

Kumar, K., Shinness, R. W., and Margerum, D. W. (1987). "Kinetics and mechanisms of the base decomposition of nitrogen trichloride in aqueous solution." *Inorganic Chemistry*, 26(21), 3430-3434.

Lodhi, A., Sen, D., Randall, C., Gold, L., Brandt, K., Rawlings, J., and Chandran, K. (2010). "Differences in GHG and nitric oxide emissions for activated sludge and biofilm ENR processes based on aeration, MCRT, mixing and media, and control of emissions and nutrients by enhancing process models in an ENR operations simulator (Aquifas)." *Proceedings of the Water Environment Federation*, 2010(13), 3539-3562.

Lodhi, A., Sen, D., Rawlings, J., Kundamal, J., Abbott, D., Wahibi, O., Mende, U., and Gold, L. (2011). "Simultaneous Optimization of Plants for Nitrogen and Phosphorus Removal, Reuse, Energy and Emissions through a Real Time Operations Controller in Middle-East-Asia and Chesapeake Bay Region of US." *Proceedings of the Water Environment Federation*, 2011(14), 3069-3092.

Martin, S. T. (2005). "Precipitation and dissolution of iron and manganese oxides." *Environmental Catalysis*, 61-81.

Mbamba, C. K., Batstone, D. J., Flores-Alsina, X., and Tait, S. (2015). "A generalised chemical precipitation modelling approach in wastewater treatment applied to calcite." *Water research*, 68, 342-353.

Metcalf, Eddy, Burton, F. L., Stensel, H. D., and Tchobanoglous, G. (2003). *Wastewater engineering: treatment and reuse*, McGraw Hill.

Morgenroth, E., van Loosdrecht, M. C. M., and Wanner, O. (2000). "Biofilm models for the practitioner." *Water Science and Technology*, 41(4-5), 509-512.

Munhoven, G. (2013). "Mathematics of the total alkalinity–pH equation–pathway to robust and universal solution algorithms: the SolveSAPHE package v1. 0.1." *Geoscientific Model Development [= GMD]*, 6, 1367-1388.

Musvoto, E., Wentzel, M., and Ekama, G. (2000). "Integrated chemical–physical processes modelling—II. Simulating aeration treatment of anaerobic digester supernatants." *Water Research*, 34(6), 1868-1880.

Plazinski, W., Rudzinski, W., and Plazinska, A. (2009). "Theoretical models of sorption kinetics including a surface reaction mechanism: a review." *Advances in colloid and interface science*, 152(1), 2-13.

Reckhow, D. A., Knocke, W. R., Kearney, M. J., and Parks, C. A. (1991). "Oxidation of iron and manganese by ozone." *Ozone: science & engineering*, 13(6), 675-695.

Rittmann, B. E., Banaszak, J. E., VanBriesen, J. M., and Reed, D. T. (2002). "Mathematical modeling of precipitationand dissolution reactions in microbiological systems." *Biodegradation*, 13(4), 239-250.

Sen, D., Lodhi, A., Gold, L., Abbott, D., Rawligns, J., Mellendick, M., Sedlack, D., Copithorn, R., Pehrson, R., and McCall, C. (2012). "Implementing an Intelligent Operations and Asset Management System that Integrates DCS, SCADA, CMMS and Process Models for Activated Sludge, IFAS and Biofilms to Improve Compliance and Optimize ENR Plants in Real Time." *Proceedings of the Water Environment Federation*, 2012(15), 1468-1487.

Sen, D., and Randall, C. W. (2008). "Improved computational model (AQUIFAS) for activated sludge, integrated fixed-film activated sludge, and moving-bed biofilm reactor systems, Part I: Semi-empirical model development." *Water environment research*, 80(5), 439-453.

Serralta, J., Ferrer, J., Borrás, L., and Seco, A. (2004). "An extension of ASM2d including pH calculation." *Water research*, 38(19), 4029-4038.

Simpson, D. R. (2008). "Biofilm processes in biologically active carbon water purification." *Water research*, 42(12), 2839-2848.

Skopp, J. (2009). "Derivation of the Freundlich adsorption isotherm from kinetics." *Journal of chemical education*, 86(11), 1341.

Sötemann, S., Musvoto, E., Wentzel, M., and Ekama, G. (2005). "Integrated biological, chemical and physical processes kinetic modelling Part 1–Anoxic-aerobic C and N removal in the activated sludge system." *WaterSA*, 31(4), 529-544.

Stumm, W., and Morgan, J. J. (1996). *Aquatic chemistry: chemical equilibria and rates in natural waters*, John Wiley & Sons.

US-EPA (1999). "Alternative disinfectants and oxidants." *Disinfectant use in water treatment, Washington DC*.

Von Gunten, U. (2003). "Ozonation of drinking water: Part I. Oxidation kinetics and product formation." *Water research*, 37(7), 1443-1467.

Weil, I., and Morris, J. C. (1949). "Kinetic studies on the chloramines. I. The rates of formation of monochloramine, N-chlormethylamine and N-chlordimethylamine." *Journal of the American Chemical Society*, 71(5), 1664-1671.

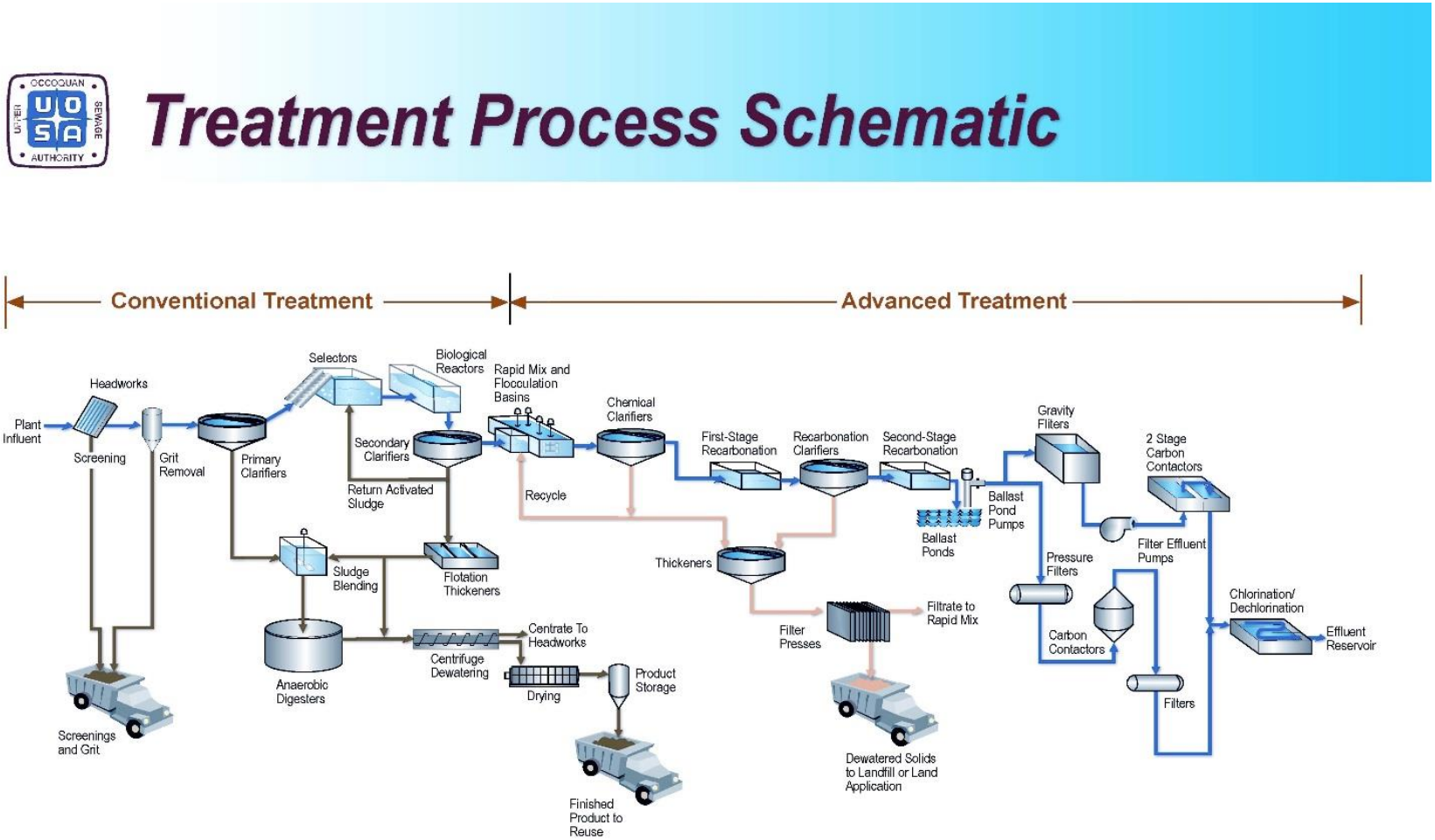

Figure 5-1. UOSA-WRF treatment process schematic *(courtesy UOSA)*

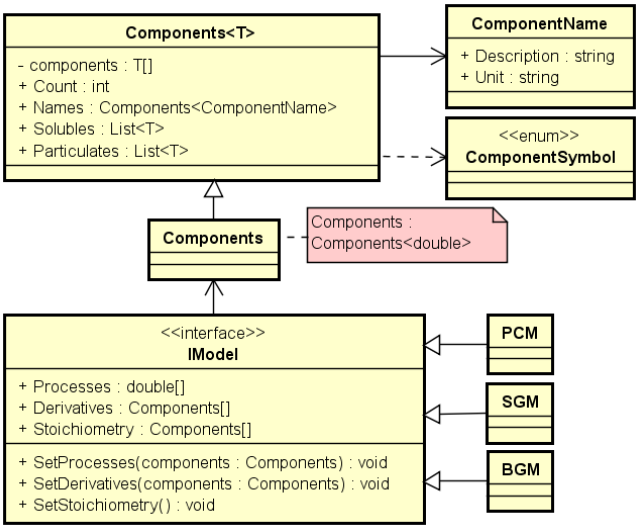

Figure 5-2. Class diagram of IViewOps model library

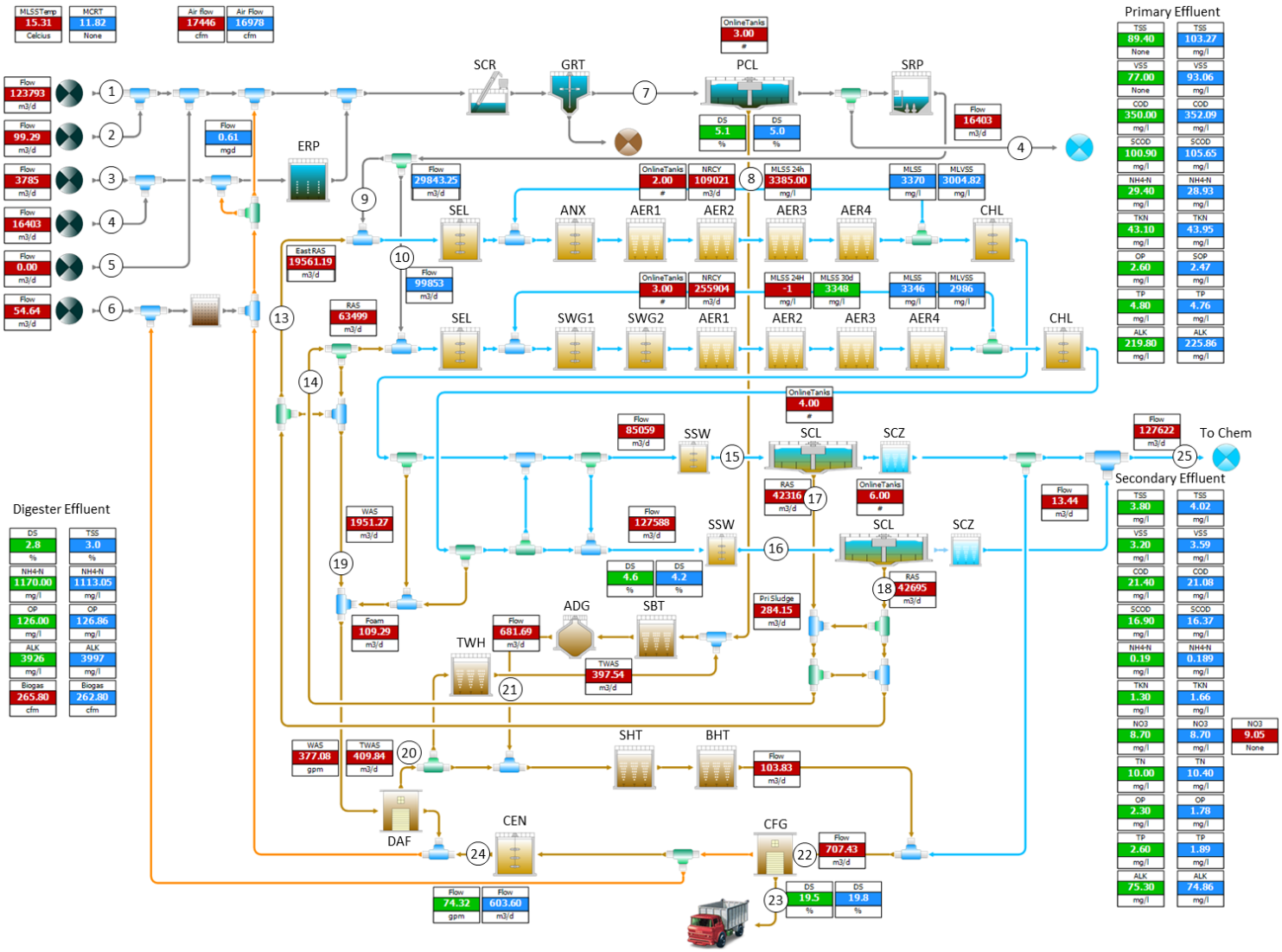

Figure 5-3. IViewOps4 model for UOSA-WRF secondary treatment system. Refer to Table 5-1 for the description of unit-processes and Table 5-2 for flows in different pipes.

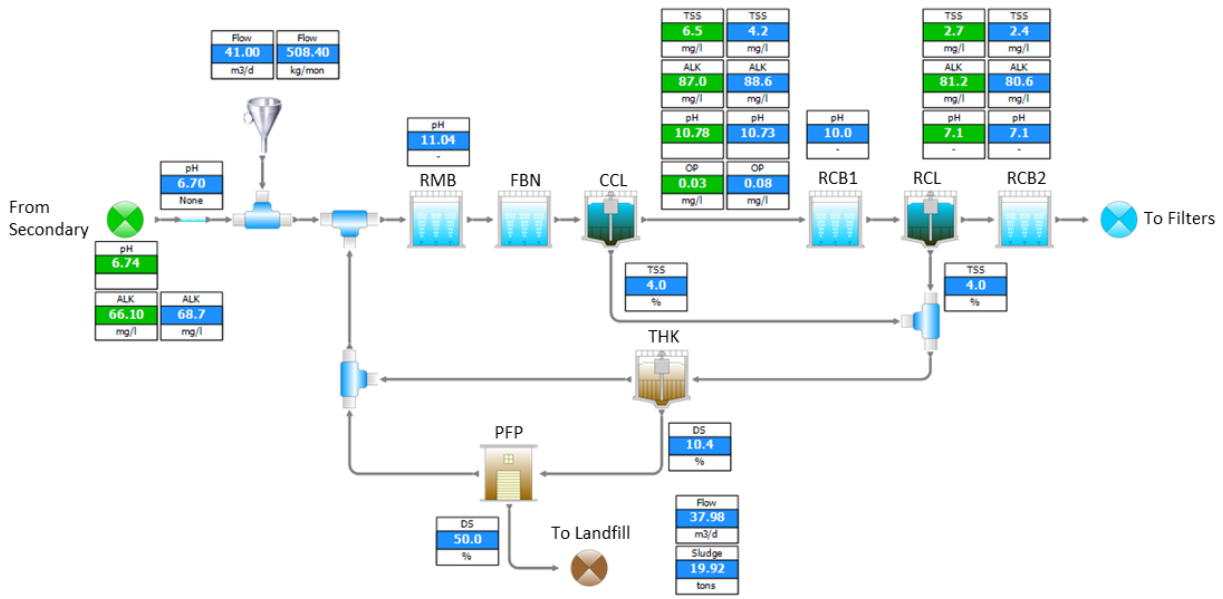

Figure 5-4. IViewOps4 UOSA-WRF model for chemical P-removal system. Refer to Table 5-1 for the description of unit-processes.

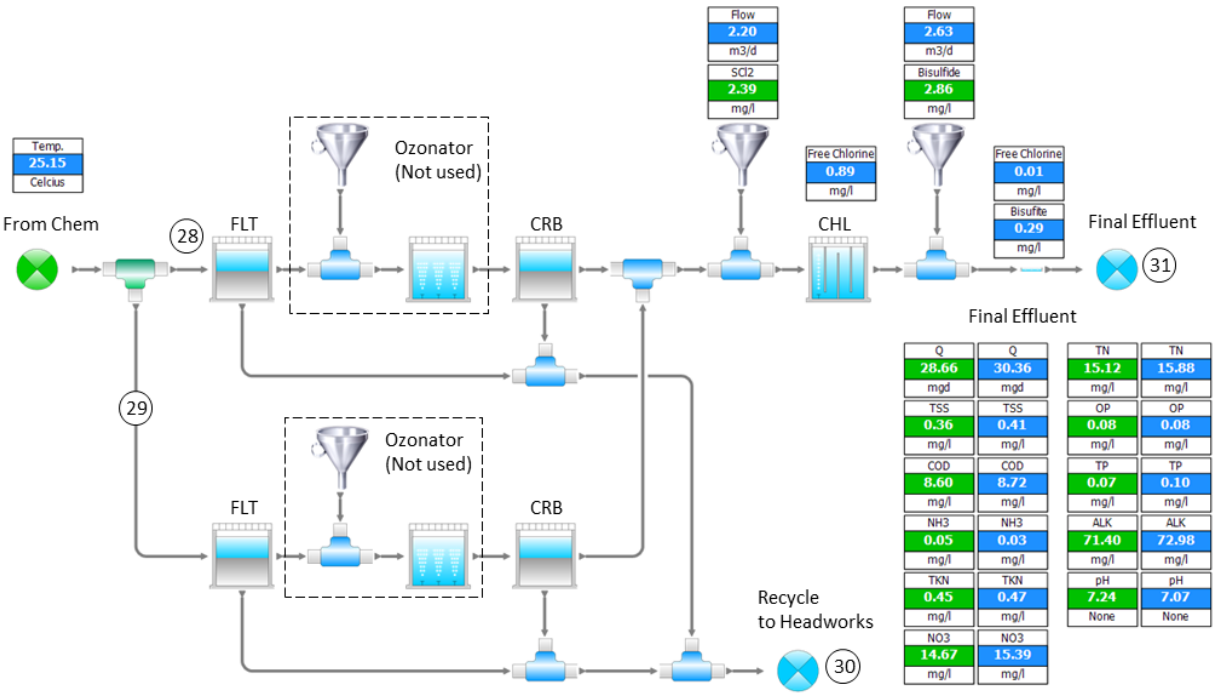

Figure 5-5. IViewOps4 model for UOSA-WRF multimedia filters, carbon contactors, and chlorination systems. Refer to Table 5-1 for the description of unit-processes and Table 5-2 for flows in different pipes.

Table 5-1. Sizes of different unit operators and unit processes in the plant

#	Description	Tag	East Side		West Side	
			No.	Size [1]	No.	Size[1]
1	Bar screen	SCR	4	Channel width 1.52 m	-	-
2	Grit chamber (Diameter)	GRT	4	7.31 ft	-	-
3	Primary clarifier (Diameter x Side water depth)	PCL	3	38.11 x 3.65	3	38.1 x 3.65
4	Anaerobic selector (Length x Width x Depth)	SEL	3	16.77 x 3.35 x 4.57	4	16.77 x 3.35 x 4.57
5	Anoxic tank (Length x Width x Depth)	ANX	3	17.37 x 35.06 x 4.57	4	17.37 x 35.06 x 4.57
6	Swing zone 1 (Length x Width x Depth)	SWG		-	4	15.55 x 31.71 x 4.57
7	Swing zone 2 (Length x Width x Depth)	SWG		-	4	15.55 x 31.71 x 4.57
8	Aeration Zone-1 (Length x Width x Depth)	AER1	3	17.37 x 35.06 x 4.57	4	17.37 x 35.06 x 4.57
9	Aeration Zone-2 (Length x Width x Depth)	AER2	3	18.45 x 36.89 x 4.57	4	17.37 x 35.06 x 4.57
10	Aeration Zone-3 (Length x Width x Depth)	AER3	3	9.45 x 36.89 x 4.57	4	17.37 x 35.06 x 4.57
11	Aeration Zone-4 (Length x Width x Depth)	AER4	3	9.14 x 36.89 x 4.57	4	17.37 x 35.06 x 4.57
12	MLSS channel (Length x Width x Depth)	CHL	1	3.04 x 110.67 x 1.83	1	3.04 x 126.83 x 1.83
13	Secondary clarifier (Diameter x Side water depth)	SCL	4	38.11 x 3.65	6	38.11 x 4.87
14	Stilling well (Diameter x Depth)	SSW	4	6.86 x 1.22	6	6.86 x 1.22
15	Clear water zone well (Diameter x Depth)	SCZ	4	35.98 x 2.44	6	35.98 x 2.44
16	Sludge blending tank (Length x Width x Depth)	SBT	-	-	2	3.04 x 3.04 x 3.04
17	Anaerobic digester (Diameter x Side water depth)	ADG	3	24.39 x 7.93	-	-
18	Thickened WAS holding tank (Length x Width x Depth)	TWH	-	-	1	3.04 x 3.04 x 3.04
19	Digested sludge holding tank (Length x Width x Depth)	SHT	-	-	2	10.67 x 10.67 x 3.04
20	Ballast sludge holding tank (Length x Width x Depth)	BHT	-	-	1	9.14 x 9.14 x 3.04

#	Description	Tag	East Side		West Side	
			No.	Size [1]	No.	Size[1]
21	Dissolved air floatation tank	DAF	2	-	2	-
22	Centrate holding tank (Length x Width x Depth)	CEN	-	-	1	30.49 x 30.49 x 3.04
23	Centrifuge	CFG	-	-	3	-
24	Wet well (Length x Width x Depth)	WWT	-	-		30.49 x 30.49 x 3.04
25	ERP basin (Length x Width x Depth)	ERP	-	-		91.46 x 91.46 x 1.52
26	Rapid mix basin (Length x Width x Depth)	RMB	2	6.40 x 6.40 x 4.27	4	4.88 x 6.10 x 4.34
27	Flocculation basin (Length x Width x Depth)	FBN	3	14.33 x 6.10 x 4.27	4	14.33 x 6.10 x 4.27
28	Chemical clarifier (Diameter x Depth)	CCL	3	38.11 x 3.65	4	38.11 x 3.65
29	1st-stage recarbonation basin (Length x Width x Depth)	RCB1	3	9.15 x 4.57 x 4.27	4	13.41 x 6.71 x 4.88
30	Recarbonation clarifier (Diameter x Depth)	RCL	3	38.11 x 3.65	4	38.11 x 4.45
31	2nd-stage recarbonation basis (Length x Width x Depth)	RCB2	3	9.15 x 4.57 x 4.27	4	13.41 x 6.71 x 4.88
32	Chemical thickener (Diameter x Depth)	THK	3	12.20 x 3.65	3	24.39 x 3.65
33	Chemical thickener (Diameter x Depth)	THK	1	22.87 x 3.65	-	-
34	Plate and frame press for chemical sludge	PFP	3	-	-	-
35	Multimedia filters (Area x media depth)	FLT	12	46.48 m^2 x 0.91	10	49.45 m^2 x 0.91
36	Activated carbon contactors (Diameter x Depth)	CRB	32	3.66 x 7	-	-
37	Activated carbon contactors (Length x Width x Depth)	CRB	-	-	8	4.27 x 10.98 x 3.05
38	Chlorine contact basin (Length x Width x Depth)	CHL	-	-	4	91.46 x 2.13 x 3.66

(1) All dimensions are in meters unless otherwise specified

Table 5-2. Plant flows

#	Location	Flow (m^3/d)[1]					
		Jul 17	Aug 17	Sep 17	Jan 18	Feb 18	Mar 18
1	Raw influent	120,445	124,739	112,995	115,176	137,062	123,793
2	Septage	99	99	99	99	99	99
3	Filtration recycle	3,785	3,785	3,785	3,785	3,785	3,785
4	ERP	18,669	12,520	10,002	16623	18,933	16,403
5	Other influent	0	0	0	0	0	0
6	Toilets	55	55	55	55	55	55
7	Primary clarifiers Inflow	144,894	143,219	129,059	137,743	162,163	146,384
8	Primary clarifiers underflow	328	355	393	344	290	284
9	East aeration tanks	0	0	0	0	17,560	29,843
10	West aeration tanks	125,897	130,344	118,662	120,776	125,380	99,853
11	East nitrogen recycle [1]	0	0	0	0	51,671	109,020
12	West nitrogen recycle[1]	0	0	0	459,000	394,184	255,904
13	East RAS	0	0	0	0	13,960	19,561
14	West RAS	97409	82,625	89,242	113,795	97,753	63,499
15	East secondary clarifier inflow	89,279	85,144	83,118	93,784	101,818	85,059
16	West secondary clarifier inflow	133,918	127,716	124,677	140,677	152,726	127,588
17	East secondary clarifier underflow	40,182	15,786	36,038	41,378	46,546	42,316
18	West secondary clarifier underflow	58,713	68,492	54,919	74,056	67,079	42,695
19	WAS	1,487	1,653	1,714	1,,641	1,930	1951
20	DAF overflow	383	546	492	300	393	383
21	Anaerobic digester effluent flow	672	726	371	636	671	655
22	Centrifuge inflow	720	914	899	634	714	682
23	Centrifuge dewatered sludge	87	104	104	98.4	110	104
24	Centrate recycle	633	810	795	560	587	576
25	Secondary effluent	124,291	128,569	116,825	119,012	140,886	127,622
26	East chemical phosphorus removal	0	0	0	0	0	0
27	West chemical phosphorus removal	124,291	128,569	116,825	119,012	140,886	127,622
28	East filters and activated carbon	0	22,790	39,713	7,432	30,824	31,560
29	West filters and activated carbon	124,291	101,500	84,578	116,858	93,467	92,731
30	Filtration backwash	3,785	3,785	3,785	3,785	3,785	3,785
31	Plant effluent	120,506	124,784	113,040	115,227	137,101	123,837

(1) All flows are calculated based on last 30-days averaged unless otherwise specified

(2) Last 24-hours averaged.

Table 5-3: Online tanks

#	Description	Tanks Available	No. of Tanks Online					
			Jul 17	Aug 17	Sep 17	Jan 18	Feb 18	Mar 18
1	Primary clarifier	6	2	2	2	6	4	3
2	East aeration	3	0	0	0	3	1	2
3	West aeration	4	4	4	4	4	4	4
4	Secondary clarifiers	10	10	10	10	10	10	10
5	Anaerobic digesters	3	3	3	3	3	3	3
6	East chemical P removal	4	0	0	0	0	0	0
7	West chemical P removal	4	4	4	4	4	4	4
8	East carbon contactors	24	0	7	8	2	8	8
9	West carbon contactors	6	6	5	4	6	6	5

Table 5-4. Raw influent characteristics

#	Parameters(1)	Units	Baseline	Jul 17	Aug 17	Sep 17	Jan 18	Feb 18	Mar 18
1	TSS	mg/L as TSS	205.0	209.4	202.2	228.0	243.5	218.6	217.2
2	VSS	mg/L as TSS	180.0	183.9	177.5	200.2	213.8	191.9	190.7
3	CCOD	mg/L as COD	58.0	59.2	57.2	64.5	68.9	61.8	61.5
4	PCOD	mg/L as COD	387.0	395.3	381.7	430.4	459.7	412.6	410.1
5	SCOD	mg/L as COD	105.0	107.3	103.6	116.8	124.7	112.0	111.3
6	VFA	mg/L as COD	25.0	25.5	24.7	27.8	29.7	26.7	26.5
7	Total COD	mg/L as COD	550.0	561.8	542.4	611.7	653.3	586.4	582.8
8	SCODnbio	mg/L as COD	13.0	13.3	12.8	14.5	15.4	13.9	13.8
9	PCODnbio	mg/L as COD	60.0	61.3	59.2	66.7	71.3	64.0	63.6
10	NH_3	mg/L as N	25.0	25.5	24.7	27.8	29.7	26.7	26.5
11	SKN	mg/L as N	26.0	26.6	25.6	28.9	30.9	27.7	27.6
12	TKN	mg/L as N	47.0	48.0	46.4	52.3	55.8	50.1	49.8
13	SKNnbio	mg/L as N	0.25	0.26	0.25	0.28	0.30	0.27	0.26
14	PKNnbio	mg/L as N	0.25	0.26	0.25	0.28	0.30	0.27	0.26
15	OP	mg/L as P	2.00	2.04	1.97	2.22	2.38	2.13	2.12
16	TSP	mg/L as P	2.00	2.04	1.97	2.22	2.38	2.13	2.12
17	TP	mg/L as P	4.75	4.85	4.68	5.28	5.64	5.06	5.03
18	SPnbio	mg/L as P	0.02	0.02	0.02	0.02	0.02	0.02	0.02
19	PPnbio	mg/L as P	0.25	0.26	0.25	0.28	0.30	0.27	0.26
20	Alkalinity	mg/L as $CaCO_3$	215.0	219.6	212.0	239.1	255.4	229.2	227.8

(1) Refer to abbreviations for description of parameters

Table 5-5. Other influent characteristics

#	Parameters[1]	Units	Septage	ERP	Filtration Recycle	Toilets
1	TSS	mg/L as TSS	1000	100	200	205
2	VSS	mg/L as TSS	800	80	40	180
3	CCOD	mg/L as COD	0	0	0	0
4	PCOD	mg/L as COD	1500	18	275	400
5	SCOD	mg/L as COD	1000	105	25	150
6	VFA	mg/L as COD	0	177	0	0
7	Total COD	mg/L as COD	2500	300	300	550
8	SCODnbio	mg/L as COD	50	10	5	10
9	PCODnbio	mg/L as COD	50	50	200	60
10	NH_3	mg/L as N	40	28	5	28
11	SKN	mg/L as N	60	29	5	29
12	TKN	mg/L as N	200	40	5	47
13	SKNnbio	mg/L as N	0.1	0.1	0.1	0.25
14	PKNnbio	mg/L as N	0.2	0.2	2	0.25
15	OP	mg/L as P	4	2.2	0.1	2
16	TSP	mg/L as P	6	2.2	0.2	2
17	TP	mg/L as P	10	4.5	10	4.2
18	SPnbio	mg/L as P	0.5	0.1	.02	0.02
19	PPnbio	mg/L as P	0.5	0.2	1.0	0.02
20	Alkalinity	mg/L as CaCO3	1000	215	80	215

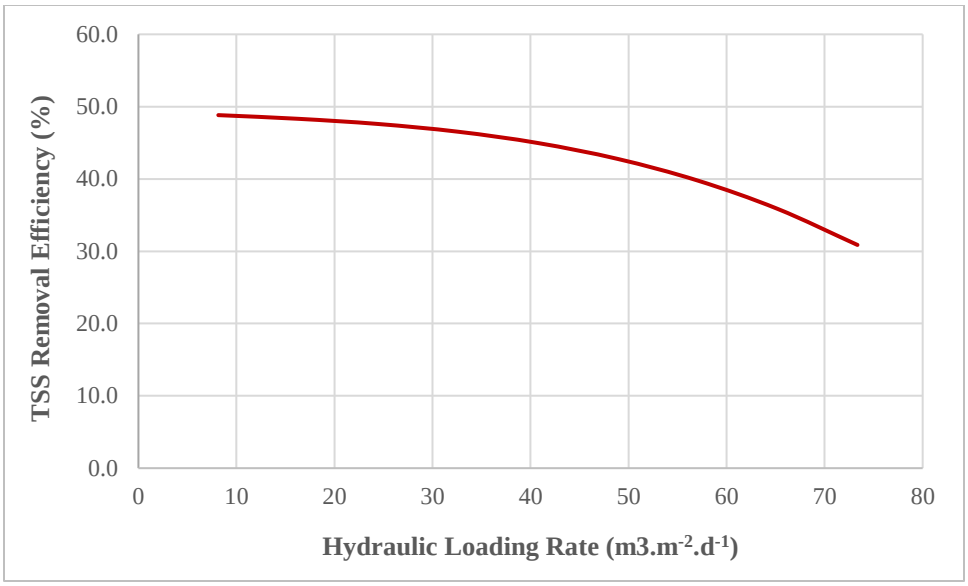

Figure 5-6. Primary clarifier TSS removal rating curve

Table 5-6. Model calibration results for primary effluent

#	Parameter(1)	Units	Jul 17		Aug 17		Sep 17		Jan 18		Feb 18		Mar 18		MAE(2)	RMSE(3)	PBIAS(4)
			Obs	Sim	Obs	Sim	Obs	Sim	Obs	Sim	Obs	Sim	Obs	Sim			
1	TSS	mg/L as TSS	115.9	113.7	106.8	112.3	134.3	119.5	118.7	105.5	108.9	91.6	89.4	103.2	11.1	12.4	4.2
2	VSS	mg/L as TSS	101.4	103.5	88.2	102.3	112.0	108.3	100.9	94.8	93.0	82.3	77.0	93.0	8.8	10.2	-2.0
3	COD	mg/L as COD	378.0	377.1	361.8	370.8	417.2	398.6	402.1	365.0	327.4	315.6	350.6	352.1	13.1	18.0	2.6
4	SCOD	mg/L as COD	100.2	107.4	114.7	104.2	103.8	113.8	121.5	111.8	89.3	96.5	100.9	105.7	8.2	8.5	-1.4
5	NH_3	mg/L as N	27.6	29.0	28.9	27.7	31.4	30.6	32.8	30.4	26.7	26.2	29.4	28.9	1.1	1.3	2.3
6	TKN	mg/L as N	41.1	44.6	43.8	43.3	48.6	47.4	51.6	47.1	37.2	39.9	43.1	44.0	2.2	2.7	-0.3
7	OP	mg/L as P	2.3	2.4	2.4	2.5	2.5	2.6	3.0	2.5	2.3	2.1	2.6	2.5	0.2	0.2	3.8
8	TP	mg/L as P	4.6	4.7	4.9	4.9	5.4	5.1	6.0	5.0	4.5	4.2	4.8	4.8	0.3	0.5	4.9
9	Alkalinity	mg/L as $CaCO_3$	223.0	225.2	227.8	217.2	243.9	241.9	226.2	226.4	194.4	205.5	219.8	225.9	5.4	6.8	-0.5

(1) Refer to abbreviations for description of parameters

(2) MAE: Mean absolute error

(3) RMSE: Root mean square error

(4) PBIAS: Percentage Bias

Table 5-7: Dissolved oxygen (DO) setpoints for different zones.

#	Zones	Dissolved oxygen setpoint (mg/L)					
		Jul 17	Aug 17	Sep 17	Jan 18	Feb 18	Mar 18
1	East Side Aer1	-	-	-	-	1.94	1.55
2	East Side Aer2	-	-	-	-	1.94	1.55
3	East Side	-	-	-	-	1.92	1.03
4	East Side Aer4	-	-	-	-	1.92	0.59
5	West Side SWG1	-	-	-	-	-	-
6	West Side SWG2	0.31	0.14	0.13	-	-	-
7	West Side Aer1	0.86	1.02	1.21	1.18	1.11	1.26
8	West Side Aer2	0.86	1.02	1.21	1.18	1.11	1.26
9	West Side Aer3	0.74	0.78	0.99	0.71	1.01	1.07
10	West Side Aer4	0.74	0.78	0.99	0.71	1.01	1.07

Table 5-8: Diffused aeration input parameters

#	Parameter	Unit	Value
1	Alpha	-	0.65~0.8
2	Beta	-	0.95
3	Theta	-	1.02
4	Fouling factor	-	0.98
5	Effective situation depth	%	50
6	Height of diffuser	meter	0.23
7	Standard efficiency @ 3.66 m	%	25

Table 5-9. Model calibration results for secondary effluent

#	Parameter(1)	Units	Jul 17		Aug 17		Sep 17		Jan 18		Feb 18		Mar 18		MAE(2)	RMSE(3)	PBIAS(4)
			Obs	Sim	Obs	Sim	Obs	Sim	Obs	Sim	Obs	Sim	Obs	Sim			
1	TSS	mg/L as TSS	3.1	2.7	7.0	6.6	8.4	7.1	5.3	5.3	9.0	8.6	3.8	4.0	0.5	0.6	6.2
2	VSS	mg/L as TSS	2.7	2.4	5.9	5.8	6.2	6.3	4.5	4.7	7.5	7.7	3.2	3.6	0.2	0.2	-1.6
3	COD	mg/L as COD	20.7	21.5	26.9	26.0	23.7	28.0	22.9	23.7	25.5	25.3	21.4	21.1	1.2	1.9	-3.2
4	SCOD	mg/L as COD	17.8	18.1	21.2	18.1	18.7	19.3	17.4	17.5	16.9	15.0	16.9	16.4	1.1	1.5	4.2
5	NH_3	mg/L as N	0.06	0.04	0.07	0.04	0.07	0.03	0.10	0.09	0.07	0.10	0.19	0.19	0.02	0.02	11.61
6	TKN	mg/L as N	1.2	1.4	1.7	1.5	1.5	1.6	1.4	1.6	1.8	1.6	1.3	1.7	0.2	0.2	-6.2
7	NO_3	mg/L as N	15.3	16.7	15.5	14.8	15.6	15.9	8.2	7.6	7.6	7.6	8.7	8.7	0.5	0.7	-0.6
8	Total N	mg/L as N	16.5	18.1	17.2	16.4	17.1	17.5	9.6	9.2	9.4	9.3	10.0	10.4	0.6	0.8	-1.5
9	OP	mg/L as P	1.8	2.4	1.9	1.3	1.9	1.9	1.8	2.1	1.8	2.0	2.3	1.8	0.4	0.4	0.6
10	TP	mg/L as P	2.0	2.5	2.2	1.5	2.2	2.1	2.1	2.3	2.4	2.2	2.6	1.9	0.4	0.5	8.2
11	Alkalinity	mg/L as $CaCO_3$	66.0	68.4	64.5	58.6	67.0	77.0	80.2	82.4	73.2	75.9	75.3	74.9	3.9	5.1	-2.6

(1) Refer to abbreviations for description of parameters

(2) MAE: Mean absolute error

(3) RMSE: Root mean square error

(4) PBIAS: Percentage Bias

Table 5-10. Model calibration results for aeration basins

#	Parameter(1)	Units	Jul 17		Aug 17		Sep 17		Jan 18		Feb 18		Mar 18		MAE(2)	RMSE(3)	PBIAS(4)
			Obs	Sim	Obs	Sim	Obs	Sim	Obs	Sim	Obs	Sim	Obs	Sim			
1	Total airflow	m^3/h	28,936	29,114	27,679	29,332	30,526	29,418	29,347	28,025	29,089	28,764	29,641	28,846	897	1039	0.98
2	MLSS (Probe)	mg/L as TSS	4427	4514	3982	3911	3192	3974	4099	4390	3730	3423	3385	3346	263	366	-3.3
3	MLSS (Lab)	mg/L as TSS	3560	4514	3518	3911	3532	3974	4508	4390	4094	3423	3348	3346	430	536	-4.4

(1) Refer to abbreviations for description of parameters

(2) MAE: Mean absolute error

(3) RMSE: Root mean square error

(4) PBIAS: Percentage Bias

Table 5-11. Model calibration results for anaerobic digestion effluent

#	Parameter(1)	Units	Jul 17		Aug 17		Sep 17		Jan 18		Feb 18		Mar 18		MAE(2)	RMSE(3)	PBIAS(4)
			Obs	Sim	Obs	Sim	Obs	Sim	Obs	Sim	Obs	Sim	Obs	Sim			
1	NH_3	mg/L as N	936	986	687	809	731	839	1016	1024	982	987	1170	1113	58.4	73.6	-4.3
2	OP	mg/L as P	88	99	71	103	82	90	150	94	99	86	126	127	20.2	27.3	2.7
3	pH	-	7.20	7.13	7.20	7.02	7.20	7.02	7.18	7.11	7.10	7.10	7.20	7.14	0.09	0.11	1.30
4	Alkalinity	mg/L as $CaCO_3$	3958	3591	3483	2880	3216	3043	4107	3691	3987	3578	3926	3997	339.8	381.6	8.4
5	Biogas	m^3/h	358.6	382.9	325.9	383.9	367.6	392.9	423.1	450.2	434.4	443.4	451.6	446.5	24.8	30.1	-5.9

(1) Refer to abbreviations for description of parameters

(2) MAE: Mean absolute error

(3) RMSE: Root mean square error

(4) PBIAS: Percentage Bias

Table 5-12. Chemical dosages

#	Location	Concentrations (mg/L)					
		Jul 17	Aug 17	Sep 17	Jan 18	Feb 18	Mar 18
1	Lime for chemical phosphorus removal (1)	132.0	131.9	117.9	124.3	136.3	125.7
2	Sodium hypochlorite for disinfection (2)	2.15	2.17	2.37	1.94	1.87	1.85
3	Sodium bisulfide for de-chlorination	2.44	2.85	2.85	2.25	2.04	1.87

(1) As $Ca(OH)_2$

(2) As chlorine

Table 5-13. Model calibration results for chemical phosphorus removal process

#	Parameter[1]	Units	Jul 17		Aug 17		Sep 17		Jan 18		Feb 18		Mar 18		MAE[2]	RMSE[3]	PBIAS[4]
			Obs	Sim	Obs	Sim	Obs	Sim	Obs	Sim	Obs	Sim	Obs	Sim			
1	Rapid mix pH[5]	-		11.0		11.1		10.8		10.9		10.8		10.9			
2	Chemical clarifier Alkalinity	mg/L as $CaCO_3$	87.0	88.9	83.6	77.6	78.6	82.9	92.5	104.4	95.7	108.9	96.0	97.0	6.4	7.9	-4.9
3	Chemical clarifier OP	mg/L as P	0.03	0.08	0.07	0.06	0.07	0.09	0.06	0.08	0.06	0.06	0.06	0.07	0.02	0.02	-25.7
4	Chemical clarifier pH	-	10.8	10.7	10.4	10.9	10.2	10.4	10.7	10.5	10.6	10.5	10.7	10.6	0.2	0.2	-0.3
5	1st stage Recarb. pH[6]	-		10.0		10.1		10.0		10.0		10.0		10.0			
6	2nd stage Recarb. pH[7]	-		7.1		7.2		7.0		7.2		7.3		7.3			
7	2nd stage Recarb. Alkalinity	mg/L as $CaCO_3$	81.2	80.9	77.5	69.9	70.1	74.7	86.4	96.3	91.0	101.6	90.6	89.4	5.7	7.0	-3.2

(1) Refer to abbreviations for description of parameters

(2) MAE: Mean absolute error

(3) RMSE: Root mean square error

(4) PBIAS: Percentage Bias

(5) Setpoint: 10.8 to 11.1

(6) Setpoint: 10.0 to 10.2

(7) Setpoint: 7.0 to 7.6

Table 5-14. Simulated sludge production and CO_2 consumption in chemical phosphorus removal process

#	Description	Units	Jul 17	Aug 17	Sep 17	Jan 18	Feb 18	Mar 18	Average
1	Chemical sludge production	tons/month	619.1	597.1	554.1	611.3	580.7	602.3	594.1
		kg/1000m^3	230	214	226	237	210	218	222
2	Carbon dioxide dosage	tons/month	59.1	57.7	43.5	50.6	55.9	52.0	54.4
		kg/1000m^3	15.3	14.5	12.4	13.7	14.2	13.2	13.9

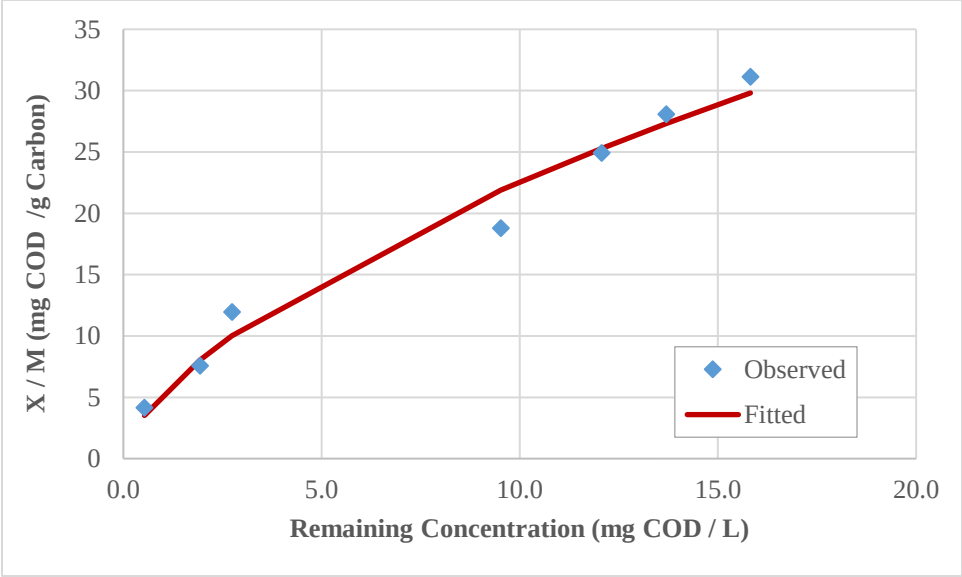

Figure 5-7. Isotherm data, provided by UOSA-WRF for new activated carbon, fitted into Equation 5-27 to calculate the isotherm coefficients. (q_{max} = 414 mg/L, a = 0.65, k_{Ads} = 1.5 d^{-1}, k_{Des} = 114 d^{-1})

Table 5-15: Design parameters for activated carbon

#	Description	Unit	Value
1	Surface Area	m^2/g	1050
2	Carbon Density	kg/m^3	2000
3	Bulk Density	kg/m^3	400
4	Porosity	-	0.8
5	Mean Particle diameter	mm	1.0
6	Sphere volume	m^3	5.24E-10
7	Sphere Weight	kg	1.05E-06
8	Sphere area	m^2	3.14E-06
9	Spheres / volume	$No./m^3$	3.82E+08
10	Specific surface area	m^2/m^3	1200

Table 5-16. Model calibration results for final effluent

#	Parameter(1)	Units	Jul 17		Aug 17		Sep 17		Jan 18		Feb 18		Mar 18		MAE(2)	RMSE(3)	PBIAS(4)
			Obs	Sim	Obs	Sim	Obs	Sim	Obs	Sim	Obs	Sim	Obs	Sim			
1	TSS	mg/L as TSS	0.4	0.4	0.5	0.4	0.4	0.4	0.4	0.4	0.4	0.4	0.4	0.4	0.04	0.05	1.7
2	COD	mg/L as COD	7.7	6.4	7.6	7.3	8.6	8.7	9.8	9.6	9.2	7.7	9.1	8.5	0.69	0.86	7.5
3	NH_3	mg/L as N	0.03	0.03	0.02	0.05	0.05	0.03	0.08	0.05	0.07	0.05	0.15	0.05	0.03	0.05	35.0
4	TKN	mg/L as N	0.5	0.3	0.5	0.5	0.5	0.5	0.6	0.5	0.5	0.5	0.6	0.6	0.06	0.08	9.2
5	NO_3	mg/L as N	15.6	16.3	16.3	14.2	14.7	15.4	8.6	7.2	7.8	7.2	8.8	8.5	0.96	1.12	3.9
6	Total N	mg/L as N	16.0	16.6	16.7	14.7	15.1	15.9	9.2	7.9	8.3	7.7	9.4	9.1	0.93	1.09	3.8
7	OP	mg/L as P	0.08	0.07	0.08	0.05	0.08	0.08	0.09	0.08	0.08	0.06	0.08	0.07	0.01	0.02	16.3
8	Alkalinity	mg/L as $CaCO_3$	79.4	79.1	81.2	68.6	71.4	73.0	86.4	94.4	91.0	100.2	90.6	87.3	5.85	7.33	-0.5
9	pH	-	7.2	7.3	7.3	7.6	7.2	7.1	7.4	7.5	7.4	7.6	7.4	7.5	0.16	0.17	-1.4

(1) Refer to abbreviations for description of parameters

(2) MAE: Mean absolute error

(3) RMSE: Root mean square error

(4) PBIAS: Percentage Bias

Table A 5-1. Existing state variables for SGM and BGM

#	Symbols	Description	Unit
1	S_F	Fermentable organic substance	*mg/L as COD*
2	S_{nF}	Non-fermentable organic substance	*mg/L as COD*
3	S_{VFA}	Fermentable acetate	*mg/L as COD*
4	S_{MET}	Methanol	*mg/L as COD*
5	S_U	Unbiodegradable organic material	*mg/L as COD*
6	$S_{PO_4^{3-}}$	Orthophosphorus	*mg/L as COD*
7	S_P	Organic phosphorus	*mg/L as P*
8	S_{PU}	Unbiodegradable organic phosphorus	*mg/L as P*
9	S_{NHx}	Total ammonium nitrogen	*mg/L as N*
10	S_{NO_3}	Nitrate	*mg/L as N*
11	S_{NO_2}	Nitrite	*mg/L as N*
12	S_{NO}	Nitric oxide	*mg/L as N*
13	S_{N_2O}	Nitrous oxide	*mg/L as N*
14	$S_{NO_2_FLOC}$	Nitrite in flocs	*mg/L as N*
15	S_N	Organic nitrogen	*mg/L as N*
16	S_{NU}	Unbiodegradable organic nitrogen	*mg/L as N*
17	S_{ALK}	Alkalinity	*mg/L as* $CaCO_3$
18	X_{PHA}	Poly-hydroxy-alkonates	*mg/L as COD*
19	X_S	Slowly biodegradable organics	*mg/L as COD*
20	X_U	Unbiodegradable organic material	*mg/L as COD*
21	X_{PP}	Poly-phosphates	*mg/L as P*
22	X_P	Organic phosphate	*mg/L as P*
23	X_{PU}	Unbiodegradable organic phosphate	*mg/L as P*
24	X_N	Organic nitrogen	*mg/L as N*
25	X_{NU}	Unbiodegradable organic nitrogen	*mg/L as N*
26	X_M	Inert inorganic minerals	*mg/L as TSS*
27	X_{OHO}	Ordinary heterotrophs	*mg/L as COD*
28	X_{OAF}	Obligate anaerobic fermenters	*mg/L as COD*
29	X_{OAM}	Obligate anaerobic methanogens	*mg/L as COD*
30	X_{PAO}	Phosphorus accumulating bacteria	*mg/L as COD*
31	X_{MET}	Methanotrophs	*mg/L as COD*
32	X_{AOB}	Ammonium oxidizing bacteria	*mg/L as COD*
33	X_{NOB}	Nitrate oxidizing bacteria	*mg/L as COD*

Table A 5-2. New state variables for PCM

#	Symbol	Description	Unit
1	S_{IC}	Inorganic Carbon	gC / m^3
2	S_{CO_2}	Carbon dioxide	gC / m^3

#	Symbol	Description	Unit
3	$S_{Al,T}$	Total Aluminum species	g/m^3
4	$S_{Fe^{3+},T}$	Total Ferric species	g/m^3
5	$S_{Fe^{2+},T}$	Total Ferrous species	g/m^3
6	$S_{Ca^{2+}}$	Calcium	g/m^3
7	$S_{Mg^{2+}}$	Magnesium	g/m^3
8	$S_{Mn^{2+}}$	Manganese	g/m^3
9	$S_{Na^{+}}$	Sodium	g/m^3
10	$S_{K^{+}}$	Potassium	g/m^3
11	. .	Chloride	gS/m^3
12	$S_{SO_4^{2-}}$	Sulfate	gS/m^3
13	$S_{SO_3^{2-}}$	Sulfite	gS/m^3
14	$S_{S^{2-}}$	Sulfide	gS/m^3
15	S_{Cl_2}	Free chlorine	gCl/m^3
16	$S_{Que,Cl}$	Dechlorination agent	g/m^3
17	S_{NH_2Cl}	Monochloramine	g/m^3
18	S_{NHCl_2}	Dichloramine	g/m^3
19	S_{NHCl_3}	Trichloramine	g/m^3
20	S_{MnO_4}	Permanganate	g/m^3
21	S_{Que,MnO_4}	Permanganate quenching agent	g/m^3
22	S_{ClO_2}	Chlorine dioxide	g/m^3
23	S_{Que,ClO_2}	Chlorine dioxide quenching agent	g/m^3
24	S_{O_3}	Ozone	g/m^3
25	S_{Que,O_3}	Ozone quenching agent	g/m^3
26	$S_{H_2O_2}$	Hydrogen peroxide	g/m^3
27	S_{Que,H_2O_2}	Hydrogen peroxide quenching agent	g/m^3
28	S_{N_2}	Nitrogen gas	g/m^3
29	S_{CH_4}	Methane	g/m^3
30	S_{H_2S}	Hydrogen sulfide	g/m^3
31	$X_{Fe(OH)_3}$	Ferric Hydroxide	g/m^3
32	X_{FePO_4}	Ferric Phosphate	g/m^3
33	$X_{Al(OH)_3}$	Aluminum Hydroxide	g/m^3
34	X_{AlPO_4}	Aluminum Phosphate	g/m^3
35	X_{FeCO_3}	Ferrous carbonate	g/m^3
36	$X_{Fe(OH)_2}$	Ferrous hydroxide $X_{Fe(OH)_3}$	g/m^3
37	$X_{Fe_3(PO_4)_2}$	Vivianite	
38	X_{CaCO_3}	Calcium Carbonate (Calcite)	g/m^3
39	$X_{Ca(OH)_2}$	Calcium hydroxide	g/m^3
40	$X_{Ca_5(PO_4)_3(OH)}$	Hydroxyapatite	g/m^3
41	X_{CaHPO_4}	Brushite	g/m^3

#	Symbol	Description	Unit
42	$X_{Mg(OH)_2}$	Magnesium hydroxide	g/m^3
43	$X_{MgNH_4PO_4}$	Struvite	g/m^3
44	$X_{Mn(OH)_2}$	Manganese hydroxide	g/m^3
45	X_{MnO_2}	Manganese Dioxide	g/m^3
46	X_A	Adsorbent	g/m^3
47	$X_{A,F}$	S_F adsorbed on X_A	$gCOD/m^3$
48	$X_{A,VFA}$	S_A adsorbed on X_A	$gCOD/m^3$
49	$X_{A,nF}$	S_{UF} adsorbed on X_A	$gCOD/m^3$
50	$X_{A,U}$	S_I adsorbed on X_A	$gCOD/m^3$

Note: In addition to above, ten soluble and ten particulate user defined components are also included for modeling custom processes.

Table A 5-3. New algebraic variables for PCM

#	Symbol	Description	Unit
1	S_{H^+}	Hydrogen	g/m^3
2	$S_{Fe^{3+}}$	Ferric	g/m^3
3	$S_{Fe^{2+}}$	Ferrous	g/m^3
4	S_{FeL^+}	Ferrous attached to organic ligand	g/m^3
5	$S_{Al^{3+}}$	Aluminum	g/m^3
6	S_{OH^-}	Hydroxide	g/m^3
7	S_{Ac^-}	Acetate	$gCOD/m^3$
8	$S_{PO_4^{3-},ion}$	Phosphate	gP/m^3
9	$S_{HPO_4^{2-}}$	Hydrogen Phosphate	gP/m^3
10	$S_{H_2PO_4^-}$	Dihydrogen Phosphate	gP/m^3
11	$S_{CO_3^{2-}}$	Carbonate	gC/m^3
12	$S_{HCO_3^-}$	Bicarbonate	gC/m^3
13	S_{HOCl}	Hypochlorous acid	gCl/m^3
14	S_{OCl^-}	Hypochlorite	gCl/m^3
15	$S_{NH_4^+}$	Ammonium	gN/m^3
16	S_{NH_3}	Ammonia	gN/m^3

Table A 5-4. Model parameters for PCM

No.	Parameter	Description	Unit
1	γ_i	Activity coefficient for component *i*	-
2	M_i	Molar mass of component *i*	$mg\ mole^{-1}$
3	k_{PRE_i}	Precipitations rate constant of component *i*	d^{-1}
4	k_{RED_i}	Redissolution rate constant of component *i*	d^{-1}
5	K_{RED}	Half saturation constant for redissolution	$mg\ L^{-1}$
6	$k_{Oxd_i_j}$	Oxidation rate constant of component *i* by oxidant *j*	$L\ mg^{-1}\ d^{-1}$
7	$k_{Oxd_i_j_1}$	First oxidation rate constant of component *i* by oxidant *j*	$L\ mg^{-3}\ d^{-3}$
8	$k_{Oxd_i_j_2}$	Second oxidation rate constant of component *i* by oxidant *j*	$L\ mg^{-1}\ d^{-1}$

9	$k_{Que,i}$	Quenching rate constant for oxidant *i*	$L\ mg^{-1}\ d^{-1}$
10	f_{Que,Cl_2}	De-chlorinating agent stoichiometric factor	-
11	$k_{Oxd_NH_4^+_HOCl}$	Oxidation rate of NH_4^+ *to* NH_2Cl by *HOCl*	$L\ mg^{-1}\ d^{-1}$
12	$k_{Oxd_NH_2Cl_HOCl}$	Oxidation rate of NH_2Cl *to* $NHCl_2$ by *HOCl*	$L\ mg^{-1}\ d^{-1}$
13	$k_{Oxd_NHCl_2_HOCl}$	Oxidation rate of $NHCl_2$ *to* NCl_3 by *HOCl*	$L\ mg^{-1}\ d^{-1}$
14	k_{0,NCl_3}	Decomposition rate constant of NCl_3	d^{-1}
15	k_{1,NCl_3}	Decomposition rate constant of NCl_3 for OH^-	$L\ mg^{-1}\ d^{-1}$
16	$k_{H_2PO_4^-,NCl_3}$	Decomposition rate constant of NCl_3 for $H_2PO_4^-$	$L\ mg^{-1}\ d^{-1}$
17	$k_{HPO_4^{2-},NCl_3}$	Decomposition rate constant of NCl_3 for HPO_4^{2-}	$L\ mg^{-1}\ d^{-1}$
18	$k_{HCO_3^-,NCl_3}$	Decomposition rate constant of NCl_3 for HCO_3^-	$L\ mg^{-1}\ d^{-1}$
19	k_{2,NCl_3}	Decomposition rate constant of NCl_3 for $(OH^-)^2$	$L\ mg^{-2}\ d^{-2}$
20	b_{Cl_2}	Free chlorine decay rate constant	d^{-1}
21	k_{ADS}	Adsorption rate constant	$L\ mg^{-1}\ d^{-1}$
22	k_{Des}	Desorption rate constant	d^{-1}
23	k_{Hyd_Ads}	Hydrolysis rate of $X_{A,U}$	d^{-1}
24	k_{Sat_Ads}	Saturation coefficient for adsorption	d^{-1}
25	$k_{L,i}$	Gas transfer coefficient of component *i*	$m\ sec^{-1}$
26	$K_{H,i}$	Henry's coefficient of component *i*	$M\ bar^{-1}$
27	P_i	Partial pressure of component *i*	*bar*
28	SSA	Surface area of tank	$m^2\ m^{-3}$
29	A_{Bubble}	Specific surface area of bubbles	$m^2\ m^{-3}$

Table A 5-5. Acidity constants for acids

#	Constant	Reaction	LogK
1	K_w	$H_2O \text{ €} \quad OH^- + H^+$	-14
2	K_{a_1,H_2CO_3}	$H_2CO_3^* \text{ €} \quad HCO_3^{1-} + H^+$	-6.35
3	K_{a_2,HCO_3^-}	$HCO_3^- \text{ €} \quad CO_3^{2-} + H^+$	-10.33
4	$K_{a_2,H_2PO_4^-}$	$H_2PO_4^{1-} \text{ €} \quad HPO_4^{2-} + H^+$	-7.20
5	K_{a_3,HPO_4^-}	$HPO_4^{2-} \text{ €} \quad PO_4^{3-} + H^+$	-12.37
6	K_{a,NH_4^+}	$NH_4^+ \text{ €} \quad NH_3 + H^+$	-9.25
7	$K_{a,Ac}$	$CH_3COOH \text{ €} \quad CH_3COO^- + H^+$	-4.76
8	$K_{a,HOCl}$	$HOCl \text{ €} \quad OCl^- + H^+$	-7.50

Table A 5-6. Solubility constants for precipitates

#	Constant	Reaction	LogK
1	$K_{sp,FePO_4}$	$FePO_{4(s)} \text{ €} \quad Fe^{3+} + PO_4^{3-}$	-28.75
2	$K_{sp,Fe(OH)_3}$	$Fe(OH)_{3(s)} \text{ €} \quad Fe^{3+} + 3OH^-$	-38.2
3	$K_{sp,AlPO_4}$	$AlPO_{4(s)} \text{ €} \quad Al^{3+} + PO_4^{3-}$	-22.2
4	$K_{sp,Al(OH)_3}$	$Al(OH)_{3(s)} \text{ €} \quad Al^{3+} + 3OH^-$	-32.3
5	$K_{sp,FeCO_3}$	$FeCO_{3(s)} \text{ €} \quad Fe^{2+} + CO_3^{2-}$	-10.24
6	$K_{sp,Fe_3(PO_4)_2}$	$Fe_3(PO_4)_{2(s)} \text{ €} \quad 3Fe^{2+} + 2PO_4^{3-}$	-35.8
7	$K_{sp,CaCO_3}$	$CaCO_{3(s)} \text{ €} \quad Ca^{2+} + CO_3^{2-}$	-8.34
8	$K_{sp,Ca_5(PO_4)_3(OH)}$	$Ca_5(PO_4)_3(OH)_{(s)} \text{ €} \quad 5Ca^{5+} + 3PO_4^{3-} + OH^-$	-58.33
9	$K_{sp,CaHPO_4}$	$CaHPO_{4(s)} \text{ €} \quad Ca^{2+} + HPO_4^{2-}$	-6.6

10	$K_{sp,Mg(OH)_2}$	$Mg(OH)_{2(s)}$ € $Mg^{2+} + 2OH^-$	-11.16
11	$K_{sp,MgNH_4PO_4}$	$MgNH_4PO_{4(s)}$ € $Mg^{2+} + NH_4^+ + PO_4^{3-}$	-13.26

Table A 5-7. Stability constants for metal complexes

#	Constant	Reaction	LogK
1	β_{1,Fe_3^+}	$Fe^{3+} + OH^-$ € $FeOH^{2+}$	11.81
2	β_{2,Fe_3^+}	$Fe^{3+} + 2OH^-$ € $Fe(OH)_2^{1+}$	23.4
3	β_{3,Fe_3^+}	$Fe^{3+} + 3OH^-$ € $Fe(OH)_3^{0}$	29.43
4	β_{4,Fe_3^+}	$Fe^{3+} + 4OH^-$ € $Fe(OH)_4^{1-}$	34.4
5	$K_{eq,FeH_2PO_4^{2+}}$	$Fe^{3+} + 2H^+ + PO_4^{3-}$ € $FeH_2PO_4^{2+}$	23.85
6	β_{1,Al_3^+}	$Al^{3+} + OH^-$ € $AlOH^{2+}$	9.0
7	β_{2,Al_3^+}	$Al^{3+} + OH^-$ € $Al(OH)_2^{1+}$	17.9
8	β_{3,Al_3^+}	$Al^{3+} + 3OH^-$ € $Al(OH)_3^{0}$	25.2
9	β_{4,Al_3^+}	$Al^{3+} + 4OH^-$ € $Al(OH)_4^{1-}$	33.3
10	$K_{eq,AlH_2PO_4^{2+}}$	$Al^{3+} + 2H^+ + PO_4^{3-}$ € $AlH_2PO_4^{2+}$	28.9

Table A 5-8. Algebraic equations for pH calculation

No.	Equation
1	$\frac{S_{ALK}}{0.5M_{CaCO_3}}+\frac{S_{H^+}}{M_H}-\frac{S_{OH^-}}{M_{OH}}-\frac{S_{HCO_3^-}}{M_C}-\frac{2S_{CO_3^{2-}}}{M_C}-\frac{S_{H_2PO_4^-}}{M_P}-\frac{2S_{HPO_4^{2-}}}{M_P}-\frac{3S_{PO_4^{3-}}}{M_P}-\frac{0.628S_{Ac^-}}{2M_O}-\frac{S_{OCl^-}}{M_{Cl}}-\frac{S_{NH_3}}{M_N}=0$
2	$\frac{\gamma_{OH^-}S_{OH^-}}{M_{OH}}\frac{\gamma_{H^+}S_{H^+}}{M_H}-K_w=0$
3	$\frac{S_{IC}}{M_C}-\frac{S_{HCO_3^-}}{M_C}-\frac{S_{CO_3^{2-}}}{M_C}-\frac{S_{CO_2}}{M_C}=0$
4	$K_{a_1,H_2CO_3}\frac{S_{CO_2}}{M_C}-\frac{\gamma_{HCO_3^-}S_{HCO_3^-}}{M_C}\frac{\gamma_{H^+}S_{H^+}}{M_H}=0$
5	$K_{a_2,HCO_3^-}\frac{\gamma_{HCO_3^-}S_{HCO_3^-}}{M_C}-\frac{\gamma_{CO_3^{2-}}S_{CO_3^{2-}}}{M_C}\frac{\gamma_{H^+}S_{H^+}}{M_C}=0$
6	$\frac{S_{PO_4}}{M_P}-\frac{S_{H_2PO_4^-}}{M_P}-\frac{S_{HPO_4^{2-}}}{M_P}-\frac{S_{PO_4^{3-},ion}}{M_P}-K_{eq,FeH_2PO_4^{2+}}\frac{\gamma_{Fe^{3+}}S_{Fe^{3+}}}{M_{Fe}}\left(\frac{\gamma_{H^+}S_{H^+}}{M_H}\right)^2\frac{\gamma_{PO_4^{3-}}S_{PO_4^{3-},ion}}{M_P}-K_{eq,AlH_2PO_4^{2+}}\frac{\gamma_{Al^{3+}}S_{Al^{3+}}}{M_{Al}}\left(\frac{\gamma_{H^+}S_{H^+}}{M_H}\right)^2\frac{\gamma_{PO_4^{3-}}S_{PO_4^{3-},ion}}{M_P}=0$
7	$K_{a_2,H_2PO_4^-}\frac{\gamma_{H_2PO_4^-}S_{H_2PO_4^-}}{M_P}-\frac{\gamma_{HPO_4^{2-}}S_{HPO_4^{2-}}}{M_P}\frac{\gamma_{H^+}S_{H^+}}{M_H}=0$
8	$K_{a_3,HPO_4^-}\frac{\gamma_{HPO_4^-}S_{HPO_4^-}}{M_P}-\frac{\gamma_{PO_4^{3-}}S_{PO_4^{3-},ion}}{M_P}\frac{\gamma_{H^+}S_{H^+}}{M_H}=0$
9	$\frac{S_{NHx}}{M_N}-\frac{S_{NH_4^+}}{M_N}-\frac{S_{NH_3}}{M_N}=0$
10	$K_{a,NH_4^+}\frac{\gamma_{NH_4^+}S_{NH_4^+}}{M_N}-\frac{S_{NH_3}}{M_N}\frac{\gamma_{H^+}S_{H^+}}{M_H}=0$
11	$K_{a,Ac}\frac{S_{VFA}}{2M_O}-\left(K_{a,Ac}+\frac{\gamma_{H^+}S_{H^+}}{M_H}\right)\frac{\gamma_{Ac^-}S_{Ac^-}}{M_{Ac}}=0$
12	$\frac{S_{Cl_2}}{M_{Cl}}-\frac{S_{HOCl}}{M_{Cl}}-\frac{S_{OCl^-}}{M_{Cl}}=0$
13	$K_{a,HOCl}\frac{S_{HOCl}}{M_{Cl}}-\frac{\gamma_{OCl^-}S_{OCl^-}}{M_{Cl}}\frac{\gamma_{H^+}S_{H^+}}{M_{Cl}}=0$
14	$\frac{S_{Fe^{3+},T}}{M_{Fe}}-\frac{S_{Fe^{3+}}}{M_{Fe}}-\beta_{1,Fe^{3+}}\frac{\gamma_{Fe^{3+}}S_{Fe^{3+}}}{M_{Fe}}\frac{\gamma_{OH^-}S_{OH^-}}{S_{OH}}-\beta_{2,Fe^{3+}}\frac{\gamma_{Fe^{3+}}S_{Fe^{3+}}}{M_{Fe}}\left(\frac{\gamma_{OH^-}S_{OH^-}}{S_{OH}}\right)^2-\beta_{3,Fe^{3+}}\frac{\gamma_{Fe^{3+}}S_{Fe^{3+}}}{M_{Fe}}\left(\frac{\gamma_{OH^-}S_{OH^-}}{S_{OH}}\right)^3-\beta_{4,Fe^{3+}}\frac{\gamma_{Fe^{3+}}S_{Fe^{3+}}}{M_{Fe}}\left(\frac{\gamma_{OH^-}S_{OH^-}}{S_{OH}}\right)^4-K_{eq,FeH_2PO_4^{2+}}\frac{\gamma_{Fe^{3+}}S_{Fe^{3+}}}{M_{Fe}}\left(\frac{\gamma_{H^+}S_{H^+}}{M_H}\right)^2\frac{\gamma_{PO_4^{3-}}S_{PO_4^{3-},ion}}{M_P}=0$
15	$\frac{S_{Al^{3+},T}}{M_{Al}}-\frac{S_{Al^{3+}}}{M_{Al}}-\beta_{1,Al^{3+}}\frac{\gamma_{Al^{3+}}S_{Al^{3+}}}{M_{Al}}\frac{\gamma_{OH^-}S_{OH^-}}{S_{OH}}-\beta_{2,Al^{3+}}\frac{\gamma_{Al^{3+}}S_{Al^{3+}}}{M_{Al}}\left(\frac{\gamma_{OH^-}S_{OH^-}}{S_{OH}}\right)^2-\beta_{3,Al^{3+}}\frac{\gamma_{Al^{3+}}S_{Al^{3+}}}{M_{Al}}\left(\frac{\gamma_{OH^-}S_{OH^-}}{S_{OH}}\right)^3-\beta_{4,Al^{3+}}\frac{\gamma_{Al^{3+}}S_{Al^{3+}}}{M_{Al}}\left(\frac{\gamma_{OH^-}S_{OH^-}}{S_{OH}}\right)^4-K_{eq,AlH_2PO_4^{2+}}\frac{\gamma_{Al^{3+}}S_{Al^{3+}}}{M_{Al}}\left(\frac{\gamma_{H^+}S_{H^+}}{M_H}\right)^2\frac{\gamma_{PO_4^{3-}}S_{PO_4^{3-},ion}}{M_P}=0$

No.	Equation
16	$\frac{S_{Fe^{2+},T}}{M_{Fe}} - \frac{S_{Fe^{2+}}}{M_{Fe}} - S_{FeL^+} = 0$
17	$K_{FeL^+} \frac{\gamma_{Fe^{2+}} S_{Fe^{2+}}}{M_{Fe}} S_U - S_{FeL^+} = 0$

Table A 5-9. Process rate equations and stoichiometry for precipitation

No.	Process[1]	Process Rate Equation	$S_{Fe^{3+},T}$	$S_{Al,T}$	$S_{Fe^{2+},T}$
1	Precipitation of $FePO_4$	$k_{PRE,FePO_4}\left(Q_{sp,FePO_4} - K_{sp,FePO_4}\right)$ where $Q_{sp,FePO_4} = \frac{\gamma_{Fe^{3+}} S_{Fe^{3+}}}{M_{Fe}} \frac{\gamma_{PO_4^{3-}} S_{PO_4^{3-},ion}}{M_P}$	$-M_{Fe}$		
2	Re-dissolution of $FePO_4$	$k_{RED,FePO_4}\left(K_{sp,FePO_4} - Q_{sp,FePO_4}\right)\frac{X_{FePO_4}}{K_{Red} + X_{FePO_4}}$	M_{Fe}		
3	Precipitation of $Fe(OH)_3$	$k_{PRE,Fe(OH)_3}\left(Q_{sp,Fe(OH)_3} - K_{sp,Fe(OH)_3}\right)$ where $Q_{sp,Fe(OH)_3} = \frac{\gamma_{Fe^{3+}} S_{Fe^{3+}}}{M_{Fe}} \left(\frac{\gamma_{OH^-} S_{OH^-}}{M_{OH}}\right)^3$	$-M_{Fe}$		
4	Re-dissolution of $Fe(OH)_3$	$k_{RED,Fe(OH)_3}\left(K_{sp,Fe(OH)_3} - Q_{sp,Fe(OH)_3}\right)\frac{X_{Fe(OH)_3}}{K_{Red} + X_{Fe(OH)_3}}$	M_{Fe}		
5	Precipitation of $AlPO_4$	$k_{PRE,AlPO_4}\left(Q_{sp,AlPO_4} - K_{sp,AlPO_4}\right)$ where $Q_{sp,AlPO_4} = \frac{\gamma_{Al^{3+}} S_{Al^{3+}}}{M_{Al}} \frac{\gamma_{PO_4^{3-}} S_{PO_4^{3-},ion}}{M_P}$		$-M_{Al}$	
6	Re-dissolution of $AlPO_4$	$k_{RED,AlPO_4}\left(K_{sp,AlPO_4} - Q_{sp,AlPO_4}\right)\frac{X_{AlPO_4}}{K_{Red} + X_{AlPO_4}}$		M_{Al}	
7	Precipitation of $Al(OH)_3$	$k_{PRE,Al(OH)_3}\left(Q_{sp,Al(OH)_3} - K_{sp,Al(OH)_3}\right)$ where $Q_{sp,Al(OH)_3} = \frac{\gamma_{Al^{3+}} S_{Al^{3+}}}{M_{Al}} \left(\frac{\gamma_{OH^-} S_{OH^-}}{M_{OH}}\right)^3$		$-M_{Al}$	
8	Re-dissolution of $Al(OH)_3$	$k_{RED,Al(OH)_3}\left(K_{sp,Al(OH)_3} - Q_{sp,Al(OH)_3}\right)\frac{X_{Al(OH)_3}}{K_{Red} + X_{Al(OH)_3}}$		M_{Al}	
9	Precipitation of $FeCO_3$	$k_{PRE,FeCO_3}\left(Q_{sp,FeCO_3} - K_{sp,FeCO_3}\right)$ where $Q_{sp,FeCO_3} = \frac{\gamma_{Fe^{2+}} S_{Fe^{2+}}}{M_{Fe}} \frac{\gamma_{CO_3^{2-}} S_{CO_3^{2-}}}{M_C}$			$-M_{Fe}$
10	Re-dissolution of $FeCO_3$	$k_{RED,FeCO_3}\left(K_{sp,FeCO_3} - Q_{sp,FeCO_3}\right)\frac{X_{FeCO_3}}{K_{Red} + X_{FeCO_3}}$			M_{Fe}
11	Precipitation of $Fe_3(PO_4)_2$	$k_{PRE,Fe_3(PO_4)_2}\left(Q_{sp,Fe_3(PO_4)_2} - K_{sp,Fe_3(PO_4)_2}\right)$ where $Q_{sp,Fe_3(PO_4)_2} = \left(\frac{\gamma_{Fe^{2+}} S_{Fe^{2+}}}{M_{Fe}}\right)^3 \left(\frac{\gamma_{PO_4^{3-}} S_{PO_4^{3-},ion}}{M_P}\right)^2$			$-M_{Fe}$
12	Re-dissolution of $Fe_3(PO_4)_2$	$k_{RED_Fe_3(PO_4)_2}\left(K_{sp,Fe_3(PO_4)_2} - Q_{sp,Fe_3(PO_4)_2}\right)\frac{X_{Fe_3(PO_4)_2}}{K_{Red} + X_{Fe_3(PO_4)_2}}$			M_{Fe}

No.	Process[1]	Process Rate Equation	$S_{Fe^{3+},T}$	$S_{Al,T}$	$S_{Fe^{2+},T}$
13	Precipitation of $CaCO_3$	$k_{PRE,CaCO_3}\left(Q_{sp,CaCO_3}-K_{sp,CaCO_3}\right)$ where $Q_{sp,CaCO_3}=\frac{\gamma_{Ca^{2+}}S_{Ca^{2+}}}{M_{Ca}},\frac{\gamma_{CO_3^{2-}}S_{CO_3^{2-}}}{M_C}$			
14	Re-dissolution of $CaCO_3$	$k_{RED,CaCO_3}\left(K_{sp,CaCO_3}-Q_{sp,CaCO_3}\right)\frac{X_{CaCO_3}}{K_{Red}+X_{CaCO_3}}$			
15	Precipitation of $Ca_5(PO_4)_3OH$	$k_{PRE,Ca_5(PO_4)_3OH}\left(Q_{sp,Ca_5(PO_4)_3OH}-K_{sp,Ca_5(PO_4)_3OH}\right)$ where $Q_{sp,Ca_5(PO_4)_3OH}\left(\frac{\gamma_{Ca^{2+}}S_{Ca^{2+}}}{M_{Ca}}\right)^5\left(\frac{\gamma_{PO_4^{3-}}S_{PO_4^{3-},ion}}{M_P}\right)^3\frac{\gamma_{OH^-}S_{OH^-}}{M_{OH}}$			
16	Re-dissolution of $Ca_5(PO_4)_3OH$	$k_{RED,Ca_5(PO_4)_3OH}\left(K_{sp,Ca_5(PO_4)_3OH}-Q_{sp,Ca_5(PO_4)_3OH}\right)\frac{X_{Ca_5(PO_4)_3OH}}{K_{Red}+X_{Ca_5(PO_4)_3OH}}$			
17	Precipitation of $CaHPO_4$	$k_{PRE,CaHPO_4}\left(Q_{sp,CaHPO_4}-K_{sp,CaHPO_4}\right)$ where $Q_{sp,CaHPO_4}=\frac{\gamma_{Ca^{2+}}S_{Ca^{2+}}}{M_{Ca}}\frac{\gamma_{HPO_4^{2-}}S_{HPO_4^{2-}}}{M_P}$			
18	Re-dissolution of $CaHPO_4$	$k_{RED,CaHPO_4}\left(K_{sp,CaHPO_4}-Q_{sp,CaHPO_4}\right)\frac{X_{CaHPO_4}}{K_{Red}+X_{CaHPO_4}}$			
19	Precipitation of $Mg(OH)_2$	$k_{PRE,Mg(OH)_2}\left(Q_{sp,Mg(OH)_2}-K_{sp,Mg(OH)_2}\right)$ where $Q_{sp,Mg(OH)_2}=\frac{\gamma_{Mg^{2+}}S_{Mg^{2+}}}{M_{Mg}}\left(\frac{\gamma_{OH^-}S_{OH^-}}{M_{OH}}\right)^2$			
20	Re-dissolution of $Mg(OH)_2$	$k_{RED,Mg(OH)_2}\left(K_{sp,Mg(OH)_2}-Q_{sp,Mg(OH)_2}\right)\frac{X_{Mg(OH)_2}}{K_{Red}+X_{Mg(OH)_2}}$			
21	Precipitation of $MgNH_4PO_4$	$k_{PRE,MgNH_4PO_4}\left(Q_{sp,MgNH_4PO_4}-K_{sp,MgNH_4PO_4}\right)$ where $Q_{sp,MgNH_4PO_4}=\frac{\gamma_{Mg^{2+}}S_{Mg^{2+}}}{M_{Mg}}\frac{\gamma_{NH_4^+}S_{NH_4^+}}{M_N}\frac{\gamma_{PO_4^{3-}}S_{PO_4^{3-},ion}}{M_P}$			
22	Re-dissolution of $MgNH_4PO_4$	$k_{RED,MgNH_4PO_4}\left(K_{sp,MgNH_4PO_4}-Q_{sp,MgNH_4PO_4}\right)\frac{X_{MgNH_4PO_4}}{K_{Red}+X_{MgNH_4PO_4}}$			

Table A 5-9. (Continued)

No.	Process[1]	$S_{Ca^{2+}}$	$S_{Mg^{2+}}$	$S_{Mn^{2+}}$	$S_{PO_4^{3-}}$	$S_{NH_4^+}$	S_{IC}	S_{ALK}	S_{O_2}	X_{FePO_4}	$X_{Fe(OH)_3}$	X_{AlPO_4}	$X_{Al(OH)_3}$	X_{FeCO_3}
1	Precipitation of $FePO_4$				$-M_P$			$-1.5M_{CaCO_3}$		M_{FePO_4}				
2	Re-dissolution of $FePO_4$				M_P			$1.5M_{CaCO_3}$		$-M_{FePO_4}$				
3	Precipitation of $Fe(OH)_3$							$-1.5M_{CaCO_3}$			$M_{Fe(OH)_3}$			
4	Re-dissolution of $Fe(OH)_3$							$1.5M_{CaCO_3}$			$-M_{Fe(OH)_3}$			
5	Precipitation of $AlPO_4$				$-M_P$			$-1.5M_{CaCO_3}$				M_{AlPO_4}		
6	Re-dissolution of $AlPO_4$				M_P			$1.5M_{CaCO_3}$				$-M_{AlPO_4}$		
7	Precipitation of $Al(OH)_3$							$-1.5M_{CaCO_3}$					$M_{Al(OH)_3}$	
8	Re-dissolution of $Al(OH)_3$							$1.5M_{CaCO_3}$					$-M_{Al(OH)_3}$	
9	Precipitation of $FeCO_3$						$-M_C$	$-M_{CaCO_3}$						M_{FeCO_3}

No.	Process[1]	$S_{Ca^{2+}}$	$S_{Mg^{2+}}$	$S_{Mn^{2+}}$	$S_{PO_4^{3-}}$	$S_{NH_4^+}$	S_{IC}	S_{ALK}	S_{O_2}	X_{FePO_4}	$X_{Fe(OH)_3}$	X_{AlPO_4}	$X_{Al(OH)_3}$	X_{FeCO_3}
10	Re-dissolution of $FeCO_3$						M_C	M_{CaCO_3}						$-M_{FeCO_3}$
11	Precipitation of $Fe_3(PO_4)_2$				$-0.67M_P$			$-M_{CaCO_3}$						
12	Re-dissolution of $Fe_3(PO_4)_2$				$0.67M_P$			M_{CaCO_3}						
13	Precipitation of $CaCO_3$	$-M_{Ca}$					$-M_C$	$-M_{CaCO_3}$						
14	Re-dissolution of $CaCO_3$	M_{Ca}					M_C	M_{CaCO_3}						
15	Precipitation of $Ca_5(PO_4)_3OH$	$-M_{Ca}$			$-0.6M_P$			$-M_{CaCO_3}$						
16	Redissolution of $Ca_5(PO_4)_3OH$	M_{Ca}			$0.6M_P$			M_{CaCO_3}						
17	Precipitation of $CaHPO_4$	$-M_{Ca}$			$-M_P$			$-M_{CaCO_3}$						
18	Re-dissolution of $CaHPO_4$	M_{Ca}			M_P			M_{CaCO_3}						
19	Precipitation of $Mg(OH)_2$		$-M_{Mg}$					$-M_{CaCO_3}$						
20	Re-dissolution of $Mg(OH)_2$		M_{Mg}					M_{CaCO_3}						
21	Precipitation of $MgNH_4PO_4$		$-M_{Mg}$		$-M_P$	$-M_{NH_4}$		$-1.5M_{CaCO_3}$						
22	Re-dissolution of $MgNH_4PO_4$		M_{Mg}		M_P	M_{NH_4}		$1.5M_{CaCO_3}$						

Table A 5-9. (Continued)

No.	Process[1]	$X_{Fe_3(PO_4)_2}$	$X_{Ca(OH)_2}$	X_{CaCO_3}	$X_{Ca_5(PO4)_3OH}$	X_{CaHPO_4}	$X_{Mg(OH)_2}$	$X_{MgNH_4PO_4}$	$X_{Mn(OH)_2}$
1	Precipitation of $FePO_4$								
2	Re-dissolution of $FePO_4$								
3	Precipitation of $Fe(OH)_3$								
4	Re-dissolution of $Fe(OH)_3$								
5	Precipitation of $AlPO_4$								
6	Re-dissolution of $AlPO_4$								
7	Precipitation of $Al(OH)_3$								
8	Re-dissolution of $Al(OH)_3$								
9	Precipitation of $FeCO_3$								
10	Re-dissolution of $FeCO_3$								
11	Precipitation of $Fe_3(PO_4)_2$	$0.33M_{Fe_3(PO4)_2}$							
12	Re-dissolution of $Fe_3(PO_4)_2$	$-0.33M_{Fe_3(PO4)_2}$							
13	Precipitation of $CaCO_3$		M_{CaCO_3}						

No.	Process[1]	$X_{Fe_3(PO_4)_2}$	$X_{Ca(OH)_2}$	X_{CaCO_3}	$X_{Ca_5(PO4)_3OH}$	X_{CaHPO_4}	$X_{Mg(OH)_2}$	$X_{MgNH_4PO_4}$	$X_{Mn(OH)_2}$
14	Re-dissolution of $CaCO_3$		$-M_{CaCO_3}$						
15	Precipitation of $Ca_5(PO_4)_3OH$				$M_{Ca_5(PO_4)_3OH}$				
16	Re-dissolution of $Ca_5(PO_4)_3OH$				$-M_{Ca_5(PO_4)_3OH}$				
17	Precipitation of $CaHPO_4$					M_{CaHPO_4}			
18	Re-dissolution of $CaHPO_4$					$-M_{CaHPO_4}$			
19	Precipitation of $Mg(OH)_2$						$M_{Mg(OH)_2}$		
20	Re-dissolution of $Mg(OH)_2$						$-M_{Mg(OH)_2}$		
21	Precipitation of $MgNH_4PO_4$							$M_{MgNH_4PO_4}$	
22	Re-dissolution of $MgNH_4PO_4$							$-M_{MgNH_4PO_4}$	

(1) Refer to Table A 5-6 for process reactions

Table A 5-10. Process rate equations and stoichiometry of oxygen

No.	Process	Process Rate Equation	$S_{Fe,Tot}$	S_{Mn}	S_{ALK}	S_{O_2}	$X_{Fe(OH)_2}$	X_{MnO_2}
1	Oxidation of Fe^{2+} to $Fe(OH)_3$ with O_2[1]	$k_{Oxd,Fe^{2+},O_2} S_{O_2} . S_{Fe^{2+}} S_{OH^-}^2$	-1		$-\frac{M_{CaCO_3}}{M_{Fe}}$	$-\frac{M_{O_2}}{2M_{Fe}}$	$\frac{M_{Fe(OH)_3}}{M_{Fe}}$	
2	Oxidation of Mn^{2+} to MnO_x with O_2[2]	$k_{1,Oxd,Mn^{2+},O_2} S_{Mn^{2+}} S_{O_2} S_{OH^-}^2 + k_{2,Oxd,Mn^{2+},O_2} S_{Mn^{2+}} X_{MnO_x}$		-1	$-\frac{M_{CaCO_3}}{M_{Mn}}$	$-\frac{M_{O_2}}{M_{Mn}}$		$\frac{M_{MnO_2}}{M_{Mn}}$

(1) $Fe^{2+} + \frac{1}{4}O_2 + 2\frac{1}{2}H_2O \rightleftharpoons Fe(OH)_3 + 2H^+$

(2) $Mn^{2+} + \frac{1}{2}O_2 + H_2O \rightleftharpoons MnO_2 + 2H^+$

Table A 5-11. Process rate equations and stoichiometry for chlorination

No.	Process	Process Rate Equation
1	Hydrolysis of XC_B to S_F	$k_{Hyd,X_{CB},Cl_2} XC_B S_{Cl_2}$
2	Hydrolysis of X_U to S_F	$k_{Hyd,X_U,Cl_2} X_U S_{Cl_2}$
3	Hydrolysis of S_U to S_F	$k_{Hyd,S_U,Cl_2} S_U S_{Cl_2}$
4	Hydrolysis of X_N to S_{NHx}	$k_{Hyd,X_N,Cl_2} X_N S_{Cl_2}$
5	Hydrolysis of X_{NU} to S_{NHx}	$k_{Hyd,X_{NU},Cl_2} X_{NU} S_{Cl_2}$
6	Hydrolysis of S_N to S_{NHx}	$k_{Hyd,S_N,Cl_2} S_N S_{Cl_2}$

No.	Process	Process Rate Equation
7	Hydrolysis of S_{NU} to S_{NHx}	$k_{Hyd,S_{NU},Cl_2} S_{NU} S_{Cl_2}$
8	Hydrolysis of X_P to S_{PO_4}	$k_{Hyd,X_P,Cl_2} X_P S_{Cl_2}$
9	Hydrolysis of X_{PU} to S_{PO_4}	$k_{Hyd,X_{PU},Cl_2} X_{PU} S_{Cl_2}$
10	Hydrolysis of S_P to S_{PO_4}	$k_{Hyd,S_P,Cl_2} S_P S_{Cl_2}$
11	Hydrolysis of S_{PU} to S_{PO_4}	$k_{Hyd,S_{PU},Cl_2} S_{PU} S_{Cl_2}$
12	Oxidation of X_{OHO}	$k_{Oxd,MIC,Cl_2} X_{OHO} S_{Cl_2}$
13	Oxidation of X_{AOB}	$k_{Oxd,MIC,Cl_2} X_{AOB} S_{Cl_2}$
14	Oxidation of X_{NOB}	$k_{Oxd,MIC,Cl_2} X_{NOB} S_{Cl_2}$
15	Oxidation of X_{PAO}	$k_{Oxd,MIC,Cl_2} X_{PAO} S_{Cl_2}$
16	Oxidation of S_F (1,2)	$k_{Oxd,S_F,HOCl} S_F S_{HOCl} + k_{Oxd,S_F,OCl} S_F S_{OCl^-}$
17	Oxidation of S_{VFA} (3,4)	$k_{Oxd,S_{VFA},HOCl} S_{VFA} S_{HOCl} + k_{Oxd,S_{VFA},OCl} S_{VFA} S_{OCl^-}$
18	Oxidation of S_{nF} (1,2)	$k_{Oxd,S_{nF},HOCl} S_{nF} S_{HOCl} + k_{Oxd,S_{nF},OCl} S_{nF} S_{OCl^-}$
19	Oxidation of S_U (1,2)	$k_{Oxd,S_U,HOCl} S_U S_{HOCl} + k_{Oxd,S_U,OCl} S_U S_{OCl^-}$
20	Oxidation of S_{NHx} to S_{NH_2Cl}	$k_{NH_4,HOCl} S_{NH_x} S_{HOCl}$
21	Oxidation of S_{NH_2Cl} to S_{NHCl_2}	$k_{NH_2Cl} S_{NH_2Cl} S_{HOCl}$
22	Oxidation of S_{NHCl_2} to S_{NCl_3}	$k_{NHCl_2} S_{NHCl_2} S_{HOCl}$
23	Oxidation of S_{NCl_3} to S_{N_2} (5)	$2\left(k_{0,NCl_3} + k_{1,NCl_3} S_{OH^-} + k_{H_2PO_4^-} S_{H_2PO_4^-} + k_{HPO_4^{2-}} S_{HPO_4^{2-}} + k_{HCO_3^-} S_{HCO_3^-} + k_{2,NCl_3} \left(S_{OH^-}\right)^2\right) S_{NCl_3}$
24	Oxidation of $S_{Fe^{2+}}$ (6)	$k_{Oxd,Fe^{2+},HOCl} S_{HOCl} S_{Fe^{2+}} S_{OH^-}$
25	Oxidation of $S_{Mn^{2+}}$ (7)	$k_{1,Oxd,Mn^{2+},HOCl} S_{Mn^{2+}} S_{O_2} S_{OH^-}^2 + k_{2,Oxd,Mn^{2+},HOCl} S_{Mn^{2+}} X_{MnO_x}$
26	Oxidization of S_{NO_2} to S_{NO_3} (8)	$k_{Oxd,NO_2,Cl_2} S_{NO_2} S_{Cl_2}$
27	De-chlorination	$k_{Que,Cl_2} S_{Que,Cl_2} S_{Cl_2}$

Table A 5-11. (Continued)

#	Process	S_F	S_{VFA}	S_{nF}	S_U	S_{NHx}	S_N	S_{NU}	S_{PO_4}	S_P	S_{PU}	$S_{Fe^{2+}}$	$S_{Mn^{2+}}$	S_{NO_2}	S_{NO_3}	S_{Cl_2}	S_{ALK}	S_{IC}
1	Hydrolysis of XC_B to S_F	1																
2	Hydrolysis of X_U to S_F	1																
3	Hydrolysis of S_U to S_F	1			-1													
4	Hydrolysis of X_N to S_{NHx}					1												
5	Hydrolysis of X_{NU} to S_{NHx}					1												
6	Hydrolysis of S_N to S_{NHx}					1	-1										3.57	

#	Process	S_F	S_{VFA}	S_{nF}	S_U	S_{NHx}	S_N	S_{NU}	S_{PO_4}	S_P	S_{PU}	$S_{Fe^{2+}}$	$S_{Mn^{2+}}$	S_{NO_2}	S_{NO_3}	S_{Cl_2}	S_{ALK}	S_{IC}
7	Hydrolysis of S_{NU} to S_{NHx}					1		-1									3.57	
8	Hydrolysis of X_P to S_{PO_4}								1									
9	Hydrolysis of X_{PU} to S_{PO_4}								1									
10	Hydrolysis of S_P to S_{PO_4}								1	-1								
11	Hydrolysis of S_{PU} to S_{PO_4}								1		-1							
12	Oxidation of X_{OHO}	1				$i_{N,BM}$			$i_{P,BM}$									
13	Oxidation of X_{AOB}	1				$i_{N,BM}$			$i_{P,BM}$									
14	Oxidation of X_{NOB}	1				$i_{N,BM}$			$i_{P,BM}$									
15	Oxidation of X_{PAO}	1				$i_{N,BM}$			$i_{P,BM}$									
16	Oxidation of S_F (1,2)	-1														$-\frac{2M_{Cl}}{M_{O_2}}$	$-\frac{M_{CaCO_3}}{M_{O_2}}$	$\frac{0.67M_C}{M_{O_2}}$
17	Oxidation of S_{VFA} (3,4)		-1													$-\frac{2M_{Cl}}{M_{O_2}}$	$-\frac{1.5M_{CaCO_3}}{M_{O_2}}$	$\frac{M_C}{M_{O_2}}$
18	Oxidation of S_{nF} (1,2)			-1												$-\frac{2M_{Cl}}{M_{O_2}}$	$-\frac{M_{CaCO_3}}{M_{O_2}}$	$\frac{0.67M_C}{M_{O_2}}$
19	Oxidation of S_U (1,2)				-1											$-\frac{2M_{Cl}}{M_{O_2}}$	$-\frac{M_{CaCO_3}}{M_{O_2}}$	$\frac{0.67M_C}{M_{O_2}}$
20	Oxidation of S_{NHx} to S_{NH_2Cl}					-1										$-\frac{M_{Cl}}{M_N}$		
21	Oxidation of S_{NH_2Cl} to S_{NHCl_2}															$-\frac{M_{Cl}}{M_N}$		
22	Oxidation of S_{NHCl_2} to S_{NCl_3}															$-\frac{M_{Cl}}{M_N}$		
23	Oxidation of S_{NCl_3} to S_{N_2} (5)																$-\frac{1.5M_{CaCO_3}}{M_N}$	
24	Oxidation of $S_{Fe^{2+}}$ (6)											-1				$-\frac{0.5M_{Cl}}{M_{Fe}}$	$-\frac{1.25M_{CaCO_3}}{M_{Fe}}$	
25	Oxidation of $S_{Mn^{2+}}$ (7)												-1			$-\frac{M_{Cl}}{M_{Mn}}$	$-\frac{1.5M_{CaCO_3}}{M_{Mn}}$	
26	Oxidization of S_{NO_2} to S_{NO_3} (8)													-1	1	$-\frac{M_{Cl}}{M_N}$	$-\frac{0.5M_{CaCO_3}}{M_N}$	
27	De-chlorination															-1		

Table A 5-10. (Continued)

No.	Process	$S_{Que,Cl}$	S_{NH_2Cl}	S_{NHCl_2}	S_{NCl_3}	X_{OHO}	X_{AOB}	X_{NOB}	X_{PAO}	X_{CB}	X_U	X_N	X_{NU}	X_P	X_{PU}	$X_{Fe(OH)_3}$	X_{MnO_2}
1	Hydrolysis of XC_B to S_F									-1							
2	Hydrolysis of X_U to S_F										-1						
3	Hydrolysis of S_U to S_F																
4	Hydrolysis of X_N to S_{NHx}											-1					
5	Hydrolysis of X_{NU} to S_{NHx}												-1				
6	Hydrolysis of S_N to S_{NHx}																
7	Hydrolysis of S_{NU} to S_{NHx}																
8	Hydrolysis of X_P to S_{PO_4}													-1			
9	Hydrolysis of X_{PU} to S_{PO_4}														-1		
10	Hydrolysis of S_P to S_{PO_4}																
11	Hydrolysis of S_{PU} to S_{PO_4}																
12	Oxidation of X_{OHO}					-1											
13	Oxidation of X_{AOB}						-1										
14	Oxidation of X_{NOB}							-1									
15	Oxidation of X_{PAO}								-1								
16	Oxidation of S_F (1,2)																
17	Oxidation of S_{VFA} (3,4)																
18	Oxidation of S_{nF} (1,2)																
19	Oxidation of S_U (1,2)																
20	Oxidation of S_{NHx} to S_{NH_2Cl}		1														
21	Oxidation of S_{NH_2Cl} to S_{NHCl_2}		-1	1													
22	Oxidation of S_{NHCl_2} to S_{NCl_3}			-1	1												
23	Oxidation of S_{NCl_3} to S_{N_2} (5)				-1												
24	Oxidation of $S_{Fe^{2+}}$ (6)															$\frac{M_{Fe(OH)_3}}{M_{Fe}}$	
25	Oxidation of $S_{Mn^{2+}}$ (7)																$\frac{M_{MnO_2}}{M_{Mn}}$
26	Oxidization of S_{NO_2} to S_{NO_3} (8)																
27	De-chlorination	$-f_{Que,Cl_2}$															

(1) $CH_3OH + 1.5O_2 \rightleftharpoons CO_2 + 2H_2O$

$$(2)\ CH_3OH + 3HOCl \rightleftharpoons CO_2 + 3Cl^- + 3H^+ + 2H_2O$$

$$(3)\ CH_3COO^- + 2O_2 \rightleftharpoons CO_2 + H_2O + HCO_3^-$$

$$(4)\ CH_3COO^- + 4HOCl \rightleftharpoons CO_2 + H_2O + HCO_3^- + 4H^+ + 4Cl^-$$

$$(5)\ 2NCl_3 + 6OH^- \rightleftharpoons N_2 + 3OCl^- + 3Cl^- + 3H_2O$$

$$(6)\ 2Fe^{2+} + HOCl + 5H_2O \rightleftharpoons 2Fe(OH)_3 + Cl^- + 5H^+$$

$$(7)\ Mn^{2+} + HOCl + H_2O \rightleftharpoons MnO_2 + Cl^- + 3H^+$$

$$(8)\ NO_2 + HOCl \rightleftharpoons NO_3 + Cl^- + H^+$$

Table A 5-12. Process rate equations and stoichiometry of $KMnO_4$

No.	Process	Process Rate Equation	S_F	S_{VFA}	S_{nF}	S_U	S_{NHx}	S_N	S_{NU}	S_{PO_4}	S_P	S_{PU}	$S_{Fe^{2+}}$	$S_{Mn^{2+}}$
1	Hydrolysis of XC_B to S_F	$k_{Hyd,X_{C_B},MnO_4} XC_B S_{MnO_4}$	1											
2	Hydrolysis of X_U to S_F	$k_{Hyd,X_U,MnO_4} X_U S_{MnO_4}$	1											
3	Hydrolysis of S_U to S_F	$k_{Hyd,S_U,MnO_4} S_U S_{MnO_4}$	1			-1								
4	Hydrolysis of X_N to S_{NHx}	$k_{Hyd,X_N,MnO_4} X_N S_{MnO_4}$					1							
5	Hydrolysis of X_{NU} to S_{NHx}	$k_{Hyd,X_{NU},MnO_4} X_{NU} S_{MnO_4}$					1							
6	Hydrolysis of S_N to S_{NHx}	$k_{Hyd,S_N,MnO_4} S_N S_{MnO_4}$					1	-1						
7	Hydrolysis of S_{NU} to S_{NHx}	$k_{Hyd,S_{NU},MnO_4} S_{NU} S_{MnO_4}$					1		-1					
8	Hydrolysis of X_P to S_{PO_4}	$k_{Hyd,X_P,MnO_4} X_P S_{MnO_4}$								1				
9	Hydrolysis of X_{PU} to S_{PO_4}	$k_{Hyd,X_{PU},MnO_4} X_{PU} S_{MnO_4}$								1				
10	Hydrolysis of S_P to S_{PO_4}	$k_{Hyd,S_P,MnO_4} S_P S_{MnO_4}$								1	-1			
11	Hydrolysis of S_{PU} to S_{PO_4}	$k_{Hyd,S_{PU},MnO_4} S_{PU} S_{MnO_4}$								1		-1		
12	Oxidation of S_F (1,2)	$k_{Oxd,S_F,MnO_4} S_F S_{MnO_4}$	-1											
13	Oxidation of S_{VFA} (2,4)	$k_{Oxd,S_{VFA},MnO_4} S_{VFA} S_{MnO_4}$		-1										
14	Oxidation of S_{nF} (1,2)	$k_{Oxd,S_{nF},MnO_4} S_{nF} S_{MnO_4}$			-1									
15	Oxidation of S_U (1,2)	$k_{Oxd,S_U,MnO_4} S_U S_{MnO_4}$				-1								
16	Oxidation of $S_{Fe^{2+}}$ (5)	$k_{Oxd,Fe^{2+},MnO_4} S_{MnO_4} S_{Fe^{2+}} S_{OH^-}$											-1	
17	Oxidation of $S_{Mn^{2+}}$ (6)	$k_{1,Oxd,Mn^{2+},MnO_4} S_{Mn^{2+}} S_{MnO_4} S_{OH^-}^{1.12} + k_{2,Oxd,Mn^{2+},MnO_4} S_{Mn^{2+}} X_{MnO_2}$												-1
18	Oxidization of S_{NO_2} to S_{NO_3} (7)	$k_{Oxd,NO_2,MnO_4} S_{NO_2} S_{MnO_4}$												
19	Quenching of oxidant	$k_{Que,MnO_4} S_{Que,MnO_4} S_{MnO_4}$												

Table A 5-12. (Continued)

#	Process	S_{NO_2}	S_{NO_3}	S_{MnO_4}	S_{ALK}	S_{IC}	S_{Que,MnO_4}	X_{CB}	X_U	X_N	X_{NU}	X_P	X_{PU}	$X_{Fe(OH)_3}$	X_{MnO_2}
1	Hydrolysis of XC_B to S_F							-1							
2	Hydrolysis of X_U to S_F								-1						
3	Hydrolysis of S_U to S_F														
4	Hydrolysis of X_N to S_{NHx}									-1					
5	Hydrolysis of X_{NU} to S_{NHx}										-1				
6	Hydrolysis of S_N to S_{NHx}				3.57										
7	Hydrolysis of S_{NU} to S_{NHx}				3.57										
8	Hydrolysis of X_P to S_{PO_4}											-1			
9	Hydrolysis of X_{PU} to S_{PO_4}												-1		
10	Hydrolysis of S_P to S_{PO_4}														
11	Hydrolysis of S_{PU} to S_{PO_4}														
12	Oxidation of S_F (1,2)			$-\frac{1.33M_{MnO_4}}{M_{O_2}}$	$\frac{0.67M_{CaCO_3}}{M_{O_2}}$	$\frac{0.67M_C}{M_{O_2}}$									$\frac{1.33M_{MnO_2}}{M_{O_2}}$
13	Oxidation of S_{VFA} (3,4)			$-\frac{1.33M_{MnO_4}}{M_{O_2}}$	$\frac{0.92M_{CaCO_3}}{M_{O_2}}$	$\frac{M_C}{M_{O_2}}$									$\frac{1.33M_{MnO_2}}{M_{O_2}}$
14	Oxidation of S_{nF} (1,2)			$-\frac{1.33M_{MnO_4}}{M_{O_2}}$	$\frac{0.67M_{CaCO_3}}{M_{O_2}}$	$\frac{0.67M_C}{M_{O_2}}$									$\frac{1.33M_{MnO_2}}{M_{O_2}}$
15	Oxidation of S_U (1,2)			$-\frac{1.33M_{MnO_4}}{M_{O_2}}$	$\frac{0.67M_{CaCO_3}}{M_{O_2}}$	$\frac{0.67M_C}{M_{O_2}}$									$\frac{1.33M_{MnO_2}}{M_{O_2}}$
16	Oxidation of $S_{Fe^{2+}}$ (5)			$-\frac{0.33M_{MnO_4}}{M_{Fe}}$	$-\frac{0.83M_{CaCO_3}}{M_{Fe}}$									$\frac{M_{Fe(OH)_3}}{M_{Fe}}$	$\frac{0.33M_{MnO_2}}{M_{Fe}}$
17	Oxidation of $S_{Mn^{2+}}$ (6)			$-\frac{0.67M_{MnO_4}}{M_{Mn}}$	$-\frac{0.67M_{CaCO_3}}{M_{Mn}}$										$\frac{1.67M_{MnO_2}}{M_{Mn}}$
18	Oxidization of S_{NO_2} to S_{NO_3} (7)	-1	1	$-\frac{0.67M_{MnO_4}}{M_N}$	$\frac{0.33M_{CaCO_3}}{M_N}$										$\frac{0.67M_{MnO_2}}{M_N}$
19	Quenching of oxidant			-1			$-f_{Que,MnO4}$								

(1) $CH_3OH + 1.5O_2 \rightleftharpoons CO_2 + 2H_2O$

(2) $CH_3OH + 2MnO_4 + 2H^+ \rightleftharpoons CO_2 + 3H_2O + 2MnO_{2(s)}$

(3) $CH_3COO^- + 2O_2 \rightleftharpoons CO_2 + H_2O + HCO_3^-$

(4) $3CH_3COO^- + 8MnO_4 + 8H^+ \rightleftharpoons 3CO_2 + 7H_2O + 3HCO_3^- + 8MnO_{2(s)}$

$$(5)\ 3Fe^{2+} + MnO_4 + 7H_2O \rightleftharpoons 3Fe(OH)_3 + MnO_{2(S)} + 5H^+$$

$$(6)\ 3Mn^{2+} + MnO_4 + 2H_2O \rightleftharpoons 5MnO_{2(s)} + 4H^+$$

$$(7)\ 3NO_2 + 2MnO_4 + 2H^+ \rightleftharpoons 3NO_3 + 2MnO_{2(s)} + H_2O$$

Table A 5-13. Process rate equations and stoichiometry of ClO_2

No.	Process	Process Rate Equation	S_F	S_{VFA}	S_{nF}	S_U	S_{NHx}	S_N	S_{NU}	S_{PO_4}	S_P	S_{PU}	$S_{Fe^{2+}}$	$S_{Mn^{2+}}$
1	Hydrolysis of XC_B to S_F	$k_{Hyd,X_{CB},ClO_2} XC_B S_{ClO_2}$	1											
2	Hydrolysis of X_U to S_F	$k_{Hyd,X_U,ClO_2} X_U S_{ClO_2}$	1											
3	Hydrolysis of S_U to S_F	$k_{Hyd,S_U,ClO_2} S_U S_{ClO_2}$	1			-1								
4	Hydrolysis of X_N to S_{NHx}	$k_{Hyd,X_N,ClO_2} X_N S_{ClO_2}$					1							
5	Hydrolysis of X_{NU} to S_{NHx}	$k_{Hyd,X_{NU},ClO_2} X_{NU} S_{ClO_2}$					1							
6	Hydrolysis of S_N to S_{NHx}	$k_{Hyd,S_N,ClO_2} S_N S_{ClO_2}$					1	-1						
7	Hydrolysis of S_{NU} to S_{NHx}	$k_{Hyd,S_{NU},ClO_2} S_{NU} S_{ClO_2}$					1		-1					
8	Hydrolysis of X_P to S_{PO_4}	$k_{Hyd,X_P,ClO_2} X_P S_{ClO_2}$								1				
9	Hydrolysis of X_{PU} to S_{PO_4}	$k_{Hyd,X_{PU},ClO_2} X_{PU} S_{ClO_2}$								1				
10	Hydrolysis of S_P to S_{PO_4}	$k_{Hyd,S_P,ClO_2} S_P S_{ClO_2}$								1	-1			
11	Hydrolysis of S_{PU} to S_{PO_4}	$k_{Hyd,S_{PU},ClO_2} S_{PU} S_{ClO_2}$								1		-1		
12	Oxidation of S_F (1,2)	$k_{Oxd,S_F,ClO_2} S_F S_{ClO_2}$	-1											
13	Oxidation of S_{VFA} (2,4)	$k_{Oxd,S_{VFA},ClO_2} S_{VFA} S_{ClO_2}$		-1										
14	Oxidation of S_{nF} (1,2)	$k_{Oxd,S_{nF},ClO_2} S_{nF} S_{ClO_2}$			-1									
15	Oxidation of S_U (1,2)	$k_{Oxd,S_U,ClO_2} S_U S_{ClO_2}$				-1								
16	Oxidation of $S_{Fe^{2+}}$ (5)	$k_{Oxd,Fe^{2+},ClO_2} S_{ClO_2} S_{Fe^{2+}} S_{OH^-}$											-1	
17	Oxidation of $S_{Mn^{2+}}$ (6)	$k_{1,Oxd,Mn^{2+},ClO_2} S_{Mn^{2+}} S_{ClO_2} S_{OH^-}^{1.12} + k_{2,Oxd,Mn^{2+},ClO_2} S_{Mn^{2+}} X_{MnO_2}$												-1
18	Oxidization of S_{NO_2} to S_{NO_3} (7)	$k_{Oxd,NO_2,ClO_2} S_{NO_2} S_{ClO_2}$												
19	Quenching of oxidant	$k_{Que,ClO_2} S_{Que,ClO_2} S_{ClO_2}$												

Table A 5-13. (Continued)

#	Process	S_{NO_2}	S_{NO_3}	S_{ClO_2}	S_{ALK}	S_{IC}	S_{Que,ClO_2}	X_{CB}	X_U	X_N	X_{NU}	X_P	X_{PU}	$X_{Fe(OH)_3}$	X_{MnO_2}
1	Hydrolysis of XC_B to S_F							-1							
2	Hydrolysis of X_U to S_F								-1						
3	Hydrolysis of S_U to S_F														

#	Process	S_{NO_2}	S_{NO_3}	S_{ClO_2}	S_{ALK}	S_{IC}	S_{Que,ClO_2}	X_{CB}	X_U	X_N	X_{NU}	X_P	X_{PU}	$X_{Fe(OH)_3}$	X_{MnO_2}
4	Hydrolysis of X_N to S_{NHx}									-1					
5	Hydrolysis of X_{NU} to S_{NHx}										-1				
6	Hydrolysis of S_N to S_{NHx}				3.57										
7	Hydrolysis of S_{NU} to S_{NHx}				3.57										
8	Hydrolysis of X_P to S_{PO_4}											-1			
9	Hydrolysis of X_{PU} to S_{PO_4}												-1		
10	Hydrolysis of S_P to S_{PO_4}														
11	Hydrolysis of S_{PU} to S_{PO_4}														
12	Oxidation of S_F (1,2)			$-\frac{0.8M_{ClO_2}}{M_{O_2}}$	$-\frac{0.4M_{CaCO_3}}{M_{O_2}}$	$\frac{0.67M_C}{M_{O_2}}$									
13	Oxidation of S_{VFA} (2,4)			$-\frac{0.8M_{ClO_2}}{M_{O_2}}$	$\frac{0.15M_{CaCO_3}}{M_{O_2}}$	$\frac{M_C}{M_{O_2}}$									
14	Oxidation of S_{nF} (1,2)			$-\frac{0.8M_{ClO_2}}{M_{O_2}}$	$-\frac{0.4M_{CaCO_3}}{M_{O_2}}$	$\frac{0.67M_C}{M_{O_2}}$									
15	Oxidation of S_U (1,2)			$-\frac{0.8M_{ClO_2}}{M_{O_2}}$	$-\frac{0.4M_{CaCO_3}}{M_{O_2}}$	$\frac{0.67M_C}{M_{O_2}}$									
16	Oxidation of $S_{Fe^{2+}}$ (5)			$-\frac{M_{ClO_2}}{M_{Fe}}$	$-\frac{1.5M_{CaCO_3}}{M_{Fe}}$									$\frac{M_{Fe(OH)_3}}{M_{Fe}}$	
17	Oxidation of $S_{Mn^{2+}}$ (6)			$-\frac{2M_{ClO_2}}{M_{Mn}}$	$-\frac{2M_{CaCO_3}}{M_{Mn}}$										$\frac{M_{MnO_2}}{M_{Mn}}$
18	Oxidization of S_{NO_2} to S_{NO_3} (7)	-1	1	$-\frac{0.4M_{ClO_2}}{M_N}$	$-\frac{0.2M_{CaCO_3}}{M_N}$										
19	Quenching of oxidant			-1			$-f_{Que,ClO_2}$								

(1) $CH_3OH + 1.5O_2 \rightleftharpoons CO_2 + 2H_2O$

(2) $5CH_3OH + 6ClO_2 \rightleftharpoons 5CO_2 + 6H^+ + 6Cl^- + 7H_2O$

(3) $CH_3COO^- + 2O_2 \rightleftharpoons CO_2 + H_2O + HCO_3^-$

(4) $5CH_3COO^- + 8ClO_2 \rightleftharpoons 5CO_2 + H_2O + 5HCO_3^- + 8Cl^- + 8H^+$

(5) $Fe^{2+} + ClO_2 + 3H_2O \rightleftharpoons Fe(OH)_3 + ClO_2^- + 3H^+$

(6) $Mn^{2+} + 3ClO_2 + 2H_2O \rightleftharpoons MnO_{2(s)} + 2ClO_2^- + 4H^+$

(7) $5NO_2 + 2ClO_2 + H_2O \rightleftharpoons 5NO_3 + 2Cl^- + 2H^+$

Table A 5-14. Process rate equations and stoichiometry of O_3

No.	Process	Process Rate Equation	S_F	S_{VFA}	S_{nF}	S_U	S_{NHx}	S_N	S_{NU}	S_{PO_4}	S_P	S_{PU}	$S_{Fe^{2+}}$	$S_{Mn^{2+}}$	S_{O_2}
1	Hydrolysis of XC_B to S_F	$k_{Hyd,X_{CB},O_3} XC_B S_{O_3}$	1												
2	Hydrolysis of X_U to S_F	$k_{Hyd,X_U,O_3} X_U S_{O_3}$	1												
3	Hydrolysis of S_U to S_F	$k_{Hyd,S_U,O_3} S_U S_{O_3}$	1			-1									
4	Hydrolysis of X_N to S_{NHx}	$k_{Hyd,X_N,O_3} X_N S_{O_3}$					1								
5	Hydrolysis of X_{NU} to S_{NHx}	$k_{Hyd,X_{NU},O_3} X_{NU} S_{O_3}$					1								
6	Hydrolysis of S_N to S_{NHx}	$k_{Hyd,S_N,O_3} S_N S_{O_3}$					1	-1							
7	Hydrolysis of S_{NU} to S_{NHx}	$k_{Hyd,S_{NU},O_3} S_{NU} S_{O_3}$					1		-1						
8	Hydrolysis of X_P to S_{PO_4}	$k_{Hyd,X_P,O_3} X_P S_{O_3}$								1					
9	Hydrolysis of X_{PU} to S_{PO_4}	$k_{Hyd,X_{PU},O_3} X_{PU} S_{O_3}$								1					
10	Hydrolysis of S_P to S_{PO_4}	$k_{Hyd,S_P,O_3} S_P S_{O_3}$								1	-1				
11	Hydrolysis of S_{PU} to S_{PO_4}	$k_{Hyd,S_{PU},O_3} S_{PU} S_{O_3}$								1		-1			
12	Oxidation of S_F (1,2)	$k_{Oxd,S_F,O_3} S_F S_{O_3} + k_{Oxd,S_F,O_3,OH} R_c S_{O_3}$	-1												2
13	Oxidation of S_{VFA} (2,4)	$k_{Oxd,S_{VFA},O_3} S_{VFA} S_{O_3} + k_{Oxd,S_{VFA},O_3,OH} R_c S_{O_3}$		-1											2
14	Oxidation of S_{nF} (1,2)	$k_{Oxd,S_{nF},O_3} S_{nF} S_{O_3} + k_{Oxd,S_{nF},O_3,OH} R_c S_{O_3}$			-1										2
15	Oxidation of S_U (1,2)	$k_{Oxd,S_U,O_3} S_U S_{O_3} + k_{Oxd,S_U,O_3,OH} R_c S_{O_3}$				-1									2
16	Oxidation of $S_{Fe^{2+}}$ (5)	$k_{Oxd,Fe^{2+},O_3} S_{O_3} S_{Fe^{2+}} S_{OH^-}$											-1		$\frac{0.5 M_{O_2}}{M_{Fe}}$
17	Oxidation of $S_{Mn^{2+}}$ (6)	$k_{1,Oxd,Mn^{2+},O_3} S_{Mn^{2+}} S_{O_3} S_{OH^-}^{1.12} + k_{2,Oxd,Mn^{2+},O_3} S_{Mn^{2+}} X_{MnO_2}$												-1	$\frac{M_{O_2}}{M_{Mn}}$
18	Oxidization of S_{NO_2} to S_{NO_3} (7)	$k_{Oxd,NO_2,O_3} S_{NO_2} S_{O_3}$													$\frac{M_{O_2}}{M_N}$
19	Dissociation to S_{O_2}	$k_{Dis,O_3} S_{O_3}$													$\frac{M_{O_3}}{M_{O_2}}$
20	Quenching of oxidant	$k_{Que,O_3} S_{Que,O_3} S_{O_3}$													

Table A 5-14. (Continued)

#	Process	S_{NO_2}	S_{NO_3}	S_{O_3}	S_{ALK}	S_{IC}	S_{Que,O_3}	X_{CB}	X_U	X_N	X_{NU}	X_P	X_{PU}	$X_{Fe(OH)_3}$	X_{MnO_2}
1	Hydrolysis of XC_B to S_F							-1							
2	Hydrolysis of X_U to S_F								-1						
3	Hydrolysis of S_U to S_F														

#	Process	S_{NO_2}	S_{NO_3}	S_{O_3}	S_{ALK}	S_{IC}	S_{Que,O_3}	X_{CB}	X_U	X_N	X_{NU}	X_P	X_{PU}	$X_{Fe(OH)_3}$	X_{MnO_2}
4	Hydrolysis of X_N to S_{NHx}									-1					
5	Hydrolysis of X_{NU} to S_{NHx}										-1				
6	Hydrolysis of S_N to S_{NHx}				3.57										
7	Hydrolysis of S_{NU} to S_{NHx}				3.57										
8	Hydrolysis of X_P to S_{PO_4}											-1			
9	Hydrolysis of X_{PU} to S_{PO_4}												-1		
10	Hydrolysis of S_P to S_{PO_4}														
11	Hydrolysis of S_{PU} to S_{PO_4}														
12	Oxidation of S_F (1,2)			$-\frac{2M_{O_3}}{M_{O_2}}$		$\frac{0.67M_C}{M_{O_2}}$									
13	Oxidation of S_{VFA} (2,4)			$-\frac{2M_{O_3}}{M_{O_2}}$	$\frac{0.25M_{CaCO_3}}{M_{O_2}}$	$\frac{M_C}{M_{O_2}}$									
14	Oxidation of S_{nF} (1,2)			$-\frac{2M_{O_3}}{M_{O_2}}$		$\frac{0.67M_C}{M_{O_2}}$									
15	Oxidation of S_U (1,2)			$-\frac{2M_{O_3}}{M_{O_2}}$		$\frac{0.67M_C}{M_{O_2}}$									
16	Oxidation of $S_{Fe^{2+}}$ (5)			$-\frac{0.5M_{O_3}}{M_{Fe}}$	$-\frac{M_{CaCO_3}}{M_{Fe}}$									$\frac{M_{Fe(OH)_3}}{M_{Fe}}$	
17	Oxidation of $S_{Mn^{2+}}$ (6)			$-\frac{M_{O_3}}{M_{Mn}}$	$-\frac{M_{CaCO_3}}{M_{Mn}}$										$\frac{M_{MnO_2}}{M_{Mn}}$
18	Oxidization of S_{NO_2} to S_{NO_3} (7)	-1	1	$-\frac{M_{O_3}}{M_N}$											
19	Dissociation to S_{O_2}			-1											
20	*Quenching of oxidant*			*-1*			$-f_{Que,O_3}$								

(1) $CH_3OH + 1.5O_2 \rightleftharpoons CO_2 + 2H_2O$

(2) $CH_3OH + 3O_3 \rightleftharpoons CO_2 + 3O_2 + 2H_2O$

(3) $CH_3COO^- + 2O_2 \rightleftharpoons CO_2 + H_2O + HCO_3^-$

(4) $CH_3COO^- + 4O_3 \rightleftharpoons CO_2 + 4O_2 + HCO_3^- + H_2O$

(5) $2Fe^{2+} + O_3 + 5H_2O \rightleftharpoons 2Fe(OH)_3 + O_2 + 4H^+$

(6) $Mn^{2+} + O_3 + H_2O \rightleftharpoons MnO_{2(s)} + O_2 + 2H^+$

(7) $NO_2 + O_3 \rightleftharpoons NO_3 + O_2$

Table A 5-15. Process rate equations and stoichiometry of H_2O_2

No.	Process	Process Rate Equation	S_F	S_{VFA}	S_{nF}	S_U	S_{NHx}	S_N	S_{NU}	S_{PO_4}	S_P	S_{PU}	$S_{Fe^{2+}}$	$S_{Mn^{2+}}$
1	Hydrolysis of XC_B to S_F	$k_{Hyd,X_{CB},H_2O_2} XC_B S_{H_2O_2}$	1											
2	Hydrolysis of X_U to S_F	$k_{Hyd,X_U,H_2O_2} X_U S_{H_2O_2}$	1											
3	Hydrolysis of S_U to S_F	$k_{Hyd,S_U,H_2O_2} S_U S_{H_2O_2}$	1			-1								
4	Hydrolysis of X_N to S_{NHx}	$k_{Hyd,X_N,H_2O_2} X_N S_{H_2O_2}$					1							
5	Hydrolysis of X_{NU} to S_{NHx}	$k_{Hyd,X_{NU},H_2O_2} X_{NU} S_{H_2O_2}$					1							
6	Hydrolysis of S_N to S_{NHx}	$k_{Hyd,S_N,H_2O_2} S_N S_{H_2O_2}$					1	-1						
7	Hydrolysis of S_{NU} to S_{NHx}	$k_{Hyd,S_{NU},H_2O_2} S_{NU} S_{H_2O_2}$					1		-1					
8	Hydrolysis of X_P to S_{PO_4}	$k_{Hyd,X_P,H_2O_2} X_P S_{H_2O_2}$								1				
9	Hydrolysis of X_{PU} to S_{PO_4}	$k_{Hyd,X_{PU},H_2O_2} X_{PU} S_{H_2O_2}$								1				
10	Hydrolysis of S_P to S_{PO_4}	$k_{Hyd,S_P,H_2O_2} S_P S_{H_2O_2}$								1	-1			
11	Hydrolysis of S_{PU} to S_{PO_4}	$k_{Hyd,S_{PU},H_2O_2} S_{PU} S_{H_2O_2}$								1		-1		
12	Oxidation of S_F (1,2)	$k_{Oxd,S_F,H_2O_2} S_F S_{H_2O_2} + k_{Oxd,S_F,H_2O_2,OH} R_c S_{H_2O_2}$	-1											
13	Oxidation of S_{VFA} (2,4)	$k_{Oxd,S_{VFA},H_2O_2} S_{VFA} S_{H_2O_2} + k_{Oxd,S_{VFA},H_2O_2,OH} R_c S_{H_2O_2}$		-1										
14	Oxidation of S_{nF} (1,2)	$k_{Oxd,S_{nF},H_2O_2} S_{nF} S_{H_2O_2} + k_{Oxd,S_{UF},H_2O_2,OH} R_c S_{H_2O_2}$			-1									
15	Oxidation of S_U (1,2)	$k_{Oxd,S_U,H_2O_2} S_U S_{H_2O_2} + k_{Oxd,S_U,H_2O_2,OH} R_c S_{H_2O_2}$				-1								
16	Oxidation of $S_{Fe^{2+}}$ (5)	$k_{Oxd,Fe^{2+},H_2O_2} S_{H_2O_2} S_{Fe^{2+}} S_{OH^-}$											-1	
17	Oxidation of $S_{Mn^{2+}}$ (6)	$k_{1,Oxd,Mn^{2+},H_2O_2} S_{Mn^{2+}} S_{H_2O_2} S_{OH^-}^{1.12} + k_{2,Oxd,Mn^{2+},H_2O_2} S_{Mn^{2+}} X_{MnO_2}$												-1
18	Oxidization of S_{NO_2} to S_{NO_3} (7)	$k_{Oxd,NO_2,H_2O_2} S_{NO_2} S_{H_2O_2}$												
19	Quenching of oxidant	$k_{Que,H_2O_2} S_{Que,H_2O_2} S_{H_2O_2}$												

Table A 5-15. (Continued)

#	Process	S_{O_2}	S_{NO_2}	S_{NO_3}	$S_{H_2O_2}$	S_{ALK}	S_{IC}	S_{Que,O_3}	X_{CB}	X_U	X_N	X_{NU}	X_P	X_{PU}	$X_{Fe(OH)_3}$	X_{MnO_2}
1	Hydrolysis of XC_B to S_F								-1							
2	Hydrolysis of X_U to S_F									-1						
3	Hydrolysis of S_U to S_F															
4	Hydrolysis of X_N to S_{NHx}										-1					
5	Hydrolysis of X_{NU} to S_{NHx}											-1				
6	Hydrolysis of S_N to S_{NHx}					3.57										
7	Hydrolysis of S_{NU} to S_{NHx}					3.57										

#	Process	S_{O_2}	S_{NO_2}	S_{NO_3}	$S_{H_2O_2}$	S_{ALK}	S_{IC}	S_{Que,O_3}	X_{CB}	X_U	X_N	X_{NU}	X_P	X_{PU}	$X_{Fe(OH)_3}$	X_{MnO_2}
8	Hydrolysis of X_P to S_{PO_4}												-1			
9	Hydrolysis of X_{PU} to S_{PO_4}													-1		
10	Hydrolysis of S_P to S_{PO_4}															
11	Hydrolysis of S_{PU} to S_{PO_4}															
12	Oxidation of S_F (1,2)				$-\frac{2M_{H_2O_2}}{M_{O_2}}$		$\frac{0.67M_C}{M_{O_2}}$									
13	Oxidation of S_{VFA} (2,4)				$-\frac{2M_{H_2O_2}}{M_{O_2}}$	$\frac{0.25M_{CaCO_3}}{M_{O_2}}$	$\frac{M_C}{M_{O_2}}$									
14	Oxidation of S_{nF} (1,2)				$-\frac{2M_{H_2O_2}}{M_{O_2}}$		$\frac{0.67M_C}{M_{O_2}}$									
15	Oxidation of S_U (1,2)				$-\frac{2M_{H_2O_2}}{M_{O_2}}$		$\frac{0.67M_C}{M_{O_2}}$									
16	Oxidation of $S_{Fe^{2+}}$ (5)				$-\frac{0.5M_{H_2O_2}}{M_{Fe}}$	$-\frac{M_{CaCO_3}}{M_{Fe}}$									$\frac{M_{Fe(OH)_3}}{M_{Fe}}$	
17	Oxidation of $S_{Mn^{2+}}$ (6)				$-\frac{M_{H_2O_2}}{M_{Mn}}$	$-\frac{M_{CaCO_3}}{M_{Mn}}$										$\frac{M_{MnO_2}}{M_{Mn}}$
18	Oxidization of S_{NO_2} to S_{NO_3} (7)		-1	1	$-\frac{M_{H_2O_2}}{M_N}$											
19	Quenching of oxidant				-1			$-f_{Que,H_2O_2}$								

(1) $CH_3OH + 1.5O_2 \rightleftharpoons CO_2 + 2H_2O$

(2) $CH_3OH + 3H_2O_2 \rightleftharpoons CO_2 + 5H_2O$

(3) $CH_3COO^- + 2O_2 \rightleftharpoons CO_2 + H_2O + HCO_3^-$

(4) $CH_3COO^- + 2H_2O_2 \rightleftharpoons CO_2 + 5HO_2 + HCO_3^-$

(5) $2Fe^{2+} + H_2O_2 + 4H_2O \rightleftharpoons 2Fe(OH)_3 + 4H^+$

(6) $Mn^{2+} + H_2O_2 \rightleftharpoons MnO_{2(s)} + 2H^+$

(7) $NO_2 + H_2O_2 \rightleftharpoons NO_3 + H_2O$

Table A 5-16. Process rate equations and stoichiometry of Adsorption

No.	Process	Process Rate Equation	S_F	S_{VFA}	S_{nF}	S_U	S_{ALK}	$X_{A,F}$	$X_{A,VFA}$	$X_{A,nF}$	$X_{A,U}$
1	Adsorption of S_F	$k_{Ads}S_F^a\left[q_{max}X_A - \left(X_{A,F} + X_{A,VFA} + X_{A,nF} + X_{A,U}\right)\right]$	-1					1			

No.	Process	Process Rate Equation	S_F	S_{VFA}	S_{nF}	S_U	S_{ALK}	$X_{A,F}$	$X_{A,VFA}$	$X_{A,nF}$	$X_{A,U}$
2	Desorption of S_F	$k_{Des}X_{A,F}$	1					-1			
3	Adsorption of S_{VFA}	$k_{Ads}S_{VFA}^{a}\left[q_{max}X_A-\left(X_{A,F}+X_{A,VFA}+X_{A,nF}+X_{A,U}\right)\right]$		-1			-2.5		1		
4	Desorption of S_{VFA}	$k_{Des}X_{A,VFA}$		1			2.5		-1		
5	Adsorption of S_{nF}	$k_{Ads}S_{nF}^{a}\left[q_{max}X_A-\left(X_{A,F}+X_{A,VFA}+X_{A,nF}+X_{A,U}\right)\right]$			-1					1	
6	Desorption of S_{nF}	$k_{Des}X_{A,nF}$			1					-1	
7	Adsorption of S_U	$k_{Ads}S_{U}^{a}\left[q_{max}X_A-\left(X_{A,F}+X_{A,VFA}+X_{A,nF}+X_{A,U}\right)\right]$				-1					1
8	Desorption of S_U	$k_{Des}X_{A,U}$				1					-1
9	Hydrolysis of $X_{A,U}$	$k_{Hyd,Des}X_{A,U}$	1								-1
10	Saturation of $X_{A,F}$	$k_{Sat}X_{A,F}$						-1			
11	Saturation of $X_{A,VFA}$	$k_{Sat}X_{A,VFA}$							-1		
12	Saturation of $X_{A,nF}$	$k_{Sat}X_{A,nF}$								-1	
13	Saturation of $X_{A,U}$	$k_{Sat}X_{A,U}$									-1

Table A 5-17. Process rate equations and stoichiometry of gas transfer

No.	Process	Process Rate Equation	S_{O_2}	S_{CO_2}	S_{CH_4}	S_{NH_3}	S_{NO}	S_{N_2O}	S_{IC}
1	Gas transfer for S_{O_2}	$86400k_{L,O_2}A_{Tank}\left(P_{O_2}K_{H,O_2}M_{O_2}-S_{O_2}\right)+\frac{SOTR\times\alpha\times F\times\left(C_{inf}-S_{O_2}\right)}{\left(C_{inf,20}\theta_{O_2}^{20-T}\right)V}$	1						
2	Gas transfer for S_{CO_2}	$86400k_{L,CO_2}\left(A_{Tank}+A_{Bubble}\right)\left(P_{CO_2}K_{H,CO_2}M_C-S_{CO_2}\right)$		1					1
3	Gas transfer for S_{CH_4}	$86400k_{L,CH_4}\left(A_{Tank}+A_{Bubble}\right)\left(P_{CH_4}K_{H,CH_4}M_C-S_{CH_4}\right)$			1				

No.	Process	Process Rate Equation	S_{O_2}	S_{CO_2}	S_{CH_4}	S_{NH_3}	S_{NO}	S_{N_2O}	S_{IC}
4	Gas transfer for S_{NH_3}	$86400k_{L,NH_3}\left(A_{Tank}+A_{Bubble}\right)\left(P_{NH_3}K_{H,NH_3}M_N-S_{NH_3}\right)$				1			
5	Gas transfer for S_{NO}	$86400k_{L,NO}\left(A_{Tank}+A_{Bubble}\right)\left(P_{NO}K_{H,NO}M_N-S_{NO}\right)$					1		
6	Gas transfer for S_{N_2O}	$86400k_{L,N_2O}\left(A_{Tank}+A_{Bubble}\right)\left(P_{N_2O}K_{H,N_2O}M_N-S_{N_2O}\right)$						1	

Chapter 6 Summary and Conclusions

6.1 Summary

The term integrated modeling commonly refers to the coupling mechanism used to automate the data exchange between linked models. However, such applications often require extensive pre- and post-processing in order to develop a fully automated integrated model. URUNME was developed with the goal of not only facilitating model coupling, but automating the entire simulation process - creating inputs from different data sources, reading outputs, analyzing data, making statistical inferences, and ultimately showing results in a visually-aesthetic and interactive way. It serves as an intelligent layer between the users, models, and data sources, practically hiding the underlying mechanics of an otherwise complex simulation process. The first study explained in detail the architecture and capabilities of URUNME and demonstrated how it can be used to perform different modeling tasks ranging from simple data analysis to complex model integration. With the increasing need to model and analyze complex environmental problems that are both multimedia and multidisciplinary (Laniak et al. 2013), a software platform such as URUNME provides a one-stop solution. Greater functionality and features is expected to be added to URUNME following user feedback. Support for several new data formats, implementation of other modeling frameworks, upgrade to OpenMI 2.0, and integration of Geographic Information System (GIS) mapping features are already part of the future software development plan.

This second study presented the development and implementation of a DSS for the Occoquan IPR system to forecast and regulate the nitrate concentrations in the augmented reservoir. The entire DSS application was powered by URUNME to fully automate the operation of the integrated reservoir and process models, forecasting products, and data sources. The reservoir model is operated weekly, running multiple future scenarios based on different combinations of natural stream inflows, plant effluent flows and nitrate concentrations, and water withdrawal by the WTP. The future weather conditions are simulated using forecasts obtained from the CFS. A 30-day forecast predicted the reservoir conditions based on the NWM stream flow forecast going out 30 days. A 90-day forecast, on the other hand, was used as a what-if analysis to simulate the effects of possible future winter drought. The forecasted nitrate-N concentrations under different scenarios are used by the WRF to identify and dynamically analyze operational strategies in

response to the reservoir's future conditions. If nitrates going out 30 to 60 days exceeds 3 mg/L, the DSS can run different optimization routines on IViewOps to determine the means to reduce the nutrient discharge. Even when the target nitrate effluent concentrations are difficult to achieve due to operational constraints, the DSS output provides a fair estimate of the time it would take for the reservoir to reach unacceptable nitrate levels. This provides valuable feedback to the plant managers for contingency planning (e.g., rescheduling maintenance of certain assets, adding supplemental carbon chemicals, changing plant configuration, etc.) to avoid future emergencies. As the DSS progresses forward in time, the optimization of the WRF is revisited every 7 days with updated outputs based on the dynamic nature of the system. For instance, a significant rain event could partially or completely wash out the entire reservoir, diluting the nitrate concentrations to much lower levels. The plant could then use the URUNME interface to simulate this with IViewOps and output relevant data in a screen adjacent to the SCADA screen.

The third study presented a new PCM that was incorporated into the latest version of IViewOps to simulate processes like pH (acid/base), precipitation, oxidation, adsorption, biofiltration, carbonation, chlorination, etc. A number of new state and algebraic variables and kinetic equations were added to this model. A new solver was developed to implicitly solve the pH model of any reactor, if desired by the user. This allows users to limit the pH calculation to only select reactors and reduce computational overhead. The setup of the full-scale model for UOSA-WRF was discussed in detail and results were presented. Initial calibration indicated that pH, precipitation, carbonations, biofiltration, and chlorination were accurately modeled by the PCM. It was shown that the addition of pH model is not only essential for modeling processes like chemical P removal but can also be helpful in predicting the undesired precipitation in dewatering systems. The model was able to accurately predict the primary and secondary clarifiers and final effluent concentrations with a PBIAS of less than 10% in most cases. Other calibration variables including total airflow, MLSS in the aeration basins, and biogas from the digester were also simulated by the model with a PBIAS of less than 5%. The model was able to accurately capture the varying nitrate concentrations during summers and winters caused by changes in plant configurations. The model also predicted the presence of phosphorus accumulating bacteria in the system throughout the year that promoted biological P uptake. The amount of sludge produced by the chemical P removal system and the carbon dioxide dosage for carbonation were simulated to be within the range generally observed at the plant. The new

architecture of IViewOps4 was also briefly explained and showed how decoupling the model code from the rest of the software and making it open-sourced allows users to modify and/or add new model equations. It is envisaged that the addition of the new open-sourced PCM in IViewOps will not only allow modeling of advanced wastewater and water reuse processes, but will also expand its application to water treatment systems.

6.2 Conclusion

Integrated modeling provides a comprehensive approach to environmental management by evaluating different components within a system in a holistic manner. It can be used as an effective tool for design, planning, and risk assessments, and can facilitate informed decision-making, enhancing the transparency and collaboration between different stakeholders. Moreover, it can be used for simulating, understanding, and managing a combination of wastewater, drinking water, and groundwater interactions, such as:

4. IPR applications in southern California (Orange County).
5. Wastewater treatment, discharge to a reservoir, extraction for drinking water supply, and drinking water treatment (IPR, Wichita Falls, Texas);
6. Raw water supply from a reservoir, water treatment, and sludge disposal to a wastewater treatment plant (WSSC [Washington Suburban Sanitary Commission], Maryland).

The use of a DSS driven by URUNME can be used in various systems in addition to water resources. These can include chemical and biological engineering systems and their models, manufacturing and supply chain management systems and their models. URUNME is available free of cost for academic use (www.urunme.com).

6.3 References

Laniak, G. F., Olchin, G., Goodall, J., Voinov, A., Hill, M., Glynn, P., Whelan, G., Geller, G., Quinn, N., and Blind, M. (2013). "Integrated environmental modeling: a vision and roadmap for the future." *Environmental Modelling & Software*, 39, 3-23.